Biochemical investigation of cation selectivity of the *Ilyobacter tartaricus* Na^+-ATP synthase rotor ring

Dissertation
Zur Erlangung des Doktorgrades
der Naturwissenschaften

vorgelegt beim Fachbereich 14
Biochemie, Chemie und Pharmazie
Der Johann Wolfgang Goethe-Universität
In Frankfurt am Main

von

Ganna Krasnoselska
aus Odessa, Ukraine

Frankfurt, 2018
(D30)

Diese Arbeit wurde in der Arbeitsgruppe von Dr. Thomas Meier der Abteilung Structurbiologie des Max-Planck-Institutes für Biophysik in Frankfurt am Main durchgefürt und vom Fachbereich 14 Biochemie, Chemie , Pharmazie der Johann Wolfgang Goethe Universität als Dissertation angenommen.

Dekan: Prof. Dr. Clemens Glaubitz

1. Gutachter: Prof. Dr. Klaas Martinus Pos
2. Gutachter: Prof. Dr. Werner Kühlbrandt

Datum der Disputation: _____

Abstract

Rotary F-type ATP synthases are essential components of cellular bioenergetics in bacteria. The bioenergetic role of membrane-integrated rotary ATP synthases is to catalyze ATP synthesis at the expense of the transmembrane electrical ion gradient (Mitchell 1961, Duncan et al. 1995, Noji et al. 1997, Kinosita et al. 1998). Rotary ATP synthases are divided into two classes according to their cation selectivity under physiological conditions, one belonging to H^+-selective and other belonging to Na^+-selective ATP synthases. Their monovalent cation selectivity (H^+ or Na^+) is a critical property that underpins the bioenergetic function. There is only a limited number of anaerobic eubacteria and archaea, which retain Na^+-coupled bioenergetics. The well-characterized examples of Na^+-selective ATP synthases are the F-type enzymes from *I. tartaricus*, *P. modestum* and V/A-type enzymes of *E. hirae* and *A. woodii*. Despite differences in cation selectivity, their organization and principles of action are similar.

In the work presented in this thesis, the aim was to investigate which factors contribute to high selectivity and affinity of ATP synthase membrane-embedded rotor c-ring with respect to protons (H^+) and Na^+. To carry out this investigation, the F-type ATP synthase c_{11}-ring from the anaerobic bacterium *Ilyobacter tartaricus* was used as a model system. The *I. tartaricus* c-ring has an inherently high binding selectivity for Na^+, but under non-physiological condition, it can also bind and operate with Li^+ and H^+ (Neumann et al. 1998).

The thesis is divided in four sections: (i) An introduction of rotary ATP synthases and how they can be experimentally approach to characterize their monovalent cation properties. (ii) The investigation of cation binding properties of the purified *I. tartaricus* wild-type and mutant c-rings.(iii) The biochemical exploration of the catalytic activity of *I. tartaricus* wild-type and mutant ATP synthases regarding their Na^+, H^+ and Li^+ selectivity and affinity. (iv)The last section discusses these findings in the context of principles of biophysics and biochemistry toward design of Na^+ and/or H^+ selectivity of rotary ATP synthases.

Two terms were used to describe the association of monovalent cations with c-rings and ATP synthases: (i) selectivity, which distinguishes between binding partners with higher and lower specificity (selectivity refers to differences in absolute binding affinities of ligands); (ii) affinity,

which describes the probability of a protein finding a ligand molecule (Jones et al. 1998, Demchenko 2001). The K_d and K_M values were used to quantify Na^+ binding affinity of the c-rings and ATP synthases, respectively. The selectivity was used to indicate cations that can bind tothe c-rings and ATP synthases (e.g., $H^+/Na^+/Li^+$-, H^+/Na^+- or only H^+). The ratio between absolute binding affinities for each of the cations (e.g., K_d (Na^+)/K_d (H^+)) was used to display a preference toward particular cation. The factors that underlie cation selectivity and affinity of *I. tartaricus* c-ring were studied by mutagenesis of its ion binding site residues. Na^+ binding in *I. tartaricus* c-ring occurs at the interface of two adjacent c-subunits of the c-ring. Amino acids participating in binding of the Na^+ are located in helix 1 (Gln32) and helix 2 (Val63, Ser66, Thr67 and Tyr70) close to the essential Glu65.In total, 19 different specific site-directed single and double mutations were introduced in the sequence of *atpE* gene encoding *I. tartaricus* ATP synthase c-subunit. In particularly, three polar residues from ion binding site in *I. tartaricus* c-ring (Ser66, Thr67 and Tyr70) were replaced with other, polar residues (Ser67, Ile67 or Leu67),or hydrophobic residues (Ala66, Gln67 and Phe70). The charged Glu65 was substituted by shorter, but still charged side chain Asp65. An approach that combines biochemical (DCCD ion competition assay) and biophysical (ITC) methods to characterize monovalent cation binding by *I. tartaricus* wild-type and mutant c-rings was used.

The ATP synthase inhibitor *N,N′*-dicyclohexylcarbodiimide (DCCD), which covalently modifies protonated Glu/Asp carboxyl group in c-subunits at different $[Na^+]/[H^+]$ molar ratios, was used to assess differences in Na^+ and/or H^+ binding to wild-type and mutant c-rings. Only c-rings with high Na^+ binding affinity could be sufficiently protected against DCCD modification of Glu/Asp carboxyl group. A result of this study was that much higher initial $[Na^+]/[H^+]$ molar ratios were required to protect the carboxyl group in T67G, T67S, E65D, Y70F, S66A/Y70F and Q32A mutant c-rings against DCCD modification and that Na^+ did not protect Glu65 carboxyl group even at very high $[Na^+]/[H^+]$ molar ratio in the Q32A/Y70F mutant c-ring. It was concluded therefore, that Q32A/Y70F mutation abolishes Na^+ binding to *I. tartaricus* c-ring and T67G, T67S, E65D, Y70F, S66A/Y70F and Q32A mutations reduce Na^+ binding affinity of *I. tartaricus* c-ring. The changes in $[Na^+]/[H^+]$ molar ratio required to protect Glu65 carboxyl group against DCCD modification were also correlated with H^+ binding properties of Glu65 carboxyl group (namely, its pKa value). Indeed, for the set of Q32A, S66A/Y70F and

Q32A/Y70F mutant c-rings it was shown that considerably reduced (Q32A and S66A/Y70F mutations) or no Na^+ protection (Q32A/Y70F mutation) against DCCD modification correlated with higher pKa values of Glu65 carboxyl group in corresponding c-rings. Another question addressed what determines high pKa in Q32A, S66A/Y70F and Q32A/Y70F mutant c-rings. This work postulates that high pKa of Glu65 carboxyl group is related to the high hydrophobicity of the ion binding site in the c-ring. In general, set of DCCD modification experiments with the c-rings gave a clear indication on changes in both, cation affinity and selectivity upon introduction of mutations in the *I. tartaricus* c-ring.

At the next step, isothermal titration calorimetry (ITC) experiments on Na^+ binding to wild-type and mutant c-rings of *I. tartaricus* were run in order to obtain accurate measurements of changes in Na^+ binding affinity of mutant c-rings. In the case of the *I. tartaricus* wild-type c-ring, solubilized in DDM detergent, the absolute binding affinity for Na^+ (the K_d (Na^+) was extrapolated at theoretical [H^+] = 0) roughed to 7.9 μM. By experimental approach, it was shown that Na^+ binds to *I. tartaricus* c-ring with equivalent affinity only at conditions of low H^+ concentration (high pH), when Glu65 carboxyl group is deprotonated and no cation competition is observed. In terms of total cation selectivity (the K_d (Na^+)/K_d (H^+) ratio was calculated) intact c-ring of *I. tartaricus* is 637 more selective to H^+ than to Na^+. However, the total cation selectivity varied depending on the local chemical environment around the ion binding site (e.g., if different detergents or even organic solvent were used for c-ring solubilisation). A mutagenesis study with the G25A, T67G and Y70F mutants additionally underpinned different principles that underlie inherently tight Na^+ binding to *I. tartaricus* c-ring. The role of atomic composition with enthalpy-driven thermodynamic mechanism of interaction was assigned for attaining high Na^+ binding affinity by *I. tartaricus* c-ring. The Na^+ binding affinity of the wild-type and mutant c-rings was divided on the basis of the contribution (favorable negative or unfavorable positive) of enthalpy and entropy energy changes into total free energy change of a Na^+ binding reaction, into three groups:

(I) high-affinity Na^+ binding (low μM range)

(II) middle-affinity Na^+ binding (high μM range)

(III) low-affinity Na^+ binding (mM range)

To address the functional significance of residues in or near the ion binding site of the c-ring in *I. tartaricus* ATP synthase, the kinetic properties of ATP synthesis of the wild-type and a selection of mutant ATP synthases, recombinantly expressed in *E. coli* cells and purified via metal affinity chromatography, were studied by assaying ATP hydrolysis and ATP synthesis measurements. The following question was addressed: How would the substitution of residues in the ion binding site of *I. tartaricus* c-ring affect the assembly and activity of ATP synthase? ATP hydrolysis assay was used to show that mutant c-rings could assemble in functional coupled ATP synthases. Next, it was determined that depending on applied conditions, *smf, pmf* or *lmf* can drive ATP synthesis by wild-type ATP synthase reconstituted in ETLE vesicles. Most of the mutations that were introduced in or near the c-ring ion binding site (namely, G25A, Y70F, S66A, T67G, S66A/Y70F, E65D, G25S, T67M, T67Q and Q32A/Y70F) altered the inherent cation selectivity of *I. tartaricus* ATP synthase, allowing Na^+ and H^+ (but not Li^+) gradients to drive ATP synthesis. This is the presence of ionisable Asp/Glu residue in the ion binding site of the rotary c-rings that makes Na^+-motive ATP synthases additionally selective to H^+, as it is seen in both, wild-type and mutant ATP synthases studied in this work. The rates of *pmf*-driven ATP synthesis differed among mutants and correlated with differences in the pKa values of Glu65 carboxyl group in the c-ring. Higher pKa values of Glu65 in Q32A, S66A/Y70F and Q32A/Y70F mutant c-rings correlated with higher turnover numbers of *pmf*-driven ATP synthesis of the corresponding mutant ATP synthases. In general, the current mutagenesis study did not reveal mutations apart from Glu65 residue in the rotor c-ring that restrict *pmf*-driven ATP synthesis activity. From other hand, the mutagenesis study revealed a total of five mutations (E65D, G25S, T67M, T67Q and Q32A/Y70F) that restrict *smf*- and *lmf*- ATP synthesis by the *I. tartaricus* ATP synthase. Further, the K_M (Na^+) values were determined for wild-type and mutant ATP synthases using Na^+ inhibition of *pmf*-driven ATP synthesis. A hybrid *I. tartaricus* ATP synthase in which the *I. tartaricus* $Na^+/Li^+/H^+$-selective c-ring was replaced by the H^+-selective c-ring from the *S. platensis* ATP synthase was used to validate the method of K_M (Na^+) determination. The obtained hybrid ATP synthase was exclusively H^+-selective and was used to test unspecific binding of Na^+ and Li^+ to *I. tartaricus* ATP synthase. In this experiment, it was shown that at the concentrations up to 100 mM there is no binding of Na^+ or Li^+ to other subunits of ATP synthase that can inhibit *pmf*-driven ATP synthesis activity of *I. tartaricus* ATP synthase. Concerning the

Na^+ binding affinity, the wild-type K_M (Na^+) value of 1.2 mM was increased up to 20 mM for the mutants T67G and G25A. Higher K_M (Na^+) values correlated with slower turnover rates for ATP synthesis (ATPs synthesised per second per nM of protein) by S66A, Y70F, G25A, T67G, Q32A and S66A/Y70F mutant ATP synthases, driven by *smf*.

The obtained changes in Na^+ binding affinity (both, K_d and K_M values were obtained in this work) and changes in turnover rates by corresponding mutant ATP synthases driven by *smf*, were related to changes in overall enzyme catalytic *smf*-driven efficiency. Namely, the ratio of the enzyme's maximal reaction rate (V_{max}, in s^{-1}) and the Na^+ binding affinity of the c-ring (K_d, in μM) was determined [V_{max}/K_d (Na^+) parameter = K_{cat}/K_M parameter]. All mutations introduced in or near the ion binding site of *I. tartaricus* c-ring caused a decrease in $V_{max}/K_d(Na^+)$ at least by one order of magnitude relative to wild-type ATP synthases. This means that the original amino acid composition of ion-binding site in *I. tartaricus* c-ring is best adapted for reaching high efficiency of *smf*-driven ATP synthesis under tested (close to physiological) conditions.

The data obtained from the experiments that were carried out in this work indicate that c-rings are selective to H^+ as far as ionisable Glu/Asp residue is present in the ion-binding site of the c-ring. The H^+ binding affinity of the c-ring is dependent on hydrophobicity of the residues that compose the ion binding site. The factors that define the Na^+ selectivity of the c-ring are far more numerous. From those that were studied in this work, the number of polar residues that contribute hydrogen bonds to Na^+, co-coordination of Na^+ by structurally present water molecule and presence of negatively charged residue should be mentioned as very important for Na^+ liganding to the c-ring. Interactions that stabilize bound Na^+ and overall atomic composition of ion binding site that favour enthalpy-driven Na^+ binding to c-ring play major role in attending the high Na^+ binding affinity of the c-ring. For the first time, this in-depth study outlines the thermodynamic settings that underlie high Na^+ binding affinity of the c-ring and traces changes imposed by mutations. The numerous experiments with ATP synthase assembled with mutant c-rings were directed to link the changes in H^+ and Na^+ binding affinities with changes in operation of ATP synthase. The main conclusion that may be derived from this work is that the Na^+/H^+-selective ATP synthases can be converted to exclusively H^+-selective fully functional ATP synthases by substituting only 1-2 residues within its rotary c-ring ion binding sit

Zusammenfassung

Die membranintegrierten, rotierenden F-Typ ATP-Synthasen zählen zu den essentiellen Komponenten der bakteriellen Energieversorgung. Ihre Rolle im zellulären Energiehaushalt bestehtin der Synthese von ATP unter Nutzung des transmembranen, elektrischen Ionengradienten (Mitchell 1961, Duncan et al. 1995, Noji et al. 1997, Kinosita et al. 1998). Die rotierenden ATP-Synthasen werden entsprechend der Kationenselektivität,die sie unter physiologischen Bedingungen zeigen, in zwei verschiedene Klassen eingeteilt, die H^+ selektiven, sowiedie Na^+ -selektiven ATP-Synthasen. Hierbei bildet die Selektivität beider Klassen für einwertige Kationen (H^+ oder Na^+) eine essenzielle Grundlage für ihre Rolle im Energiehaushalt der bakteriellen Zellen. Jedoch gibt es nur eine begrenzte Anzahl von anaeroben Eubakterien und Archaeen, die noch einen auf Na^+- Ionen basierenden Energiehaushalt besitzen. Gut charakterisierte Beispiele für Na^+ selektive ATP-Synthasen bilden die F-Typ-Synthasen von *I. tartaricus*, *P. modestum*, sowie die V/A-Typ-Enzyme von *E. hirae* und *A. woodii*. Trotz der Unterschiede in der Kationenselektivitätder unterschiedlichen F-Typ ATP-Synthasen sind sie jedoch sowohl inihre Organisation, als auch hinsichtlich ihre Wirkungsweisen ähnlich.

Das Ziel, der im Rahmen dieser Arbeit durchgeführten Forschung, bestand in der Identifizierung der Faktoren, die sowohl die hohen Selektivität, als auch die Affinität des in der Membran-eingebetteten Rotor-C-Rings der ATP-Synthasezu Protonen (H^+) und Na^+- Ionen beeinflussen. Die Untersuchungen wurden hierbei andem c_{11}-Ring der F-Typ-ATP-Synthase aus dem anaeroben Bakterium *Ilyobacter tartaricus*durchgeführt, das hierbei als Modellsystem diente. Der untersuchte Ring zeigt unter physiologischen Bedingungen eine hohe Bindungsselektivität für Na^+ Ionen, kann jedoch unter nicht-physiologischen Bedingungen auch Li^+ und H^+ Ionen binden und zur ATP-Synthese verwenden (Neumann et al. 1998).

Die K_d- und K_M-Werte wurden verwendet, um die Na^+ -Bindungsaffinität der C-Ringe bzw. ATP-Synthasen zu quantifizieren. Über die Selektivität wurdebeschrieben, welche Kationen an die C-Ringe und ATP-Synthasen binden können (z. B. $H^+/Na^+/Li^+$, H^+/Na^+ - oder nur H^+ Ionen).Das Verhältnis der absoluten Bindungsaffinitäten zwischen zwei Kationen (z. B. K_d (Na^+)/K_d (H^+)) wurde verwendet, um die Präferenz des Enzyms für eines der Ionen zu quantifizieren. Die Faktoren, diederKationenselektivität und der Affinität des *I. tartaricus* c-Rings zugrunde liegen, wurden mit Hilfe von Mutageneseexperimenten der Aminosäuren in der Ionenbindungsstelle untersucht. Im *I. tartaricus*-c-Ring erfolgt die Na^+ Bindung an der

Grenzfläche von zwei benachbarten c-Untereinheiten des c-Rings.

An der Bindung der Na^+-Ionen sind sowohl Aminosäuren aus Helix 1 (Gln32), sowie von Helix 2 (Val63, Ser66, Thr67 und Tyr70) beteiligt, die in der Nähe, des für den Mechanismusessentiellen Glu65 liegen. Insgesamt wurden 19 verschiedene, spezifische Einzel- und Doppelmutationen in die Sequenz des *atpE*-Gens eingeführt, die für die *I. tarticus*-ATP-Synthase-c-Untereinheit kodiert. Bei den Experimenten mit dem *I. tartaricus* c-Ring (Ser66, Thr67 und Tyr70) wurden drei polare Reste der Ionenbindungsstelle durch die polaren Reste (Ser67, Ile67 oder Leu67) oder hydrophobe Reste (Ala66, Gln67 und Phe70) ersetzt, während das geladene Glu65 durch die kürzere, aber immer noch geladene Seitenkette Asp65 ausgetauscht wurde. Zur Charakterisierung der monovalenten Kationenbindung durch die Wildtyp, sowie die mutierten C-Ringe von *I.-tartaricus*, wurde ein Ansatz verwendet, der biochemische (DCCD-Ionen-Kompetitionsassay) und biophysikalische (ITC) Methoden kombiniert.

Der ATP-Synthase-Inhibitor N, N'-Dicyclohexylcarbodiimid (DCCD), der protonierte Glu/Asp-Carboxylgruppen in c-Untereinheiten kovalent modifiziert, wurde verwendet, um Unterschiede in der Na^+ und / oder H^+ Bindung an die untersuchten Wildtyp- und mutierten C-Ringe zu untersuchen, da die Stärke der Modifikation Abhängig vommolaren $[Na^+]/[H^+]$ Verhältnis ist. C-Ringe mit hoher Na^+-Bindungsaffinität waren besser gegen eine DCCD Modifikation der Glu/Asp-Carboxylgruppe geschützt. Die Ergebnisse der Experimente zeigen,dass bei den Mutanten T67G, T67S, E65D, Y70F, S66A/Y70F und Q32A der C-Ringe ein höheres anfänglichesmolares $[Na^+]/[H^+]$ Verhältnis erforderlich war um die Carboxylgruppe gegen die DCCD-Modifikation zu schützten, während im Fall der Q32A/Y70F-Mutanten-c-Ring auch bei einem sehr hohen $[Na^+]/[H^+]$ - Molverhältnis die Glu65-Carboxylgrupp nicht geschützt war. Auf Grundlage dieser Ergebnisse wurde geschlossen, dass die Mutationen Q32A/Y70F die Na^+-Bindung an den *I.-tartaricus*-Ring aufhebt, während die Mutationen T67G-, T67S, E65D, Y70F, S66A/Y70F und Q32A die Na^+-Bindungsaffinität des *I.-tartaricus*-c-Rings reduzieren. Die Änderungen des molaren Verhältnisses von $[Na^+]/[H^+]$, die erforderlich waren, um die Glu65-Carboxylgruppe gegen DCCD-Modifikation zu schützen, wurde ebenfalls mit den H^+ Bindungseigenschaften, in Form ihres pKa-Wertes, der Glu65-Carboxylgruppe korreliert (nämlich ihrem pKa-Wert).

Für die Kombination der Mutationen Q32A-, S66A/Y70F- und Q32A/Y70F des C-Rings, für die ein stark eingeschränkter Schutz (Q32A- und S66A/Y70F-Mutationen) bzw. kein Schutz durch Na^+-Ionen (Q32A/Y70F-Mutation) gegenüber der DCCD-Modifikation beobachtet werden konnte, war eine Korrelation mit höheren pKa-Werten von Glu65-Carboxylgruppe in entsprechenden C-Ringen gemessen.Woraus sich die Frage ergab, was den hohen pKa in den mutierten c-Ringen Q32A, S66A/Y70F und Q32A/Y70F bestimmt.

Diese Arbeit postuliert, dass ein hoher pKa-Wert der Glu65-Carboxylgruppe mit der hohen Hydrophobizität der Ionenbindungsstelle im C-Ring zusammenhängt. Im Allgemeinen gab eine Reihe von DCCD-Modifikationsexperimenten mit den C-Ringen einen deutlichen Hinweis auf Veränderungen sowohl der Kationenaffinität als auch der Selektivität durch die Einführung der Mutationen in den *I.-tartaricus*-c-Ring.

Im nächsten Schritt wurden isothermale titrations Kalorimetrie (ITC) Experimente durchgeführt, um exakte Änderungen in der Na^+ Bindungsaffinität der Wildtyp und der c-Ring Mutanten zu bestimmen. Im Falle des Wildtyp *I.-tartaricus*-c-Rings, der in DDM Detergenz gelöst wurde, wurde eine absolute Bindungsaffinität von Na^+ (der K_d (Na^+)) wurde zu einem theoretischen Wert von $[H^+] = 0$ extrapoliert) von ca. 7.9 µM bestimmt. Experimentell konnte gezeigt werden, dass die Na^+ Bindung an den *I.-tartaricus*-c-Ringnur mit equivalenter Affinität bei niedriger H^+-Konzentration (hohem pH) erfolgt, bei dem die Carboxylgruppe des Glu65 deprotoniert vorliegt und keine Kationen Kompetition beobachtet wird. In Bezug auf die totale Kationenselektivität (die über den $K_d(Na^+)/K_d$ (H^+) Quotient berechnet wurde) zeigt der intakte C-Ring von *I.-tartaricus*eine 637 mal höhere Selektivität für H^+ als für Na^+. Jedoch variiert die totale Kationen Bindungsaffinität in Abhängigkeit von der lokalen chemischen Umgebung der Ionenbindestelle (z.B. wenn verschiedene Detergenzien oder organische Lösungsmittel für die Solubilisierung des C-Rings verwendet wurden).

Durch Experimente mit den Mutanten G25A-, T67G und Y70F konnten zusätzlich die verschiedenen Prinzipien untermauert werden, die einer inhärent engen Na^+-Bindung an den *I. tartaricus*-c-Ring zugrunde liegen. Die Rolle der atomaren Zusammensetzung wurde im Zusammenhang mit dem enthalpie-getriebenem thermodynamischen Wirkmechanismus der Interaktion bestimmt, die für den Erhalt einer hohen Na^+-Bindungsaffinität durch den *I. tarticus* c-Ring notwendig ist. Um die funktionelle Bedeutung der Amionsäureresten in oder in der Nähe

der Ionenbindungsstelle des C-Rings der *I. tarticus* ATP-Synthaseweiter zu charakterisieren, wurdensowohl die kinetischen Eigenschaften der wildtyp ATP-Synthese, als auch die einer Auswahl von mutierten ATP-Synthasenin ATP-Hydrolyse- und ATP-Synthesemessungen bestimmt. Die hierbei verwendeten Proteinewurdenrekombinant in *E. Coli* Zellen exprimiert und über Metallaffinitätschromatographie gereinigt.

Des Weiteren wurde die Frage untersucht, wie die Substitution von Aminosäureresten in der Ionenbindungsstelle des *I. tartaricus* c-Rings den Aufbau und die Aktivität der ATP-Synthase beeinflusst. Hierfür wurde zunächst mit Hilfe des ATP-Hydrolyse-Assays gezeigt, dass sich die mutiertenc-Ringe zu funktionellen gekoppelten ATP-Synthasen assemblieren können. Im nächsten Schritt wurde gezeigt, dass die in ETLE-Vesikeln rekonstituiert Wildtyp-ATP-Synthase, in Abhängigkeit von den angewandten Bedingungen, smf, pmf or lmf zur ATP-Synthese in der Lage ist. Die Ergebnisse der Experimente mit den Mutanten zeigten, das die meisten der Mutationen, die in oder nahe der c-Ring-Ionenbindungsstelle eingeführt wurden (nämlich G25A, Y70F, S66A, T67G, S66A/Y70F, E65D, G25S, T67M, T67Q und Q32A/Y70F) einen Einfluss auf die inhärente Kationenselektivität der *I. tartaricus* ATP-Synthase, hatten, sodass die ATP- Synthese sowohl über Na^+, als auch über einen H^+ (aber nicht Li^+) Gradienten angetrieben werden konnte. Die zusätzliche H^+-Ionen Selektivität der Na^+-Ionen abhängigen ATP-Synthase wird hauptsächlich durch die Anwesenheit des ionisierbaren Asp-/Glu-Rests in der Ionenbindungsstelle des rotierenden c-Rings der ATP-Synthasenvermittelt, was im Rahmen dieser Arbeit, sowohl an der untersuchten Wildtyp-, als auch den mutierten ATP-Synthasen beobachtet werden konnte.

Die Raten der pmf-abhängigen ATP-Synthese unterschieden sich zwischen den Mutanten und korrelierten mit Unterschieden in den pKa-Werten der Glu65-Carboxylgruppe im c-Ring. Die höheren pKa-Werte von Glu65 die für die c-Ringe mit den Mutationen Q32A-, S66A/Y70F- und Q32A/Y70F gemessen werden konnten, korrelierten mit höheren Umsatzraten der pmf-gesteuerten ATP-Synthese der jeweiligen Mutanten. Im Rahmen der durchgeführten Mutagenesestudie konnten, abgesehen von der Mutation des Glu65-Rests, keine anderen Mutationenidentifiziert werden, die die pmf-abhängige ATP-Synthese eingeschränkt haben. Im Gegensatz dazu wurden im Rahmen dieser Studien insgesamt fünf Mutationen (E65D, G25S, T67M, T67Q und Q32A/Y70F) identifiziert, die sowohl die smf-, als auch die lmf-abhängige

ATP-Synthese der *I.-tarticus*-ATP-Synthase eingeschränkt haben. Des Weiteren wurden für Wildtyp- und mutierte ATP-Synthasen die K_M (Na^+) - Werte über die Na^+-Hemmung der *pmf*-getriebenen ATP-Synthese bestimmt.

In Bezug auf die Na^+-Bindungsaffinität erhöhte sich für die Mutanten T67G und G25A der $K_M(Na^+)$-Wert auf bis zu 20 mM im Vergleich zu 1.2 mM beim Wildtyp. Die höheren K_M (Na^+)-Werte korrelierten mit langsameren Umsatzraten der *smf* getriebenen ATP-Synthese (synthetisierte ATPs pro Sekunde pro nM Protein) im Fall der ATP-Synthasen mit den Mutationen S66A, Y70F, G25A, T67G, Q32A und S66A/Y70F.

Die Daten der in dieser Arbeit durchgeführten Experimente, zeigen, dass c-Ringe selektiv für H^+ sind, solange in der Ionenbindungsstelle des c-Rings ein ionisierbarer Glu/Asp-Rest vorhanden ist. Die H^+-Bindungsaffinität des c-Rings hängt von der Hydrophobizität der Reste ab, aus der die Ionenbindungsstelle aufgebaut ist.Jedoch ist die Zahl der Faktoren, die die Na^+-Selektivität des C-Rings bestimmen, weitaus größer. Von den in dieser Arbeit untersuchten Faktoren war die Zahl der polaren Reste, die Wasserstoffbrücken zu Na^+ bilden, die Co-Koordination von Na^+ durch strukturell vorhandene Wassermoleküle und die Anwesenheit von negativ geladenen Resten besonders wichtig für die Bindung der Na^+-Ionen an den Ring. Die hohe Bindungsaffinität des c-Rings für Na^+-Ionen, wird sowohl durch Wechselwirkungen begünstigt die das gebundene Na^+-Ion stabilisieren, als auch den gesamten atomaren Aufbau der Ionenbindestelle, der die enthalpiegetriebene Na^+-Bindungan den c-Ring begünstigen. Im Rahmen dieser eingehenden Studien konnten zum ersten Mal die thermodynamischen Eigenschaften aufgeklärt werden, die der hohen Na^+-Bindungsaffinität des c-Rings zugrunde liegen, sowie der Einfluss von Mutationen auf diese Parameter ermittelt werden. Durch zahlreiche Experimente mit ATP-Synthasen, die mit mutierten c-Ringen zusammengesetzt wurden, sollte eine Verbindung zwischen Veränderungen der H^+- und der Na^+-Bindungsaffinitäten und Unterschiede im Betrieb der ATP-Synthase aufgeklärt werden. Die wichtigste Schlussfolgerung, die sich aus dieser Arbeit ableiten lässt, ist, besteht darin, dass sich Na^+/H^+-selektiven ATP-Synthasen durch den Austausch von 1-2 Aminosäureresten innerhalb der rotierenden c-Ring-Ionenbindungsstelle in ausschließlich H^+-selektive, vollfunktionelle ATP-Synthasen umwandeln lassen.

Table of Contents

Abstract ……	II
Zusammenfassung ……	VII
Table of Contents ……	XII
List of Symbols and Abbreviations ……	XXI
List of Figures ……	XXV
List of Tables ……	XXXI
2. Introduction……	1
2.1. Adenosine-5´-triphosphate (ATP) and energy transduction coupled to transmembrane electrochemical gradient……..	1
2.2. Role of ATP synthases……	3
2.3. Classification of rotary ATPases……	3
2.4. Proton-motive force (*pmf*) coupled bioenergetics……	4
2.5. Sodium-motive force (*smf*) coupled bioenergetics……..	5
2.5.1. SMF in pathogens……..	7
2.5.2. SMF in methanogens…….	7
2.5.3. SMF in the fermenting, anaerobic bacterium *Ilyobacter tartarcus*…….	7
2.6. Overall organization of rotary ATP synthases…….	9
2.6.1. Structure of catalytic soluble F_1 domain……..	10
2.6.2. Rotation sub-steps of ATP synthase during catalysis……	11
2.6.3. Mechanism of rotary ATP synthase operation……..	14
2.6.4. Structure of a peripheral stalk……..	14
2.6.5. Organization of membrane F_o domain…….	15
2.6.6. Structure of the c-ring……..	15
2.6.7. Structure of the ion-binding site in the c-rings of different species……	17
2.6.8. Water molecule in the Na^+ ion-binding sites……	23
2.6.9. Designated conserved residues in Na^+-binding motif of c(K)-rings……	23
2.6.10. Structure of the a-subunit……	25
2.6.11. Ion-translocation mechanism…….	28

2.7. Implementation of mutagenesis approach to study the ion selectivity of rotary ATP synthases……	31
2.8. Isothermal titration calorimetry (ITC) and applications for cation affinity measurements ……	33
2.8.1. Principles of isothermal titration calorimetry (ITC)…….	33
2.8.2. Use of ITC technique for assessing Na^+ binding affinity and selectivity of *I. tartaricus* c-ring…….	37
2.9. Principles and application of *N,N´*-dicyclohexylcarbodiimide (DCCD) modification of ionisable residues……	40
2.10. Free energy change of deprotonation and the pKa value of carboxyl group	43
3. Aim of this work……	45
4. Materials and Methods……	47
4.1. Materials……..	47
4.2. Methods ……	48
4.2.1. Cloning of the expression vectors …….	48
4.2.1.1. Recombinant DNA techniques ……..	48
4.2.1.2. Characteristic of pt7cIT and pITtr5Hisa vector plasmids used to clone mutants of *I. tartaricus* c-ring……	48
4.2.1.3. Genetic manipulations with pt7cIT and pltTr5Hisa vector plasmids…….	50
4.2.1.4. PCR amplification of pt7cIT plasmid……	51
4.2.1.5. PCR amplification of DNA fragments from pltTr5Hisa plasmid	52
4.2.1.6. Restriction digest and ligation of PCR amplified DNA fragments and pITtr5Hisa vector plasmid…….	53 54
4.2.1.7. *Xba*I test restriction of cloned pt7cIT plasmid……..	54
4.2.1.8. *Hind*III/*Sal*I test restriction of cloned pItTr5Hisa plasmid….:..	54
4.2.1.9. Transformation of the *E. coli* DK8 competent cells…….	55

4.2.1.10. Transformation of the *E. coli* BL21 competent cells……..	55
4.2.1.11. Preparation of the glycerol stocks……	56
4.2.1.12. Obtained constructs for the mutants of *I. tartaricus* c-ring….	56
4.2.2. *E. coli* recombinant protein expression by auto-induction……..	56
4.2.2.1. Strains used for protein expression……	56
4.2.2.2. Recombinant expression of the protein…….	57
4.2.2.3. Expression of γ_{His}/ε complex ……	59
4.2.3. Extraction and purification of wild-type and mutant forms of ATP synthase from *E. coli* DK8 pItTr5Hisa cells……	59
4.2.4. Different approaches for extraction and purification of *I. tartaricus* wild-type and mutant c-rings ……..	61
4.2.5. Extraction of *I. tartaricus*γ_{His}/ε complex from *E. coli* BL21 (DE3) cells	63
4.2.6. Isothermal titration calorimetry (ITC) measurements……..	64
4.2.6.1. Preparation of solutions and handling……	64
4.2.6.2. Refining the Na^+ baseline level in the protein samples…….	64
4.2.6.3. Equilibration of the protein samples for ITC measurements…	64
4.2.6.4. ITC experiment setup for measuring Na^+ and Li^+ binding to *I. tartaricus* wild-type and mutant c-rings……	66
4.2.6.5. Evaluation of the ITC data……..	67
4.2.6.6. Evaluation and subtraction of heats from Glu65 deprotonation mediated by Na^+ and Li^+ binding to *I. tartaricus* wild-type and mutant c-rings…….	68
4.2.6.8. Statistical analysis of the data……	69
4.2.7. Mass spectrometry-based measurements……	70
4.2.7.1. Mass spectrometry-based determination of the c-subunits masses from *I. tartaricus* c-ring mutants…….	70
4.2.7.2. Measuring the kinetic of Glu65 modification by DCCD in detergent solution…….	70
4.2.7.3. Measuring the kinetic of Glu65 modification by DCCD in	

lipids……	71
4.2.7.4. Chloroform/methanol extraction of the c-subunits for mass-spectrometry analysis……	71
4.2.7.5. DCCD modification of Glu65 in wild-type and mutant c-rings under different pH and salt conditions…….	72
4.2.7.6. DCCD profile-based evaluation of the pKa values for Glu65 residue……..	72
4.2.7.7. Specific rates of DCCD modification of Glu65 residue……	73
4.2.8. Measurements of functional activity of *I. tartaricus* wild-type and mutant ATP synthases……..	73
4.2.8.1. Preparation of lipids……	73
4.2.8.2. Reconstitution of recombinant wild-type and mutant ATP synthases in pre-formed lipid vesicles……..	74
4.2.8.3. Real-time measurements of *smf*-driven ATP synthesis ……	74
4.2.8.4. Real-time measurements of *lmf*-driven ATP synthesis……	76
4.2.8.5. Real-time measurements of *pmf*-driven ATP synthesis……	77
4.2.8.6. Na^+ inhibition of *pmf*-driven ATP synthesis……..	77
4.2.8.7. Estimation of the Hill plot coefficient and Linewear-Burk transformation of the data……..	78
4.2.8.8. Evaluation of B_{max} (Na^+) values. Fitting data to one-site binding equation……	78
4.2.8.9. Evaluation of protein concentration in proteoliposomes……	79
4.2.8.10. Evaluation of the efficiencies (V_{max}/K_d) of *smf*-driven ATP synthesis by lipid-reconstituted ATP synthases……..…	79
4.2.8.11. Statistics and data analysis…….	79
4.2.9. 3D crystallization of selected c-ring mutants……	80
5. Results…….	81
5.1. Oligomeric state, SDS-stability and rotor reassembly properties of *I. tartaricus*	

c-ring mutants …….	81
5.1.1. In-gel electrophoretic mobility and (SDS-)stability of *I. tartaricus* wild-type and mutant c-rings……..	82
5.1.2. Assembly and co-elution of the rotor complex from *I. tartaricus* mutant c-rings and γ_{His}/ε subunits……..	84
5.2. DCCD modification assay with *I. tartaricus* wild-type and mutant c-rings…	87
5.2.1. Identification of mutant c-subunits and determination of their molecular masses by mass spectroscopy……..	88
5.2.2. Rates of Glu65 modification by DCCD in wild-type and mutant *I. tartaricus* c-rings……..	91
5.2.3. pH-dependent rates of Glu65 modification by DCCD in the wild-type and mutant c-rings…….	93
5.2.4. pH of the maximal rateof Na^+ protection of Glu65 carboxyl group against DCCD modification in the wild-type and mutant *I. tartaricus* c-rings….	94
5.2.5. Low Na^+ protection of Glu65 against DCCD modification in the S66A/Y70F mutant c-ring …….	95
5.2.6. DCCD modification of Glu65 in Q32A/Y70F mutant c-ring in1,2-dimyristoyl-*sn*-glycero-3-phosphocholine (DMPC) lipids……	97
5.2.7. Summary of DCCD modification experiments…….	98
5.3. Isothermal titration calorimetry (ITC) measurements of cation selectivity of *I. tartaricus* wild-type and mutant c-rings ……	100
5.3.1. Insights into measuring Na^+ binding affinity of *I. tartaricus* wild-type c-ring with ITC…….	100
5.3.1.1. Initial tests, detection of cation binding to *I. tartaricus* wild-type c-ring……	100
5.3.1.2. Relative constants for Na^+ binding. Competitive mode of Na^+/H^+ binding to *I. tartaricus* wild-type c-ring……..	102
5.3.1.3. Total binding selectivity and absolute constants for Na^+ and H^+ binding to *I. tartaricus* wild-type c-ring……	104

5.3.1.4. Effect of different detergents and DMSO on Na^+ binding to *I. tartaricus* wild-type c-ring…….	107
5.3.1.5. Effect of the detergent concentration on Na^+ binding to *I. tartaricus* wild-type c-ring…….	110
5.3.1.6. Contribution of Glu65 carboxyl group deprotonation to observed enthalpies of Na^+ binding……	111
5.3.1.7. Thermodynamics of Li^+ binding to *I. tartaricus*wild-type c-ring	114
5.3.1.8. Comparing the thermodynamic signatures of Na^+ and Li^+ binding to *I. tartaricus* wild-type c-ring……	119
5.3.2. Effect of mutations on apparent Na^+bindingaffinity of *I. tartaricus* c-ring	120
5.3.3. Evaluation of protonation states for Glu65 carboxyl groups in mutant c-rings……	125
5.3.4. Differences in thermodynamic settings of Na^+ binding to mutant c-rings	126
5.3.5. Grouping of the *I. tartaricus*c-ring mutants depending on the thermodynamic signature of Na^+ binding …….	127
5.3.6. Estimation of the pKa values for Glu65 by combining ITC and DCCD data……	128
5.3.7. Summary of ITC experiments……..	131
5.4. Functional characterization of wild-type and mutant forms of *I. tartaricus* ATP synthase ……	132
5.4.1. Functional insights into cation-coupled ATP synthesis of *I. tartaricus* ATP synthase……..	132
5.4.1.1. Heterologous expression and purification of *I. tartaricus* wild-type ATP-synthase ……..	132
5.4.1.2. Cation selectivity of *I. tartaricus* wild-type ATP synthase and kinetic of ATP synthesis depending on applied ion-driving force…….	133
5.4.1.3. Requirements of *I. tartaricus* wild-type ATP synthase for *pmf*-driven ATP synthesis……..	135
5.4.1.4. Requirements of *I. tartaricus* wild-type ATP synthase in	

membrane potential ($\Delta\psi$) for ATP synthesis…… 139

5.4.1.5. The*pmf*-driven ATP synthesis of hybrid *I. tartaricus* ATP synthase harboring the H^+-selective*Spirulina platensis* c-ring…… 142

5.4.2. Heterologous expression and purification of *I. tartaricus* ATP synthase with mutations in the c-ring……. 147

5.4.3. Coupled ATP hydrolysis activity of wild-type and mutant forms of *I. tartaricus* ATP synthase…….. 149

5.4.4. Incorporation of *I. tartaricus* wild-type and mutant ATP synthases in lipid vesicles: The ATP hydrolysis activity in reconstituted ATP synthases is enhanced…….. 151

5.4.5. Characterization of the cation selectivity by lipid-reconstituted *I. tartaricus* mutant ATP synthases……. 154

5.4.6. Effect of Na^+ on *pmf*-driven ATP synthesis of *I. tartaricus* wild-type and mutant ATP synthases…….. 156

5.4.7. Estimation of K_M values for Na^+ binding to *I. tartaricus* wild-type and mutant ATP synthases…….. 159

5.4.8. Maximal Na^+ occupancy of ion binding sites in *I. tartaricus* wild-type and mutant ATP synthases…….. 160

5.4.9. Verification of the binding model describing Na^+ binding to *I. tartaricus* wild-type and mutant ATP synthases……. 162

5.4.10. Verification of cooperativity in Na^+ binding to *I. tartaricus* wild-type and mutant ATP synthases…… 163

5.4.11. Li^+-inhibition of *pmf*-driven ATP synthesis by *I. tartaricus* wild-type and mutant ATP synthases…… 165

5.4.12. Effect of mutations on initial rates (V_i) of cation-driven ATP synthesis 167

5.4.13. Efficiency of *smf*-driven ATP synthesis, V_{max}/K_d parameter……. 169

5.4.14. Summary of functional studies…….. 172

5.5. 3D crystallization of Q32A/Y70F mutant c-ring…… 173

5.5.1. Extraction and 3D crystallization of Q32A/Y70F mutant c-ring…….	175
5.5.2. Electroelution of Q32A/Y70F mutant c-ring from SDS-PAGE and its 3D crystallization……..	177
5.6. Summary of all obtained results…….	181
6. Discussion……	184
6.1. The pKa values of ionisable chemical groups in proteins …….	184
6.1.1. The pKa values of Glu/Asp carboxyl groups in the ion-binding site of the c-rings……..	187
6.1.2. High pKa of Glu65 carboxyl group in *I. tartaricus* wild-type c-ring …..	191
6.1.3. Functional implication of high pKa values of the Glu/Asp in *I. tartaricus* mutant ATP synthases……..	193
6.1.4. Factors that determine high pKa and H^+ selectivity of Glu/Asp residue in the c-rings…….	196
6.2. Principles that underlie high Na^+ binding affinity and selectivity of the proteins ……..	197
6.2.1. Determined Na^+ binding affinity and selectivity of *I. tartaricus* wild-type c-ring…….	199
6.2.2. Effect of microenvironment on Na^+ binding to *I. tartaricus* wild-type c-ring ……..	200
6.2.3. Thermodynamic principles that underlie Na^+ binding affinity and selectivity of *I. tartaricus* wild-type and mutant c-rings ……	203
6.2.4. Match of the size of the ion-binding site……	210
6.2.5. Importance of water molecule in the ion binding site of c-ring (T67M and T67Q mutations) …….	210
6.2.6. Importance of the negatively charged carboxylic group for Na^+ transport by rotary ATPases (E65D mutation)……	212
6.3. Comparison of K_d (Na^+) and K_M (Na^+) values obtained for *I. tartaricus* c-ring and ATP synthase…….	218

6.4. Summary and outlook……	219
7. Appendix ……	220
8. Acknowledgements……...	228
9. Curriculum Vitae……..	229
10. References……	230

List of Symbols and Abbreviations

°C	degrees Celsius
3D	three dimensional
Å	Angstrom(s)
M	micro
AAS	atomic absorption spectroscopy
ADP	adenosine-5´-diphosphate
AMP-PNP	adenylyn imidodiphosphate
ATP	adenosine-5´-triphosphate
B_{max}	maximal occupancy
Bp	base-pairs
Cal	calorie
CCCP	carbonylcyanide m-chlorophenylhydrazone
CDI	carbodiimides
CHES	2-(cyclohexylamino)ethanesulfonic acid
Cmc	critical micellar concentration
DCCD	*N,N´*-dicyclohexylcarbodiimide
DCOU	dicyclohexyl-O-acylurea
DCNU	dicyclohexyl-N-acylurea
DDM	dodecyl-β-D-maltopyranoside
DHAP	2,5-dihydroxyacetophenone
DHB	2,5-dihydroxybenzoic acid
DMPC	1,2-dimyristoyl-*sn*-glycero-3-phosphocholine
DMSO	dimethyl sulfoxide
DNA	deoxyribonucleic acid
DTT	dithiothreitol
E. coli	*Escherichia coli*
EDTA	ethylenediaminetetraacetic acid
EPL	*E. coli* polar lipids

et al	*et alia*
ETLE	*E. coli* total lipid extract
G	G-force
H	cooperativity
HEPES	4-(2-hydroxyethyl)piperazine-1-ethanesulfonic acid
H/S	enthalpy/entropy compensation
ICG	ionisable chemical group
I. tartaricus	*Ilyobacter tartaricus*
IPTG	isopropyl β-D-1-thiogalactopyranoside
ITC	isothermal titration calorimetry
K	Kelvin
K_d	dissociation constant
K_M	Michaelis constant
kDa	kilo Dalton
LB	Luria Bertani
Lmf	lithium-motive force
L	liter
LPMOs	lytic polysaccharide mono-oxygenase
LPR	lipid-to-protein ratio
LS	N-lauryl sarcosine
M	Moles per liter
M	milli
MALDI-MS	matrix assisted laser desorption/ionization mass spectrometry
Mbh	membrane-bound Na^+/H^+ antiporter modules containing hydrogenase
MES	2-(N-morpholino)ethanesulfonic acid
Min	minute
MOPS	3-(N-morpholino)propanesulfonic acid
MS	mass spectrometry

MTR	Na^+-translocating coenzyme M methylase
mQ	MilliPore
MR	molar ratio
mV	millivolts
m/z ratio	mass-to-charge ratio
N	stoichiometry
NaR	Na^+-translocating rhodopsin
NTA	nitrilotriacetic acid
NQR	Na^+-translocating NADH:ubiquinone oxidoreductase
OADC	Na^+-translocating oxaloacetate decarboxylase
OD	optical density
OG	octyl β-D-glucopyranoside
PCR	ploymerase chain reaction
PEG	polyethylen glycol
P_i	inorganic phosphate
pKa	acid dissociation constant
Pmf	proton-motive force
Psi	pound-force per square inch
PVDF	polyvinylidene difluoride
Q	phosphate potential
RNF	Na^+-translocating ferredoxin:NAD^+ oxidoreductase
Rpm	rotations per minute
RT	room temperature
S. platensis	*Spirulina platensis*
SDS	sodium dodecyl sulfate
S/H	entropy/enthalpy compensation
PAGE	polyacrylamide gel electrophoresis
S.E.	standard error
Sec	second

smf	sodium-motive force
T	temperature
TCA	trichloroacetate
TMAOH	tetramethylammonium hydroxide
Tris	2-amino-2-(hydroxymethyl)-1,3-propanediol
Tricine	N-[Tris(hydroxymethyl)methyl]glycine
$\mathbf{V_{max}}$	maximal velocity
U	unit
UV	ultraviolet
V	volt
v/v	volume per volume
w/w	weight per weight
w/v	weight per volume
$\mathbf{\Delta C_p}$	heat capacity
ΔH	enthalpy change
$\mathbf{\Delta H_{obs}}$	observed enthalpy change
$\mathbf{\Delta H_{binding}}$	enthalpy change of binding
$\mathbf{\Delta H_{ion}}$	ionization enthalpy
ΔG	free energy change
-TΔS	entropy change
Δψ	membrane potential
Δμ	electrochemical gradient

List of Figures

Figure 2-1: Visual characteristic and taxonomic assignment of I. tartaricus……..	8
Figure 2-2: Schematic illustration of organization of bacterial rotary ATP synthases	9
Figure 2-3: Structure of catalytic F_1 domain from bovine……..	11
Fig. 2-4: Rotation scheme and arrangement of the α- and β-subunits of the bacterial F_1-ATPase for the 360° rotation of the γ-subunit……	13
Figure 2-5: The binding change mechanism of the F_1 ATPase……	14
Figure 2-6: Overall structure of I. tartaricus c-ring……	16
Figure 2-7: 2.35 Å resolution structure of Na^+ ion-binding site in I. tartaricus c-ring…	18
Figure 2-8: 2.2 Å resolution structure of F. nucleatum Na^+ ion-binding site.……	19
Figure 2-9: 2.1 Å resolution structures of Na^+ ion–binding site in the c-ring from hybrid F/V-type ATPases of A. woodii……	20
Figure 2-10: 2.1 Å resolution structure of Na^+ ion-binding site in bacterial V-type c-ring from E. hirae……	21
Figure 2-11: 2.1 Å crystal structure of the H^+-binding site in S. platensis c-ring……	22
Figure 2-12: 2.5 Å structure of H^+-binding site in Bacillus pseudofirmus OF4 c-ring….	22
Figure 2-13: Na^+ and H^+-binding signatures in the sequence of the c(K)-subunits from rotary ATP synthase……	24
Figure 2-14: Arrangement of helices in a-subunit dedicated from cryo-EM structures	27
Figure 2-15: 6.9 Å cryo-EM structure of V_o domain from S. cerevisiae V-ATPase……	28
Figure 2-16: 6.4 Å cryo-EM structure of a-subunit from bovine mitochondrial ATP synthase……..	28
Figure 2-17: Two-half channel model and principles of ion-translocation mechanism	
Figure 2-18: H^+ translocation through F-type ATP synthases……..	29
Figure 2-19: Difference in DCCD modification profiles of I. tartaricus ATP synthase harbouring wild-type and mutant c-rings……	30
Figure 2-20: Schematic illustration of working principles of isothermal titration calorimetry (ITC)……	33
Figure 2-21: ITC measurements of Na^+ binding to natively produced I. tartaricus wild-type c-ring……	38

Figure 2-22: Extrapolation of absolute binding constants for Na^+ and H^+ binding to the I. tartaricus wild-type c-ring……	39
Figure 2-23: Principles of carbodiimides modification……	41
Figure 4-1: pt7cIT vector plasmid……	49
Figure 4-2: pITtr5Hisa vector plasmid……	50
Figure 5-1: Representative SDS-PAGE of I. tartaricus mutant c-rings extracted directly from host E. coli membranes……	83
Figure 5-2: Co-elution of wild-type and mutant c-rings with I. tartaricus γ_{His}/ε rotor subunits from Ni-NTA resin……	85
Figure 5-3: SDS-PAGE of (SDS-)unstable and (SDS-)stable c-rings of I. tartaricus with mutation……	87
Figure 5-4: Representative MALDI-MS spectra of I. tartaricus c-subunit with Q32A/Y70F mutation……	89
Figure 5-5: Representative DCCD modification of Glu65 carboxyl group in I. tartaricus wild-type c-subunit detected by MALDI-MS……	90
Figure 5-6: Na^+ protection of Glu65 in S66A/Y70F c-ring mutant against DCCD modification under various $[Na^+]/[H^+]$ ratios……	96
Figure 5-7: Na^+-unprotected DCCD modification of Glu65 in Q32A/Y70F mutant c-ring in DMPC lipids……	97
Figure 5-8: Detecting cation binding to I. tartaricus wild-type c-ring……	102
Figure 5-9: pH-dependent, apparent Na^+-binding affinities of I. tartaricus wild-type c-ring……	103
Figure 5-10: Estimation of the absolute Na^+ and H^+ binding affinities for I. tartaricus wild-type c-ring……	105
Figure 5-11: Estimation of total Na^+/H^+ binding-selectivity of I. tartaricus wild-type c-ring……	106
Figure 5-12: Effect of microenvironment on thermodynamic settings of Na^+ binding to I. tartaricus wild-type c-ring at pH 5.4……	109
Figure 5-13: Effect of detergent-to-protein ratios (DPR) on Na^+ binding to I. tartaricus	

wild-type c-ring in 10 mM HEPES pH 7.2……	110
Figure 5-14: Effect of buffers with different heats of ionization on observed enthalpies upon Na^+ binding to I. tartaricus wild-type c-ring……	112
Figure 5-15: Evaluation of contribution from deprotonation of Glu65 to observed enthalpies upon Na^+ binding……	113
Figure 5-16: Thermodynamic signature (ΔG, ΔH and $-T\Delta S$) of Na^+ binding to I. tartaricus wild-type c-ring at pH 7.5……	114
Figure 5-17: Effect of detergent on Li^+ binding to I. tartaricus wild-type c-ring recombinantly produced in E. coli DK8 cells……	115
Figure 5-18: Effect of detergent on Li^+ binding to wild-type c-ring natively produced in I. tartaricus cells……	116
Figure 5-19: Effect of buffers with different heats of ionization on observed enthalpies upon Li^+ binding at pH 7.5……	117
Figure 5-20: Dissection of the heats of Li^+-mediated deprotonation of Glu65 from overall observed enthalpies upon Li^+ binding……	118
Figure 5-21: Energy profile of Li^+ binding to I. tartaricus wild-type c-ring……	119
Figure 5-22: Comparison of energy profiles for Na^+ and Li^+ binding to I. tartaricus wild-type c-ring at pH 7.5……	120
Figure 5-23: Representative thermograms of Na^+ binding to wild-type and mutant forms of I. tartaricus c-ring at pH 7.5……	121
Figure 5-24: Titration of Q32A and S66A/Y70F mutant c-rings with different concentrations of NaCl……	124
Figure 5-25: Titration of Q32A/Y70F mutant c-ring with different concentrations of NaCl……	125
Figure 5-26: Different thermodynamic settings of Na^+ binding to I. tartaricus c-ring depending on chemical oscillation of the ion-binding site……	127
Figure 5-27: Representative SDS-PAGE of purified I. tartaricus wild-type ATP synthase heterologously expressed in E. coli DK8 cells……	133
Figure 5-28: ATP synthesis of I. tartaricus wild-type ATP synthase driven by different	

ion-motive forces……	135
Figure 5-29: ATP synthesis by H^+-selective.E. coli wild-type ATP synthase……	139
Figure 5-30: Requirements of I. tartaricus wild-type ATP synthase in Δψ for lmf-driven ATP synthesis……	140
Figure 5-31: Requirements of I. tartaricus wild-type ATP synthase for ATP synthesis depending on applied ion-motive force……	141
Figure 5-32: SDS-PAGE of a hybrid H^+-selective S. platensis c-ring/I. tartaricus ATP synthase……	143
Figure 5-33: MALDI-MS spectra of extracted c-subunits of S. platensis c-ring produced recombinantly in E. coli DK8 cells as a part of I. tartaricus hybrid ATP synthase……	144
Figure 5-34: NaCl- and LiCl-mediated unspecific inhibition of pmf-driven ATP synthesis of hybrid S. platensis/I. tartaricus ATP synthase……	146
Figure 5-35: Comparative SDS-PAGE of extracted wild-type and mutant ATP synthases expressed recombinantly in E. coli DK8 cells……	148
Figure 5-36: Representative freeze fracture electron microscopy of I. tartaricus wild-type and mutant ATP synthases incorporated in pre-formed lipid vesicles composed of ETLE……	152
Figure 5-37: Verification of smf-driven ATP synthesis activity of I. tartaricus wild-type and mutant ATP synthases reconstituted in lipids……	155
Figure 5-38: Na^+-inhibition of pmf-driven ATP synthesis of I. tartaricus wild-type and mutant ATP synthases……	158
Figure 5-39: Lineweaver–Burk plots for Na^+ binding to the c-rings in the wild-type and mutant ATP synthases……	159
Figure 5-40: Comparison of the kinetic equilibrium constants K_M (Na^+) and B_{max} (Na^+) for the ATP synthases with wild-type and mutant c-rings……	161
Figure 5-41: Patterns of Na^+-dependent inhibition of pmf-driven ATP synthesis fitted to one-site binding model……	163
Figure 5-42: Estimation of cooperativeness of Na^+ binding to I. tartarcius ATP	

synthase containing wild-type and mutant c-rings……	164
Figure 5-43: Unspecific Li^+-inhibition of pmf-driven ATP synthesis of I. tartaricus wild-type ATP synthase……	166
Figure 5-44: pmf-driven ATP synthesis of mutant ATP synthases at high LiCl concentration……	167
Figure 5-45: Relative changes in efficiencies of smf-driven ATP synthesis by mutant ATP synthases……	171
Figure 5-46: Q32A/Y70F mutant c-ring purified by two different approaches……	174
Figure 5-47: Refining sample for further crystallization……	175
Figure 5-48: Crystals of Q32A/Y70F mutant c-ring……	176
Figure 5-49: Example of diffraction pattern for one of the obtained crystal forms of Q32A/Y70F mutant c-ring……	177
Figure 5-50: Electroelution of Q32A/Y70F c-ring from SDS-PAGE stained with Coomassie brilliant blue R-250 dye……	178
Figure 5-51: Electroelution of Q32A/Y70F c-ring from SDS-PAGE negatively stained with $CuCl_2$……	179
Figure 5-52. Electroeluted and prepared for crystallization probable c_{12}-oligomer of Q32A/Y70F mutant……	180
Figure 6-1: Multiple sequence alignment of c(K)-subunits from different species……	187
Figure 6-2: Examples of indirect assays used for estimation of pKa values for ionisable Glu/Asp residues in the c-rings/ATP synthases from different species……	189
Figure 6-3: pKa of Glu65 carboxyl group in I. tartaricus wild-type and mutant c-rings and its effect on rates of pmf-driven ATP synthesis……	195
Figure 6-4: Effect of detergent on energetics of melibiose binding by $MelB_{St}$……	203
Figure 6-5: Differences in free energy change of Na^+ binding ($\Delta\Delta G$) between I. tartaricus wild-type and mutant c-rings……	204
Figure 6-6: Effect of Y70F (polar-to-hydrophobic) mutation……	207
Figure 6-7: Effect of T67G (polar-to-hydrophobic) mutation……	209
Figure 6-8: Effect of E65D (charge-to-charge) mutation……	213

Figure 6-9: Na^+ coordination involving negative charge in different transporters……..	216
Figure 7-1: Sequence alignment of I. tartaricus and S. platensis wild-type c-subunits and I. tartaricus c-subunits with mutations……	220
Figure 7-2: pH-dependent and Na^+-protected DCCD modification of the wild-type c-ring……	221
Figure 7-3: pH-dependent DCCD-modification of Q32A mutant……	222
Figure 7-4: pH-dependent and Na^+-protected DCCD modification of T67G mutant…….	223
Figure 7-5: pH-dependent and Na^+-protected DCCD modification of S66A/Y70F mutant……	224
Figure 7-6: pH-dependent DCCD-modification of Q32A/Y70F mutant……..	225
Figure 7-7: pH-dependent and Na^+-protected DCCD modification of Y70F mutant……	226
Figure 7-8: pH-dependent and Na^+-protected DCCD modification of T67S mutan……	227

List of Tables

Table 2-1: Classes of primary Na^+ pumps that perform Na^+ extrusion in bacteria and archaea	6
Table 4-1: Modifications of pITtr5Hisa plasmi	49
Table 4-2: List of mutagenic primers used for site-directed mutagenesis	51
Table 4-3: PCR amplification of pt7cIT plasmid	52
Table 4-4: PCR amplification of DNA fragments from pltTr5Hisa plasmid	52
Table 4-5: Sequencing primers for atp operon of I. tartaricus ATP synthase	55
Table 4-6: List of cloned constructs	56
Table 4-7: List of E. coli strains used for protein overexpression	57
Table 4-8: Composition of 1x ZY auto-induction medium	58
Table 4-9: Composition of Buffers used for protein extraction	60
Table 4-10: Composition of buffers used for c-ring extraction	63
Table 4-11: Characteristic of the solutions implemented in ITC measurements	65
Table 4-12: Parameters of the MicroCal machine used in ITC measurements	67
Table 4-13: Buffers used for reconstitution of mutant ATPases	74
Table 5-1: Summarizing table: Characteristic properties of I. tartaricus mutant c-rings	86
Table 5-2: Molecular masses of the explored c-subunits determined by MALDI-MS	88
Table 5-3: Specific rates of Glu65 modification by DCCD in wild-type and mutant c-rings	92
Table 5-4: pH properties of Glu65 modification by DCCD	94
Table 5-5: Na^+ protection of Glu65 carboxyl group against DCCD modification	95
Table 5-6: Grouping of I. tartaricus wild-type and mutant c-rings according to characteristic parameters of Glu65 modification by DCCD	98
Table 5-7: Effect of themicroenvironmenton apparent K_d (Na^+) values	107
Table 5-8: Mutant specific differences in Na^+-binding affinities and ΔG (Na^+) values	122
Table 5-9: Molar excess of Na^+ over H^+ required to promote Na^+ binding to mutant c-rings at pH 7.5	123
Table 5-10: Protonation state of Glu65 carboxyl group at pH 7.5 depending on mutation	126

Table 5-11: Grouping of c-ring mutants depending on ITC data……	128
Table 5-12: Estimated apparent pKa values ϕmɵdeprotonation energies for Glu65 in wild-type and mutant c-rings……	130
Table 5-13: Ion-motive forces tested for generation of ATP synthesis by I. tartaricus ATP synthase……	134
Table 5-14: Optimization of conditions for pmf-driven ATP synthesis by I. tartaricus wild-type ATP synthase.……	137
Table 5-15: Specific ATP hydrolysis activity of I. tartaricus wild-type and mutant ATP synthases……	150
Table 5-16: Rates of specific ATP hydrolysis activity of I. tartaricus wild-type and mutant ATP synthases incorporated in vesicles……	153
Table 5-17: Coupling of ATP synthesis to different monovalent cations by wild-type and mutant forms of I. tartaricus ATP synthase……	156
Table 5-18: Initial and maximal velocities of ATP synthesis driven by different monovalent cation-motive forces……	168
Table 6-1: The extreme pKa values of Asp and Glu residues reported for folded proteins	185
Table 6-2: Estimates of pKa values of ionisable Glu/Asp residues in the c-rings/c-subunits/ATP synthases of different species in respect to their ion-binding selectivity…	190
Table 6-3: Na^+ binding affinity and ion selectivity of the c-rings of different species……	199
Table 6-4: Na^+ and Li^+ binding to I. tartaricus wild-type c-ring in different microenvironments……	200
Table 6-5: Effect of T67M and T67Q mutations on activity of I. tartaricus ATP synthase	211

2. Introduction

2.1. Adenosine-5´-triphosphate (ATP) and energy transduction coupled to transmembrane electrochemical gradient

Adenosine-5´-triphosphate (ATP) is the universal energy currency in cellular processes and the driver of many biochemical reactions. Therefore, the production of ATP is a chemical reaction of major importance in living organisms. The biochemical standard free energy (ΔG) of ATP hydrolysis to adenosine-5´-diphosphate (ADP) and inorganic phosphate (P_i) is -30-60 kJ/mol depending on reaction conditions (e.g., solvent, salt and pH conditions) (Rosing and Slater 1972, Junge et al. 2001, Alberty 2003).

$$\mathbf{ATP + H_2O \rightarrow ADP + P_i + \Delta G\ (30\text{-}60\ kJ/mol)}$$

The energy stored in the phosphate bond of ATP can be used for a variety of biochemical reactions to fill any energy need of the cell such as movements of cytoskeletal motor proteins fuelled by ATP hydrolysis (myosins, dyneins and kinesins) (Kull 2000, Schliwa and Woehlke 2003), muscle contraction (myosin, actin) (Lymn and Taylor 1971, Espindola et al. 1992), phosphorylation-dephosphorylation of proteins (protein kinases) (Krebs and Fischer 1955, Roskoski 2015), protein folding (chaperons) (Gething and Sambrook 1992, Buchner 1996), building and maintenance of ion gradients (ATP synthases), synthesis of new proteins etc. From this point of view, production of ATP is substantial process for all domains of life. For living systems, there are two ways to conserve energy in the form of ATP: chemiosmotic coupling via membrane-integral ATP synthases and substrate-level phosphorylation (Mitchell 1961, Gottschalk and Thauer 2001).

Most of ATP is synthesized during operation of ATP synthases (Junge 2013) by utilizing energy via oxidative- or photophosphorylation in energy-transforming membranes of mitochondria, chloroplasts, and bacteria. Already in early 60s Peter Mitchell proposed membrane-integrated ATP synthases to play the important bioenergetic role in coupling of membrane electrochemical potential and synthesis (or hydrolysis) of ATP (Chemiosmotic Theory, (Mitchell 1961)). In 1966 first evidence for chemiosmotic theory was obtained by Jagendorf and Uribe (Jagendorf and

Uribe 1966), which demonstrated ATP formation by spinach chloroplasts due to acid-base transition.

The two components that constitute the transmembrane electrochemical potential (Δμ) are the concentration ion gradient (gradient of H^+ or Na^+) and electrical potential (Δψ). The electrochemical gradient of protons, proton-motive force (*pmf*, expressed in mV) can be written as:

$$\Delta\mu_{H+} (pmf) = F\Delta\psi - 2.3RT\Delta pH$$

Where F is the Faraday constant, R is the gas constant and ΔpH is the difference in H^+ concentration across the membrane. For the room temperature, RT (25°C), the equation can be rewritten as:

$$\Delta\mu_{H+} (pmf) = \Delta\psi - 59\Delta pH$$

The effect of 1pH unit difference between cytoplasm and external medium corresponds to 59 mV at 25°C. The resulting *pmf* is negative for most of the organisms (Konings et al. 2002).

The formula of the electrochemical gradient of Na^+, sodium-motive force (*smf*, expressed in mV) is:

$$\Delta\mu_{Na+} (smf) = \Delta\psi + 2.3RT/F*\log[Na^+_{in}]/[Na^+_{out}]$$

Ion gradients play an important role in energy storage and the use of ion gradients across membranes for energy conservation is a universal principle for all living cells. H^+ and Na^+ are the only used coupling ions in energy transduction in the domains of life from Bacteria and Eukarya. Two important cation (H^+ or Na^+)-linked energy processes are the synthesis of ATP by ATP synthases and active transport by secondary active transporters.

2.2. Role of ATP synthases

The bioenergetic role of membrane-integrated ATP synthases is energy conversion via coupling of membrane electrochemical potential of H^+ or Na^+ to synthesis (or hydrolysis) of ATP by rotary operation of F_1F_o ATP synthase (Mitchell 1961, Duncan et al. 1995, Noji et al. 1997, Kinosita et al. 1998). Energy-conserving rotary ATP synthases are ubiquitous to all three domains of life (Bacteria, Archaea and Eukarya) and are found in the bacterial plasma membrane, in the thylakoid membrane of chloroplasts and in the inner mitochondrial membrane. Rotary ATP synthases catalyze ATP synthesis at the expense of the transmembrane electrical ion gradient according to equation:

$$\mathbf{ADP + P_i + \mathit{n}\ ions_{out} \leftrightarrow ATP + \mathit{n}\ ions_{in}}$$

ATP synthases enable ATP synthesis reaction to occur away from equilibrium under cellular conditions that favor the ATP hydrolysis reaction by a factor of 2×10^5 (Nam et al. 2014). However, ATP synthases are capable of both, consuming and generating an ion gradient. In ATP synthesis direction, ATP synthases use the energy stored in electrochemical gradient to synthesize ATP. In the reverse direction, ATP synthases act as ATP-driven ion pumps to build up the ion gradient across the membrane. The primary function of the proton-motive force acting on F_1F_o-ATP synthase is to provide the torque required to rotate the γ-subunit in the direction for ATP synthesis (Itoh et al. 2004, Walker 2013).

2.3. Classification of rotary ATPases

ATP synthases are evolutionally related complexes and are classified by their origin, function and number of peripheral stalks in the complex into F-, A- and V-type ATPases (Cross and Muller 2004, Lee et al. 2010). While F- and A-type ATP synthases are rotary ATP synthesizing enzymes, the V-type ATPases are ATP-driven proton pumps that do not synthesize ATP (Kane 2006, Forgac 2007). Peripheral stalks are present in F-, A-type ATP synthases and V-type ATPases but their number differs. Bacterial F-type ATP synthases contain only one peripheral

stalk, whereas prokaryotic A/V-type ATP synthases contain two peripheral stalks. Only eukaryotic V-type ATPase contains three peripheral stalks (Cross and Muller 2004, Muench et al. 2011).

2.4. Proton-motive force (*pmf*) coupled bioenergetics

The majority of free-living organisms (as well as mitochondria and plastids) maintain a transmembrane gradient of H^+ to convert the free energy released by different chemical reactions, into electrochemical energy that can be used to sustain a variety of processes, such as ATP synthesis. Most anaerobic and all aerobic bacteria rely on the transmembrane electrochemical gradient of H^+ (proton-motive force, *pmf*) as a source of energy for a variety of cellular processes. Usually, the H^+ cycle includes generation of *pmf* by diverse primary transport systems (H^+ pumps) and its use for ATP synthesis, solute transport, motility, reverse electron transport, etc. (Skulachev 1991, Skulachev 1992, Harold 1996).

The respiration metabolism is the predominant energy pathway in living cells. This catabolic process is fundamental to all kingdoms of life (Nicholls 2002). Fewer organisms that lack respiratory chains rely on glycolysis or fermentation for the production of ATP. The respiratory chain plays a crucial role for bacteria in translocation of H^+ across the membrane and establishing the primary electrochemical gradient of H^+. Electron transport systems are located in the cytoplasmic membrane of numerous species of obligate or facultative aerobic bacteria and the inner mitochondrial membrane of eukaryotes. The underlying mechanism involves the coupling of an electron transfer along a chain of redox enzymes to H^+ translocation across an organellar membrane in which the redox components are embedded (Mitchell 1961). The canonical mitochondrial electron transport chain includes:

- complex I (NADH-ubiquinone oxidoreductase),
- complex II (succinate-quinone oxidoreductase),
- complex III (cytochrome bc_1 complex),
- complex IV (cytochrome c oxidase).

While many organisms have this type of respiratory chain complexes, the composition of the

electron transport chain is not overall conserved, particularly in bacteria and archaea. Presumably, the great diversity in bacterial and archaeal respiration chains is due to their diverse metabolic pathways and is critical for the surviving in extreme habitats. Bacteria utilize multiple electron transport chains, often simultaneously in order to respond to different electron acceptors and donors available in the environment (Haddock and Schairer, 1973; Anraku, 1988). The bacterial component of respiratory chain can be highly diversified between organisms, or even within the same organism depending on growth conditions (Rea et al. 2010). In addition to the respiratory chain complexes, bacteria can have a number of different dehydrogenases, oxidases and reductases (as well as a variety of different electron donors and acceptors) that are also implemented in generation of electrochemical gradient across a membrane (Wada et al. 1999, Rea et al. 2010).

2.5. Sodium-motive force (*smf*) coupled bioenergetics

Certain anaerobic bacteria and archaea use Na^+ instead, or in addition to H^+ for energy coupling (Dimroth 1992, Speelmans et al. 1993, Dimroth 1994, Muller et al. 2001). So far, no aerobic organisms were found to couple energy transduction to *smf*. Some archaeal species lack cytochromes and other H^+-pumping electron transfer chains that can sustain efficient H^+ cycling. These archaea have only the Na^+-translocating methyltransferase or hydrogenase for membrane energization and therefore, are proposed to use the Na^+ potential to drive ATP synthesis (Thauer et al. 2008, Mayer et al. 2012, Mayer and Muller 2014).

The *smf* is established by primary Na^+ pumps such as decarboxylases, ATPases or Na^+-dependent electron transport complexes or by the action of Na^+/H^+ antiporters which primary use the *pmf* (Dimroth 1987, Junge, et al. 2001). Na^+ cycle includes a primary Na^+ pump that directly couples Na^+ translocation to a chemical reaction. There is only limited number of the Na^+-translocating pumps (**Table 2-1**). For instance, *smf* is established by the function of Na^+-translocating methylmalonyl-Coa decarboxylase in case of *Propionigenium modestum* (Hilpert and Dimroth 1984, Dimroth et al. 2006, von Ballmoos et al. 2008) and Na^+-translocating ferredoxin:NAD^+ oxidoreductase (RNF) sets up *smf* in case of *Acetobacterium woodii* (Biegel and Muller 2010, Poehlein et al. 2012).

Table 2-1: Classes of primary Na^+ pumps that perform Na^+ extrusion in bacteria and archaea (adapted from (Dibrova et al. 2015))

Na^+ primary pump
1. Decarboxylases (Dimroth 1980, Hilpert and Dimroth 1983):
Bacteria and archaea: Na^+-translocating oxaloacetate decarboxylase (OADC)
Bacteria: Na^+-translocating methylmalonyl-CoA decarboxylase
Bacteria: Na^+-translocating malonate-CoA decarboxylase
Bacteria: Na^+-translocating glutaconyl-CoA decarboxylase
2. Oxidoreductases (Unemoto and Hayashi 1979, Schmehl et al. 1993, Muller et al. 2008, Verkhovsky and Bogachev 2010):
Bacteria: Na^+-translocating NADH:ubiquinone oxidoreductase (NQR)
Bacteria and archaea: Na^+-translocating ferredoxin:NAD^+ oxidoreductase (RNF)
3. Methyltransferases (Becher et al. 1992):
Archaea: Na^+-translocating coenzyme M methylase (MTR)
4. Pyrophosphatases (Malinen et al. 2007):
Bacteria: Na^+-translocating pyrophosphatase
5. ATPases (Laubinger and Dimroth 1988, Takase et al. 1993, Solioz and Davies 1994, Dibrova et al. 2010):
Bacteria: Na^+-translocating F_1F_o ATPases
Bacteria and archaea: Na^+-translocating A/V-type ATPases
Bacteria and archaea: Na^+-translocating N-type ATPases
6. Hydrogenases (Gottschalk and Thauer 2001):
Archaea: membrane-bound Na^+/H^+ antiporter modules containing hydrogenase (Mbh)
Archaea: Na^+-translocating formylmethanofuran dehydrogenase
7. Light driven ion pumps (Inoue et al. 2013, Yoshizawa et al. 2014):
Bacteria: Na^+-translocating rhodopsin, (NaR)

* - The multi-subunit membrane-bound hydrogenase (Mbh) is used in *Pyrococcus furiosus* to generate the *smf* for transport processes and other energy-consuming membrane reactions but most of the cellular ATP is generated by substrate level phosphorylation during glycolysis (Sapra et al. 2003).

2.5.1. SMF in pathogens

There are few reasons to assume that the generation of a Na^+ gradient is essential for survival of bacterial parasites (Skulachev 1989, Hase and Barquera 2001):

- Some parasites were shown to encode primary membrane Na^+ pumps (Hase et al. 2001). Sequence-based comparison of many human and animal pathogens (e.g. *Vibrio cholerae*, *Neisseria meningitidis*, *Salmonella enterica serovar Typhi*, *Yersinia pestis*, *Treponema pallidum*, *Chlamydia trachomatis* and *Chlamydia pneumoniae*) revealed they encode primary membrane Na^+ pumps, Na^+-transporting dicarboxylate decarboxylases or Na^+-translocating NADH:ubiquinone oxidoreductase, and a number of Na^+-dependent permeases.
- The established inwardly directed Na^+ electrochemical gradient is supposed to be widespread and important for number of pathogens (Hase et al. 2001) (Dibrov 2017). Use of Na^+ instead of H^+ is a good virulence factor and therefore, can be essential for survival of bacterial parasites (Skulachev 1989, Hase, et al. 2001).
- Na^+ is the most common cation in human extracellular fluids (e.g., blood plasma).

2.5.2. SMF in methanogens

Methanogens are strictly anaerobic organisms found in different anoxic environments (Ferry 2011). To date, methanogens are the only microorganisms known to produce two primary ion gradients, Na^+ and H^+, at the same time (Muller et al. 2005). Moreover, other bioenergetically crucial membrane proteins in methanogens and acetogens, notably Ech hydrogenase and respiratory enzyme RNF, are also apparently selective for Na^+ and H^+ (Buckel and Thauer 2013). Even complex I (NADH dehydrogenase) displays intriguing Na^+/H^+ heterogeneity (Batista et al. 2012).

2.5.3. SMF in the fermenting, anaerobic bacterium *Ilyobacter tartarcus*

Ilyobacter tartaricus (strain GraTa2) was isolated from canal mud in Venice (Italy) (Schink

1984) and assigned to the family of *Fusobacteriaceae* (Krieg and Holt 1984). *I. tartaricus* is a marine L-tartrate-fermenting strictly anaerobic gram-negative bacterium. It is non-sporeforming, has short, straight rods, 1.0 x 1.2-1.2- 2.5 micrometre in size, often in chains, surrounded by slime capsules and non-motile (Schink 1984), **Figure 2-1**.

A

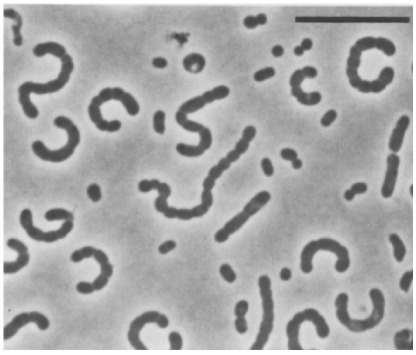

B

Domain: Bacteria
→ **Phylum:** *Fusobacteria*
→ **Class:** *Fusobacteriia*
→ **Order:** *Fusobacteriales*
→ **Family:** *Fusobacteriaceae*
→ **Genera:** *Ilyobacter*
→ **Species:** *Ilyobacter tartaricus*

Figure 2-1: Visual characteristic and taxonomic assignment of *I. tartaricus*. (**A**) Phase contrast photomicrographs of marine isolate *I. tartaricus* strain (from (Schink 1984)). (**B**) Assignment of *I. tartaricus* across all taxonomic levels.

Physiological characteristics of *I. tartaricus* fit this habitat: As anaerobic fermenting bacterium *I. tartaricus* lacks an efficient H^+ cycling system and therefore, energy transduction for *I. tartaricus* solely depends on Na^+ cycling (Neumann, et al. 1998). The Na^+-translocating ATP synthase from *I. tartaricus* utilizes the *smf* generated by one of the Na^+ primary pumps (e.g., Na^+-translocating oxaloacetate decarboxylase). Indeed, *P. modestum* from the same *Fusobacteriaceae* family uses metylmalonyl-CoA decarboxylase to establish *smf* (Bott et al. 1997).

2.6. Overall organization of rotary ATP synthases

ATP synthase complex in a simplest case of bacterial F-type ATP synthases has a molecular weight of 550-650 kDa and comprises 8 subunits with a stoichiometry of α_3:β_3:γ_1:a_1:δ_1:b_2:ε_1:$c_{8\text{-}15}$ (**Figure 2-2A**). The prokaryotic V/A-type ATPases found in archaea and few eubacteria are larger (~ 700 kDa) and are more complex than F-type ATPases (Muench et al. 2009, Vonck et al. 2009, Lau and Rubinstein 2012). Typically, V/A-type ATPases are composed of 9 subunits in a stoichiometry of $A_3B_3CDE_2FG/H_2ac_{10\text{-}12}$ (Vonck, et al. 2009, Lee, et al. 2010, Lau and Rubinstein 2012) (**Figure 2-2B**). The eukaryotic V-type ATPases contain at least 15 subunits forming functional complex (Muench, et al. 2009, Stewart et al. 2013), which may be due to the greater need for regulation in the eukaryotic cell. The additional subunits are mostly located in the peripheral and central stalks region.

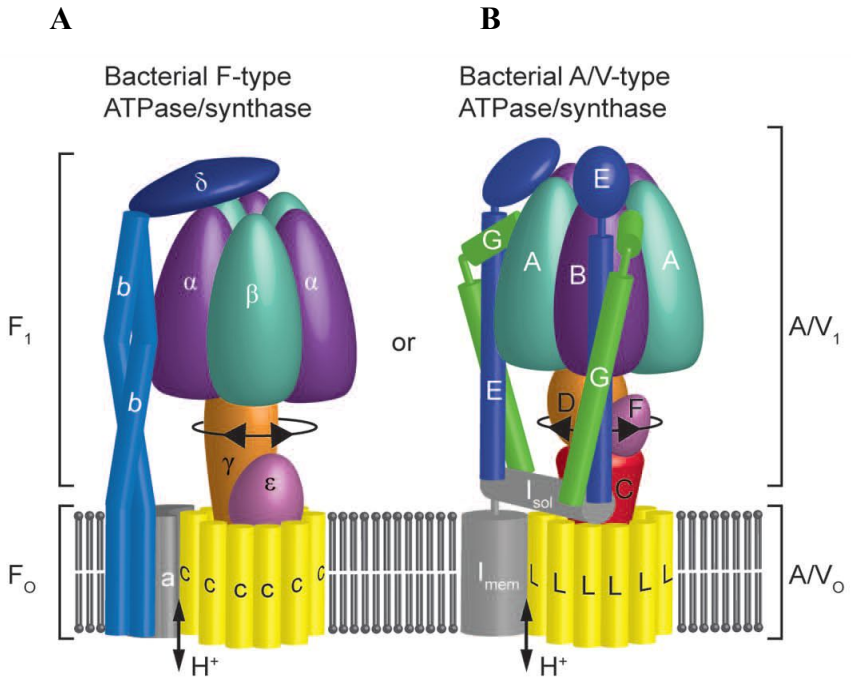

Figure 2-2: Schematic illustration of organization of bacterial rotary ATP synthases (figure is taken from (Stewart, et al. 2013)). (**A**) F- and (**B**) V/A-type ATPases have a related structure and mechanism (Toei et al. 2010) and both can operate in either directions, synthesising or hydrolysing ATP. ATP synthases consist and are separable into water-soluble $F_1/V_1/A_1$ domain (upper part) and membrane embedded $F_o/V_o/A_o$ domain, which are connected by one central and one (F-type) or two (V/A-type) peripheral stalks.

A soluble ATP synthesising/hydrolysing domain ($\alpha_3\beta_3\gamma\delta\varepsilon$ for F_1) runs on ATP. The trans-membrane domain ($ab_2c_{8\text{-}15}$ for F_o) is powered by a gradient of monovalent cations (mostly H^+, much more rare Na^+ and in laboratory conditions Li^+) (Oster and Wang 1999, von Ballmoos, et al. 2008, Krah, et al. 2010, Pogoryelov et al. 2010). These two complexes are tightly coupled to the central stalk for torque transmission and to additional peripheral stalk for counteracting rotation, stabilization and regulation. Particularly, the ε-subunit is essential for F_1 and F_o assembly (Duncan et al. 2014). The c-ring is in contact with the central stalk of F_1 formed by γδε subunits (Stock et al. 1999, Dautant et al. 2010).

2.6.1. Structure of catalytic soluble F_1 domain

F_1-ATPase ($\alpha_3\beta_3\gamma\delta\varepsilon$) is a structural and functional subcomplex of ATP synthase that contains catalytic centres for ATP synthesis and hydrolysis. John Walker and co-workers described the first crystal structure of the F_1 domain from bovine heart mitochondria in 1994 (Abrahams et al. 1994). Several subsequent high-resolution structures of F_1complexes from bovine and yeast mitochondria provided a detailed understanding of how ATP is synthesized by the F_1F_o-ATP synthase (for example, (Menz et al. 2001, Yasuda et al. 2001, Kabaleeswaran et al. 2009, Rees et al. 2012)). Later on, the list of available structures was expanded with structure of bacterial F_1 from *E. coli* (EF_1-δ, depleted of subunit δ) (Cingolani and Duncan 2011, Roy et al. 2012). In addition, the 3.5 Å resolution structures of F_1-c-ring complexes from bovine and yeast mitochondria were solved (Stock, et al. 1999, Watt et al. 2010). All these structures showed a high overall similarity that allows talking about overall structural organization of the F_1 complex. The F_1 domain is composed of five proteins with a stoichiometry of $\alpha_3\beta_3\gamma\delta\varepsilon$ (**Figure 2-3**). Three α- and three β-subunits form the core hexagonal subcomplex that is arranged around elongated α-helical structure of γ-subunit. The α- and β-subunits have similar folds consisting of an N-terminal domain with six β-strands, a central nucleotide binding domain made of both α-helices and β-strands and an α-helical C-terminal domain containing six α-helices in β-subunits and seven in α-subunits (Bowler et al. 2007).Subunits γεδ form the central stalk. The 'foot' made by protruding γ-subunit attaches the $\alpha_3\beta_3\gamma$ subcomplex to rotary c-ring embedded in the membrane (Kayalar et al. 1977, Abrahams, et al. 1994, Walker 2013).

The catalytic nucleotide binding sites are located mainly on the β-subunits, at the interface with α-subunits. Three additional nucleotide binding sites were located at the other interfaces of αβ. However, they are non-catalytic, and all contained adenylyn imidodiphosphate (AMP-PNP) in 3D X-ray structures.

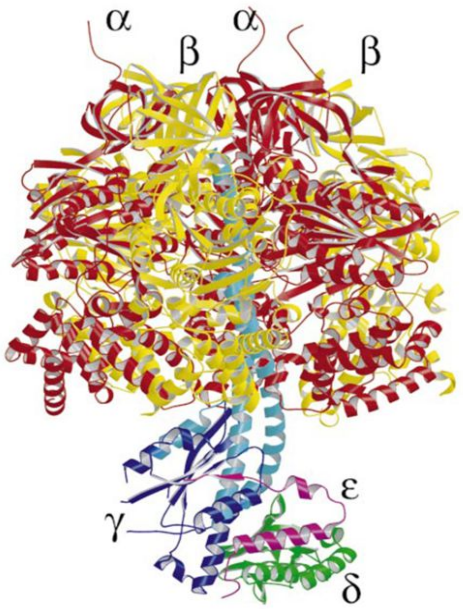

Figure 2-3: Structure of catalytic F_1 domain from bovine (Figure is taken from (Stock et al. 2000)). (**A**) Side view of F_1 complex with $\alpha_3\beta_3\gamma\delta\varepsilon$ subunit composition (9 polypeptide chains) with pseudo-6-fold-symmetry. Subunits α, β, γ, δ, and ε are shown with red, yellow, dark blue, green and magenta colours, respectively.

2.6.2. Rotation sub-steps of ATP synthase during catalysis

The rotation of the central stalk (γεδ) within the core of F_1 ($\alpha_3\beta_3$) was shown to effect sequential conformational changes in within the three active sites of β-subunits, that catalyze ATP synthesis and release. Namely, because of the asymmetry of the γ-subunit, the catalytic β-subunits adopt three different conformations with different nucleotide occupancies each (Bowler, et al. 2007). Each catalytic site performs ATP hydrolysis in a highly cooperative manner to induce the unidirectional rotation of the *γ* subunit (Uchihashi et al. 2011). The direction of rotation is counter clockwise as viewed from the membrane domain of the enzyme (Noji, et al. 1997,

Tsunoda et al. 2001). Most crystal structures trap the three *β*-subunits in different states: two closed states and one open state, which correspond to the catalytic dwell (Okuno et al. 2008). Traditionally, the numbering of β-subunits corresponds to conserved β-γ interaction and is based on mitochondrial nomenclature (MF_1): β_{TP}, β_E and β_{DP} conformation states correspond to "tight", "empty" and "loose" catalytic sites, respectively, in a binding change mechanism of ATP hydrolysis and synthesis (Boyer 1993):

- β1 = β_{DP} (closed, ADP + P_i bound state; "loose catalytic site)
- β2 = β_E (open state, no nucleotide bound; "open" catalytic site)
- β3 = β_{TP} (closed ATP-bound state; "tight" catalytic site)

The interconversion of catalytic sites during ATP hydrolysis by F_1-ATPase is affected by 360° mechanical rotation of the *γ*-subunit (Boyer 1981, Abrahams, et al. 1994, Noji, et al. 1997, Kinosita et al. 2000, Weber and Senior 2000, Yoshida et al. 2001, Kinosita et al. 2004). Sambongi et al. first observed the rotation of purified *E. coli* F_1F_o ATP synthase (Sambongi et al. 1999). The rotation of F_1-ATPase occurs in steps of 120°, each driven by hydrolysis of one ATP molecule (Yasuda et al. 1998, Adachi et al. 2000). The rotation of the γ-subunit is not continuous, it proceeds in 90° and 30° substeps (Yasuda, et al. 2001)or 80° and 40° substeps in other more recent experiments (Hirono-Hara et al. 2001, Shimabukuro et al. 2003, Nishizaka et al. 2004, Masaike et al. 2008). The 80° substep is triggered by ATP binding and ADP release that occur on different *β*-subunits (Nishizaka, et al. 2004, Adachi et al. 2007). The 40° substep is initiated by ATP hydrolysis and release of inorganic phosphate (P_i), which also occurs on different *β*-subunits (Shimabukuro, et al. 2003, Adachi, et al. 2007, Watanabe et al. 2008). In early experiments, the 80° and 40° substeps were found to be triggered by ATP binding and ATP hydrolysis, respectively (Yasuda, et al. 2001, Shimabukuro, et al. 2003). Therefore, the angles from which the 80° and 40° substeps begin are referred to as the binding angle and the catalytic angle, respectively (Arai et al. 2014).

Single-molecule experiments using the bacterial F_1-ATPase gave the scheme of the structural change of the *β* subunit associated with the nucleotide changes in the binding site (Sambongi, et al. 1999, Tsunoda et al. 2000, Ueno et al. 2005, Ishmukhametov et al. 2010, Sielaff and Borsch 2013) (**Figure 2-4**).

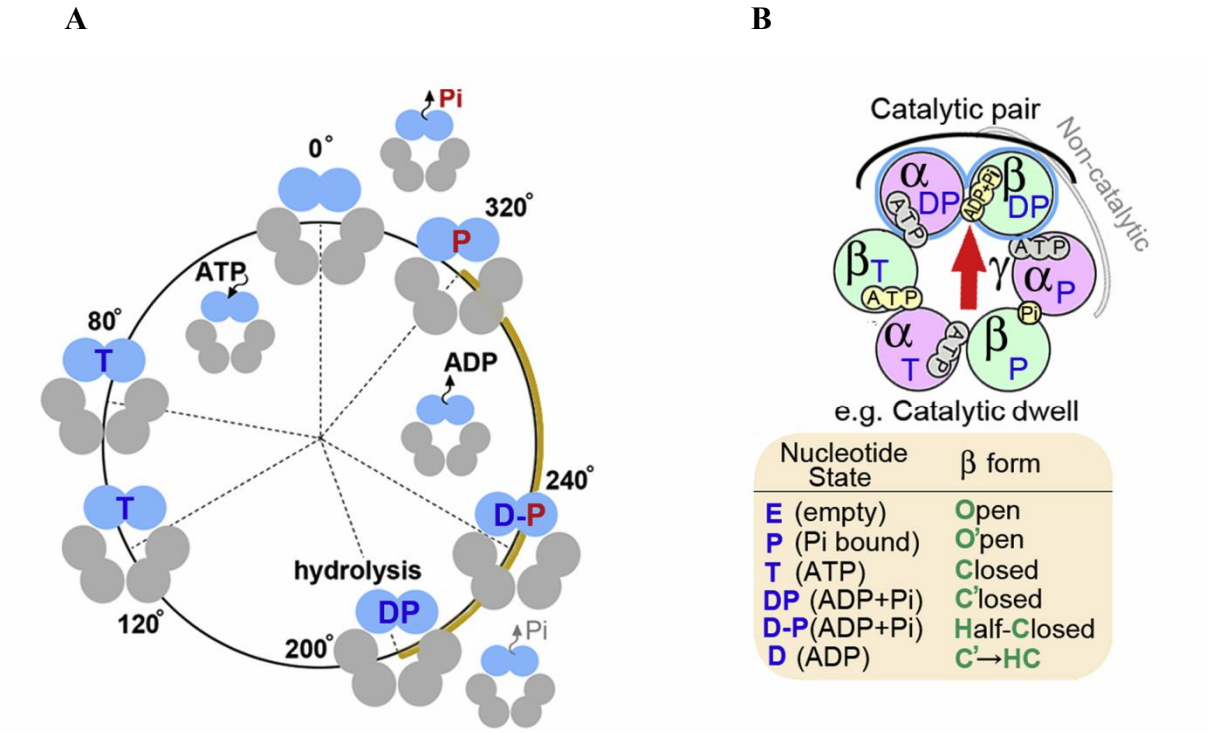

Fig. 2-4: Rotation scheme and arrangement of the α- and β-subunits of the bacterial F_1-ATPase for the 360° rotation of the γ-subunit (figure was taken and modified from (Ito and Ikeguchi 2015)). (**A**) Complete 360° catalytic turnover of ATP hydrolysis by one of the β-subunits (highlighted in blue) and (**B**) its 200° rotation angle with description/abbreviations of the nucleotide states. Individual β subunit completes one turnover of ATP hydrolysis in a turn of the γ-subunit, where the β subunits vary in their catalytic phase by one step of the γ-subunit rotation - 120° (Yasuda, et al. 1998). ATP binds to each β-subunit at the different angles related to γ-subunit (± 120°). After 200° rotation of γ-subunit, the ATP is hydrolyzed by β-subunits into ADP and P_i (Ariga et al. 2007). The release of ADP and P_i occurs after additional 40° and 120° rotations, respectively and is induced by conformational changes of β-subunit (closed → half-closed nucleotide states) (Nishizaka, et al. 2004, Adachi, et al. 2007, Masaike, et al. 2008, Watanabe et al. 2010, Okazaki and Hummer 2013). The next round of ATP catalysis starts only when γ-subunit returns to initial angular position. One turnover of ATP hydrolysis includes ATP binding (0°), ATP hydrolysis (200°), ADP release (240°) and P_i release (320°) and sequential open→closed→half-closed→open β-subunit conformations regarding their nucleotide bound state.

F_1-ATPase is a reversible molecular machine and when γ-subunit is rotated in the reverse direction by an external force, ATP is synthesized in the catalytic sites (Itoh, et al. 2004). It is

assumed that the order of the structural changes accompanying ATP hydrolysis is reversed also (Walker 2013). The reversibility is the exclusive feature of F_1 among other motor proteins.

2.6.3. Mechanism of rotary ATP synthase operation

The transport of ions (H^+ or Na^+) downhill electrochemical gradient causes the release of energy used to rotate c-ring relative to a-subunit in F_o portion (Cox et al. 1984) along with subunits γ, δ and ε in F_1 (Boyer 1981). Ions reach c-ring through half channels made by a-subunit in the F_o sector (Wittig and Schägger 2008). The rotation of subunit γ within the $\alpha_3\beta_3$ hexamer provides energy for ATP synthesis. This is called "rotary catalysis" (Devenish et al. 2008) and can be explained by the "binding-change" mechanism (**Figure 2-5**), first proposed by Boyer (Boyer 1975).

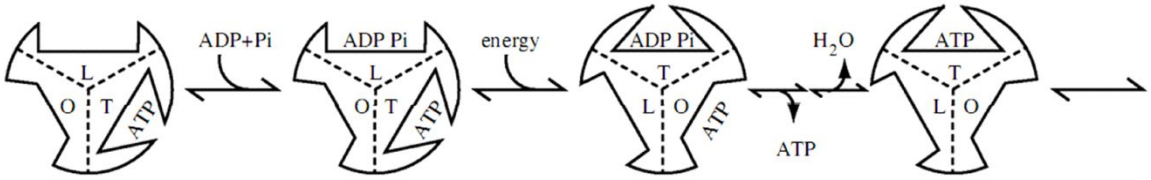

Figure 2-5: The binding change mechanism of the F_1 ATPase. Binding-change mechanism proposes that during ATP synthesis or hydrolysis the three catalytic binding sites in the *β*-subunits sequentially pass through the same conformations (Boyer 1993, Boyer 2000): O (open), L (loose), and T (tight) (according to Cross 1981). They correspond to β_E, β_{TP} and β_{DP} in the structure of Abrahams (Abrahams, et al. 1994). Each site alternates between these three states when ATP hydrolysis or ATP synthesis (in the reverse direction) proceeds.

2.6.4. Structure of a peripheral stalk

Peripheral stalk links catalytic soluble domain to membrane-embedded subunit a. Together, they form the stator complex (Walker and Dickson 2006). The F-type ATP synthases from mitochondria, chloroplasts and bacterial plasma membrane can have different subunit composition of the peripheral stalk depending on the organism (Gabellini et al. 1988, Herrmann

et al. 1993, Dunn et al. 2001, Dickson et al. 2006, Peng et al. 2006, Rees et al. 2009). In bacterial ATP synthases, the peripheral stalk is composed of homodimer of b-subunits (b_2) with one transmembrane helix and a soluble domain extending from the membrane to top of F_1 (Wilkens and Capaldi 1998, Revington et al. 1999) and the δ-subunit. The peripheral stalk is important for avoiding the $\alpha_3\beta_3$ hexamer to follow the rotation of the rotor and to keep it fixed in relation to a-subunit (von Ballmoos, et al. 2008, Junge et al. 2009, von Ballmoos et al. 2009). The peripheral stalk links the core $\alpha_3\beta_3$ domain to a-subunit in the F_o domain. Mechanically, they form together the "stator" part of the enzyme ($\alpha_3\beta_3$, b_2, a).

2.6.5. Organization of membrane F_o domain

The F_o domain contains a motor, which generates rotation using the energy stored in electrochemical gradient of ions (Na^+ and/or H^+). The rotation energy of the motor is transmitted to the catalytic domain by the central stock (γδε), which is attached directly to the motor. The F_o domain of bacterial F-type ATP synthase has a stoichiometry of ab_2c_8-c_{15}. The c-ring is embedded in the membrane, where it interacts with a-subunit (Jiang and Fillingame 1998, Hakulinen et al. 2012, Allegretti et al. 2015) and b_2 (Jones et al. 2000, Fillingame and Dmitriev 2002). The c-ring interacts also with F_1 domain through γε subunits (Stock, et al. 1999, Tsunoda, et al. 2001).

2.6.6. Structure of the c-ring

The c-ring is a major component of the membrane-embedded F_o domain and interacts with the a-subunit (Hakulinen et al., 2012). The c-ring is able to rotate with respect to the stator ab_2complex and transport ions (Na^+ and/or H^+) across membrane. The c-ring rotates within the membrane in steps determined by the number of c-subunits in the c-ring. The stepped rotation of the c-ring was visualized directly under optical microscope (Duser et al. 2009, Ishmukhametov et al. 2010). The c-ring is a membrane-inserted symmetrical oligomer composed of multiple c-subunits (**Figure 2-6**). The overall structure of the c-ring usually resembles hourglass due to narrowing of the c-ring diameter in the middle and has a central pore (Meier, et al. 2005, Meier, et al. 2009,

Schulz et al. 2013)

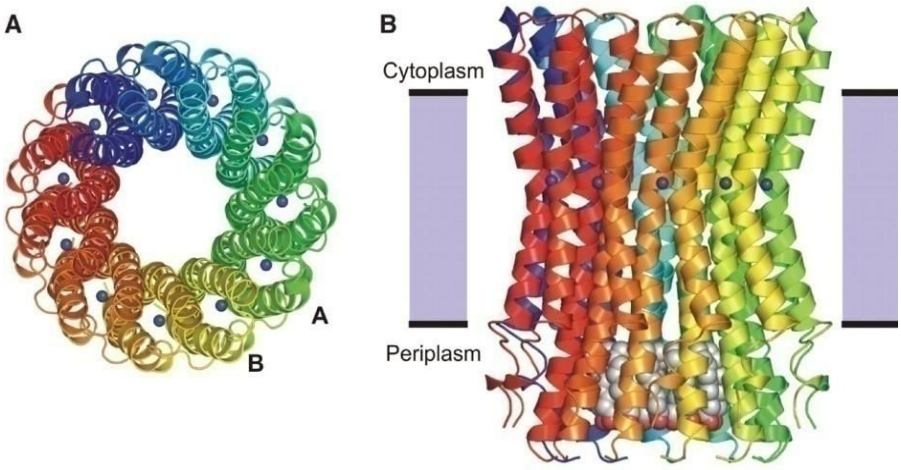

Figure 2-6: Overall structure of *I. tartaricus* c-ring (figure is taken from (Meier, et al. 2005)). (**A**) Top view of the *I. tartaricus* c-ring from the cytoplasmic side. The 11 c-subunits that form c-ring are depicted in different colours. (**B**) The side view of *I. tartaricus* c-ring with a membrane plane depicted in grey. Bound Na^+ ions are shown in blue.

The first resolved high-resolution structure of c-ring was the 2.4 Å crystal structure of *I. tartaricus* c-ring (Meier et al. 2005, Meier et al. 2009). *I. tartaricus* c-ring is a 96.7 kDa integral membrane protein composed from 11 hydrophobic c-subunits each per 89 amino acids. Amino acids of each c-subunit fold into a hairpin of two transmembrane helixes: N- and C-terminal helixes and short polar cytoplasmic connecting loop (**Figure 2-7**). The c-ring exists as an oligomer in the membrane and each monomer performs ion binding exchange activity only at c-subunit/c-subunit interface that forms the ion-binding pocket.

Usually, c-ring harbours a number of identical ion-binding sites that corresponds to a number of c-subunits in the c-ring (Meier et al., Science 2005). The number of c-subunits that form the c-ring varies between species (Meier et al., 2011). To date, the c-ring from the mitochondrial enzyme from bovine heart possesses the smallest number of c-subunits in the c-ring – 8 (Watt, et al. 2010). The largest c-rings so far were purified from cyanobacterial ATP synthase – 15 c-subunits (Pogoryelov et al. 2005, Pogoryelov et al. 2009) and from *F. nucleatum* ATP synthase – 17 c-subunits (Schulz et al., 2017). As result, movement of 8-17 H^+ (or Na^+ ions) are needed to

rotate the c-ring 360° and drive the synthesis of 3 molecules of ATP. Thus, number of c-subunits provides theoretical values for ATP/H^+ (or Na^+) ratios (Watt, et al. 2010, Pogoryelov et al. 2012).

2.6.7. Structure of the ion-binding site in the c-rings of different species

Ion binding site in the c-rings is formed by the network of amino acid residues that, independently of coordinating ion (Na^+ and/or H^+), include at least one conserved ionisable Glu or Asp residue in the sequence of second α-helix of the c-ring (Meier, et al. 2009, Pogoryelov, et al. 2010, Preiss et al. 2010, Schulz, et al. 2013, Matthies et al. 2014). The general principles of Na^+ coordination in the rotor c-rings have been described for the ion binding sites of *I. tartaricus*, *F. nucleatum*, *A. woodii* and *E. hirae* rotor c(K)-rings.

Na^+ coordination in *I. tartaricus* c-ring occurs at the interface of two adjacent c-subunits, involving the amino acid residues of three helices: One N-terminal helix (provided by the first c-subunit) and two C-terminal helices (provided by the first and its neighbouring c-subunit). The Na^+ coordination site of *I. tartaricus* harbours a conserved Glu65 present in helix 2 and three more amino acid residues that directly coordinate the Na^+: Gln32, Val63 and Ser66. Tyr70 forms a hydrogen bond with Glu65 and stabilizes the geometry of the ion coordination shell, but is not directly involved in Na^+ coordination. Thr67 itself is also not directly involved in Na^+ binding but coordinates a buried structural water molecule in the Na^+ binding site (Meier, et al. 2009) (**Figure 2-7**). The Na^+-bound c-ring has only one Na^+ ion per ion-binding site.

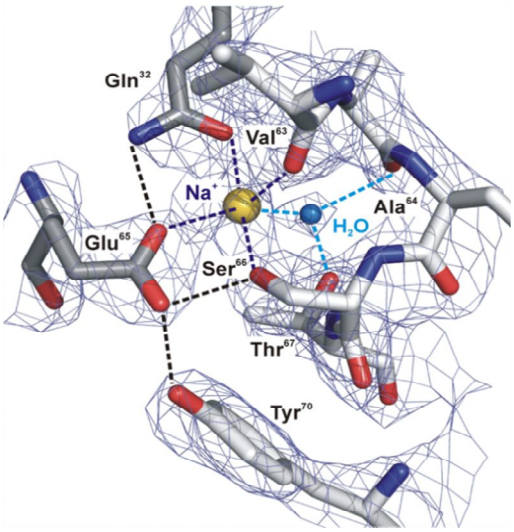

Figure 2-7: 2.35 Å resolution structure of Na^+ ion-binding site in *I. tartaricus* c-ring (figure is taken from (Meier, et al. 2009)). The structure represents the Na^+-bound, ion-locked conformation of *I. tartaricus* ion-binding site. Formed 11 inter-subunit ion-binding sites are of single ion occupancy (one Na^+ per each ion binding site). Residues from helix 1 and helix 2 (specifically Gln32, Glu65, Val63 and Ser66) form a stable coordination of the Na^+. Thr67 coordinates a buried structural water molecule and Tyr70 forms a hydrogen bond with Glu65 and stabilizes the geometry of the ion coordination shell.

The c-ring of the Na^+-coupled ATP synthase from *Fusobacterium nucleatum*, another representative of family *Fusobacteriaceae*, shares similar overall structure and arrangement of the ion-binding site with the c-ring of *I. tartaricus* ATP synthase (Schulz, et al. 2013) (**Figure 2-8**). The most notable difference is the presence of second glutamate residue (Glu32) in the ion-binding site of *F. nucleatum* c-ring. The side-chain of Glu32 also contributes to Na^+ coordination through the carboxylate oxygen atom and harbours the second H^+ in addition to one bound to Glu65. However, only one of these H^+ is likely to be transported (Schulz et al., 2013).

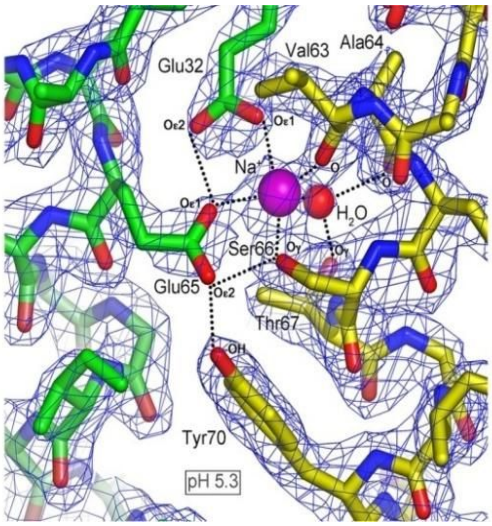

Figure 2-8: 2.2 Å resolution structure of *F. nucleatum* Na^+ ion-binding site (figure is taken from (Schulz, et al. 2013)). Na^+ binding motif in *F. nucleatum* c-ring includes two Glu side-chains (in *I. tartaricus* c-ring at the position of second Glu is located Gln), Ser66:Oγ and Val63:O from the adjacent c-subunit and water molecule. Ser66:Oγ and Tyr70:OH also provide hydrogen bonds to Glu65 and stabilize the geometry of the Na^+-bound state. Thr67:Oγ and Ala64:O are involved in coordination of water molecule through hydrogen bonds.

Another Na^+-selective c-ring, the hybrid c-ring of *A. woodii* F-type ATPase is composed of the c-subunits with distinct transmembrane helix topologies. The c-ring of *A. woodii* comprises both, single-hairpin F-type c-subunits ($c_{2/3}$) that are structurally similar to single-hairpin subunits of *I. tartaricus* c-ring and double-hairpin V-type c-subunit (c_1) in a stoichiometry of 9:1, respectively (Matthies, et al. 2014) (**Figure 2-9**). The Na^+ binding sites are localized at $c_{2/3}c_{2/3}$, $c_{2/3}c_1$ and $c_1c_{2/3}$ interface. The bound Na^+ is co-coordinated by water molecule in the formed ion-binding sites. However, the binding site within the c_1 subunit lacks Na^+ ion due to substitution of key glutamate to glutamine.

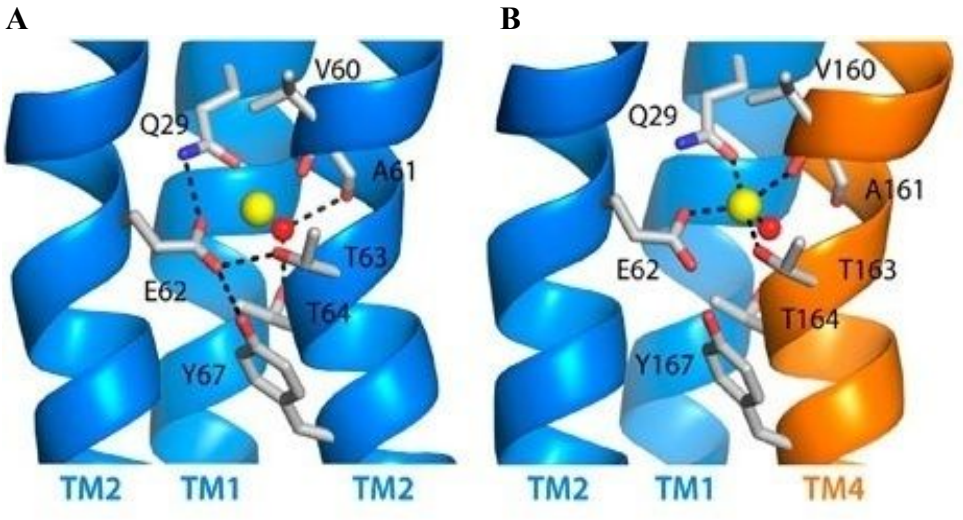

Figure 2-9: 2.1 Å resolution structures of Na^+ ion–binding site in the c-ring from hybrid F/V-type ATPases of *A. woodii* (figure is taken from (Matthies, et al. 2014)**.** (**A**) The Na^+-binding site of *A. woodii* at the $c_{2/3}c_{2/3}$ interface and (**B**) $c_{2/3}/c_1$interface at 2.1 Å resolution. Na^+ (depicted in yellow) is stabilized by Glu carboxylate and Gln carbonyl groups from one c-subunit, by Thr hydroxyl and backbone carbonyl groups from adjacent c-subunit and water molecule (depicted with red). Hydrogen bonds between Glu and Tyr and Thr and water molecule stabilizes the formed ion-binding network.

Structure of another Na^+-selective K-ring was solved from *E. hirae* V-type ATPase. In the case of *E. hirae*, the high resolution crystal structures of both, Na^+- and Li^+-bound K-rings were obtained (Murata et al. 2005, Murata, et al. 2008). The bound ion was occluded by Glu139 and the position of the Glu139γ carboxylate was stabilized by the hydrogen bonds with the side chains of Gln110, Tyr68 and Thr64 (**Figure 2-10**). The Na^+- and Li^+-bound K-rings had similar ion coordination (Murata, et al. 2005, Murata, et al. 2008). Interestingly, Na^+ and Li^+ bound states lack water molecule co-coordination observed in the Na^+ binding sites of *I. tartaricus*, *F. nucleatum* and *A. woodii* c-rings.

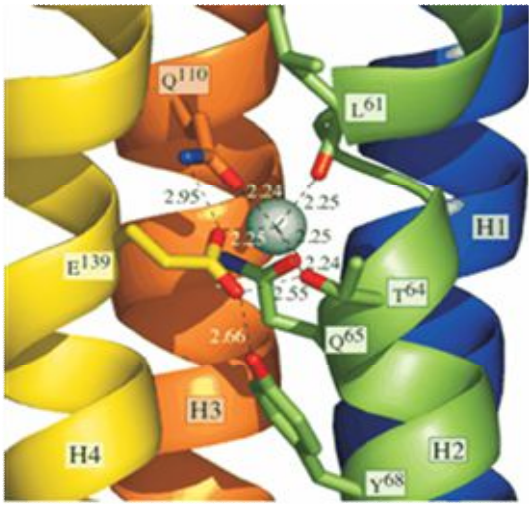

Figure 2-10: 2.1 Å resolution structure of Na^+ ion-binding site in bacterial V-type c-ring from *E. hirae* (figure is taken from (Murata, et al. 2005)). In the obtained structure, Na^+ion is surrounded by five oxygen atoms, four in the side chains of Thr64, Gln65, Gln110 and Glu139 and the fifth in the main-chain carbonyl of Leu61.

The first high-resolution crystal structure of H^+ ion-binding site in the c-ring was solved from alkaliphilic cyanobacterim *S. platensis* (Pogoryelov, et al. 2009) (**Figure 2-11**). Similar coordination pattern in the H^+-binding site was suggested for *Pea sativum* c-ring (Saroussi et al. 2012). Different H^+ coordination was observed in c_{13}-ring of the alkaliphilic *Bacillus pseudofirmus* OF4 ATP synthase (Preiss, et al. 2010) (**Figure 2-12**).

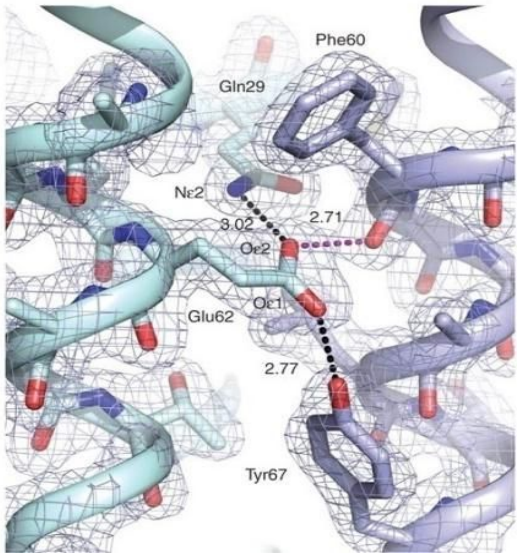

Figure 2-11: 2.1 Å crystal structure of the H^+-binding site in *S. platensis* c-ring (figure is taken from (Pogoryelov, et al. 2009)). H^+ is bound to Glu62 and is additionally coordinated by hydrogen bond network formed by Gln29, Phe60 and Tyr67 residues from the two C-terminal and one N-terminal helixes of the adjacent c-subunits.

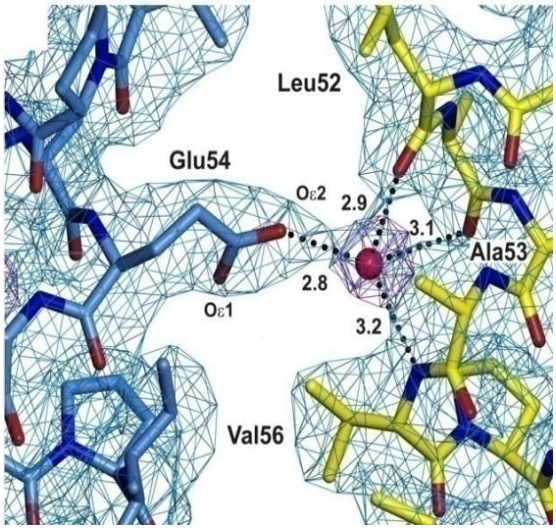

Figure 2-12: 2.5 Å structure of H^+-binding site in *Bacillus pseudofirmus* OF4 c-ring (figure is taken from (Preiss, et al. 2010)). H^+-binding site includes side chain carboxyl group of Glu54, backbone carbonyl groups of Leu52 and Ala53, backbone nitrogen of Val56 from the two outer helixes of neighbouring c-subunits and a water molecule (shown in red).

The majority of the solved to date c-ring structures trap the closed, ion-locked conformations of the ion-binding site. Exceptional is the c_{10}-ring structure from *Saccharomyces cerevisae*, which was solved in open conformation due to unique crystallization conditions (Symersky et al. 2012).

2.6.8. Water molecule in the Na^+ ion-binding sites

A water molecule is a prominent feature of Na^+-selective ion-binding site. X-ray crystal structure of the rotor ring isolated from the *I. tartaricus*, *F. nucleatum* and *A. woodii* ATP synthases favour this hypothesis (Meier, et al. 2009, Schulz, et al. 2013, Matthies, et al. 2014). In these structures, a water molecule contributes to ion(Na^+)-coordination in the binding sites in ion-locked conformation. However, no water molecule is observed in Na^+-binding pocket of the *E. hirae* c-ring (Murata, et al. 2005). Conversely, a bound water molecule was found in the H^+-binding pocket of the *Bacillus pseudofirmus* OF4 c-ring (Preiss, et al. 2010). Therefore, the unambiguous role of water molecule in attaining high affinity Na^+ binding by c-rings is still under investigation.

2.6.9. Designated conserved residues in Na^+-binding motif of c(K)-rings

It is believed that the primary structure of the c-ring determines the ion specificity of the ATP synthases/ATPases (Krah, et al. 2010, Preiss, et al. 2010, Pogoryelov, et al. 2012, Preiss et al. 2013, Preiss et al. 2014). High-resolution crystal structures of Na^+-bound c-rings allow comparing available Na^+ binding motifs in the c-rings. The residues of the c-subunits that are involved in Na^+-coordination form a conserved Na^+-binding motif formed by Gln/Glu + Glu + Ser/Thr → Q/E…ES/T motif (illustrated at **Figure 2-13**). The acidic Glu/Asp and Tyr residues in helix 2 of the c-ring are generally present in the ion-binding motifs independently on inherent ion-binding selectivity.

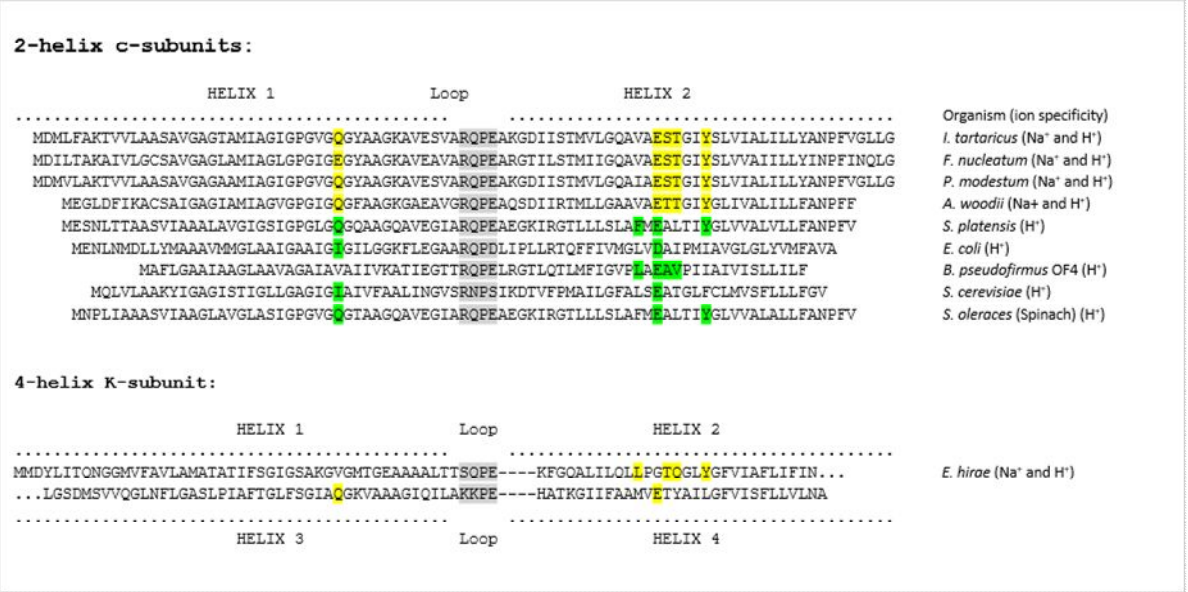

Figure 2-13: Na^+ and H^+-binding signatures in the sequence of the c(K)-subunits from rotary ATP synthases. The sequence alignment of c-subunits from a selection of bacteria is shown. Each c-subunit consists of two (or two duplicated) α-helices, helix 1 and helix 2 (shown on top of the figure). The amino acids of the c-subunit hairpin loop region or the ones, which are involved in either H^+ or Na^+ coordination, are displayed. The Na^+-binding motif is designated (yellow marked amino acids). The H^+ binding motifs are more variable and include only conserved Asp or Glu in helix 2 of the rotor ring (green marked amino acids).

Q/E…ES/T motif is adequately conserved among resolved Na^+-binding sites. Indeed, Q...ES Na^+ binding motif is present in the c-ring of *I. tartaricus* (Meier, et al. 2005, Meier, et al. 2009). E…ES Na^+ binding motif is present in the c-ring of *F. nucleatum* (Schulz, et al. 2013). Q…ET motif in the K-ring of bacterial V-type ATP synthase from *E. hirae* (Murata, et al. 2005) and Q…ET motif in F/V-hybrid rotor of *A. woodii* (Matthies, et al. 2014).

Based on sequence analysis, many A-type ATP synthases from archaea containing Q/E…ES/T motif in the c(K)-rings were predicted to use Na^+ as a coupling ion: methanogens and halobacteria, as well as in species of the genera *Pyrococcus*, *Thermococcus*, *Desulfurococcus*, *Ignisphaera*, *Staphylothermus* and *Nanoarchaeum* (Gruber et al. 2014). However, only for some of these species (e.g. *Pyrococcus furiosus*, *Methanobrevibacter ruminantium*, *Methanosarcina acetivoran, and Thermococcus onnurineus*) coupling to Na^+ was shown mainly by indirect

biochemical methods. These methods include measuring Na^+-activation of ATP hydrolysis, Na^+ protection against covalent DCCD modification, Na^+-dependence of ATP synthesis and ATP hydrolysis-based Na^+-accumulation in inverted membrane vesicles or proteoliposomes (Pisa et al. 2007, McMillan et al. 2011, Mayer, et al. 2012, Schlegel, et al. 2012, Mayer et al. 2015). Nonetheless, the sequence-based prediction is not ultimate for defining the ion selectivity of the c-rings. There are few examples for this:

- *M. acetivorans* (E…ET ion-binding motif, predicted coupling to Na^+): It was evidentially shown that ATP synthase of *M. acetivorans* uses both H^+ and Na^+ for energy transduction.
- *Methanosarcina mazei* (E…ET ion binding motif, predicted coupling to Na^+): The predicted Na^+ ion coupling for ATP synthase was not confirmed by experiments (Pisa et al. 2007).

Therefore, the presence of the designated Na^+-binding motif in the sequence of the c-subunits does not provide ample evidence for Na^+ selectivity of the corresponding ATP synthases. A more complex biochemical approach is needed to judge on the ion-selectivity of the c-rings in ATP synthases.

2.6.10. Structure of the a-subunit

The a-subunit is a part of ion-translocation F_o domain in ATP synthase. LILBID-MS and gel filtration analysis shows that a-subunit is present in a single copy in bacterial F_o domain (Hakulinen et al., 2012). Mutagenesis studies and crosslinking experiments shed some light on the fold and helix topology of a-subunit and identified residues important for ion-translocation in F_o sector (Long et al. 1998, Valiyaveetil and Fillingame 1998, Wada, et al. 1999, Schwem and Fillingame 2006, DeLeon-Rangel et al. 2013). The a-subunit is supposed to form two ion-conducting half channels at two sides of the membrane that provide the pathway for the ions (Na^+ and/or H^+). However, up to now, there is no high-resolution structure for the stator membrane bound a-subunit, which interacts with rotor c-ring.

First insights on a structure of a-subunit were obtained recently by single-particle cryo-electron microscopy: An overall 7 Å resolution map of mitochondrial F-type ATP synthase dimer from

Polytomella sp gave structural information on arrangement of helixes in the a-subunit and gave new arguments to elucidate the mechanism of ion-translocation through a/c-subunit interface (Allegretti, et al. 2015). More specifically, it was shown that a-subunit is formed by 4 long horizontal α-helixes that form two hairpin-like structures and are tilted in relation to c_{10}-ring (**Figure 2-14A**). All previous cryo-electron microscopy structures showed remarkable 4-helix bundle but proposed not tilted vertical orientation of helixes (Hakulinen, et al. 2012, Lau and Rubinstein 2012). The long hairpin of a-subunit of *Polytomella sp* F-type ATP synthase is proposed to contain the conserved arginine residue (R239) that was shown to be crucial for H^+ translocation (Mitome et al. 2010, Allegretti et al., 2015). The helices are oriented in way that Arg239 is situated in a closest proximity next to the conserved glutamate residue in c-ring (Glu235) (Allegretti et al., 2015). In more recent cryo-EM work (Hahn et al., 2016), more details on a-subunit topology and more proper helices assignment were obtained using ATP synthase dimer of *Yarrowia lypolitica*. Despite low sequence identity with *Polytomella sp* a-subunit and reverse helices assignment, similar long tilted hairpin was identified in *Y. lypolittica* a-subunit (**Figure 2-14B**). The essential and highly conserved charged R182 residue in a-subunit is also assigned in the long horizontal hairpin at a/c interface, where it is proposed to be interacting with conserved protonatable Glu residue in c-ring.

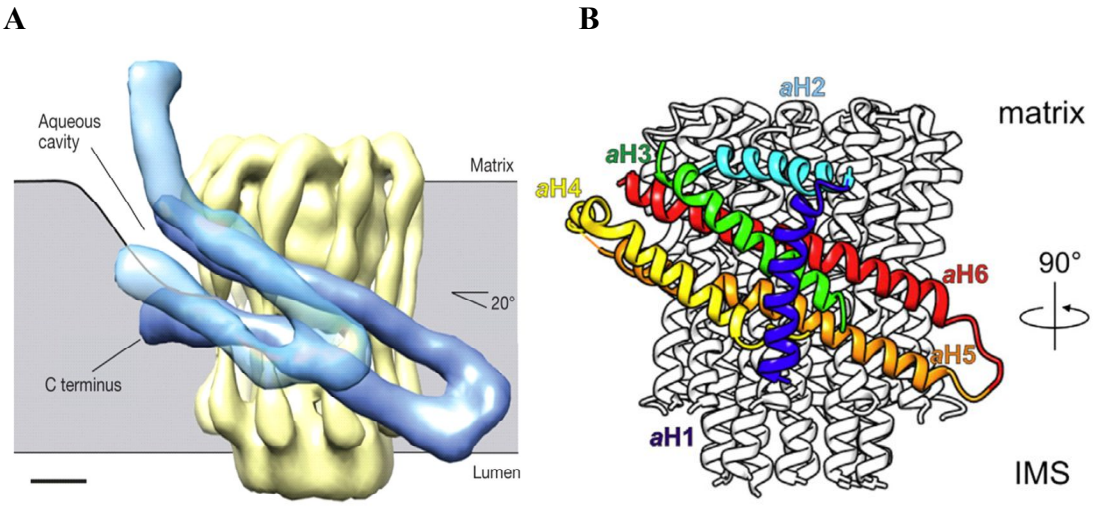

Figure 2-14: Arrangement of helices in a-subunit dedicated from cryo-EM structures (**A**) 7 Å cryo-EM structure of a-subunit from ATP synthase dimer of *Polytomella sp* (figure is taken from (Allegretti, et al. 2015)). Four transmembrane α-helixes that constitute a-subunit (colored in blue) are arranged into two hairpins of different length: short outer hairpin (35 Å) and long hairpin (80 and 65 Å length). Both helixes of the long hairpin contact c_{10}-ring (colored in yellow) (Allegretti, et al. 2015). (**B**)6.2 Å cryo-EM structure of a-subunit from ATP synthase dimer of *Yarrowia lypolitica*(figure is taken from (Hahn et al., 2016)). In a-subunit of ATP synthase dimer of *Yarrowia lypolitica* is also present long hairpin tilted by 20°-25° degree relative to membrane plane. The long hairpin is formed by 2 α-helices (aH5 shown in orange and aH6 shown in red) (Hahn et al., 2016).

Similar arrangement of α-helices from the a- and c-subunits was shown for the *Saccharomyces cerevisiae* V-type ATPase (Zhao et al. 2015) and bovine mitochondrial ATP synthase (Zhou et al., 2015). Namely, from the eight determined transmembrane α-helixes that constitute the a-subunit in *Saccharomyces cerevisiae* V-type ATPase, two were shown to be highly tilted with respect to plane of lipid bilayer and contact α-helixes of the c-ring (**Figure 2-15**). For the case of a-subunit from bovine ATP synthase, 6 α-helices are also unambiguously determined and two of them are also highly tilted (**Figure 2-16**).

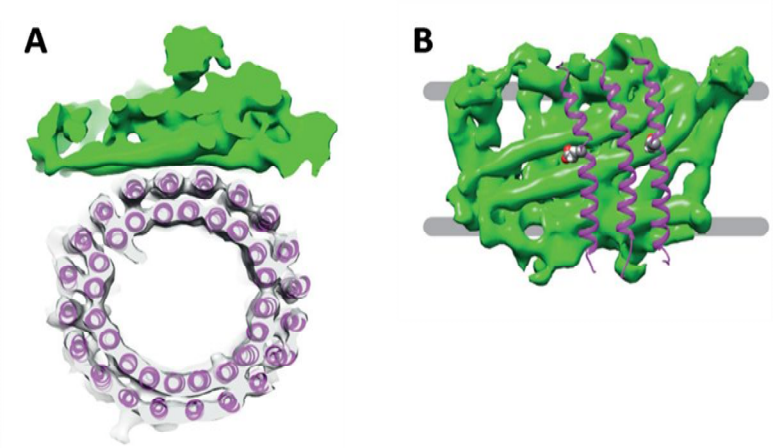

Figure 2-15:6.9 Å cryo-EM structure of V_o domain from *S. cerevisiae* V-ATPase (figure is taken from (Zhao et al., 2015)). (**A**) The cryo-EM map shows interaction of c-ring consisting of 10 c-, c-′ and c′′-subunits (magenta) with a-subunit (green). (**B**) The a-subunit was shown to have two long highly tilted α-helixes.

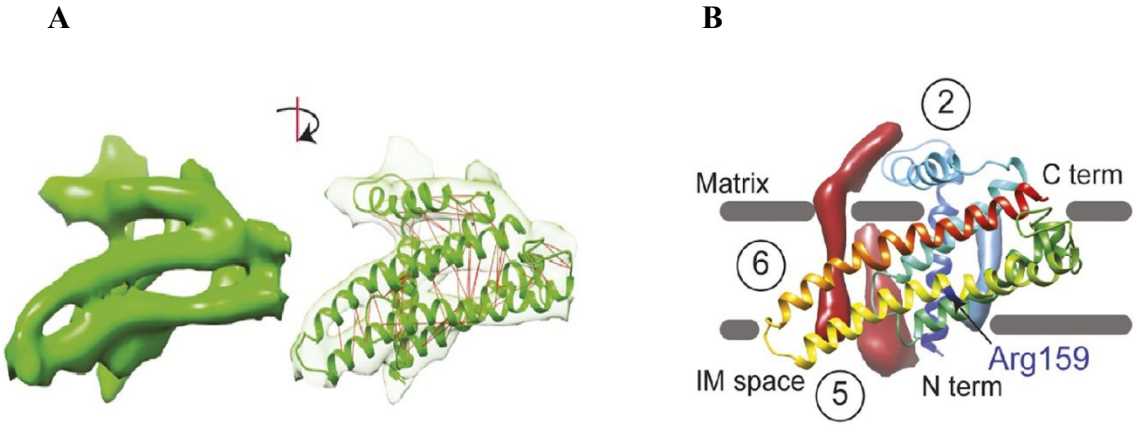

Figure 2-16: 6.4 Å cryo-EM structure of a-subunit from bovine mitochondrial ATP synthase (figure is adapted from (Zhou et al., 2015). (**A**) Nice fitting of a-subunit sequence into obtained cryo-EM map. (**B**) Horizontally tilted helix 5 and helix 6 are indicated. Helix 5 contains essential charged Arg159 residue.

2.6.11. Ion-translocation mechanism

Many models for ion-translocation mechanism by rotary ATP synthases exist. However, the two-half aqueous channel model (Junge et al. 1997) is more favourable and broadly accepted

(Dimroth, et al. 2006, Angevine et al. 2007). This model suggests that ion translocation occurs through two half channels at the a-subunit/c-subunit interface (Junge, et al. 1997, Junge and Nelson 2005). The a-subunit constitutes 'entry' channel for ions from the cytoplasmic side and 'exit' channel to the periplasm side. The two half channels are offset to one another and each is connected to different sides of the membrane (Elston et al. 1998) (**Figure 2-17**).

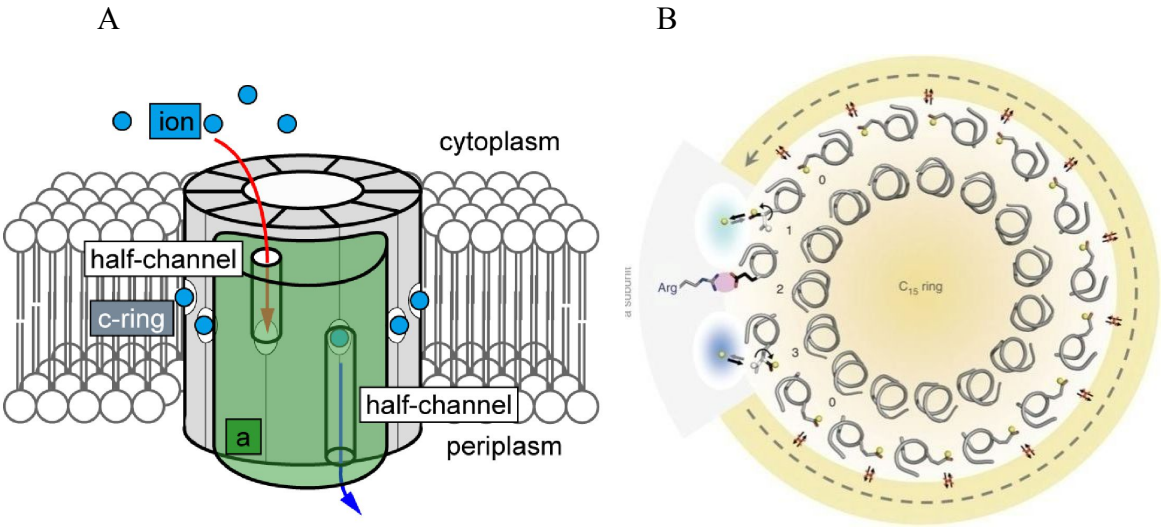

Figure 2-17: Two-half channel model and principles of ion-translocation mechanism (Figures are taken from (Kandori et al. 2015) and (Pogoryelov, et al. 2009)). (**A**) Two-half channel model (Junge, et al. 1997) assumes that loaded rotor sites release and bind new ions at stator/rotor interface made by a/c-subunits. The hydrophobic a-subunit forms two aqueous half-channels that allow ions to flow through and (**B**) the electrostatic interaction between conserved Arg in the a-subunit and the Glu/Asp in the ion-binding site of the c-ring is important for ion release/binding and unidirectional translocation mechanism.

The strictly conserved Glu/Asp in the c-subunit is the ion acceptor and donor at the c-ring/a-subunit interface and therefore, is crucial for ion-translocation mechanism (Vik and Antonio 1994, Junge, et al. 1997, Pogoryelov, et al. 2010, Allegretti, et al. 2015) (**Figure 2-18**). Generally, the ion-translocation mechanism is based on adjustable (tunable) pKa of Glu/Asp in the c-ring (Pogoryelov, et al. 2009). Thus, one-half channel of a-subunit is used to protonate conserved ionisable Glu/Asp residue in the second α-helix of one of the c-subunit and another half channel is used to deprotonate Glu/Asp in the adjacent c-subunit (Vik and Antonio, 1994;

Junge et al., 1997; Steed and Fillingame, 2008; Lau and Rubinstein 2012). This proposed ion-translocation mechanism seems to be conserved among F/V-type ATPases (Murata, et al. 2005; Allegretti, et al. 2015; Hahn et al., 2016).

The c-ring sites that face the membrane bilayer have to be protonated and hold the H^+ tightly in order to ensure effective proton supply to the stator part. The H^+ can dissociate only when it is placed in close proximity to positively charged Arg residue in one the α-helixes of the stator a-subunit. This Arg residue is highly conserved among rotary ATP synthases and was shown to be important for function of ATP synthase (Cain and Simoni 1989, Hatch et al. 1995, Valiyaveetil and Fillingame 1997, Vik et al. 1998). It is assumed that the electrostatic interaction reduces the c-ring pKa and mediates H^+ release and the proximity of two opposing charges an electrostatic force that impedes the rotation of c-ring. However, the unprotonated (=charged) rotor sites cannot rotate from the a-subunit/c-subunit interface due to large free energy penalty and must be loaded with H^+ for the next revolution cycle (Elston, et al. 1998).

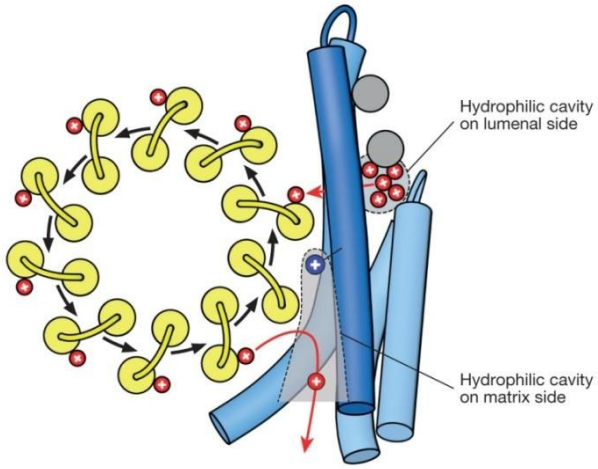

Figure 2-18: H^+ translocation through F-type ATP synthases (figure is taken from (Allegretti, et al. 2015)). H^+ (red) reach the conserved glutamate in the c-subunit via the aqueous luminal half-channel (dashed grey circle). The H^+ competes with the strictly conserved aArg239 (blue) for interaction with c-ring glutamates, which carry the H^+ around the c-ring. When the c-subunit approaches the hydrophilic half-channel on the matrix side (dashed grey outline), the glutamate becomes hydrated and adopts an open conformation, from which the H^+ can escape into the matrix. Solid grey circles indicate transmembrane helices.

2.7. Implementation of mutagenesis approach to study the ion selectivity of rotary ATP synthases

Some of the mutationally constructed hybrid ATP synthases in which intact c-rings were substituted with homologues c-rings from other organism were shown to be functional. For instance, the F_1 domains from H^+- and Na^+- specific F-type ATP sythases are functionally interchangeable. The hybrid *P. modestum* F_o that assembles with *E. coli* F_1 domain can perform catalysis driven by *smf* (Laubinger et al. 1990). These experiments point that there are no restriction on ion selectivity from the side of other subunits of ATP synthase (e.g., from subunit a).

Some work was performed to address the possibility to interchange the Na^+ ion-selectivity of the c-rings and linked ion selectivity of ATP synthases, using a single point mutagenesis approach. In these works, c-rings of *P-modestum* and *I. tartaricus* F-type ATP synthases and K-ring of *E. hirae* V/A-ATPase were used.*P. modestum* c-ring has high sequence identity with *I. tartaricus* c-subunit (only leucine at position 5 and alanine at position 20 are different). Early works on random mutagenesis of *P. modestum* c-subunit identified double F84L/L87V mutation that lead to switch from Na^+- to H^+-coupled ATP synthesis when *P. modestum* ATP synthase was expressed in the *E. coli* host cells (Kaim and Dimroth 1998). However, Phe84 and Leu87 residues are not a part of determined functional ion-binding site (Meier, et al. 2005, Meier, et al. 2009) and their effect was attributed to alteration of the inter-helix interactions and displacement of the Gln32 from the Na^+ coordination sphere (Kaim and Dimroth 1998). It was also shown that Q32I mutation leads to Na^+-independent activity of *P. modestum* ATP synthase, although the Li^+- and H^+-dependent activities of ATP synthase stayed intact (Kaim et al. 1997). However, no comprehensive biophysical or structural analysis of F84L/L87V and Q32I mutations explaining the observed phenomena was performed.

Intense mutagenesis studies were carried out with *E. hirae* K-ring. *E. hirae* V-ATPase is a unique variant of V-type ATPase, which recognizes Na^+ and Li^+ with nearly equal affinities (Murata et al. 2001). The rotor K-ring ring of *E. hirae* V-ATPase binds Li^+ with only 5-fold lower affinity than Na^+. The K_M values for Na^+ and Li^+ of ATP hydrolysis of the purified enzyme are 20 μM and 60 μM, respectively (Murata et al. 1997). K-ring binds one Na^+ ion per K-subunit,

which is competitively inhibited by Li^+ or H^+ (Murata, et al. 2008). Number of mutants was obtained that influenced ion selectivity of *E. hirae* V-ATPase and the rates of its catalysis. Namely, Kawano-Kawada (Kawano-Kawada et al. 2012) had identified residues critical for ion translocation by *E. hirae* V-ATPase. According to this study, Q110A mutation abolishes coupling of *E. hirae* ATPase to Li^+, even in the presence of conserved Glu139 and Thr64 residues. It was suggested therefore, that residues forming the ion-binding pocket are all indispensable for the Na^+ and Li^+ coupling of *E. hirae* V-ATPase and Gln65 and Tyr68 play an important role in the enzymatic reaction (Kawano-Kawada, et al. 2012). In other mutants (e.g. Q65A, Y68A and E139D) ATP hydrolysis activity by purified mutant V-ATPases was activated by Na^+ and Li^+ but showed reduced V_{max} values for ATP hydrolysis activity in comparison to wild-type ATPase. Interestingly, E139D mutant cells show no tolerance to high concentrations of Na^+ salts at pH 10 and almost equal tolerance to Li^+ salts as wild-type did. These results suggested that the arm length of the important carboxyl group at the Glu139 residue of K-ring is critical for Na^+-coupled catalytic turnover of *E. hirae* V-ATPase. Only T64A and Q110A mutants showed both reduced enzymatic activity and no effect of Na^+ and Li^+ on it (Kawano-Kawada et al. 2011, Kawano-Kawada, et al. 2012).

Mutagenesis studies of Na^+ protection against DCCD modification (Chapter 2.10) of target Glu65 residues in *I. tartaricus* c-ring was done by (von Ballmoos and Dimroth 2007) (**Figure 2-19**). In the case of the *I. tartaricus* Y70F mutant, it was shown that Y70F ATP synthase is still able to bind Na^+ but with much lower affinity (reference). Moreover, Na^+ activation of ATP hydrolysis activity by Y70F mutant and wild-type ATP synthases confirmed the decrease in Na^+ affinity for Y70F mutant. In particularly, Y70F mutant requires roughly 40 times higher concentration of Na^+ to activate half of possible ATP hydrolysis activity in comparison to wild-type enzyme. In the case of the S66A mutant, results of DCCD modification of Glu65 in S66A ATP synthase showed clear shift in pKa for Glu65 carboxyl group. Estimated pKa of Glu65 in wild-type c-ring was around pH 7.5 while S66A mutant demonstrated up-shifted pKa of ~8.5. Another important feature of S66A mutant was its Na^+-independent DCCD modification of Glu65. No Na^+ protection against DCCD modification suggested that S66A mutation abolish Na^+ binding to the c-ring. However, no other biochemical/structural data confirmed this statement. It can be summarized that despite performed mutagenesis studies, we still lack a comprehensive

answer on the principles that underlie Na^+ affinity and selectivity of rotary ATP synthases and the way it can be modulated in the c-rings of corresponding ATP synthases.

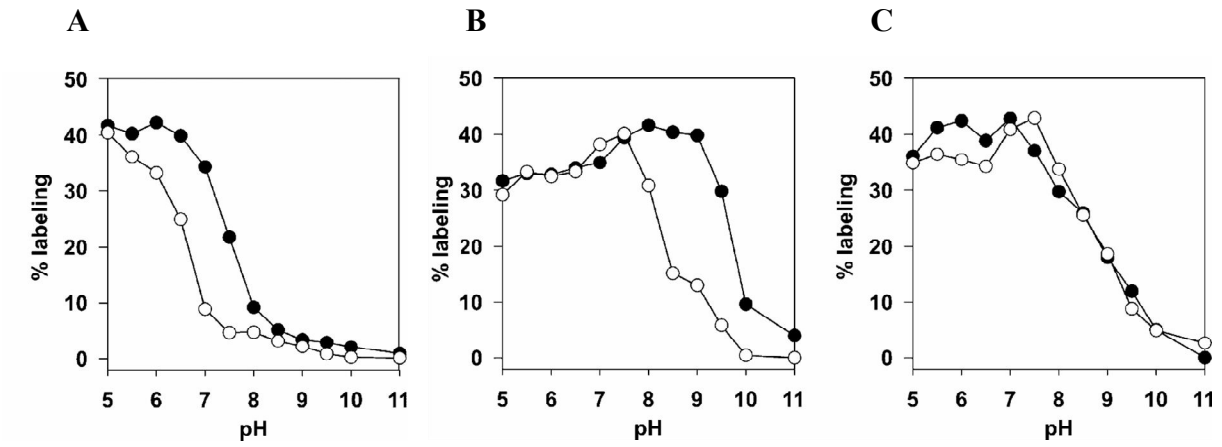

Figure 2-19: Difference in DCCD modification profiles of *I. tartaricus* ATP synthase harbouring wild-type and mutant c-rings (figure is modified from (von Ballmoos and Dimroth 2007)). (**A**) DCCD modification of Glu65 in wild-type ATP synthase. (**B**) DCCD modification profile of Glu65 in Y70F mutant ATP synthase was postulated to demonstrate lower Na^+ affinity due to lower Na^+ protection of Glu65 against DCCD modification (open circles). (**C**) DCCD modification profile of Glu65 carboxyl group in S66A mutant ATP synthase remains similar in presence (open circles) or absence of Na^+ (black circles), indicating no Na^+-protection for Glu65 modification in S66A c-ring. Additionally, estimated pKa value for target Glu65 carboxyl group was one pH unit up-shifted upon S66A mutation.

2.8. Isothermal titration calorimetry (ITC) and applications for cation affinity measurements

2.8.1. Principles of isothermal titration calorimetry (ITC)

Isothermal titration calorimetry (ITC) is an experimental technique that can accurately provide a complete thermodynamic descriptionof a ligand molecule binding to a target protein (or other molecule) using single titration experiments. The thermodynamic description includes the change of the Gibb's free energy (ΔG), the change of enthalpy (ΔH) and the change of the entropy ($-T\Delta S$), the dissociation constant K_d, the stoichiometry n and the heat capacity ΔC_p

parameters can be obtained from an ITC experiment (Leavitt and Freire 2001). Small aliquots of a ligand are introduced to a solution containing the protein and mixed, in a stepwise manner. The resulting heat is measured and converted to enthalpy by mathematical integration for each titration step. The principle of ITC measurements is shown in **Figure 2-20**.

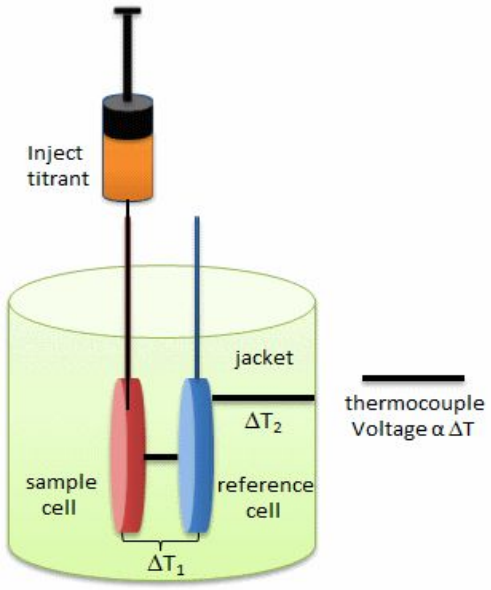

Figure 2-20: Schematic illustration of working principles of isothermal titration calorimetry (ITC). A protein solution is placed in the sample cell (~2 mL volume) and the syringe is filled with a solution of ligand of interest. Titration is performed by slow additions of small portions of the ligand into the protein solution under mixing. Upon binding, the formed ligand/protein complex either releases (exothermic reactions) or absorbs heat (endothermic reaction). The heat changes in the sample cell are detected through temperature (temperature-compensation-mode) or power (power-compensation mode) required to kept constant temperature in the reference cell. These heat changes in the system, both endothermic and exothermic, are detected by power compensation (µcal/sec) of the ITC machine. The most common temperature for data to be recorded at is 25°C (298.15 K).

ITC technique is label-free. The ligand binding is performed in solution and therefore, does not introduce artefacts due to protein immobilization on supporting material that can involve or affect ligand-binding area in protein. ITC can measure binding affinities over 5 log units from ~100 µM to 1 nM that is not easily achieved with other label-free methods (Rajarathnam and

Rosgen 2014). One of the important applications of ITC is the possibility to measure noncatalytic binding of macromolecules that otherwise is hard to detect and evaluate with other techniques. In principle, any binding reaction (e.g., protein-ligand, protein-protein, protein-nucleic acid, nucleic-acid-drug interactions) or physical change (e.g. folding/unfolding of the protein) that is accompanied by a change in enthalpy can be measured by ITC. Moreover, ITC allows to work with both, soluble and membrane proteins. The gained valuable insights into the thermodynamic signatures of ligand binding can be used for drug discovery studies (Ladbury et al. 2010, Ruhmann et al. 2015).

Analysis of the ITC data gives ΔH and $\Delta G = RT\ln K_a$ values. The $-T\Delta S$ parameter is obtained from thermodynamic equation $\Delta G = \Delta H - T\Delta S$ (Leavitt and Freire 2001). In general, prior knowledge from the literature or other biochemical assays on the binding affinities and/or stoichiometry of binding is useful and desirable prior to ITC experiments. Otherwise, only proper evaluation of the concentrations of the two components (e.g., ligand and protein) allows the stoichiometry of the binding reaction (n) to be determined (Wiseman et al. 1989, O'Brien 2001). If ITC titration is conducted at least at two temperatures (T_1 and T_2) and at constant pressure, the change in another fundamental thermodynamic parameter, heat capacity ΔC_p, can be determined:

$$\mathbf{\Delta C_p = \Delta H_{T1} - \Delta H_{T2} / T_2 - T_1}$$

ΔC_p is characteristic for a particular biomolecular interaction upon complex formation. It describes the temperature dependence of the enthalpy change, which is strongly linked to changes in both biomolecular and solvent hydrogen bonding. Since temperature (T) is held constant during ITC experiment, the free energy (ΔG) of the binding reaction can be determined by:

$$\mathbf{\Delta G = RT\ln K_d = -RT\ln K_a}$$

Meaning, binding affinity, K_a, is dictated by the Gibbs energy of binding (ΔG):

$$\mathbf{K_a = e^{-\Delta G RT}}$$

However, ΔG is the sum of two different terms:

$$\mathbf{\Delta G = \Delta H - T\Delta S}$$

A spontaneous binding process must have a negative ΔG (ΔG < 0), and ΔG will become more negative with tighter binding of the ligand. Consequently, extremely high affinity is only achieved when both enthalpy (ΔH) and entropy (ΔS) contribute favorably to the binding (Carbonell and Freire 2005, Ohtaka and Freire 2005, Ruben et al. 2006, Sarver et al. 2007, Freire 2008). It must also be remembered that there is no correlation between enthalpy change and binding affinity; if the binding is predominantly entropically driven, the signal could be weak even for high-affinity interactions, and easily misinterpreted as lack of binding.

Many binding reactions are accompanied by a change in protonation state of either protein or ligand. In that case, the buffer will respond by taking up or releasing protons, resulting in buffer-dependent enthalpy change that must be either added or subtracted from the experimentally observed heat release. The relationship is given by the following equation:

$$\mathbf{\Delta H_{ITC} = \Delta H_{binding} + n\Delta H_{ionization}}$$

Where ΔH_{ITC} is the experimental observed enthalpy, $\Delta H_{binding}$ is the buffer-independent binding enthalpy, $\Delta H_{ionization}$ is the ionization enthalpy of the buffer, and *n* is the number of protons transferred during binding. Thus, it can be helpful to use alternative buffers with large protonation enthalpies of opposite sign. Buffer ionization enthalpies are available in the literature (Fukada and Takahashi 1998).

Up to now, number of works demonstrated that ITC can be used in particularly to study the interaction of the proteins with metals:

- ITC was successfully implemented in the studies of the thermodynamics of Ca^{2+} and Mg^{2+} (as well as competitive Ca^{2+} versus Mg^{2+}) binding to the small soluble calcium binding protein (CaBP, 14.7 kDa) from *Entamoeba histolytica* (Gopal et al. 1997);
- ITC was used to study interaction of Zn^{2+}, Ni^{2+}, Co^{2+}, Mn^{2+}, and Cd^{2+} with *Mycobacterium tuberculosis* recA intein and its mutants (Zhang et al. 2009);

- ITC was used to study Zn^{2+} displacement by Cu^{2+} in catalytic domain of A_0, lytic polysaccharide mono-oxygenase (LPMOs) of family AA11 (Hemsworth et al. 2014);
- ITC was used to quantify the Fe^{3+} affinity of the GmPM1 and GmPM9 soluble proteins, members of LEA4 (late embryogenesis abundant prateins) plant proteins (Liu et al. 2011).

However, most of the studied interactions belong to the soluble proteins or domains. Several complications exist in studying membrane proteins: Protein has to be produced and purified in sufficient amount (~20 μM of protein is recommended to use for initial screening;); it has to be stable over time (days); the proper detergents have to be chosen. For the case of *I. tartaricus* c-ring, 0.2 mg of protein is needed to get nice thermograms. From this point of view, the calorimetric studies of the membrane protein interactions are feasible but challenging to perform.

2.8.2. Use of ITC technique for assessing Na^+ binding affinity and selectivity of *I. tartaricus* c-ring

Recently ITC was successfully implemented for measuring high Na^+ binding affinity of the isolated *I. tartaricus* wild-type c-ring (Leone, et al. 2015). Established protocol allows for accurate and reproducible assessment of both, the relative to pH and absolute Na^+ binding affinities of *I. tartaricus* wild-typec-ring (**Figure 2-21** and **2-22**). The high Na^+ against H^+ competition for binding to *I. tartaricus* c-ring within selected pH range 5.5-7.5 was observed. In former studies, the cation competition for binding to *I. tartaricus* c-ring was observed by DCCD modification experiments with target Glu65 residue (von Ballmoos and Dimroth 2007, Krah, et al. 2010).

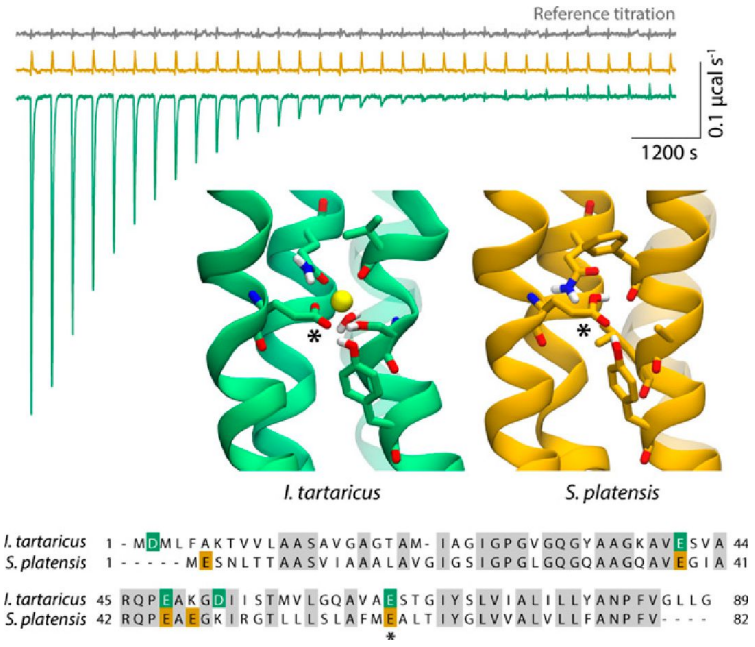

Figure 2-21: ITC measurements of Na^+ binding to natively produced *I. tartaricus* wild-type c-ring (Figure is taken from (Leone, et al. 2015)). Figure demonstrates NaCl ITC titration signals in respect to known sequence and structure of the c-rings of *I. tartaricus* and *S. platensis* ATP synthases. For the case of Na^+-selective c-ring of *I. tartaricus*, clear signals of Na^+ binding were detected (shown in green). Anticipated results demonstrate no Na^+ binding signals when H^+-selective c-ring from *S. platensis* was used as a reference (depicted in yellow).

A novel approach to evaluate the absolute binding constants for Na^+ and H^+ was offered based on the dependency of Na^+ affinities on H^+ concentrations (**Figure 2-22**) (Leone et al., 2015). In this work, the apparent absolute binding affinity to Na^+ = 290 µM and apparent absolute binding affinity to H^+ = 280 nM for the *I. tartaricus* wild-type c-ring solubilised in OG were calculated.

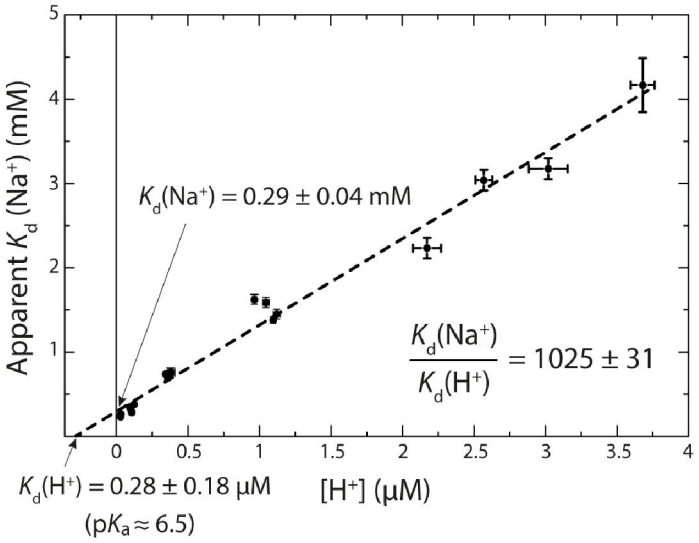

Figure 2-22: Extrapolation of absolute binding constants for Na^+ and H^+ binding to the *I. tartaricus* wild-type c-ring (Figure is taken from (Leone, et al. 2015)). The plot shows the approach to dissect the set of pH-dependent apparent Na^+ binding affinities into separated absolute binding affinity for Na^+ and absolute binding affinity for H^+. To do so, the set of ITC measurements was transformed into linear dependency of Na^+ dissociation constants as a function of H^+ concentrations. Further evaluation implied to extrapolate the K_d (Na^+) at zero concentration of H^+ (K_d (Na^+) = y-axis intercept at [H^+] = 0) and the K_d (H^+) at zero Na^+ concentration (K_d (H^+) = -x-axis intercept at [Na^+] = 0). Only extrapolation of the data can answer on Na^+ binding properties in H^+-free and Na^+-free conditions, that otherwise are not achievable in experiment.

I. tartaricus c-ring was shown to be very stable in harsh detergents (e.g., sodium dodecyl sulphate, SDS and Lauroylsarcosine, LS) within pH range 4.5-11.5 at low Na^+ concentration and in respect to high temperatures (Meier and Dimroth 2002). (Leone, et al. 2015) additionally demonstrated that *I. tartaricus* wild-type c-ring is stable at RT over reasonable time (days) at Na^+-free conditions ([Na^+] << 10 µM) after long dialysis procedure in 1% octyl β-D-glucopyranoside (OG) and different buffers. High stability of the c-ring sample in detergent solution together with high Na^+ binding affinity that can be reproducibly recorded over broad pH range allows to implement ITC in evaluation of many parameters of Na^+ and H^+ binding, namely:

- Measure relative to pH (apparent) dissociation constants for Na^+ binding to c-ring (shown

by (Leone, et al. 2015));

- Extrapolate absolute(maximal) binding constants for Na^+ binding and H^+ binding to c-ring (shown by (Leone, et al. 2015));
- Evaluate/verify stoichiometry of Na^+ binding to c-ring;
- Evaluate/verify protonation state of titratable groups in the c-ring at selected pH (protonation state of conserved Glu65 carboxyl group was evaluated in this thesis);
- Study competitive binding of different cations (shown for Na^+, H^+ and Li^+ competitive binding to c-ring, in this thesis);
- Make complete thermodynamic profile of Na^+ and Li^+ binding to c-ring (this thesis);
- Study the effect of mutations on parameters of Na^+, Li^+ and H^+ binding to the c-ring (this thesis);
- Study effect of temperature on parameters of cation binding (heat capacity parameter, ΔC_p);
- Study effect of microenvironment on thermodynamic parameters of cation binding to c-ring (this thesis)

2.9. Principles and application of *N,N′*-dicyclohexylcarbodiimide (DCCD) modification of ionisable residues

Carbodiimides (CDI) are classified as zero-length crosslinking agents used to mediate the formation of amide linkages between carboxyl and amine groups (Hermanson 1996). Since 1960-s, cross-linking of carboxyl and amino groups by carbodiimides has been used to modify proteins covalently in order to study the structure and function of enzymes and proteins in biological membranes and cytoplasm (Hoare and Koshland 1967, Frater 1971, Pennington and Fisher 1981). Carbodiimides react only with protonated carboxyl groups (Khorana 1953, Hoare and Koshland 1967). The reaction takes place in two steps. At the initial rapid step, addition of the carboxyl groups to the carbodiimides provides formation of O-acylisourea. At the second step, the O-acylisourea subsequently forms N-acylurea (Figure 2-23).

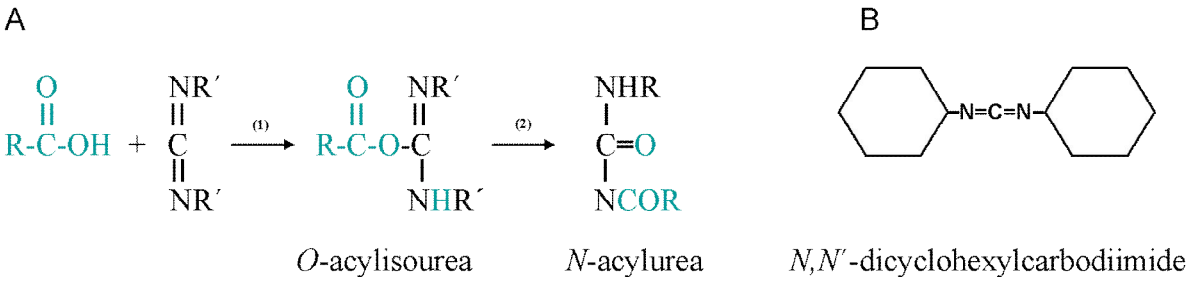

Figure 2-23: Principles of carbodiimides modification. (A) Two-step reaction of carboxylic acids with carboodiimides (adapted from (Azzi et al. 1984, Joullie and Lassen 2010)). **1** - First rapid step of the addition of the carboxyl group to the carbodiimide ends with formation of unstable intermediate – *O*-acylisourea (in case of DCCD - dicyclohexyl-O-acylurea, DCOU). **2** - Further rearrangements lead to a formation of the stable end product *N*-acylurea (in case of DCCD - dicyclohexyl-N-acylurea, DCNU). **(B)** Chemical structure of DCCD molecule.

Water-insoluble carbodiimides (in particularly *N,N′*-dicyxlohexylcarbodiimid, DCCD) are widely useful for site-specific modification of carboxyl groups (Hassinen and Vuokila 1993). DCCD is a small 206 Da hydrophobic molecule that modifies carboxyl groups in hydrophobic environment. DCCD modification was also proposed to be a two-step reaction. At first step, unstable intermediate is formed – dicyclohexyl-O-acylurea (DCOU). At the next step rearrangement of the residues leads to a formation of a more stable dicyclohexyl-N-acylurea (DCNU) (Azzi, et al. 1984). Therefore, binding site forming DCNU structure is not able to accommodate anymore H^+ or Na^+ as the acidic Glu/Asp is neutralized. DCCD was used for modification of different protein complexes, such as cytochrome bc1 complex (Beattie and Clejan 1982, Lenaz et al. 1982, Nalecz et al. 1986) and complex I (NDH-1) from enterobacterium *Klebsiella pneumoniae* (Vgenopoulou et al. 2006). DCCD was also use to study modification of thrombin (Chan et al. 1988, Borders et al. 1989).

DCCD turned out to interact covalently thus inhibiting a number of enzymes involved in H^+ translocation across biological membranes. What makes DCCD a very unusual cross-linker is its exceedingly hydrophobic nature combined with its reactivity. With these properties and specificities carbodiimides have become a sensitive probe of H^+ translocating enzymes (Solioz 1984, Lichtenberger et al. 2000).

DCCD is known to penetrate into the inner mitochondrial membrane phospholipid bilayer and to

selectively bind to protonated carboxylic groups of the ion-binding site in the middle of the second α-helix in the c-subunit (Sebald et al. 1980) leading to irreversible F_o inhibition (Nalecz, et al. 1986). DCCD was shown to modify conserved carboxyl acid (Glu/Asp) involved in functional Na^+ and/or H^+ binding sites in ATP synthases (Fillingame 1975, Negrin et al. 1980, Sebald, et al. 1980). DCCD binds to the c-ring in a way that structurally mimics the arginine residue in the a-subunit (Kluge and Dimroth 1993, Meier et al., 2003, Pogoryelov, et al. 2009, Mizutani et al. 2011). The distinct feature of Na^+ in Na^+-selective c-rings is the ability to protect Glu/Asp carboxyl group against DCCD modification. This is a case for both, F-type and V-type Na^+-specific c(K)-rings (Kluge and Dimroth 1993, Murata et al. 1999, Murata et al. 2000, Murata, et al. 2008, Mizutani, et al. 2011). The principles of Glu/Asp modification by DCCD can be used to judge on the ion-specificity of the ATP synthases through clear Na^+ protection effect against DCCD modification observed for Na^+ ion binding sites (Kluge and Dimroth 1993, Meier et al., 2003, von Ballmoos and Dimroth 2007, Schulz, et al. 2013). For this case, MALDI-MS technique serves for comparative evaluation of the DCCD modification reaction by detecting precisely the masses of not modified and DCCD-modified c-subunits (+ 206 Da) at different pH and NaCl conditions (Preiss, et al. 2014). This principle allows precise evaluation of the ratio between DCCD-labelled and DCCD-unlabelled probes and thereby investigates the effect that different factors (salts, pH, solvents and mutations) may impose.

The covalent irreversible c-ring modification by DCCD also inhibits ATP synthase activity for well-coupled F_1F_o complexes (Kluge and Dimroth 1993; Hermolin and Fillingame, 1989). In this prospective, DCCD was widely investigated as an inhibitor of rotary ATP synthases (Toei and Noji 2013). One molecule of DCCD per one F_o domain (= one DCCD-modified c-subunit per one c-oligomer) is enough to inhibit rotation of F_o and thereby inhibit ATP synthase coupling (Hermolin and Fillingame 1989, Toei and Noji 2013). The potential mechanism of inhibition is that once the c-ring is modified by DCCD, its rotation is locked due to the steric hindrance of the protruding DCCD and a subunit (Toei and Noji 2013).

However, it was found that there is also a secondary DCCD binding site on the F_1 subunit (Pougeois et al. 1979). Therefore, at high concentrations (> 300 μM) DCCD may also inhibit F_1 domain. However, this inhibition is less specific and is highly dependent on presence of bivalent cations, e.g. DCCD binds to Glu residue in F_1 domain (e.g., $\beta_{DP}Glu^{199}$) at Mg^{2+}-free conditions

(Yoshida and Allison 1983)(Gibbons et al,. 2000). Therefore, the membrane-embedded F_o sector is recognized as the primary target of the inhibitor.

With respect to ATP synthase, the covalent DCCD modification can be used for:

- To inhibit rotation of F_o domain in ATP synthase (Panke et al., 2000; Tanabe et al., 2001);
- To assess assembling of F_1 and F_o domains in ATP synthase (Hermolin and Fillingame, 1989);
- To test the functionality of the ion-binding site in the c-ring (Mayer et al., 2012);
- To judge on competitive binding of Na^+ and H^+ to the c-rings (Murata, et al. 2008);
- To evaluate the pKa of titratable groups in the c-ring (Murata, et al. 1999, Meier et al., 2003);
- To assess the effect of mutations on Na^+ and/or H^+ affinity of c-ring (von Ballmoos and Dimroth 2007).

One of the drawbacks of using DCCD modification assay is the nonequilibrium covalent nature of DCCD modification reaction that implies verification of estimated pKa values of Glu/Asp carboxyl groups by other techniques. In general, DCCD modification assay is rather comparative than one given absolute values. Moreover, it was not studied yet whether the differences in the reaction conditions such as detergent may affect the protonation state of Glu/Asp residues in the c-rings and accordingly DCCD modification rates.

2.10. Free energy change of deprotonation and the pKa value of carboxyl group

One of the means of describing the proton interaction with Glu/Asp groups depending on their chemical oscillation is comparing the free energies of Glu/Asp carboxyl group deprotonation. The experimentally estimated pKa values of the Glu/Asp carboxyl groups can be re-calculated in free energy change of deprotonation.

The experimental pKa values of ionisable groups are related to the free energies of protonation and hence correlate with their proton affinity. The equilibrium constant (K_a) of a deprotonation reaction of titratable groups depends on their free energy. The pH at which the protonation (or

deprotonation) probability is 50% is called pKa or $pK_{1/2}$. The relationship between the standard Gibbs free energy ΔG_{depr} of deprotonation and the pKa of the acid, is given by the equation:

$$\Delta G_{depr} = -RT\ pKa\ \ln 10 = -\ 2.3RT\ pKa$$

The 2.3 prefactor is due to the convention of the natural to decimal logarithms. R is a Gas constant (R = 1.98722 cal/K mol). T is a temperature (T = 298.15 K). The free energy difference of the ionisable groups being protonated or deprotonated at a given pH is given by:

$$\Delta G = -2.3RT\ pKa + 2.3RT\ pH$$

The free energy difference is related to K_a by the following expression:

$$\Delta G = -RT \ln K_a = -2.303\ RT \log K_a = 2.303\ RT\ pKa$$

The actual cost of creating negative charge at the internal positions (free energy of ionization, ΔG_{ion}) can be calculated from the difference between the apparent pKa values and the normal pKa of 4.5 for glutamate in water (Isom et al. 2010):

$$\Delta G_{ion} = 2.303\ RT\ (pKa' - pKa'')$$

Where ΔG_{ion} is a free energy change upon ionization; pKa is the apparent pKa of reprotonation for Glu residue buried in the protein and pKa´´ is a pKa of glutamate in water (standard value of 4.5).

3. Aim of this work

F-type ATP synthases can be divided into two classes with respect to their cation selectivity under physiological conditions: one belonging to H^+-selective and other belonging to Na^+-selective ATP synthases. To date, only little effort has been expended on altering the intact cation selectivity of rotary ATP synthases (Kaim et al., 1997; Kaim and Dimroth 1998; von Ballmoos and Dimroth 2007; Kawano-Kawada et al., 2012). This experimental data indicates that cation binding selectivity of the ATP synthases is defined solely by the ion binding motif in their membrane-embedded rotor c-rings responsible for ion translocation.

The goal of this thesis was to explore the conserved Na^+-binding motif present in the c-ring from *I. tartaricus* ATP synthase, which is common to all Na^+-selective c-rings and defines Na^+ selectivity of ATP synthases. In the past 10-15 years, a variety of three-dimensional high-resolution X-ray structures of c-rings have become available along with methods to modify them by site directed mutagenesis. This opened possibility to rationally mutate selected amino acids in the c-ring and evaluate the contribution to its cation binding properties in a c-ring ion binding site. In the present study the aim was to use the current knowledge on structure of the *Ilyobacter tartaricus* (Meier et al., 2009), *Fusobacterium nucleatum* (Schulz et al., 2013), *Acetobacterium woodii* (Matthies et al., 2014), *Enterococcus hirae* (Murata et al., 2005), *Spirulina platensis* (Pogoryelov et al., 2009) and *Bacillus pseudophirmus* OF4 c-rings (Preiss et al., 2010) to re-design the intact cation selectivity of *I. tartaricus* ATP synthase into exclusive H^+ selectivity. The work intended to obtain a better understanding of the individual roles of coordinating residues for monovalent cation selectivity (Na^+ and H^+) of rotary ATP synthases.

The goal requires methods for *in vitro* identification of even minor changes in cation binding and cation transport-related properties of c-rings. The spectroscopic assays are not suitable for obtaining experimentally the precise K_d values for Na^+ affinity of c-rings due to small size of ligand (Na^+) and very tight binding that required very sensitive detection techniques. Therefore, from the methodological point of view, the aim was to establish method to monitor even small changes in Na^+ and H^+ binding affinities of the c-rings. As such, in this study was tried a combinatorial approach that includes direct characterization of Na^+ binding to c-rings with a help of isothermal titration calorimetry (ITC) and indirect characterization of Na^+ binding to c-rings with a help of ion/DCCD competition assay. Namely, ITC technique was used because it enables

direct measurements of equilibrium constants for Na^+ binding to high-affinity (K_d< 10 μM).At the last step, it was important to check whether the ion affinity and selectivity principles are consistent between biochemical studies with c-rings and functional studies with ATP synthases assembled with corresponding c-rings.

The knowledge of the molecular mechanisms, and in particular, the thermodynamic basis of interactions of Na^+ with the c-ring would aid our understanding of the operation of these remarkable rotary nanomachines. It is important to take into account that genetic variation in ion binding site sequence is a key driver of evolution and re-design of ion selectivity would help to understand the evolution of cation selectivity in rotary ATP synthases. Moreover, the acquired clear understanding of c-ring structure and reaction mechanisms can be further exploited for the engineering of rotary ATP synthases with novel properties.

4. Materials and Methods

4.1. Materials

Luciferase (American firefly) and DNaseI were purchased from Roche Diagnostics GmbH; lipids were from Avanti Polar Lipids, Inc.; Macro-Prep® Ceramic Hydroxyapatite Type I (40 μm) was from Bio-Rad Laboratories, Inc.; Pefabloc® SC-Protease Inhibitor was from Carl Roth GmbH & Co. KG; Polycarbonate membranes from Avestin Inc.; Chelating Sepharose™ Fast Flow was from GE Healthcare Bio-Science AB. All other materials were purchased from Sigma-Aldrich Chemie GmbH, unless otherwise indicated.

4.2. Methods

4.2.1. Cloning of the expression vectors

4.2.1.1. Recombinant DNA techniques

General procedures for cloning and DNA manipulation were performed essentially as described by Sambrook et al. (Sambrook et al. 2001). Site-directed mutagenesis was performed using QuikChange mutagenesis method (Kunkel 1985, Ishii et al. 1998, Li et al. 2008) with QuikChange II site-directed mutagenesis kits (Stratagene) for pt7cIT plasmid harbouring the *atpE* gene encoding the single c-subunit of *I. tartaricus* ATP synthase. The PCR overlap extension method (Ho et al. 1989) was used to introduce the mutations in the *atpIBEFHAGDC* operon encoding full-length *I. tartaricus* ATP synthase on the pITtr5Hisa expression plasmid.

4.2.1.2. Characteristic of pt7cIT and pITtr5Hisa vector plasmids used to clone mutants of *I. tartaricus* c-ring

Two vector plasmids were used for cloning a set of *I. tartaricus* mutant c-rings by site directed mutagenesis: pt7cIT plasmid (Meier and Dimroth 2002, Meier, et al. 2005), which expresses single *atpE* gene encoding c-subunit of *I. tartaricus* ATP synthase and pITtr5Hisa plasmid (Oberfeld 2006, Vorburger et al. 2008), which enables to express entire ATP synthase of *I. tartaricus.*

pt7cIT plasmid is a 2,756 bp plasmid that employs *ampR* gene as a selectable marker, multiple restriction sites (**Figure 4-1**) and allows overexpressing protein under control of T7 promoter system by auto-induction protocol described in corresponding section (section 4.2.2.2).

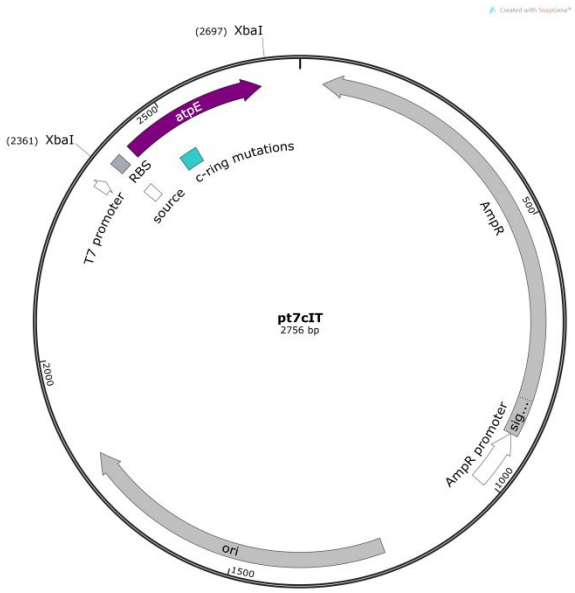

Figure 4-1: pt7cIT vector plasmid (Meier and Dimroth 2002, Meier, et al. 2005)**.** The detailed plasmid map shows the important features of the pt7cIT vector plasmid. pt7cIT plasmid was used for recombinant overexpression of *I. tartaricus* c-ring (*atpE* gene) in the sequence of which were introduced different point mutations.

pItTr5Hisa plasmid is a 11,531 bp plasmid carrying entire *atp* operon (*atpIBEFHAGDC*) of *I. tartaricus* ATP synthase (**Figure 4-2**). The genes of *atpIBEFHAGDC* operon encode assembly subunit i (does not become a part of assembled ATP synthase) and eight subunits that constitute the functional ATP synthase complex: a, c, b, δ, α, γ, β and ε. The cloned pltTr5Hisa plasmid was used to produce the *I. tartaricus* ATP synthase in *E. coli* cells. The introduced modifications are listed in **Table 4-1**.

Table 4-1: Modifications of pITtr5Hisa plasmid

ATP synthase subunit	**Encoding gene**	**Genetic manipulation**
i,b, δ, α, γ, β, ε	*atpI, atpF, atpH, atpA, atpG, atpD, atpC*	No
a	*atpB*	N-His_{12}-tag
c	*atpE*	point mutations

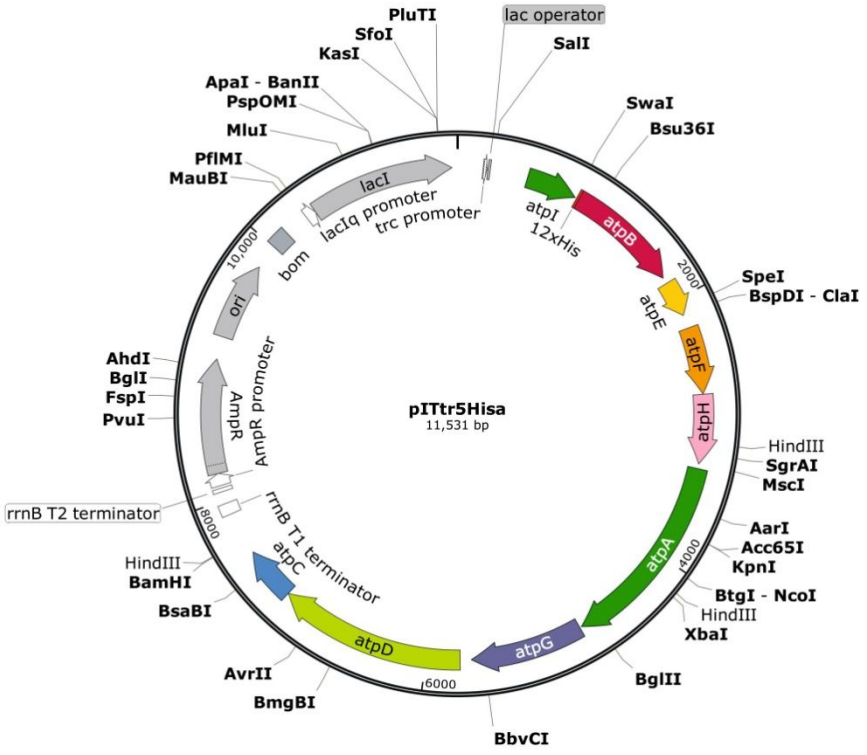

Figure 4-2: pITtr5Hisa vector plasmid (Oberfeld 2006, Vorburger et al. 2008)**.** The detailed plasmid map of pITtr55Hisa plasmid used for recombinant expression of ATP synthase from *I. tartaricus*. Map illustrates genes order and all single restriction sites (in bold). Sites used for cloning: *Eco81*I/*Bsu15*I sites for restriction digestion and subsequent ligation of the DNA fragments and *Hind*III/*Sal*I for test restriction of the plasmid. N-termini of a-subunit was modified with 12xHis for further metal affinity purification step.

4.2.1.3. Genetic manipulations with pt7cIT and pltTr5Hisa vector plasmids

Two approaches were used to clone the *atpE* gene encoding c-subunit of *I. tartaricus* c-ring: For the case of smaller pt7cIT plasmid, intended point mutations were introduced in the sequence of *I. tartaricus* c-subunit by QuickChange site-directed mutagenesis method (Kunkel 1985, Ishii, et al. 1998, Li, et al. 2008). For the case of pITtr5Hisa plasmid, the same nucleotide change(s) in the sequence of c-subunit were conferred by PCR Overlap method as described below.

4.2.1.4. PCR amplification of pt7cIT plasmid

The vector plasmid was cloned by PCR amplification of pt7cIT plasmid with a use of specific mutagenic primers. The proof-reading thermostable polymerase, *Pfu* (Finnzyme´ Phusion™ High-Fidelity), was used for the synthesis of mutant pt7cIT plasmids. The conditions for the synthesis of the mutant DNA strand were based on the annealing temperature of the used primers (60-63°C) and length of the synthesized fragment (~ 3 kbp). Primers used for the site-directed mutagenesis were designed with 13-17 flanking residues around mutation point. Overall size of the primers was in the range of 27-34 base-pairs and melting temperatures higher than 55°C (**Table 4-2**). The conditions used for PCR are listed in **Table 4-3** (in a total volume of 50 µL):

Table 4-2: List of mutagenic primers used for site-directed mutagenesis

Mutation	Sequence of mutagenic primer, →
T67I	5´-CGTTGCGGAATCAATAGGTATCTACTC-3´
S66A/T67I	5´-CGTTGCGGAAGCAATAGGTATCTACTC-3´
S66A/Y70F	5´-GTTGCGGAAGCAACAGGTATCTTCTCACTAG-3´
T67I/Y70F	5´-GCGGAATCAATAGGTATCTTCTCACTAGTTATTG-3´
T67A	5´-CGTTGCGGAATCAGCAGGTATCTACTCACTAG-3´
T67L	5´-CGTTGCGGAATCCCTAGGTATCTACTCAC-3´
Q32A	5´-CCAGGGGTAGGAGCAGGTTACGCAGCTG-3´
G25S	5´-GCAATGATCGCGAGCATTGGACCAG-3´
G25A	5´-GCAATGATCGCAGCTATTGGACCAGG-3´
E65D	5´-GGACAAGCCGTTGCGGATTCAACAGGTATCTACTC-3´
S66A	5´-CGTTGCGGAAGCAACAGGTATCTACTC-3´
T67S	5´-CGTTGCGGAATCATCAGGTATCTACTCACTAG-3´
T67G	5´-CGTTGCGGAATCAGGAGGTATCTACTCACTAG-3´
T67Q	5´-CGTTGCGGAATCACAAGGTATCTACTCACTAG-3´
T67M	5´-CGTTGCGGAATCAATGGGTATCTACTCACTAG-3´
Y70F	5´-GCGGAATCAACAGGTATCTTCTCACTAGTTA-´3

Table 4-3: PCR amplification of pt7cIT plasmid

Quick change method, PCR mixture:	PCR program:
50 ng template DNA 4 pmol forward mutagenic primer 4 pmol reverse complement mutagenic primer 1x thermostable polymerase buffer 200 µmol each dNTP 1 U *Pfu* polymerase	1 cycle: initial denaturation for 3 min at 96°C 30 cycles: denaturation for 1 min at 96°C; annealing for 0.5 min at 60-63°C, extension for 1 min per 1 kbp at 68°C 1 cycle: final extension for 20 min at 68°C

4.2.1.5. PCR amplification of DNA fragments from pltTr5Hisa plasmid

Intended PCR fragments were obtained after two rounds of PCR amplification: PCR I and PCR II (details in **Table 4-4**). *Pfu* proof-reading thermostable polymerases (Thermo Scientific Phusion High-Fidelity) was used for the synthesis of mutant fragments. The conditions for the synthesis of mutant DNA strands were based on the annealing temperature of the used primers and length of the synthesized fragment. The conditions used for PCR are as follows, in a total volume of 50 µL:

Table 4-4: PCR amplification of DNA fragments from pltTr5Hisa plasmid

PCR I mixture:	PCR II mixture:
50 ng template DNA 4 pmol flanking primer (Iti67→ or ItΔ44←) 4 pmol mutagenic primer (← or →) 1x thermostable polymerase buffer 200 µmol each dNTPs 2.5 U *Pfu* polymerase	50 ng of fragment 1 + 50 ng of fragment 2 DNA 4 pmol forward flanking primer (Iti67→) 4 pmol reverse flanking primer (ItΔ44←) 1x thermostable polymerase buffer 200 µmol each dNTPs 2.5 U *Pfu* polymerase
PCR program:	
1 cycle: initial denaturation for 2 min at 96°C 30 cycles: denaturation for 1 min at 96°C; annealing for 0.5 min at 60-63°C; extension for 1 min per 1 kb at 72°C 1 cycle: final extension for 20 min at 72°C	

After PCR amplification, all probes were centrifuged (13,000 *g* for 3 min) and subsequently purified with a use of PCR purification kit from Seqlab. Fragments were eluted in 20 µL final volume. Purified probes were subsequently digested with *Dpn*I enzyme in order to remove template DNA remaining in the PCR reaction mixtures. *Dpn*I restriction was performed for 6 hours at 37°C according to standard recommendation of the manufacturer (New England BioLabs) in 50 µL final volume. Following the restriction, the thermal inactivation of the enzyme was performed at 80°C for 15 min.

The resulting DNA products from pt7cIT amplification (10-20 ng) were used to transform *E. coli* BL21 (DE3) expression strain according to standard procedure (see below section 4.2.1.10).

The resulting DNA fragments from pltTr5Hisa amplification (10-20 ng) were used for subsequent restriction digestion and ligation as it is described below.

4.2.1.6. Restriction digest and ligation of PCR amplified DNA fragments and pITtr5Hisa vector plasmid

Obtained PCR fragments and intact pITtr5Hisa vector plasmid were subjected to restriction digest for 1-6 hour at 37°C with *Eco81*I and *Bsu15*I restriction enzymes, following the protocol provided by the manufacturer (Fermentas). Digested fragments were loaded on agarose gel and run for 1 hour at 100 V in 1x TAE running buffer (40 mM Tris, 20 mM Acetic acid and 1 mM EDTA, pH 8.2). DNA fragments < 4 kbp were run in 1% agarose gel. Larger vector fragments > 10 kbp were run in 0.75 % agarose gel. After staining with ethidium bromide and subsequent UV visualization, the bands that correspond to the size of restricted fragments were excised from agarose gel and extracted with QIAquick gel extraction kit (QIAGEN). The final concentration of DNA fragments after extraction was 10-40 ng/µL.

A gel-purified DNA fragments were ligated with T4 DNA ligase into the corresponding site of prepared vector on a basis of pItTr5Hisa plasmid. Ligation was performed for 1 hour at RT in presence of 20 % PEG-4000, 90 ng of target vector and 50 ng of insert fragments. Ligation was done with T4 DNA ligase from Fermentas in 20 µL volume. Afterwards, 1-2 µL of ligation mixture was used for transformation in *E. coli* DH5α cells. The orientation of the inserted fragment was determined by *Hind*III/*Sal*I restriction enzyme analysis.

4.2.1.7. *Xba*I test restriction of cloned pt7cIT plasmid

The plasmid DNA in the positive clones after transformation in *E. coli* BL21 cells was extracted and linearized with single cutter restriction enzyme – *Xba*I (recognition site for *Xba*I enzyme has position 2361:2366 on a plasmid). *Xba*I test restriction was done for 1 hour at 37°C according to standard recommendations of the manufacturer (New England BioLabs) in 50 µL final volume. Aliquots of the linearized plasmids were run for 1 hour in 1% agarose gel. Plasmids that showed correct 2.7 kbp size were sequenced with T7_sense primer (5´-TAATACGACTCACTATAGGG-3´) and glycerol stocks of correct constructs were prepared and used for large-scale expression/production of the protein.

4.2.1.8. *Hind*III/*Sal*I test restriction of cloned pItTr5Hisa plasmid:

The plasmid DNA in the positive clones after transformation in *E. coli* DH5α cells was extracted. pltTr5Hisa plasmid harbouring the inserted PCR fragments was test restricted to check the correctness of restriction fragment length. Restriction with a combination of *Hind*III/*Sal*I enzymes results in fragmentation of an intact plasmid into 4 fragments that roughs to 1042, 2843, 3531 and 4124 bp. In case of correct test-fragmentation of the plasmid, the appropriate probe was sent for sequencing with series of primers covering the *atp* operon (**Table 4-5**). DNA sequencing was performed at the MicroSynth (former SeqLab, Goettingen, Germany). For the case, the sequence confirmed introduction of only intended mutations, the appropriate plasmids (10-50 ng) were used for further re-transformation in *E. coli* expression DK8 strain.

Table 4-5: Sequencing primers for *atp* operon of *I. tartaricus* ATP synthase

Subunit location	Primer	Sequence of primer
Subunit i, Iti160	←	5′-GGTCACAGTTCTCTGAAAGG-3′
Subunit a, Itb1	←	5′-GGAAGAGCATAACGCACC-3′
Subunit a, Ita610	→	5′-CCCTTATGTTTCCAATTAACC-3′
Subunit b, Itb59	→	5′-GAGGTAGACGACTTGGCACC-3′
Subunit δ, Itδ479	←	5′-TAGACGGAAGCGTGAGAAGG-3′
Subunit α, Itα818	→	5′-GTAATTTCAATTACAGACGG-3′
Subunit γ, Itγ110	→	5′-GCTCTTGTAAATCAGTCAAAACC-3′
Subunit β, Itβ1	←	5′-CTGCCTCCTCTTCAATAAGG-3′

4.2.1.9. Transformation of the *E. coli* DK8 competent cells

E. coli DK8 highly competent cells were prepared using the low temperature method: Preparation is a modification of old protocol (Gene 1990, 96:23) as it is described in (Ausubel et al., 2002) and transformed with the constructs described above. Plasmid DNA from the transformants was prepared and the DNA sequenced using T7_sense primer (5′-TAATACGACTCACTATAGGG-3′). *Sal*I/*Hin*dIII fragments from the above-mentioned constructs were checked again for correct restriction size.

4.2.1.10. Transformation of the *E. coli* BL21 competent cells

Competent BL21 cells were prepared by $CaCl_2$ method as it is described in (Ausubel et al. 2002). 1 µl of plasmid (10-20 ng) was used for standard transformation. After transformation 50-250 µl volume of cells was spread on freshly prepared LB agar plates containing 100 µg/ml ampicillin or carbenicillin and incubated overnight at 37°C. Grown cultures from obtained single colonies were used for preparing the glycerol stacks.

4.2.1.11. Preparation of the glycerol stocks

10 mL of LB media was inoculated with a single colony from a recent (1–2-day) transformation of $CaCl_2$-treated (or low temperature method grown), frozen competent cells and grown for 8 hours at 37°C at 250 rpm. 1 mL of this culture was mixed with 1 mL of autoclaved 100% glycerol and stored at -80°C.

4.2.1.12. Obtained constructs for the mutants of *I. tartaricus* c-ring

Table 4-6: List of cloned constructs

c-ring mutants cloned in pt7cIT plasmid	T67I, S66A/T67I, S66A/Y70F, T67I/Y70F, T67A, T67L, Q32A, G25S, G25A, E65D, S66A, T67S, T67G, T67Q, T67M, Q32A/Y70F, Y70F
c-ring mutants cloned in pltTr5Hisa plasmid	S66A/Y70F, Q32A, G25S, G25A, E65D, S66A, T67S, T67G, T67Q, T67M, Q32A/Y70F, Y70F

In total 18 mutations of the ion binding site and its close surrounding were introduced on a basis of pt7cIT plasmid. Only 13 of these mutations were further introduced in a sequence of pltTr5Hisa plasmid (**Table 4-6**).

4.2.2. *E. coli* recombinant protein expression by auto-induction

4.2.2.1. Strains used for protein expression

Different *E. coli* expression strains were used depending on used expression vector (**Table 4-7**). For the case of pltTr5Hisa expression vector, production of *I. tartaricus* ATP synthase was done in three different *E. coli* expression strains. Among them, *E. coli* DK8 (*Δatp*) strain (Klionsky et al., 1984) has an advantage over others of lacking in chromosome its own host *E. coli* ATP synthase and therefore, allowed expressing *I. tartaricus* ATP synthase without risk of cross

contamination. For the case of pt7cIT expression vector, protein expression was done in commercially available *E. coli* strains: BL21 (DE3) and its derivatives.

Table 4-7: List of *E. coli* strains used for protein overexpression

Strains for c-ring expression	**Genotype**	**Source**
E. coli BL21 (DE3) (Grodberg and Dunn 1988)	F^-ompT gal dcm $hsdS_B$ (r_B^- m_B^-) (DE3)	Stratagene
E. coli Rosetta 2 (DE3) (Novy et al. 2001)	derived from C41 (DE3)	Novagen
Strains for ATP-synthase expression	**Genotype**	**Source**
E. coli C41 (DE3) (Miroux and Walker 1996); (Dumon-Seignovert et al. 2004)	derived from BL21 (DE3)	Novagen
E. coli C43 (DE3) (Miroux and Walker, 1996); (Dumon-Seignovert et al., 2004)	derived from C41 (DE3)	Novagen
E. coli DK8 (Klionsky et al. 1984)	derived from K-12	Novagen

4.2.2.2. Recombinant expression of the protein

Pre-cultures: Overnight cultures (LB medium) were inoculated with a glycerol stock culture. Pre-cultures were cultivated at 37°C in 20 mL media in presence of 100 µg/ml ampicillin with intensive shaking (250 rpm). After 8 hours, pre-cultures were checked spectrophotometrically for optical density. For the case of *E. coli* DK8 cells carrying pltTr5His constructs, low OD_{600} pre-cultures (0.2-0.3) were used for inoculation of large cultures in amount not exceeding 0.2% of total expression volume. For the case of *E. coli* BL21 strain, carrying pt7cIT constructs, larger volumes of inoculated pre-culture were used (1% instead of 0.2%).

I. tartaricus ATP synthase was expressed in *E. coli* DK8 cells either by auto-induction (Studier 2005, 2014) or by 1 mM isopropyl-β-D-thiogalactopyranoside (IPTG) induction at OD_{600} = 0.5-

0.6. Time of the expression was adjusted accordingly to signals from performed western blot analysis against N-His_{12}-tagged a-subunit. Thus, samples (disrupted cells and extracted membranes) were separated by SDS-PAGE and transferred to polyvinylidene difluoride (PVDF) membranes, and immunoblotting was performed using anti-c-subunit and anti-his antibodies. In case of the low yields for ATP synthase production, the optimization of the expression was done. One of the step optimization included introduction of the long cold shock step during cell growth (details below).

Large cultures: Expression of mutant variants from pT7cIT-derived plasmids was done in BL21 strain of *E. coli* in a manner similar to that for DK8 strain. Large cell cultures from transformed *E. coli* expression strains were grown at 37°C in 2-liter 1x ZY medium (**Table 4-8**) as it was described elsewhere (Studier, 2005) with some modifications (see below) and supplemented with 100 μg/ml ampicillin.

Table 4-8: Composition of 1x ZY auto-induction medium

Compound for each 2-L medium	**Final concentrations**
1950 mL ZY	1 % bacto tryptote; 0.5 % yeast extract
40 mL 50x M	25 mM Na_2HPO_4; 25 mM KH_2PO_4; 50 mM NH_4Cl; 5 mM Na_2SO_4
40 mL 50x 5052	0.5 % glycerol; 0.05 % glucose; 0.2 % α-lactose
2 mL 1 M $MgSO_4$	2 mM $MgSO_4$
0.4 mL 1000x trace elements mix	0.2x trace elements

For large-scale production (approximately 10-15 mg of protein), six-twelve 5-liter Erlenmeyer flasks with baffles containing 1 Liter each of 2x auto-induction medium (2x YZ; 100 μg/ml ampicillin) were taken. Separately 900 mL of autoclaved MilliPore-filtered water was used to dissolve trace elements (0.2 % of total volume). Only after this step 2x auto-induction media was diluted twice with water and supplemented with remaining 50x M, 50x 5052 and $MgSO_4$ buffers. Media with additives was inoculated with 1 mL (1:2000 final dilution) of an overnight pre-culture of the host expression strain *E. coli* DK8 (*Δatp*) transformed with the pItTr5Hisa

construct or 5 mL (5:2000 final dilution) of an overnight pre-culture of the host expression strain *E. coli* BL21 transformed with the pt7cIT construct. The cultures were grown overnight at 37°C to OD ~ 2-2.5 at 600 nm in a rotary shaking incubator. Expression was held at 37°C for 14 hours at 130 rpm. After expression, cells were harvested and either kept frozen at -80°C, either used for further membrane preparation and protein extraction.

Induction of protein expression by cold shock: Above described protocol for protein expression was modified in order to increase production of less stable proteins. Initially, cultures in 12x 5-liter Erlenmeyer flasks with baffles were grown overnight (14 hours) at 30°C and rotation speed of 130 rpm. Afterwards, cultures were subjected to 4-6 hours of cold shock (4°C) and back expressed with vigorous shaking at elevated temperature (37°C) and rotation speed of 130 rpm. Cells after expression were collected and immediately used for membranes preparation and subsequent protein extraction. No freezing steps were used at any of stages.

4.2.2.3. Expression of γ_{His}/ε complex

γ_{His}/ε complex cloned was expressed overnight for 14 hours at 30°C and 150 rpm in auto-induction medium. 4x 5-liter Schikane-type Erlenmeyer flasks with low volume of media (0.5L) were used to promote aeration and produce 75-100 mg of γ_{His}/ε complex.

4.2.3. Extraction and purification of wild-type and mutant forms of ATP synthase from *E. coli* DK8 pItTr5Hisa cells

The cells from 24 L of culture were pelleted by centrifugation (10,000 *g*, 20 min, 4°C, Beckman J6-MI centrifuge adapted with 1-liter centrifuge bottles) and resuspended in ice-cold Buffer 1 (**Table 4-9**). 50 μg DNase I (wt/vol) and 0.5 mM Pefabloc® SC-Protease Inhibitor were added shortly before cell disruption. The cells were passed twice through a French pressure cell at 16,000 psi and constantly kept at 4°C. After low-speed centrifugation (15,500 *g*, 35 min, 4°C) non-broken cells were removed and the supernatant was ultracentrifugated at 250,000 *g* for 1 hour at 4°C using a Beckman Avanti™ J-30 I ultracentrifuge. The membranes were next solubilized for 35 min at 4°C with gentle stirring in Buffer 2. The solubilizate was collected

again by ultracentrifugation, supplemented by 45 mM $MgCl_2$ and the protein was precipitated by adding 12.5% (wt/vol) PEG-6000.After 15 min of vigorous stirring on ice, samples were centrifuged for 30 min at 130,000 *g*, 4°C. The protein pellet contained the ATP synthase and was resolved in 35 mL (10 mL buffer for each gram of wet pellet) Buffer 3. To remove undissolved material the slurry was filtrated through a 0.2 µM sterile non-pyrogenic cellulose filter (Sarstedt AG & Co, Numbrecht, Germany) and supplemented with 0.01% (wt/vol) of *E. coli* polar lipids (EPL).

Table 4-9: Composition of Buffers used for protein extraction

Buffer	**Final concentrations**
Buffer 1 (*E. coli* DK8 cell resuspension)	50 mM K_2HPO_4/KH_2PO_4 pH 7.0; 100 mM KCl; 5 mM $MgCl_2$; 5% glycerol (vol/vol)
Buffer 2 (membrane solubilisation)	50 mM K_2HPO_4/KH_2PO_4 pH 7.0; 100 mM KCl; 5 mM $MgCl_2$; 5% glycerol (vol/vol); 1.2% DM (wt/vol)
Buffer 3 (PEG-pellet solubilisation; washing of Ni-NTA resin)	50 mM K_2HPO_4/KH_2PO_4; 100 mM KCl; 5 mM $MgCl_2$; 150 mM sucrose; 5% glycerol (vol/vol); 75 mM imidazole; 20 mM succinate; 2 mM histidine; 0.15% DDM (wt/vol); +/- 0.01% EPL (wt/vol); pH 7.0 with HCl
Buffer 4 (protein elution from Ni-NTA resin)	20 mM Tris; 5 mM K_2HPO_4/KH_2PO_4;5 mM $MgSO_4$; 5% glycerol (vol/vol); 150 mM sucrose; 400 mM imidazole; 20 mM histidine; 20 mM succinate; 0.15% DDM (wt/vol); 0.02% EPL (wt/vol); pH 7.0 with HCl

The solubilized protein was left for binding to Ni^{2+}-charged Chelating Sepharose™ Fast Flow resin (1 mL resin per 10 mL of sample) overnight in batch mode (as opposed to on-column binding) in a cold room slowly shaking at horizontal shaker. After binding, the complete material was poured into a 25 mL plastic column (BIO-RAD) and after sedimentation of the sepharose, it was washed by gravity flow with 2 column volumes (2x 25 mL) of solubilization buffer. Finally,

the ATP synthase protein was eluted in 1 mL steps using Buffer 4. The ATP hydrolysis activity was measured directly in the elution fractions and specific activity (U/mg) and coupling ratio (%) were determined as described in (Hakulinen et al., 2012).

4.2.4. Different approaches for extraction and purification of *I. tartaricus* wild-type and mutant c-rings

Extraction of *I. tartaricus* mutant c-rings from cell membranes expressed with pt7cIT was performed using three different strategies depending on the stability of the c-rings.

Extraction of SDS-stable c-rings from *E. coli* BL21 (DE3) crude membranes. Approach 1: Cells were harvested after expression by centrifugation (8,000 *g*, 30 min, 4°C) and resuspended in Buffer 5 (**Table 4-8**). DNase I (50 µg) and Pefabloc® SC-Protease Inhibitor (0.5 mM) were added shortly before cell disruption. Cells were broken using a Microfluidizer (2 passes at 12,000 psi and 4 °C). Unbroken cell debris was removed by centrifugation (15,500 *g*, 35 min, 4°C). Membranes were collected by ultracentrifugation (250,000 *g*, 1 hour, 4°C) and washed once with Buffer 6 and subjected again to ultracentrifugation. Solubilization of membranes was performed by stirring the membranes in the Buffer 6 containing 2% (wt/vol) *N*-lauroylsarcosine (LS) as a detergent for 12 min at 65°C. The solubilized material was ultracentrifuged and the protein was precipitated by addition of 2 volumes (65%) of saturated (wt/vol) $(NH4)_2SO_4$ solution, prepared in 50 mM Tris/HCl pH 8.0. The pellet was separated by centrifugation (12,500 *g*, 25 min, RT) and the supernatant was dialyzed overnight in 8-10 kDa cut-off dialysis membranes against 5 L of 20 mM Tris/HCl pH 8.0. The dialyzed sample was mixed with 400 mg of pre-equilibrated Macro-Prep® Ceramic Hydroxyapatite Type I (BIO-RAD) 40 µm beads in the presence of 20 mM Tris/HCl pH 8.0, 0.05% DDM (wt/vol) for 2 hours. The mixture was then loaded to the 5 mL plastic column (BIO-RAD).Elution was performed using 100 mM K_2HPO_4/KH_2PO_4 pH 8.0, 0.05% DDM (wt/vol). To remove contaminating proteins the samples were further purified by two consecutive sucrose density gradient (10-35%) centrifugations with concomitant pelleting of the c-ring by removing detergent during dialysis against 20 mM $CH_3CO_2NH_4$pH 6.9. The first sucrose gradient was carried out in 20 mM Tris/HCl pH 8.0, 0.1 M

NaCl, 0.05% DDM (wt/vol). For the second sucrose gradient 20 mM $CH_3CO_2NH_4$pH 6.9, 0.02% Zwittergent® 3-14 (wt/vol) buffer was used with the same sucrose gradient. The c-ring samples migrated into the 20-25% sucrose zone. The corresponding fractions were collected and dialyzed for 2 days against 20 mM $CH_3CO_2NH_4$(pH 6.9) to reduce detergent concentration below critical micelle concentration (cmc) and thereby force the refolding and precipitation of the protein. The pellet was collected by short centrifugation (8,000 *g*, 10 min and 4°C) and stored as a wet pellet at 4°C.

Extraction of c-ring mutants with reduced stability directly from *E. coli* BL21 (DE3) cells. Approach 2:

After overnight expression the cells were harvested and broken by passing twice through French pressure cell (16,000 psi, 4°C). Non-broken cell debris was collected at low-speed centrifugation (15,500 *g*, 35 min, 4°C) and discarded. A 1 mg-aliquot of purified γ_{His}/ε complex (stored at -20°C, details below) was added to the supernatant. Prior to the usage, aliquots of γ_{His}/ε protein were diluted 10 times in reconstitution Buffer 7 (**Table 4-10**). Samples were gently mixed for 30 min on ice. After 1 hour ultracentrifugation (250,000 *g*, 4°C) supernatant containing associated complex was collected and applied to a Ni-charged resin. The material was thoroughly washed with 2 column volumes (25 mL) of reconstitution buffer at 4°C. Elution was made with an imidazole step gradient (200-400 mM). Finally, ammonium sulphate precipitation without 65°C heating step was performed to extract c-rings (see approach 1).

Extraction of c-ring mutants with a reduced stability from purified recombinant ATP synthase. Approach 3:

The samples of purified ATP synthase (see below) were dialyzed 3 days against 20 mM $CH_3CO_2NH_4$pH 6.9 and pelleted with following short (2 hours) dialysis against 20 mM $CH_3CO_2NH_4$ pH 4.7. The pellet was collected by centrifugation (8,000 *g*, 20 min, 4°C), than washed with 20 mM Tris/HCl pH 8.0, centrifuged again and solubilized at 60°C for 10 minutes in the buffer containing 20 mM Tris/HCl pH 8.0, 10 mM EDTA 8.0, 10 mM DTT and 0.2% Zwittergent 3-14 (wt/vol). The solubilizate was subjected to 10-35 % sucrose density gradient centrifugation (250,000 *g* and 4°C) in 20 mM Tris/HCl pH 8.0, 0.1 M NaCl and 0.05% DDM

(wt/vol) for 20 hours. The fractions of c-ring were collected and used for biochemical analysis within few days after extraction.

Table 4-10: Composition of buffers used for c-ring extraction

Buffer	Final concentrations
Buffer 5 (*E. coli* BL21 cell resuspension)	20 mM Tris/HCl pH 8.0; 5 mM EDTA pH 8.0; 5 mM DTT
Buffer 6 (membrane washing)	20 mM Tris/HCl pH 8.0; 10 mM EDTA pH 8.0; 10 mM DTT
Buffer 7 (rotor γ_{His}/ε-c-ring reconstitution)	10 mM K_2HPO_4/KH_2PO_4 pH 7.0; 200 mM KCl; 5 mM $MgCl_2$; 5% glycerol (vol/vol); 0.05% DDM (wt/vol)

4.2.5. Extraction of *I. tartaricus*γ_{His}/ε complex from *E. coli* BL21 (DE3) cells

The γ_{His}/ε complex was expressed and purified from an *E. coli* BL21 (DE3) expression strain. Harvested cells from total 2 L of overexpression culture were re-suspended in 10 mM K_2HPO_4/KH_2PO_4 pH 7.0, 200 mM KCl, 5 mM $MgCl_2$, 75 mM imidazole pH 7.0 and 5% glycerol (vol/vol). Cells were supplemented with 50 µg DNase I (wt/vol) and 0.5 mM Pefabloc® SC-Protease Inhibitor and passed twice at 16.000 psi through a French pressure cell. Unbroken cells were collected and discarded after low-speed centrifugation (15,500 *g*, 35 min, 4°C). After the following ultracentrifugation step (250,000 *g*, 1 hour, 4°C) the supernatant was passed twice trough Ni^{2+}-NTA resin by gravity flow (2 mL resin per each 10 mL of supernatant). The column was washed with 3 column volumes of the same buffer. Elution was performed with the same buffer containing additionally 400 mM imidazole. The elution fractions were collected, aliquoted, supplemented with one volume of autoclaved glycerol (50% final concentration) and kept at -20°C to avoid precipitation of the protein.

4.2.6. Isothermal titration calorimetry (ITC) measurements

4.2.6.1. Preparation of solutions and handling

TraceSELECT® (Fluka) water containing $Li^+ \leq 1$ µg/kg and $Na^+ \leq 5$ µg/kg was used in the preparation of all solutions. Only sterile plastic tubes were used for buffer preparation and storage. No metal/glass parts were used during preparation of buffers and for storage. The buffers used in ITC measurements were pH titrated indirectly: So that, the reference buffer was pH adjusted with a known volume of base or acid (e.g., tetramethylammonium hydroxide, TMAOH or phosphoric acid) under pH-meter and the appropriate volume of titrant was added in the experimental buffer in parallel. Afterwards, the small aliquot of experimental buffer was checked for correctness of the adjusted pH.
The concentrations of the components in experimental buffers were made with precision up to 0.1 mM. Before the measurements, the trace Na^+ concentration in prepared buffers was controlled by atomic absorption spectroscopy (AAS). Shortly before ITC measurements, buffers were centrifuged for 30 min at 8,000 *g* (4°C) in order to remove air bubbles.

4.2.6.2. Refining the Na^+ baseline level in the protein samples

The extracted and refined in homogeneity c-ring protein was prepared for ITC measurements as follows. Samples of 2 mL volume containing 1-5 µM of the c-ring protein (calculated per mass of the c-ring) were placed in closed from the bottom dialysis membrane tubes (8-9 kDa cut-off) and placed vertically in sterile 50 mL plastic tubes for dialysis against 5 mM $CH_3CO_2NH_4$ pH 6.9. Dialysis was performed for 3-6 days at RT under intense stirring. The buffer exchange was performed consequently for 3-5 times within 3-6 days to reach final $[Na^+] < 5$ µM.

4.2.6.3. Equilibration of the protein samples for ITC measurements

After decreasing Na^+ concentration in protein samples, samples were solubilized by addition of 0.15% DDM (wt/vol), 1% OG (wt/vol) or 5% dimethyl sulfoxide (DMSO) (vol/vol).

Equilibration of the samples for ITC measurements was done was by dialysis for 4 days with intense stirring against equilibration buffer (2x 47 mL). All dialysis steps were performed at RT. Na^+ contamination levels in equilibration buffers were assessed by AAS technique. The characteristics of buffers implemented in sample preparation and ITC measurements are listed in **Table 4-11.**

Table 4-11: Characteristic of the solutions implemented in ITC measurements

Buffer	**[Na^+], µM***	**ΔH_{ion}, kcal/mol ****
10 mM MES pH 6.5		3.54
10 mM HEPES/TMAOH pH 7.5		5.02
10 mM Tricine/TMAOH pH 7.42	3.08	7.49
10 mM MOPS/TMAOH pH 7.38	2.62	5.04
10 mM phosphate dibasic/phosphoric acid 7.35	1.59	1.22
10 mM N-ethyl morpholine/TMAOH 7.44	1.03	6.55
10 mM Tris/phosphoric acid pH 7.55	3.14	11.34
10 mM CHES/TMAOH pH 9.14	3.23	9.47
10 mM imidazole pH		8.75
Salt	**[Na^+], µM***	
100 mM CsCl	2.09	
100 mM LiCl	3.61	
Solvent	**[Na^+], µM***	
0.15% DDM	1.37	
5% DMSO	1.06	
1% OG		
Other	**[Na^+], µM***	
MilliPore-filtered water	0.61	

* - data were obtained by AAS measurements

** - (Goldberg et al., 2002)

Titration buffers that contained NaCl or LiCl were counterbalanced with the same concentration of CsCl in equilibration (protein) buffer. For example, in case the protein titration was performed with use of 10 mM NaCl buffer, the protein sample contained 10 mM CsCl in equilibration buffer as well. Addition of CsCl to samples aimed to avoid large heat dilution signals coming from mismatch in ionic strength between buffers.

4.2.6.4. ITC experiment setup for measuring Na^+ and Li^+ binding to *I. tartaricus* wild-type and mutant c-rings

ITC measurements were performed in Malvern MicroCal VP-ITC machine (1.4255 mL sample cell volume, fitted with 290 μL volume automated syringe system). The sample cell contained c-ring equilibrated in 10 mM buffer, 1-250 mM CsCl and detergent of choice. Syringe was filled with the titration buffer containing 10 mM buffer, 1-250 mM NaCl or LiCl and detergent of choice. Equilibration (=sample) and titration solutions were made to match with regard to pH, buffer and salt ionic strength The ITC experiment was performed according to standard recommendations: Solution of ligand (NaCl or LiCl) was titrated into c-ring protein solution. The conditions of the ITC run are presented below in **Table 4-12.**

Table 4-12: Parameters of the MicroCal machine used in ITC measurements

Parameter	Settings
T, °C	25
Initial delay, sec	1800
Feedback mode/gain	high or low*
ITC equilibration options	Auto/fast equilibration
Reference power, µcal/sec	10
Protein concentration, µM (calculated for c-oligomer)	1-5
NaCl concentration in syringe, mM	1-250
CsCl concentration in sample, mM	1-250
Stirring speed, rpm	351
First injection, µM	3
Rest of injections, µM	3-10
Total number of injections	25-55
Spacing, sec	350-450**
Filter period	2
Purge/refill distance, inches	0.039

* - low feedback mode was used for low intensity signals of reference buffer/buffer titrations

** - 450 sec spacing was used for the titrations of large intensity in order to complete the k_{off} part

Each NaCl or LiCl titration of protein was followed by reference buffer/buffer titration. In the reference titration, the protein sample was substituted with an equilibration buffer from last dialysis step. The thermograms obtained from reference titrations were used for baseline correction in data evaluation procedure.

4.2.6.5. Evaluation of the ITC data

Evaluation of the raw data from ITC measurement was done by Origin® software (Origin Lab, Northampton, MA). The signal noise data that correspond to given initial delay time (first 1800

sec) was deleted from the file. The baseline was adjusted manually for each injection by moving it to the average value of the noise before and after the peak. Last heat dilution signal of reference buffer/buffer titration was subtracted mathematically from protein titration by simple math option. Another approach for data correction was carried out by point-by-point subtraction of buffer dilution signals. At the next step, the initial molar ratios, MR (Na^+-to-protein molar ratio at time of first injection) were re-adjusted according to AAS measurements of Na^+ contamination. After baseline and MR corrections, the data were integrated from the baseline and fitted with one-site binding model. The stoichiometry of binding, n = 11, was used as a fixed parameter to fit obtained curve and calculate K_d and ΔH values. The final binding signature (free energy change ΔG, binding enthalpy ΔH and entropy factor $-T\Delta S$) were calculated only after the heat from Glu65 deprotonation was subtracted as it is indicated below.

4.2.6.6. Evaluation and subtraction of heats from Glu65 deprotonation mediated by Na^+ and Li^+ binding to *I. tartaricus* wild-type and mutant c-rings

The deprotonation events that accompanied Na^+ or Li^+ binding to *I. tartaricus* c-rings were evaluated in three buffer systems differing in ionization enthalpies (**Table 4-7**). Plot of the observed enthalpies (ΔH_{obs}) against the inoization enthalpies of used buffers (ΔH_{ion}) yielded a negative slope that equaled to a number of released H^+ per each bound Na^+ or Li^+ (N_{H+}) as it is shown by equation:

$$\mathbf{\Delta H_{obs} = \Delta H_{binding} + N_{H+} * \Delta H_{ion}}$$

Where ΔH_{obs} is observed enthalpy in kcal/mol; $\Delta H_{binding}$ is enthalpy of Na^+ or Li^+ binding in kcal/mol; ΔH_{ion} is ionization enthalpy of used buffer and N_{H+} is a number of released protons. The y axis intercept yielded the pure binding enthalpy ($\Delta H_{binding}$) of Na^+ (or Li^+) binding to the c-ring.

4.2.6.7. Evaluation of ΔG and –TΔS parameters for Na^+ and Li^+ binding

Free energy change (ΔG) upon Na^+ or Li^+ binding to the c-ring was calculated according to equation:

$$\mathbf{\Delta G = -RTlnK_d}$$

Where R is a gas constant (1.9872 cal/mol*K) and T is an absolute temperature in K (Celsius + 273.15).

The entropy contribution –TΔS was calculated from previously estimated ΔG and $\Delta H_{binding}$ parameters according to equations:

$$\mathbf{\Delta G = \Delta H - T\Delta S}$$

$$\mathbf{-T\Delta S = \Delta G - \Delta H_{binding}}$$

4.2.6.8. Statistical analysis of the data

NaCl and LiCl titrations of the protein samples were run at least in triplicate at found optimal MR conditions. All data are presented as means ± S.E., $n \geq 3$.

4.2.7. Mass spectrometry-based measurements

4.2.7.1. Mass spectrometry-based determination of the c-subunits masses from *I. tartaricus* c-ring mutants

Mutant c-rings were extracted from purified ATP synthases according to described procedure (section 4.2.4). Samples were refined in purity and homogeneity and dialyzed for 3-5 days at RT against 3x 2 L of 5 mM $CH_3CO_2NH_4$ pH 6.9. After dialysis, samples were solubilized at RT with 0.01 % DDM (wt/vol) in 100 mM MES pH 6.5 for at least 1-2 hours. In the next step, samples were mixed in 1:1 ratio with 2,5-dihydroxyacetophenone (DHAP, prepared in ethanol) or 2,5-dihydroxybenzoic aced (DHB) and spotted on a standard steel target. As alternative, mass spectrometry measurements were performed with the c-subunits extracted by chloroform/methanol extraction protocol (described in part 4.2.7.4). The volume of samples used for organic extraction of the c-subunits varied in the range 50-1000 µL depending on the protein concentration.

4.2.7.2. Measuring the kinetic of Glu65 modification by DCCD in detergent solution

0.1-1 M stocks of DCCD were prepared in 100% DMSO (Bioultra, 99.5%) and stored frozen at -20°C. Protein samples (~ 0.1 mg/mL) were solubilized in 0.01 % DDM (wt/vol) and 100 mM MES pH 6.5. The incubation time (1-60 min) and DCCD concentration (0.2-1 mM) were varied in order to optimize the efficiency of Glu65 modification by DCCD. The optimized conditions for DCCD modification implied roughly 50% efficiency of DCCD labelling at tested conditions. The DCCD labelling efficiency of Glu65 modification was calculated as a ratio between peak intensity of DCCD-modified c-subunits in relation to total intensity obtained for c-subunits peaks accordingly to the formula:

Labelled c-subunits (in %) = modified c-subunits/(not modified c-subunits + modified c-subunits)*100

4.2.7.3. Measuring the kinetic of Glu65 modification by DCCD in lipids

Purified c-ring sample was mixed with 1,2-dimyristoyl-*sn*-glycero-3-phosphocholine (DMPC) in lipid-to-protein ratio (LPR) of 10. OG was added to a final concentration of 1%. Thoroughly mixed sample was further subjected to ~ 1-week dialysis against 10 mM $CH_3CO_2NH_4$ pH 6.9 at RT unless sample became turbid. Afterwards, sample was collected and 100 µl of the DMPC-reconstituted sample was mixed with 400 µl of 200 mM MES pH 5.5 (adjusted with NH_4) or 200 mM $(NH_4)HCO_3$ pH 7.0 and 8.5 (adjusted with NH_4/Acetic acid). Mixture was equilibrated for 2 hours at RT. After equilibration, the DCCD modification was performed under following final conditions: 0.17 mg/ml protein, 400 µM DCCD and +/-1 mM NaCl. DCCD-modification reaction was performed overnight (19 hours) at RT. Afterwards, 5 µl of the reaction sample was mixed with 5 µl of DHAP matrix and 0.5 µl of the mixture was spotted on a standard steel target.

4.2.7.4. Chloroform/methanol extraction of the c-subunits for mass-spectrometry analysis

To the desired volume of the c-ring samples (50-1000 µL of 0.01-1 mg/mL c-ring) were added 5-10 volumes of freshly prepared chloroform/methanol mixture (1:1). Mixture was thoroughly vortexed for 5 minutes. After 3 volumes of water were added in order to initiate phase separation, mixture was vortexed again for 5 minutes and subjected to 20 minutes centrifugation at 11,500 rpm at RT. The lower chloroform phase containing extracted c-subunits was carefully collected with an extended extra-long tip. The solvent of the chloroform phase was removed by roto-evaporation in UNIVAPO rotational vacuum centrifuge 150M (UniEquip GmbH) at RT using the vacuum from a UNIJET water-aspirator with a temperature control. The remaining pellet was washed twice with chloroform/methanol/water (50:50:30) and consequently dissolved in 10 µL of chloroform/methanol (1:1) or acetonitrile and 1 µl was spotted on a target coated previously with 1µL of DHAP or DHB matrix.

4.2.7.5. DCCD modification of Glu65 in wild-type and mutant c-rings under different pH and salt conditions

The c-ring samples (6x 200 µl, each per ~0.1 mg/ml) were solubilized and pre-incubated at the pH to be tested (0.01% DDM (wt/vol) and 0.2 M buffers in the pH range 5.0-9.0) for at least 1-2 hours at RT. To cover the broad pH range, two different buffers were used: MES/NH_4OH (pH 5.0-7.0) and NH_4HCO_3/CH_3COOH, NH_4OH (pH 7.5-9.0). As stability and accordingly the reactivity of DCCD in water solution is limited to few hours, only fresh DCCD solutions were used in reactions.

To the detergent-containing buffer the double concentration of DCCD was given (0.2-2 mM DCCD, depending on the mutant), the suspension was vigorously mixed by vortexing for at least 1 min and immediately vigorously mixed with the pre-incubated samples in a ratio of 1:1 (final DCCD concentration 0.1-1 mM). The time for reaction varied in a range of 8-60 min. The reaction was stopped by the addition of 2,6-dihydroxyacetophenone (DHAP) matrix solution mixture in a ratio of 1:1 or with chloroform/methanol (1:1) mixture. 0.3 µL of this reaction mixture was further spotted on a standard steel target and dried for 2 min at RT for further mass spectrometric analysis.

4.2.7.6. DCCD profile-based evaluation of the pKa values for Glu65 residue

The pH-dependent profile of DCCD modification was used to trace the changes in protonation state of Glu65 carboxyl group. The full (100%) protonation of Glu65 was assigned to pH-maximum of Glu65 modification by DCCD at which the most efficient DCCD modification was observed. The full deprotonation (0%) of Glu65 was attributed to pH-minimum of Glu65 modification by DCCD at which maximally diminished efficiency was observed. The 50% protonation that corresponds to pKa value was extrapolated from the plot of DCCD modification efficiency as a function of pH.

4.2.7.7. Specific rates of DCCD modification of Glu65 residue

Specific rates of Glu65 modification by DCCD were calculates as follows, equation:

ν = % of the DCCD-modified c-subunits/min/μM DCCD/mg of the c-ring

Time of DCCD labelling and DCCD concentration in reaction mixture varied depending on the mutant. The protein concentration equalled to 0.1 mg/mL.

4.2.8. Measurements of functional activity of *I. tartaricus* wild-type and mutant ATP synthases

4.2.8.1. Preparation of lipids

A 2 mL aliquot of *E. coli* total lipid extract (ETLE, 25 mg/ml) in chloroform was distributed as a thin layer in a 50 mL glass bulb and dried overnight using a continuous nitrogen stream. The layer of lipids was next rehydrated in 2 mL of reconstitution Buffer 8 (**Table 4-13**) or 2 mL of reconstitution Buffer 9 or 10 (**Table 4-13**) under intensive stirring for 45 min at RT. Buffer 8 and Buffer 9 were used for ΔpNa- and ΔpH-dependent ATP synthesis activity measurements, respectively. For the case of ΔpLi-driven ATP synthesis activity measurements, Buffer 5 was modified and 50 mM KCl was replaced with 150 mM sucrose (Buffer 10). Liposomes of defined size were pre-formed by multiple extrusions (15-20 times) through a polycarbonate membrane with a pore diameter of 100-200 nm in a mini-extruder fitted with 1 mL Hamilton syringes (Hamilton Company, Reno, NV). The size range of the prepared vesicles and the incorporation efficiency were later checked by freeze-fracture electron microscopy. A high lipid-to-protein (LPR) ratio in the range of 20-25 (wt/wt) was used to incorporate just a few molecules of ATP synthase per vesicle.

Table 4-13: Buffers used for reconstitution of mutant ATPases

Reconstitution buffer	Final concentrations
Buffer 8 (ΔpNa-dependent measurements)	15 mM Tris/HCl pH 7.5 (HCl); 5 mM $MgSO_4$; 5 mM K_2HPO_4/KH_2PO_4; 50 mM KCl
Buffer 9 (ΔpH-dependent measurements)	20 mM Tris/HCl pH 7.0 (NH_4OH); 5 mM $MgSO_4$; 5 mM K_2HPO_4/KH_2PO_4; 150 mM sucrose ; 20 mM succinate
Buffer 10 (ΔpLi-dependent measurements)	15 mM Tris/HCl pH 7.5 (HCl); 5 mM $MgSO_4$; 5 mM K_2HPO_4/KH_2PO_4; 150 mM sucrose

4.2.8.2. Reconstitution of recombinant wild-type and mutant ATP synthases in pre-formed lipid vesicles

Fractions of purified ATP synthases that showed coupled ATP hydrolysis activity (19-98%) were used for incorporation into pre-formed ETLE vesicles (see above). The reconstitution buffer varied based on implemented ion-driving force for measurements (see above). For each reconstitution 1.5-2 nM (0.8-1.1 mg) of ATP synthase protein was taken.

25 mg of pre-formed liposomes were solubilized in 1% DDM (wt/vol) and added to enzyme solution in a LPR ratio of 20:1. The total volume of 660 µL was kept for each reconstitution. The mixture was incubated for 20 min with gentle mixing on a horizontal rotating platform. To initiate vesicle formation the detergent was removed stepwise. First, the protein-lipid-detergent mixture was incubated for 20 min with Heptakis (2,6-di-O-methyl)-β-cyclodextrin (final concentration: 50mg/ml) with mild agitation. Second, cyclodextrin-complexed detergent was removed by passing through Sephadex® G-50 pre-packed columns (1 mL volume). Elution of the formed proteoliposomes was performed using 1.5 mL of reconstitution buffer. All reconstitution steps were performed at 4°C or on ice. To concentrate proteoliposomes as well as to remove detergent or Na^+ traces (important for getting tight vesicles) samples were pelleted by short, ultrafast centrifugation steps (95,000 rpm, 25 min, 4 °C) and washed once more with reconstitution buffer. Finally, the pellet was resuspended in 100 µL of one of the reconstitution

buffers (**Table 4-11**) and 3 µL (3-33 pM of reconstituted ATP synthase) were added for each ATP synthesis measurement.

For the case of low-concentrated samples of ATP synthase (≤0.1 mg/ml), in case it was required, few reconstitution reactions were performed in the parallel according to above described protocol. After eluting proteoliposomes from Sephadex columns, all the fractions were poured into one probe, pelleted and later homogenized in 100-200 µL of one of the reconstitution buffers.

4.2.8.3. Real-time measurements of *smf*-driven ATP synthesis

The four stock solutions were prepared and stored at -80°C: (1) 25 µM valinomycin in 100% ethanol; (2) 0.5 mg/ml luciferase in 20 mM Tris/HCl pH 8.0 and 1 mM DTT; (3) 5 mM luciferin in 20 mM Tris/HCl pH 8.0 and 0.1 M KCl; (4) 2 mM ADP in water, titrated with 27 % (wt/vol) NH_4OH to pH 7.0. ΔpNa was created by the unequal distribution of NaCl on the two sides of the proteoliposomes. The Nernst equation was then used (with internal and external concentrations of NaCl) to calculate the defined ΔpNa at a given T:

$$\mathbf{E_k = RT/zF*ln*[K^+]_0/[K^+]_i}$$

Where R is a gas constant (1.9872 cal/mol*K) and T is an absolute temperature in K (Celsius + 273.15). F is Faraday constant ($9.65x10^4$ coulomb/mole), z is the valence of the ion, in this case 1. $[K^+]_0$ is extracellular K concentration in mM and $[K^+]_i$ is intracellular K concentration in mM. At room temperature (25°C), this equation was reduced to equation:

$$\mathbf{E = 25.69*ln[out]/[in]}$$

Accordingly, at 25°C 100/150 mM NaCl inside and 1 mM NaCl outside the proteoliposomes results in -118/-129 mV of ΔpNa (negative inside), respectively. 100/150 mM NaCl was kept constant through experiments involving proteoliposomes of different ATP synthase mutants. Proteoliposomes containing wild-type or mutant ATP synthases were either preloaded with

100/150 mM NaCl either equilibrated overnight with 100/150 mM NaCl in presence of 4.5 µM valinomycin. The ΔpNa was supplemented with 34/95 mV of membrane potential (Δψ), oriented internally positive and generated by a K^+ diffusion potential (1/50 mM KCl inside and 200 mM KCl outside the proteoliposomes, respectively). The total driving ion-motive force (Δi)was calculated according to equation:

$$\mathbf{\Delta i = \Delta\psi + \Delta pNa = 154/224\ mV}$$

The phosphate potential (Q value) was set as a default value (Q = 0.19) in order to force ATP synthase operate in direction of ATP synthesis. Q value was calculated according to equation:

$$\mathbf{Q = [ATP,\ nM]/[ADP,\ \mu M]*[P_i,\ mM]}$$

ATP production was continuously monitored by luciferin/luciferase solution in Sirius L Tube Luminometer (Berthold Detection Systems GmbH). A luminometer-adapted well stirred cuvette (0.33 mL maximal capacitance) was filled with 300 µL of buffer (15 mM Tris/HCl, 5 mM $MgSO_4$, 5 mM K_2HPO_4/KH_2PO_4, 0.2 M KCl titrated to pH 7.5 with 37% HCl). First, 33 µM luciferin, 83 nM valinomycin and 5 µg luciferase were added to the assay mixture and some time was given until the baseline was stable. Then 53 µM K^+-ADP was added and the second baseline was recorded. ATP synthesis was initiated by the fast addition of 3 µl of proteoliposomes. At the end of activity measurement 67 nM of ATP (1 µL of stock solution) was added as a reference to quantify the arbitrary luminescence units into produced ATP amount.

4.2.8.4. Real-time measurements of *lmf*-driven ATP synthesis

The similar protocol was used for the *lmf*-driven ATP synthesis but with minor modifications: (1) 95 mV of ΔΨ was imposed to proteoliposomes for these measurements. (2) KCl was completely excluded from the interior compartment of the proteoliposomes and replaced with 150 mM sucrose. The proteoliposomes were loaded with Li^+ by overnight incubation with 100/150 mM LiCl in presence of 4.5 µM valinomycin. Alternatively, the interior of

proteoliposomes was loaded with 100/150 mM LiCl in the presence of 10 µM lithium ionophore VI (6,6-dibenzyl-1,4,8-11-tetraoxacyclotetradecane).

4.2.8.5. Real-time measurements of *pmf*-driven ATP synthesis

For the energization of the proteoliposomes with ΔpH (ΔpH = 4 units) the acid-to-base transition method was used: Firstly, 160 µL of alkaline buffer (200 mM Tris/HCl, 158 mM KCl, 242 mM KOH pH 8.0) was mixed with 33 µM luciferin, 83 nM valinomycin and 5 µg luciferase and time was given until a stable baseline was visible. Then 53 µM K^+-ADP (8 µL), 5 µg luciferase and 5 mM K_2HPO_4/KH_2PO_4 pH 7.0 was added and the second baseline was followed until is stabilized. In parallel the 3 µL proteoliposomes were acidified for 5 min on ice with 160 µL of 20 mM Tris, 5 mM $MgSO_4$, 5 mM K_2HPO_4/KH_2PO_4, 20 mM succinate with a pH adjusted to 4.0 with 37% HCl. The ATP synthesis reaction was started and followed in the luminometer by fast addition of pre-incubated proteoliposomes to the alkaline buffer. The luminescence was controlled and quantified to ATP levels by addition of a defined reference amount of ATP (1 µL, 67 nM) at the end of the measurement.

4.2.8.6. Na^+ inhibition of *pmf*-driven ATP synthesis

The previous protocol (section 4.2.8.5) was adapted in order to investigate the effect of different concentrations of NaCl on the *pmf*-driven ATP synthesis at low acidic pH. The *pmf*-driven ATP synthesis was performed with increasing (1/5/10/20/30/50/100 mM) NaCl concentrations in the acidified proteoliposomes. For low NaCl concentrations (1, 5 and 10 mM) only short 5 min incubation was applied during proteoliposomes acidification step. For higher NaCl concentrations (20-100 mM), proteoliposomes were incubated with addition of 4.5 µM valinomicyn and appropriate concentration of NaCl. The same concentrations of NaCl were added to the alkaline buffer in order to exclude the formation of reverse ΔpNa potential.

4.2.8.7. Estimation of the Hill plot coefficient and Linewear-Burk transformation of the data

Data on Na^+-inhibition of *pmf*-driven ATP synthesis (in %) were fitted to Hill plot equation and presented as $\log(V/V_{max}-V)$ *versus* log[NaCl]. Where V represents the rates of *pmf*-driven ATP synthesis at taken [NaCl] and V_{max} is a catalytic rate at maximal Na^+-inhibition of *pmf*-driven ATP synthesis. The slopes of obtained linear fits where assigned to Hill coefficients, *h*. Data were presented as mean ± S.E., n = 3. Data were further transformed and presented as a Linewear-Burk plot: 1/% of Na^+-inhibition of *pmf*-driven ATP synthesis against 1/[NaCl]. The -1/x intercept was equalled to K_M (Na^+) values.

4.2.8.8. Evaluation of B_{max} (Na^+) values. Fitting data to one-site binding equation

The inhibition of *pmf*-driven ATP synthesis by 100 mM NaCl was attributed to maximal Na^+-occupancy (B_{max} (Na^+), %) of ATP synthase assembled wild-type or mutant c-rings. B_{max} (Na^+) values were estimated only for mutants that demonstrated saturated hyperbolic dependency of Na^+-inhibition of *pmf*-driven ATP synthesis. The defined B_{max} (Na^+) and K_M (Na^+) values were used as fitting parameters in one-site saturation (hyperbolic) equation:

$$\mathbf{B_{max}*abs(x)/(K_M + abs(x))}$$

Where variables were set in a range of min = 0, max = 100 with intervals = 10. B_{max} (Na^+) and K_M (Na^+) values were taken from previous evaluations. For the case some unspecific Na^+ binding to ATP synthase occurred at high NaCl concentrations, the modified equation was used that accounts for unspecific factor (Ns). The modified equation was following:

$$\mathbf{B_{max}*abs(x)/(K_M + abs(x)) + Ns*x}$$

Use of Ns parameter was dictated by necessity of better graphical representation of the data but did not affect the defined K_M (Na^+) and B_{max} (Na^+) values. Ns parameter varied in a range of

0.01-0.135 depending on taken binding curve.

4.2.8.9. Evaluation of protein concentration in proteoliposomes

The protein concentration in proteoliposomes was evaluated indirectly: ATP hydrolysis activity of ATP synthase samples was measured before and after lipid reconstitution step and according to initial amount of total ATP hydrolysis coupled activity ($U_{total\ activity}$) activity-based determination of protein concentration in proteoliposomes was made. Usually not more than 30-40% of the protein was lost during lipid reconstitution steps.

4.2.8.10. Evaluation of the efficiencies (V_{max}/K_d) of *smf*-driven ATP synthesis by lipid-reconstituted ATP synthases

Efficiencies of *smf*-driven ATP synthesis by lipid-reconstituted wild-type and mutant ATP synthases were evaluated according to equation:

$$\textbf{Efficiency} = V_{max}/K_d\ (Na^+)$$

Where V_{max} (nM ATP/nM protein*sec) is the rate of ATP synthesis attributed to maximal curvature of the ATP synthesis activity curve and K_d (Na^+) (in nM) is the equilibrium binding constant obtained in a series of ITC measurements at pH 7.5.

4.2.8.11. Statistics and data analysis

Experimental results were expressed in the form of mean ± S.E, n = 3 for each value, where S.E. represents the standard error in the fitting estimates. The curve-fitting procedures were performed using the SigmaPlot program (Version 10.0, Dundas Software GmbH, Germany), and each fitted parameter was expressed in the form parameter ± S.E. All set of experiments were performed at least twice for two independent protein expression and purifications for every mutant sample.

4.2.9. 3D crystallization of selected c-ring mutants

4.2.9.1. Protein sample preparation for crystallization

Anion exchange chromatography. Mono Q purification of *I. tartaricus* wild-type and mutant c-rings: If desired, the purity and homogeneity of extracted c-rings were further improved on pre-packed anion exchanger Mono Q 5/50 GL column (GE Healthcare Life Sciences) on ÄKTA purifier chromatography system (GE Healthcare Life Sciences).
The wet protein pellet of c-ring(obtained as it is described in part 4.2.4.1., method 1) was dissolved in 4 mL of solubilization buffer (20 mM Tris/HCl pH 8.0, 10 mM EDTA pH 8.0, 10 mM DTT and 1.2 % DM), centrifuged for 10 min at 5,000 rpm and the supernatant was subjected to anion exchange chromatography.
MonoQ column was first equilibrated in 20 mL of buffer B [10 mM Tris/HCl pH 8.0, 1 M NaCl, 0.2 % DM] and after in 20 mL of buffer A [10 mM Tris/HCl pH 8.0, 0.2 % DM].After injecting the c-ring containing fraction, the column was washed with 20 mL of buffer A and the protein was eluted in 0.5 mL fractions with a gradient of 100% buffer B.

Solubilization of the c-ring prior to crystallization setups: Detergent solutions from Detergent Screen HT™ (Hamilton Research) in the final concentration of 1-10 cmc were used to solublize pelleted samples of the purified c-ring. Solubilization was held at RT for 1-2 hours, with a short (5 min) heating at 65ºC or overnight at 4ºC. After solubilization, undissolved protein was removed by short centrifugation (7 min, 7000 rpm, RT). The supernatant was carefully collected and used for crystallization setups.

Crystallization setups: Method of vapour diffusion with hanging drop was used for growing crystals of *I. tartaricus* mutant c-rings. 0.5-1.5 μL of the sample was mixed with 0.5-2 μL of the mother liquor in a final ratio 1:1-1:4. Crystals were grown at 4, 12 and 18ºC.

.

5. Results

5.1. Oligomeric state, SDS-stability and rotor reassembly properties of *I. tartaricus* c-ring mutants

In the crystal structure of *I. tartaricus* wild-type c-ring (Meier et al., 2005, 2009) Na^+ binding occurs at the interface of two adjacent c subunits of the c-ring. Amino acids participating in Na^+ coordination are located on helices 1 and 2. The residue of major importance is the overall conserved Glu65 on helix 2 and a carboxylated side chain can be found in both, H^+ and Na^+ binding, c-rings. While on helix 1 only 1 residue is directly involved in Na^+ coordination (Gln32), several other residues, structurally close to the essential Glu65, are directly involved (Val63 and Ser66). The amino acid sequence of *I. tartaricus* wild-type c-subunit was used to introduce a selection of mutations into the ion binding site. The selected mutations were chosen from the proposals in (Krah et al., 2010). In particularly, four polar residues from ion binding site in *I. tartaricus* c-ring (Gln32, Ser66, Thr67 and Tyr70) were replaced with other polar residues (Ser67, Ile67 or Leu67) or hydrophobic residues (Ala32, Ala66, Gln67 and Phe70). The charged Glu65 was substituted by shorter side chain Asp65.

Generally, the method to produce *I. tartaricus* c-ring in *Escherichia coli* cells along with its subsequent purification has been established and is available (Meier and Dimroth 2002; Meier et al., 2005). We took advantage of these established methods to produce and purify a number of *I.tartaricus* c_{11} mutants. In the following chapter, the production, purification and its biochemical analysis is described. Briefly, we first (5.1.1) produced a series of c-ring mutants and compared the c-rings by their migration profile on SDS polyacrylamide gels. This analysis was carried out to visualize their purity, estimate their stoichiometry (c_{11}, or different from c_{11}) and test their stability towards the detergent SDS in which the wild-type c-ring is stable (Meier et al., 2003). Second (5.1.2), the isolated c-rings were probed with respect to their ability to form the ATP synthase rotor complex consisting of γ_{His}/ε and the c-ring (the $\gamma_{His}\varepsilon c_n$ rotor).

5.1.1. In-gel electrophoretic mobility and (SDS-)stability of *I. tartaricus* wild-type and mutant c-rings

This chapter describes the production of a collection of *I. tartaricus* c-ring mutants that harbour their mutations in or at the ion-binding site. An analysis to study their impact on the c-ring stability is presented. For simplicity, only mutations that did not impair oligomeric state of the c-ring were taken further in the biochemical analyses of ion binding affinities (section 5.2-5.3). A total of 19 different specific site-directed mutations were introduced in the sequence of *atpE* gene encoding *I. tartaricus* c-subunit as it is described in Methods (section 4.2.1.4). The mutant c-rings are: G25A, G25S, Q32A, E65D, S66A, T67A, T67L, T67I, T67S, T67G, T67Q, T67M, Y70F, S66A/T67I, S66A/Y70F, T67I/Y70F, Q32A/Y70F and Q32A/S66A/Y70F.The initial expression and purification trials were done for the set of the c-subunit mutants expressed in *E. coli* BL21 cells and purified by *N*-lauroyl sarcosine solubilisation and ammonium sulphate precipitation as it is described in Methods (sections 4.2.2.2 and 4.2.4). The finally purified c-ring mutants were analyzed by SDS polyacrylamide gel electrophoresis (PAGE) (**Figure 5-1**). Notably, not all of the obtained mutants formed SDS stable c-ring and the isolated c-rings apparently dissociated while loading on the gel (SDS containing loading buffer).

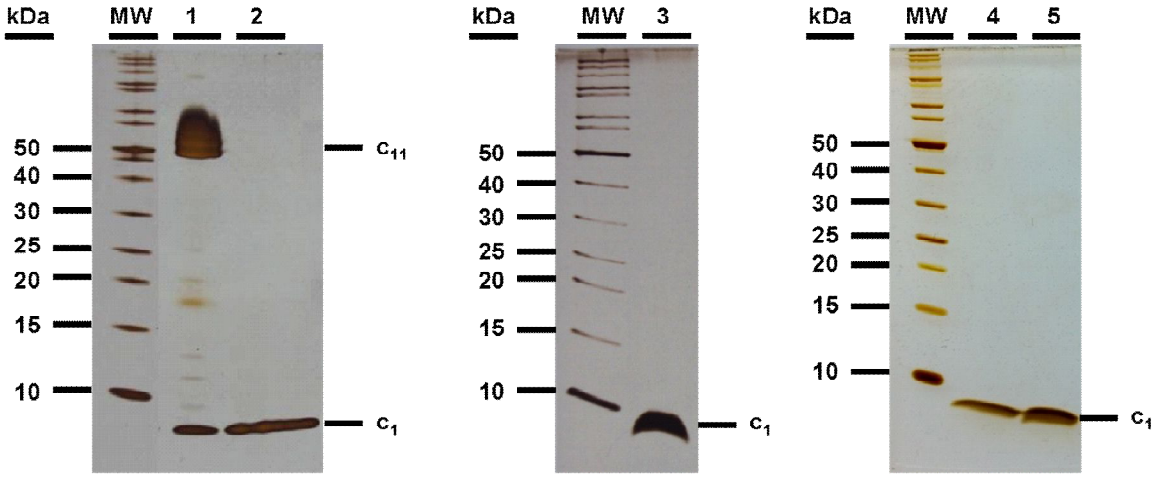

Figure 5-1: Representative SDS-PAGE of *I. tartaricus* mutant c-rings extracted directly from host *E. coli* membranes. Samples 1, 3, 4 and 5 illustrate different impact of the introduced mutations on formation and stability of the c-ring. **1** – (SDS-)stable c-ring with Q32A/Y70F mutation. **2** – Trichloroacetate (TCA) treatment of Q32A/Y70F mutant c-ring dissociates c-ring into monomeric c-subunits. **3** – c-subunits of (SDS-)unstable T67G mutant c-ring. **4, 5** – T67L and T67I monomeric c-subunits.

The c-ring mutants were distributed in three groups as follows:

1. (SDS-)stable mutant c-rings: This group comprises c-rings that appear to be fully stable on SDS-PAGE, comparable to the *I. tartaricus* c_{11} wild-type c-ring. The mutant c-rings are: Q32A, T67S, Y70F, S66A/Y70F and Q32A/Y70F. These mutant c-rings were expressed as a single *atpE* gene in *E. coli* BL21 cells and were extracted directly from cell membranes under harsh conditions [65ºC, 2% *N*-lauroyl sarcosine (LS) and saturated $(NH_4)_2SO_4$]. Extracted mutant c-rings are stable on SDS-PAGE and migrate on SDS-PAGE with no mass shifts related to wild-type c-ring.

2. (SDS-)unstable mutant c-rings: Unlike the *I. tartaricus* c_{11} wild-type c-ring and also unlike group 1 described above, this group comprises c-rings that are not stable when analysed by SDS-PAGE. This group 2 comprises the c-ring mutants G25A, G25S, E65D, S66A, T67G, T67M and T67Q. These c-ring mutants tolerate only mild detergent extraction (e.g., 0.05% DDM and 1% DM), but are immediately dissociated to monomeric c-subunits, when challenged by SDS. These

mutants also require the addition of 0.01% *E. coli* total lipid extract to membrane solubilizate for stabilization of c-rings (details in section 4.2.4). When extracted, (SDS-)unstable mutant c-rings run as c-monomers on SDS-PAGE. As described in the next chapter (5.1.2) these mutant c-rings form complex with γ/ε subunits of ATP synthase rotor (see **Table 5-1**, shown in blue**)**. The c-rings harbouring following mutations: G25A, G25S, E65D, S66A, T67G, T67M and T67Q, had higher stability when purified from the entire ATP synthase complex (section 5.4). G25A, G25S, E65D, S66A, T67G, T67M and T67Q mutations reduce intact (SDS-)stability of *I. tartaricus* c-ring.

3. Mutant c-subunits that do not form oligomers: This group comprises the single and double mutants T67A, T67I, T67L, G25S/T67G, S66A/T67I, T67I/Y70F and Q32A/S66A/Y70F. They can be purified only in the form of c-monomers, independent of the detergent used during the purification procedure (**Figure 5-1**). These mutants also do not bind to γ/ε complex (**Table 5-1,** shown in red**)**. All mutants from group 3 were excluded from the subsequent analyses.

5.1.2. Assembly and co-elution of the rotor complex from *I. tartaricus* mutant c-rings and γ_{His}/ε subunits

To discriminate between (SDS-)unstable and unstable mutant c-rings a new interaction assay was established. In this assay, the intact property of wild-type c-ring to reassemble complete ATP synthase rotor complex (γ_{His}/ε/c-ring) was tested for-all purified mutant c-rings. Using this assay, first, the His-tagged γ/ε complex and mutated c-rings were expressed and purified separately as it is described in Methods (Chapters 4.2.3-4.2.5). Then, the two fractions of purified proteins were mixed in the presence of 0.05% DDM at 4°C in order to assemble the γ_{His}/ε/c-ring complex. After ultracentrifugation the supernatant was immediately subjected to Ni-NTA affinity chromatography. The γ_{His}/ε/c-ring complex was assembled and co-eluted from Ni-NTA column as one fraction (**Figure 5-2B**). In case of the c-monomers, the only fractions of γ_{His}/ε subcomplex were detected in the elution fraction from Ni-NTA column (**Figure 5-2C**).

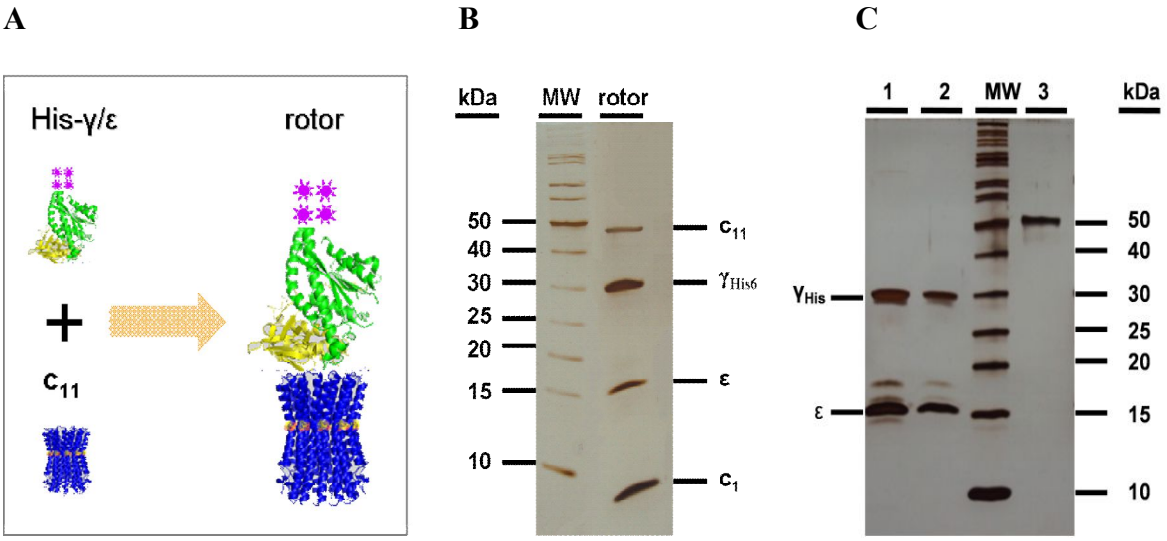

Figure 5-2: Co-elution of wild-type and mutant c-rings with *I. tartaricus* γ_{His}/ε rotor subunits from Ni-NTA resin. (**A**) Schematic illustration of the interaction between γ_{His}/ε and c-ring. (**B**) Representative SDS-PAGE of Q32A mutant γ_{His}/ε/c-ring rotor complex co-eluted from Ni-NTA column as one fraction. (**C**) SDS-PAGE of γ_{His}/ε complex (lanes 1 and 2) eluted form Ni-NTA resin and E65D mutant c-ring (lane 3) that did not form γ_{His}/ε/c-ring complex.

A summarizing table lists the mutant c-rings that can assemble into rotor γ_{His}/ε/c-ring complex (**Table 5-1**). From the set of analyzed c-rings, only the E65D mutant c-ring was not capable to assemble γ_{His}/ε/c-ring complex *in vitro*.

Table 5-1: Summarizing table: Characteristic properties of *I. tartaricus* mutant c-rings

Mutant	Sequence	Formed c-ring	Formed γ_{His}/ε/c-ring
Wild-type	-G-Q-ESTG-Y-	yes/SDS-stable	yes
Q32A	-G-A-ESTG-Y-	yes/SDS-stable	yes
T67S	-G-Q-ESSG-Y-	yes/SDS-stable	yes
Y70F	-G-Q-ESTG-F-	yes/SDS-stable	yes
Q32A/Y70F	-G-A-ESTG-F-	yes/SDS-stable	yes
S66A/Y70F	-G-Q-EATG-F-	yes/SDS-stable	yes
***S. platensis* wild-type**	**-S-Q-EALT-Y-**	yes/SDS-stable	yes
G25A	-A-Q-ESTG-Y-	yes/SDS-unstable	yes
G25S	-S-Q-ESTG-Y-	yes/SDS-unstable	yes
E65D	-G-Q-DSTG-Y-	yes/SDS-unstable	no
S66A	-G-Q-EATG-Y-	yes/SDS-unstable	yes
T67G	-G-Q-ESGG-Y-	yes/SDS-unstable	yes
T67M	-G-Q-ESMG-Y-	yes/SDS-unstable	yes
T67Q	-G-Q-ESQG-Y-	yes/SDS-unstable	yes
T67A	-G-Q-ESAG-Y-	No	no
T67I	-G-Q-ESIG-Y-	No	no
T67L	-G-Q-ESLG-Y-	No	no
G25S/T67G	-S-Q-ESGG-Y-	No	no
S66A/T67I	-G-Q-EAIG-Y-	No	no
T67I/Y70F	-G-Q-ESIG-F-	No	no
Q32A/S66A/Y70F	-G-A-EATG-F-	No	no

A modified version of the above mentioned protocol in which the assembly of γ_{His}/ε/c-ring complex could be performed directly in the cell lysate was used. Namely, unbroken cells were removed and resulting cell lysate was supplemented with a portion of purified γ_{His}/ε complex. After short incubation, the mixture was ultracentrifugated and supernatant was subjected to

Ni^{2+}affinity chromatography. Assembled γ_{His}/ε/c-ring rotor complex was eluted from Ni-NTA as one fraction. This approach was beneficial for purification of some of the unstable c-ring mutants (T67G, G25A and S66A) as lead to higher yields of purified mutant c-rings. In summary, following eight mutant c-rings were qualified for a subsequent biochemical analysis: G25A, Q32A, E65D, T67S, T67G, Y70F, S66A/Y70F and Q32A/Y70F mutants (shown in **Figure 5-3** and summarized in **Table 5-1**).

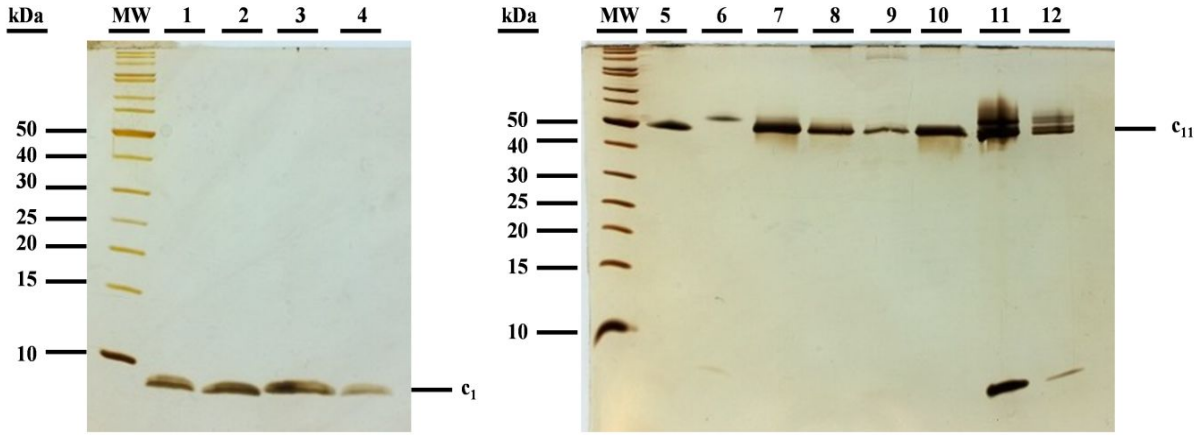

Figure 5-3: SDS-PAGE of (SDS-)unstable and (SDS-)stable c-rings of *I. tartaricus* with mutations. Lanes 1-4 show c-subunits of (SDS-)unstable mutant c-rings: G25S (1), T67M (2), T67Q (3), S66A (4). Lanes 5-12 show (SDS-)stable mutant c-rings: Q32A (5), G25A (6) (SDS-stable when purified with addition of lipids), Y70F (7), E65D (8), T67S (9), T67G (10) (SDS-stable when purified with addition of lipids), S66A/Y70F (11), Q32A/Y70F (12).

5.2. DCCD modification assay with *I. tartaricus* wild-type and mutant c-rings

To study the protonation state of the ion-binding site in *I. tartaricus* c-ring mutants, the chemical modification of the c-subunit by using *N,N′*-dicyclohexylcarbodiimide (DCCD) was performed. DCCD reacts with the c-subunit Glu65 protonated carboxyl group that is directly involved in coordination of monovalent cations (Na^+ and/or H^+). This assay, to modify DCCD labelling has been established previously (Meier et al., 2003) and was used to study DCCD modification of other c-rings (von Ballmoos and Dimroth 2007, Krah et al., 2010). The time course of

thereaction was monitored by using matrix assisted laser desorption/ionization time of flight (MALDI)-TOF mass spectrometry technique at different time points during the reaction at various pH of the buffer, as the DCCD reaction is proton dependent (Intoduction, section 2.9). The reactivity of Glu65 was probed with respect to DCCD modification in response to introduced mutations in the *I. tartaricus* c-ring. By adding Na^+ to the reaction mixture, we explored for its ability to protect Glu65 against modification by DCCD, as Na+ and DCCD compete for reaction with Glu65 carboxyl group.

5.2.1. Identification of mutant c-subunits and determination of their molecular masses by mass spectroscopy

As a quality control, all purified c-ring samples were first subjected to MALDI-MS analysis, in collaboration with Dr. Julian Langer, Department of Membrane Biology, Max-Planck-Institute of Biophysics, Frankfurt. The obtained molecular masses of wild-type and mutant c-subunits were compared with the theoretically calculated masses of corresponding c-subunits (**Table 5-2**).

Table 5-2: Molecular masses of the explored c-subunits determined by MALDI-MS

Mutant	Calculated molecular mass, Da	Measured molecular mass, Da	Observed difference in mass, Da
Wild-type	8795.4	8798.8 ± 1.9	3.4
E65D	8781.4	8783.8 ± 0.5	2.4
T67S	8781.4	8784.1 ± 0.1	2.7
T67G	8751.4	8753.9 ± 0.5	2.5
Y70F	8779.4	8783.3 ± 0.9	3.9
S66A/Y70F	8763.4	8765.7 ± 2.2	2.3
Q32A	8738.4	8740.2 ± 0.8	1.8
Q32A/Y70F	8722.4	8727.8 ± 1.1	5.4
S66A	8779.4	8780.3 ± 1.0	0.9

The mass spectrometric analysis was used to control the purity of samples (**Figure 5-4**).

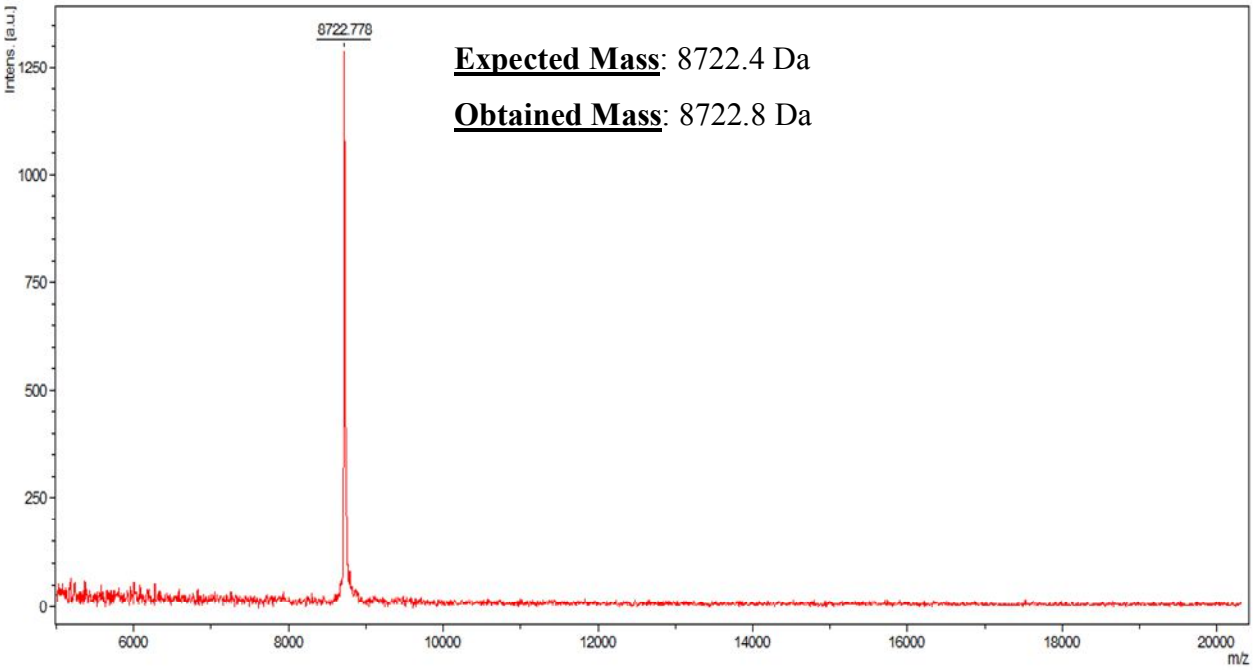

Figure 5-4: Representative MALDI-MS spectra of *I. tartaricus* c-subunit with Q32A/Y70F mutation. Analysis of purified c-ring with Q32A/Y70F mutation by MALDI-MS analysis confirmed correct molecular mass for its c-subunits with no observed modifications (e.g., formylation). No other proteins in the analyzed m/z range (5,000-20,000 Da) were detected. MALDI-MS analysis was performed by Dr. Julian Langer, Department of Membrane Biology, Max-Planck-Institue of Biophysics, Frankfurt.

After confirmation of the correct c-subunit masses, the c-rings with correct mass of c-subunits were used for modification with DCCD (**Figure 5-5**.The labelling of c-subunit with DCCD as presented in **Figure 5-5** confirmed binding of the inhibitor to this subunit as it has been shown in previous works (von Ballmoos and Dimroth, 2007, Meier et al., 2003).

The following parameters were assessed and compared between wild-type and the mutant c-rings:

- Reactivity of the Glu65 carboxyl group towards covalent DCCD modification in detergent and in lipids;

- pH-dependency of DCCD modification reaction of Glu65 carboxyl group;
- Effect of Na^+ protection of Glu65 carboxyl group against DCCD modification.

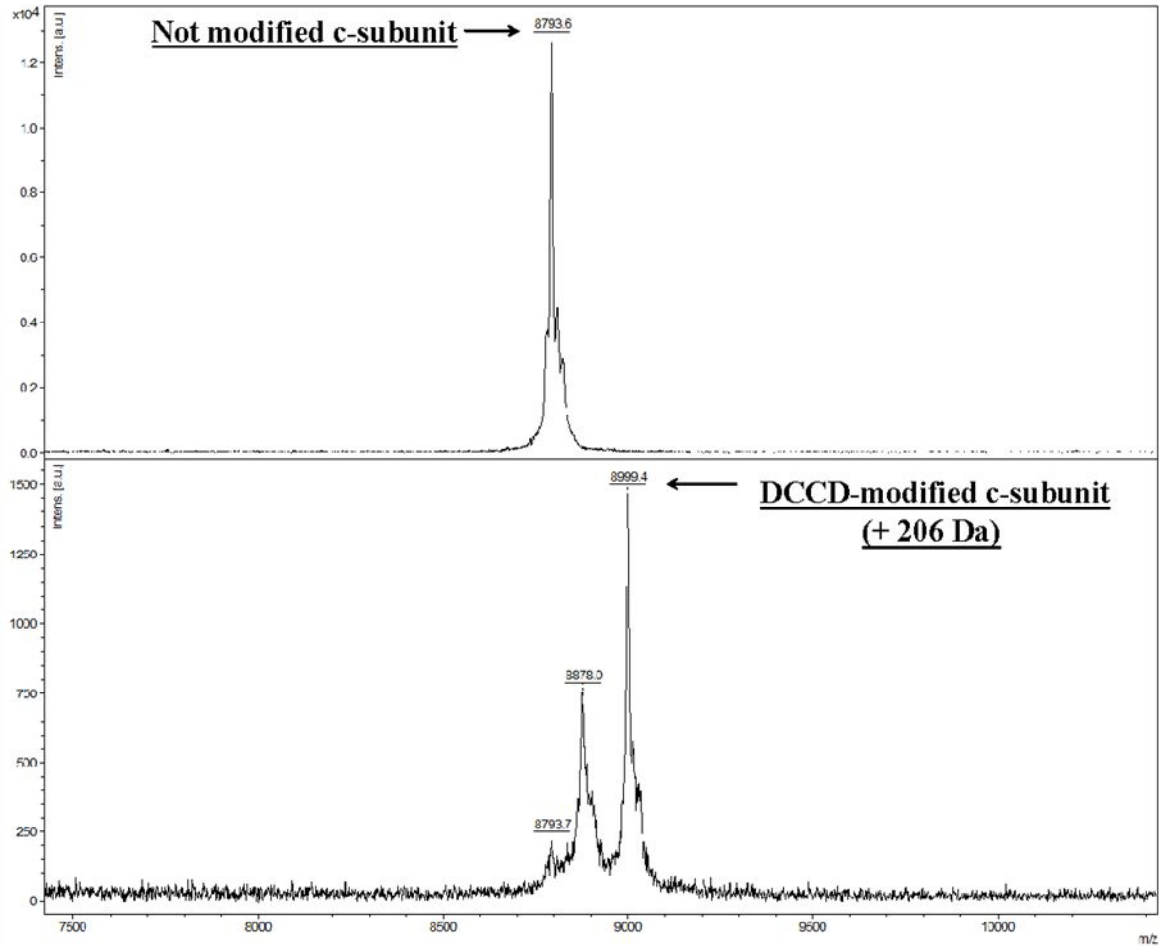

Figure 5-5: Representative DCCD modification of Glu65 carboxyl group in *I. tartaricus* wild-type c-subunit detected by MALDI-MS. A sample containing 100 µg of *I. tartaricus* wild-type c-ring was labelled for 10 min with 100 µM DCCD in 100 mM MES pH 6.5 containing 0.01% DDM. DCCD-labelled sample was subjected to MS analysis according to description in Methods (section 4.2.7.5). Upper panel: MALDI-MS spectra of not modified c-subunits in wild-type c-ring. Lower panel: MALDI-MS spectra of wild-type c-subunits covalently modified with DCCD. DCCD-modified c-subunits have 206 Da (= mass of one DCCD molecule) higher mass than non-modified ones. The intermediate peak corresponds to a fragment of DCCD-modified c-subunit (+121 Da increase in mass relative to nonmodified c-subunit) and was observed due to laser desorption of DCCD-modified c-subunit.

5.2.2. Rates of Glu65 modification by DCCD in wild-type and mutant *I. tartaricus* c-rings

In the first series of experiments, we studied the reactivity of Glu65 carboxyl group towards DCCD modification using isolated c-ring in the detergent dodecyl-β-D-maltopyranoside (DDM). For this purpose, the specific rates of Glu65 modification by DCCD were evaluated for *I. tartaricus* wild-type and mutant c-rings solubilized in 0.01% DDM at pH 6.5. We determined the amount of DCCD (μM concentrations) and time of incubation (min) required to modify approximately 50% of the c-subunits in the c-ring. The obtained differences in DCCD labelling conditions were used to calculate the specific rates of Glu65 modification by DCCD (more details of samples preparation and procedure are described in Methods, sections 4.2.7.2 and 4.2.7.7).

After a few minutes of incubation in 100 μM DCCD at pH 6.5, ≥ 90% DCCD modification was achieved using 0.1 mg of *I. tartaricus* wild-type c-ring. The measured high specific rate of DCCD labelling of thisc-ring is consistent with previously published data on DCCD labelling parameters of *I. tartaricus* wild-type c-ring (von Ballmoos and Dimroth, 2007, Meier et al., 2003). The same concentration of protein (0.1 mg/ml) was used to define specific rates of DCCD modification of mutant c-rings. The mutant c-rings were measured under the same conditions (?). According to the obtained data, among seven analyzed mutant c-rings (**Table 5-3**), only the E65D mutant showed similarly high reactivity of Glu65 with DCCD while reduced rates of DCCD modification were observed in all other mutant c-rings (Q32A, T67S, T67G, Y70F, S66A/Y70F and Q32A/Y70F).

Table 5-3: Specific rates of Glu65 modification by DCCD in wild-type and mutant c-rings

Mutant	ν*	Reactivity of Glu65 with DCCD
Wild-type	65.2 ± 5	++++
E65D	71.0 ± 1.3	++++
T67S	24.1 ± 1.9	+++
T67G	36.2 ± 1.8	+++
Y70F	23.7 ± 2.5	+++
S66A/Y70F	32.2 ± 6	+++
Q32A	4.9 ± 0.4	++
Q32A/Y70F	0.5 ± 0.2	+

* - The symbol "ν" was assigned to the specific rates of Glu65 modification by DCCD calculated as % of the DCCD-modified c-subunits/μM DCCD/μM protein/min (Methods, section 4.2.7.7). '++++', '+++' and '++/+' were assigned to high (wild-type scale), reduced and low specific rate of Glu65 modification by DCCD; respectively.

These experiments indicate that the reaction rates of DCCD with the carboxyl group of the c-ring was reduced by 1-2 orders of magnitude, when the chemical environment around Glu65 was changed from polar into a more hydrophobic amino acids, for example in the single mutant Q32A but also in the Q32A/Y70F double mutant. In particular, the Q32A/Y70F double mutant was 130 times slower as compared with the wild-type c-ring. The slower reaction of DCCD was also observed in the *S. platensis* and *B. pseudofirmus* OF4 H^+-selective c-rings and was identified by hours of sample incubation in mM concentration of DCCD required to achieve detectable DCCD modification of target carboxylic group (Pogoryelov et al., 2005; Preiss et al., 2014). According to the specific rates of DCCD modification of Glu65 carboxyl group, the studied c-rings were distributed in three groups:

I. WT-like c-rings: c-rings with ***high*** reactivity of Glu65 carboxyl group towards DCCD modification. This fastest reacting group contains the wild-type and E65D mutant c-rings.

II. c-rings with a ***reduced*** reactivity of Glu65 carboxyl group towards DCCD modification: T67S, T67G, Y70F and S66A/Y70F mutant c-rings.

III. c-rings with a ***low*** reactivity of Glu65 carboxyl group toward DCCD modification (Q32A, and Q32A/Y70F mutant c-rings).

The difference in reactivity attributed to each group was later correlated with changes in H^+ binding affinity of the Glu65 in c-rings (section 6.1 of Discussion).

5.2.3. pH-dependent rates of Glu65 modification by DCCD in the wild-type and mutant c-rings

In the view of the fact, that Na^+ and the H^+ share the same binding site within the *I. tartaricus* ATP synthase subunit c (Neumann et al., 1998; Meier et al., 2003; Krah et al., 2012; Leone et al., 2015), it was hypothesised that mutations in the c-ring's ion binding sites would alter its H^+ affinity. In order to evaluate this hypothesis experimentally, the pH-dependency of DCCD modification of Glu65 was recorded and compared between wild-type and mutant c-rings. For this experiment, 0.1 mg of DDM solubilised c-ring was incubated with DCCD for the same period of time but in buffers with different pHs (Details in section 4.2.7.2. of Methods).
According to the obtained pH profiles of DCCD labelling (see Appendix, **Figure 7.2**), the *I. tartaricus* wild-type c-ring shows the strongest pH-dependence for Glu65 modification with DCCD in the pH range 5.5-8.5, in agreement with literature values (Meier et al., 2003). The maximal rate for DCCD modification was observed at acidic pH 6.5; it decreased at pH above 6.5 (**Table 5-4**) and increases at pH below 6.5. In the case of mutant c-rings, we also observed pH-dependence for Glu65 modification by DCCD (see Appendix **Figures 7.3-7.8**), however, the maximal rates of DCCD modification were offset regarding the pH and were dependent on type of mutant c-ring (**Table 5-4**). Specifically, we detected the 0.5 pH unit up-shifted maximum of DCCD modification of Glu65 carboxyl group in the Q32A and S66A/Y70F mutant c-rings, and 1.5 pH unit up-shifted maximum of Glu65 modification by DCCD in the Q32A/Y70F mutant c-ring.

Table 5-4: pH properties of Glu65 modification by DCCD

Mutant	pH-dependence of DCCD modification	pH for maximal rate of DCCD modification
Wild-type	Yes	6.5
T67G	Yes	6.5
T67S	Yes	6.5
E65D	Yes	6.5
Y70F	Yes	6.5
S66A/Y70F	Yes	7.0
Q32A	Yes	7.0
Q32A/Y70F	Yes	8.0

5.2.4. pH of the maximal rateof Na^+ protection of Glu65 carboxyl group against DCCD modification in the wild-type and mutant *I. tartaricus* c-rings.

To determine next to what extent the *I. tartaricus* wild-type c-ring and c-ring mutants are able to be protected by Na^+ from DCCD labelling, the DCCD modification of Glu65 in the T67G, T67S, E65D, Y70F, S66A/Y70F, Q32A and Q32A/Y70F mutant c-rings in absence and in presence of 1 mM NaCl and over a pH range of 5.5-8.5 was performed (see Appendix, **Figures 7.2-7.8**). Only Q32A/Y70F mutant c-ring did not show any Na^+ protection of Glu65 modification by DCCD at any testes concentration of NaCl (1-10 mM) within the extended pH range (5.5-9.5) (**Table 5-5**). For the remaining c-ring mutants the competition between Na^+ and H^+ for the same binding site was quantified as the initial molar excess of Na^+ over H^+ (molar ratio, MR) required to protect the Glu65 carboxyl group from DCCD modification of (**Table 5-5,** graph 5). While for the wild-type c-ring DCCD labelling of Glu65 carboxyl group in the c-ring was inhibited by 1 mM NaCl already at pH 6.5 ($MR = 3.2*10^3$), the T67G, T67S, E65D, Y70F, S66A/Y70F, Q32A and Q32A/Y70F mutant c-rings showed Na^+ protection against DCCD modification at 3-100 times higher MR values (**Table 5-5**). In particular, T67S and T67G mutant c-rings demonstrated protection effect of Na^+ on Glu65 modification by DCCD at pH $\geq$ 7.0 at 3 times higher MR with

respect to the wild-type. E65D and Y70F mutant c-rings were protected by Na^+ at 10 times higher MR than wild-type. S66A/Y70F mutant c-ring was protected by Na^+ roughly at 100 times higher MR than wild-type.

Table 5-5: Na^+ protection of Glu65 carboxyl group against DCCD modification

Mutant	Na^+ protection	pH*	[NaCl]	$[Na^+]/[H^+]$, MR	% of Na^+ protected c-subunits
Wild-type	yes	6.5	1 mM	0.32 $x10^4$	51.3 ± 2.6
T67G	yes	7.0	1 mM	1 $x10^4$	13.7 ± 0.7
T67S	yes	7.0	1 mM	1 $x10^4$	12.5 ± x
E65D	yes	8.0	1 mM	10 $x10^4$	32.2 ± 2
Y70F	yes	8.0	1 mM	10 $x10^4$	24.8 ± 1.4
S66A/Y70F	yes	8.5	1 mM	31.6 $x10^4$	16.2 ± 0.8
Q32A	yes	8.5	10 mM	312.5 $x10^4$	21.6 ± 2.0
Q32A/Y70F	no	9.5	10 mM	3125 $x10^4$	no

* - pH at which Na^+ protection against DCCD modification of Glu65 was observed

On the basis of these results, it was concluded that Na^+ and H^+ are competing for binding to mutant c-rings that displayed Na^+ protection and only H^+ bind to Q32A/Y70F mutant to c-ring that did not display Na^+ protection against DCCD modification.

5.2.5. Low Na^+ protection of Glu65 against DCCD modification in the S66A/Y70F mutant c-ring

The DCCD modification of Glu65 carboxyl group in S66A/Y70F mutant c-ring was tested under broader Na^+-to-protein molar ratios, MR: 0.03-3162.28 $x10^4$ (**Figure 5-6).** S66A/Y70F mutant c-ring showed weak Na^+ protection of Glu65 against DCCD modification, although high MR was used. S66A/Y70F mutant c-ring requires 31.62 $x10^4$ molar excess of Na^+ over H^+ to protect

~50% of c-subunits against DCCD modification. For the case of wild-type c-ring, 0.32 x10^4 molar excess of Na^+ over H^+ is required to protect ~50% of c-subunits in the c-ring against DCCD modification. Low Na^+ protection of S66A/Y70F mutant c-ring against DCCD modification implies low Na^+ against H^+ competition for binding to S66A/Y70F mutant c-ring.

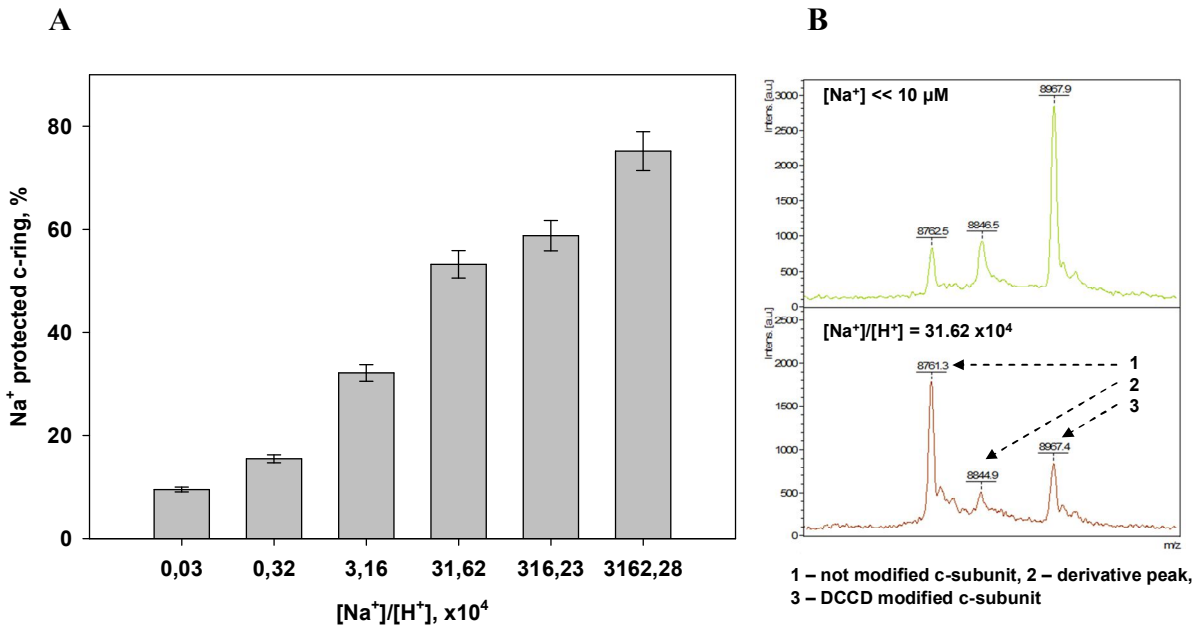

Figure 5-6: Na^+ protection of Glu65 in S66A/Y70F c-ring mutant against DCCD modification under various [Na^+]/[H^+] ratios. (**A**) Summary of results obtained from DCCD modifications experiments with S66A/Y70F mutant c-ring. S66A/Y70F c-ring was modified with 200 µM DCCD for 12 min in Na^+-free conditions and with addition of 1 mM and 10 mM NaCl at pHs of 5.5, 6.5, 8.5 and 9.5 in order to achieve different [Na^+]/[H^+] molar ratios. At [Na^+]/[H^+] = 31.62 x10^4 roughly 50% of the Glu65 carboxylates in S66A/Y70F c-ring were protected against DCCD modification. At [Na^+]/[H^+] = 3162.28 x10^4, less than 80% of the Glu65 carboxylates in S66A/Y70F c-ring were protected against DCCD modification. (**B**) Upper panel: MALDI-MS spectrum of DCCD-modified c-subunits of S66A/Y70F mutant c-ring (colored green). Majority of Glu65 carboxyl groups in S66A/Y70F c-ring are modified with DCCD at [Na^+] < 10 µM and pH = 8.5. Lower panel: MALDI-MS spectrum of Na^+-protected c-subunits of S66A/Y70F mutant c-ring (colored red). Half of Glu65 carboxyl groups in S66A/Y70F c-ring are protected against DCCD modification at pH = 8.5 and with addition of Na^+ (final [Na^+]/[H^+] molar ratio is 31.62 x 10^4).

5.2.6. DCCD modification of Glu65 in Q32A/Y70F mutant c-ring in1,2-dimyristoyl-*sn*-glycero-3-phosphocholine (DMPC) lipids

Ion competition assay showed no Na^+ protection against DCCD modification for Q32A/Y70F mutant c-ring in DDM at broad pH range (**Table 5-6**). Therefore, the investigation was done on further DCCD labelling of Q32A/Y70F mutant c-ring. We checked whether a lipidic and, therefore, hydrophobic microenvironment would promote Na^+ protection against DCCD modification of Glu65 carboxyl group in Q32A/Y70F mutant c-ring. To do so, DCCD labelling was performed in the Q32A/Y70F c-rings incorporated into 1,2-dimyristoyl-*sn*-glycero-3-phosphocholine (DMPC) lipids (section 4.2.7.3). According to performed measurements, Q32A/Y70F c-ring demonstrated Na^+-unprotected DCCD modification of Glu65 in DMPC microenvironment at pH range 7.0-8.5 (**Figure 5-7**).

A **B**

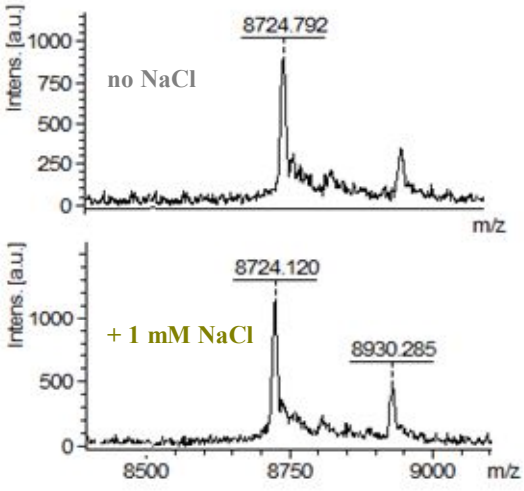

pH	DCCD labeling, % no NaCl	DCCD labeling, % + 1 mM NaCl
7.0	45.1 ± 2.19	43.8 ± 2.25
8.5	42.0 ± 2.09	40.6 ± 2.03

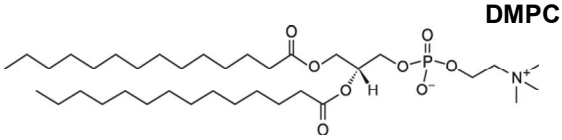

Figure 5-7: Na^+-unprotected DCCD modification of Glu65 in Q32A/Y70F mutant c-ring in DMPC lipids. Purified Q32A/Y70F mutant c-ring was reconstituted in DMPC lipids (right corner) and consequently Glu65 residues were modified with DCCD in presence of 1 mM NaCl (dark yellow) and in Na^+-free conditions (grey) at pH 7.0 and 8.5. (**A)** MALDI-MS spectrum of DCCD-modified Glu65 in Q32A/Y70F c-subunit illustrates similar efficiency of DCCD modification of Glu65 carboxyl groups in or without 1 mM NaCl. (**B**) DCCD labelling efficiency of Glu65 was Na^+ and pH-insensitive in a strictly hydrophobic microenvironment for Q32A/Y70F mutant c-ring.

This experiment illustrated that Na^+ (in the tested $[Na^+]/[H^+]$ molar ratio range) is not competing with H^+ for binding to carboxylic group of Glu65 in the Q32A/Y70F mutant c-ring neither in a lipidic (or hydrophobic) microenvironment nor in a detergent (section 5.2.4.).

5.2.7. Summary of DCCD modification experiments

To summarize the obtained results the *I. tartaricus* wild-type and mutant c-rings were grouped on the basis of similarities in parameters of DCCD modification of Glu65 carboxyl group (**Table 5-6**).

Table 5-6: Grouping of *I. tartaricus* wild-type and mutant c-rings according to characteristic parameters of Glu65 modification by DCCD

Group	Mutant	Relative reactivity of Glu65	pH for maximal rate of DCCD modification	Relative Na^+ protection of Glu65
I.	*I. tartaricus* wild-type, E65D, T67S, T67G, Y70F	High	~6.5	high
II.	Q32A, S66A/Y70F	Reduced	~7.0	low
III.	Q32A/Y70F**,** *S. platensis* wild-type	Low	~8.0	no protection

Most of the analyzed mutations in the c-ring had an influence on specific rates of Glu65 carboxyl group modification by DCCD, making *I. tartaricus* c-ring 1.8-130-fold less sensitive to DCCD. In addition, it was found that T67G, T67S, E65D, Y70F, S66A/Y70F and Q32A mutations reduced and Q32A/Y70F mutation abolished Na^+ protection of Glu65 carboxyl group against DCCD modification. The same mutations also affected pH-dependent profile of DCCD modification. From performed set of experiments, it was concluded that introduced polar-to-hydrophobic Q32A and S66A mutations and their combination with Y70F mutation reduce both, the reactivity of Glu65 carboxyl group to DCCD modification and Na^+ protection of Glu65

carboxyl group against DCCD modification. The assumption is that differences in DCCD modification reaction of Glu65 residue are linked to changes in both, H^+ and Na^+ binding affinities in mutant c-rings. However, the precise quantification of the differences in Na^+ and H^+ binding affinities are required to manifest the effect of Q32A and S66A polar-to-hydrophobic mutations. Therefore, next, the series of ITC experiments were run with wild-type and mutant c-rings (section 5.3).

5.3. Isothermal titration calorimetry (ITC) measurements of cation selectivity of *I. tartaricus* wild-type and mutant c-rings

The correct characterization of the ligand binding to protein requires intense experimental work in order to determine a variety of parameters including the stoichiometry of ligand binding; ligand binding affinity and relationship between the occupied and empty sites in the macromolecule (Martinez et al., 2009)**.** Our molecular level understanding of the relative cation selectivity of c-rings in rotary ATP synthases remains very limited due to the lack of the corresponding biochemical and thermodynamic data. Thus, first, ITC-based cation binding studies were used to provide the answer to some fundamental questions related to the thermodynamic aspects of the interaction of the cations with c-ring protein. Namely, isothermal titration calorimetry (in the following abbreviated with ITC) was used to learn more about the Na^+ binding properties, and with it the protonation state of the Glu65 carboxyl group, in the*I. tartaricus* wild-type and mutant c-rings, depending on the local structural situation within or near the ion-binding site. A second goal was to identify residues that directly or indirectly contribute to the free energy of Na^+ binding.

5.3.1. Insights into measuring Na^+ binding affinity of *I. tartaricus* wild-type c-ring with ITC

5.3.1.1. Initial tests, detection of cation binding to *I. tartaricus* wild-type c-ring

Primarily, ITC technique was used to determine multiple parameters of cation binding to *I. tartaricus* wild-type c-ring. Four different monovalent cations with different radii of ions were used to reveal the cation-binding selectivity pattern of *I. tartaricus* wild-type c-ring at the pH range 6.5-7.5: Li^+, Na^+, K^+ and Cs^+. The radii of these ions, *r* in Å, increases in a row $Li^+ > Na^+ > K^+ > Cs^+$ (Mähler and Persson 2012).The H^+ were not implemented directly in ITC titration series due to challenges to setup H^+ binding measurements at conditions where H^+ will be always present in the reaction. Experiments were performed over a 1-250 mM range of cation concentrations. Solution of DDM-solubilized and buffer-equilibrated target protein was placed in

the sample cell of ITC machine. The portions of titration solution containing NaCl, LiCl, KCl or CsCl were titrated by portions into the solution of protein. In case the binding reaction occurred, the heat release was detected (**Figure 5-8A**).ITC titrations indicated that only Na^+ and Li^+ could be specifically bound to *I. tartaricus* wild-type c-ring (**Figure 5-8**). Both associations were the exergonic processes that resulted in exothermic signals of Na^+ or Li^+ binding to wild-type c-ring. With larger cations (e.g., Cs^+ or K^+) no binding selectivity was detected.

A **B**

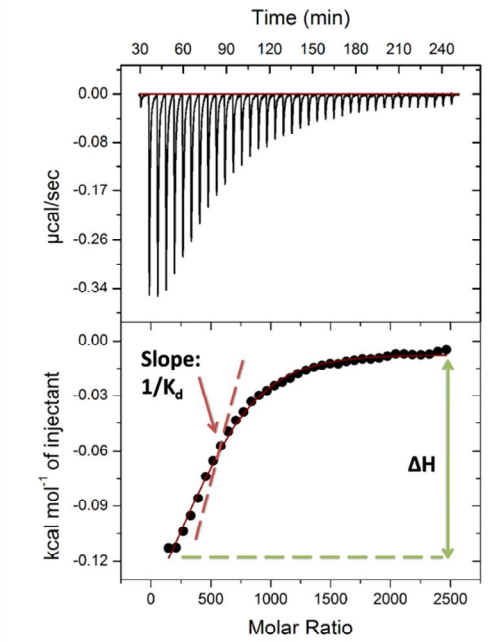

Cation	*r* , Å*	Binding	Sign of binding enthalpy
Li^+	0.60-0.79	yes	exothermic
Na^+	1.02-1.07	yes	exothermic
K^+	1.38-1.46	no	No
Cs^+	1.73	no	No

Figure 5-8: Detecting cation binding to *I. tartaricus* wild-type c-ring. (**A**) Upper panel: Characteristic data generated by ITC experiment representing the heat released (µcal/sec) during NaCl titration into solution of *I. tartaricus* wild-type c-ring. The titration profile shows that injection of aliquiots of NaCl into *I. tartaricus* wild-type c-ring suspension gives exothermic heats of binding, which decrease in magnitude with subsequent injections, showing saturation behavior. For the current experiment 2 µM of the wild-type c-ring solubilized in 0.15% DDM was titrated by consecutive additions of 5 µL of 10 mM MES pH 6.5 containing 15 mM NaCl and 0.15% DDM. Lower panel: The raw data is converted into the binding isotherm and are fitted to one-site binding model (more details are in Methods, Chapter 4.2.6.4). From this binding isotherm the change in enthalpy ΔH (green arrow) and dissociation constant K_d (red arrow) were derived. Free energy change ΔG and entropy ΔS were calculated from ΔH, K_d and T. (**B**) Summarizing table for cation binding to *I. tartaricus* wild-type c-ring.

5.3.1.2. Relative constants for Na^+ binding. Competitive mode of Na^+/H^+ binding to *I. tartaricus* wild-type c-ring

The consequence of not exclusive cation binding selectivity of *I. tartaricus* wild-type c-ring attributed to the same functional binding site is that cations competitively bind to wild-type c-ring depending on their concentrations and their apparent affinities. In order to verify this

statement, Na^+/H^+ competitive binding experiments at series of Na^+ and H^+ concentrations and Na^+/H^+ ratios were performed. Measured Na^+-binding affinities were in the range of 1616.0 ± 80.8 → 7.6 ± 0.4µM and were strictly dependent on pH (**Figure 5-9B**).

A

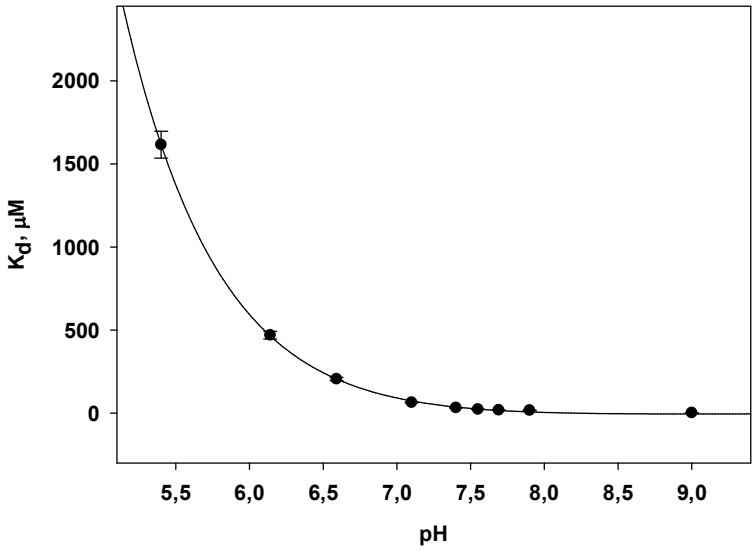

B

pH	$[H^+]$, µM	K_d (Na^+), µM
5.4	3.981	1616.0 ± 80.8
6.1	0.724	469.4 ± 23.5
6.6	0.257	205.7 ± 10.3
7.1	0.081	64.5 ± 3.2
7.4	0.039	32.8 ± 1.6
7.6	0.028	23.0 ± 1.2
7.7	0.020	18.4 ± 0.9
7.9	0.013	16.9 ± 0.8
9.0	0.001	7.6 ± 0.4

Figure 5-9: pH-dependent, apparent Na^+-binding affinities of *I. tartaricus* wild-type c-ring. (**A**) Apparent Na^+ binding affinities (●) were assessed under different pH conditions. Strong Na^+/H^+ competition for binding to wild-type c-ring was observed and is depicted by exponential decay dependency (▬), with subtle change in Na^+ affinity between pH 7.9 and 9.0. (**B**) Estimated K_d (Na^+) values at different pH and respective H^+ concentrations. The stronger Na^+ binding was observed at lower concentration of H^+.

The obtained overall pH profile of Na^+ dissociation constants demonstrates that H^+ evidently compete with Na^+ for binding. At high H^+ concentration ($[H^+]$ = 3.98 µM), the estimated Na^+ binding affinity lays in the mM range (low-affinity Na^+ binding). However, when the H^+ concentration in the reaction was lowered, the measured Na^+-binding affinities were indeed in µM range (high-affinity Na^+ binding). Hence, the Na^+-binding constants for *I. tartaricus* wild-type c-ring are always apparent and relative to the pH at which they have been determined.

5.3.1.3. Total binding selectivity and absolute constants for Na^+ and H^+ binding to *I. tartaricus* wild-type c-ring

In contrast to apparent binding affinities, absolute binding affinities are the maximal binding affinities at conditions, where Na^+ and H^+ are not competing with each other for binding. In order to dissect the absolute (=maximal) Na^+ and absolute (=maximal) H^+ binding affinities of *I. tartaricus* wild-type c-ring, obtained apparent K_d (Na^+) values were plotted as a function of appropriate concentrations of H^+ (**Figure 5-10**). Obtained dependency has a sharp linear character. The absolute binding constants for H^+ and Na^+ were extrapolated as it is described in (Leone et al., 2015).

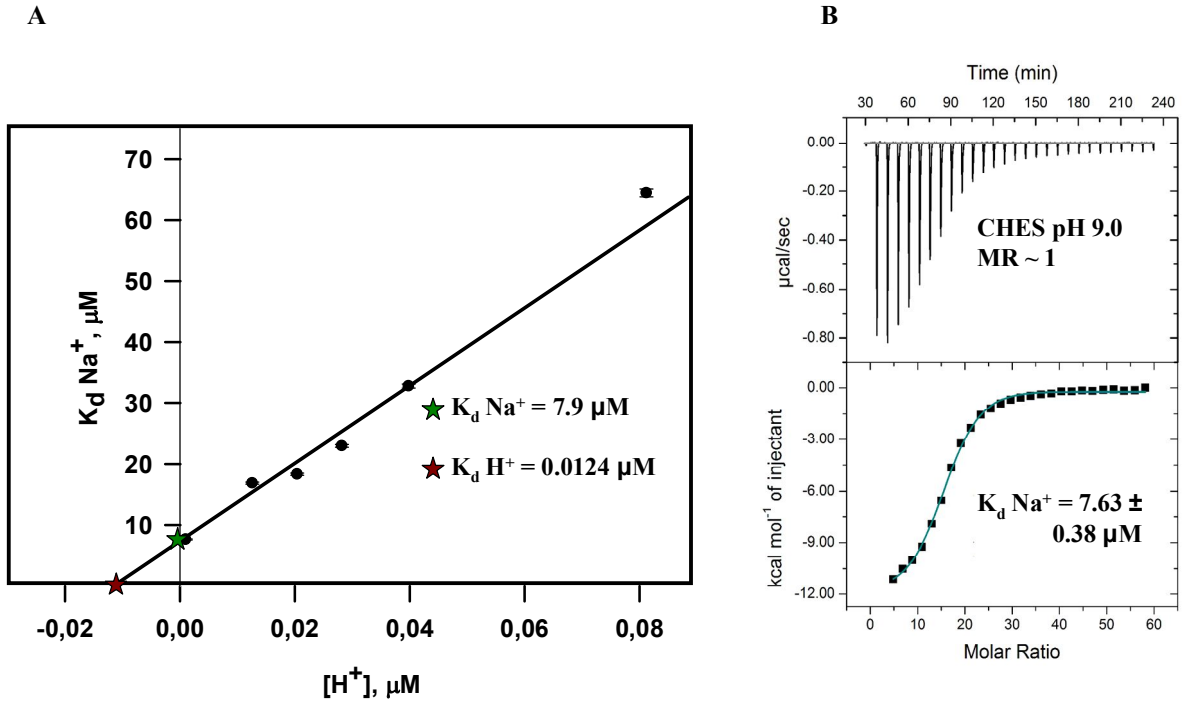

Figure 5-10: Estimation of the absolute Na^+ and H^+ binding affinities for *I. tartaricus* wild-type c-ring. (**A**) Evaluation of the absolute binding constant for Na^+ and absolute binding constant of H^+ for the wild-type c-ring in 0.15% DDM. The apparent K_d (Na^+) values were plotted against appropriate concentrations of H^+ (presented is the zoomed plot of **Figure 5-10** with K_d values between pH 6.14 and pH 9.0). At conditions of theoretical [H^+] = 0 and [Na^+] = 0, the appropriate absolute K_d (Na^+) (depicted with green star) and absolute K_d (H^+) (depicted with a red star) were extrapolated from y- and -x-axis intercepts, respectively. (**B**) Non-competitive binding of Na^+ to *I. tartaricus* wild-type c-ring at pH 9.0. Na^+ binding was observed roughly at 1:1 Na^+-to-protein molar ratio when the initial excess of Na^+ over H^+ per each µM of the protein equals to 8.55 x 10^5. According to the evaluated absolute binding constant for Na^+ (7.9 µM), Na^+ binding at pH 9.0 occurs with its absolute maximal binding affinity (7.6 ± 0.4 µM). The low H^+ concentration ([H^+] = 0.001 µM) together with conditions of total Glu65 deprotonation (0 from 11 sites are loaded with protons) promote Na^+ binding activity that is no more competitive with H^+ binding.

Interestingly, at pH 9.0, at very low H^+ concentration and expected full deprotonation of the Glu65 carboxyl group, Na^+ binds non-competitively to *I. tartaricus* wild-type c-ring with affinity identical to the evaluated absolute Na^+ binding affinity (**Figure 5-10B**). Therefore, it is assumed

that further alkalization above pH 9.0 (pH ≥ 9.0) should no longer contribute to increased apparent affinity of Na^+ binding.

The total ion selectivity for the c-ring was defined as a ratio between its absolute binding affinity for Na^+ and absolute binding affinity for H^+ (K_d (Na^+)/K_d (H^+)) (**Figure 5-11**).As follows from the plotted data, *I. tartaricus* wild-type c-ring is more selective toward H^+ over Na^+ in DDM.

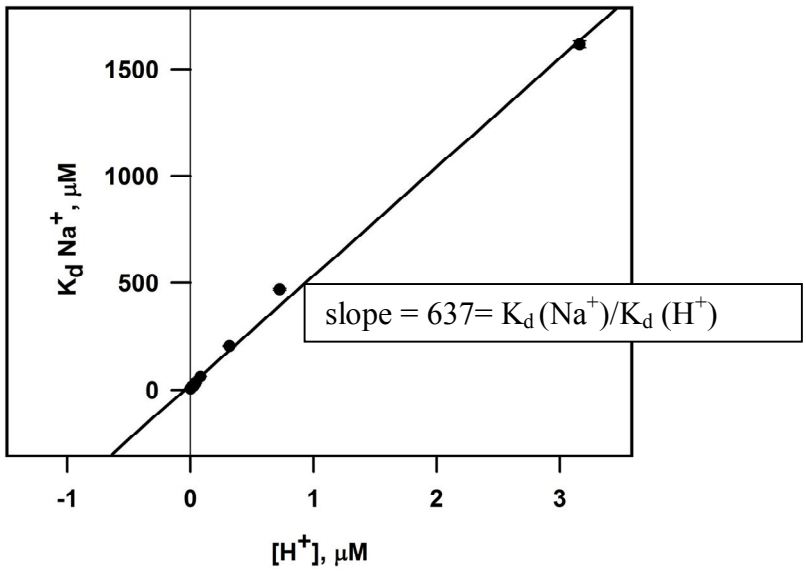

Figure 5-11: Estimation of total Na^+/H^+ binding-selectivity of *I. tartaricus* wild-type c-ring. Apparent K_d values for Na^+ binding were plotted as a function of appropriate H^+ concentrations over pH range 5.4 - 9.0. Data were fitted to a linear regression function and the estimated slope of the line was defined as total Na^+ vs H^+ ion-selectivity. According to obtained data, in 0.15% DDM *I. tartaricus* wild-type c-ring is 637 times more selective toward H^+ over Na^+.

It is important to consider that absolute binding constants for Na^+ and H^+ and the total Na^+/H^+ selectivity of wild-type c-ring were estimated in particular microenvironment (DDM microenvironment was used in current work). Different microenvironments may influence ion binding to the c-ring (section 5.3.1.4).

5.3.1.4. Effect of different detergents and DMSO on Na^+ binding to *I. tartaricus* wild-type c-ring

The microenvironment (in this case detergents and DMSO) was defined to be the local chemical neighbourhood around the protein in which its structure and function exists. In this section, the aim was to test whether there are changes in the apparent Na^+ binding constants with respect to the polarity of the used microenvironment for ITC measurements (hydrophobic detergent or hydrophilic organic solvent). Therefore, Na^+ binding experiments were performed in a similar way for one batch of wild-type c-ring equilibrated in parallel in DDM, OG or DMSO. The experiments indicated a strong effect of microenvironment on Na^+ binding to *I. tartaricus* wild-type c-ring (**Table 5-7**). The results demonstrated that independently on taken pH, DMSO provided environment for strongest Na^+-c-ring binding. Na^+ binding to c-ring was weaker in detergent. The length of detergent alkyl chain also had an impact on Na^+ binding to the c-ring.

Table 5-7: Effect of the microenvironment on apparent K_d (Na^+) values

pH	K_d (Na^+) in 5% DMSO	K_d (Na^+) in 0.15% DDM	K_d (Na^+) in 1% OG
5.4	1.01 ± 0.05	1.62 ± 0.08	2.73 ± 0.13

There were evaluated accurate sets of thermodynamic parameters for Na^+ interaction with c-ring in microenvironments with different polarity. A low pH of 5.4 was chosen as one of the reference points (**Figures 5-12)**. The thermodynamic settings of Na^+ binding to wild-type c-ring did not change in different detergents or DMSO. The obtained energy profiles of Na^+ binding to *I. tartaricus* wild-type c-ring in different microenvironments show relevant results for the sign of energy contributions (favorable or unfavourable contribution of ΔH and $-T\Delta S$ to total free energy change ΔG). Independently of the chosen microenvironment, the enthalpy term dominated in the Na^+ binding reaction and entropy unfavored Na^+ binding in all three microenvironments. However, we observe that apparent values of entropy and enthalpy contributions upon Na^+ binding differ over the change in chemical microenvironment. The difference in apparent values increases by 5 and 6.6 kcal/mol when the DMSO microenvironment is changed to long alkyl-

chain length DDM and short alkyl-chain OG detergent, respectively.

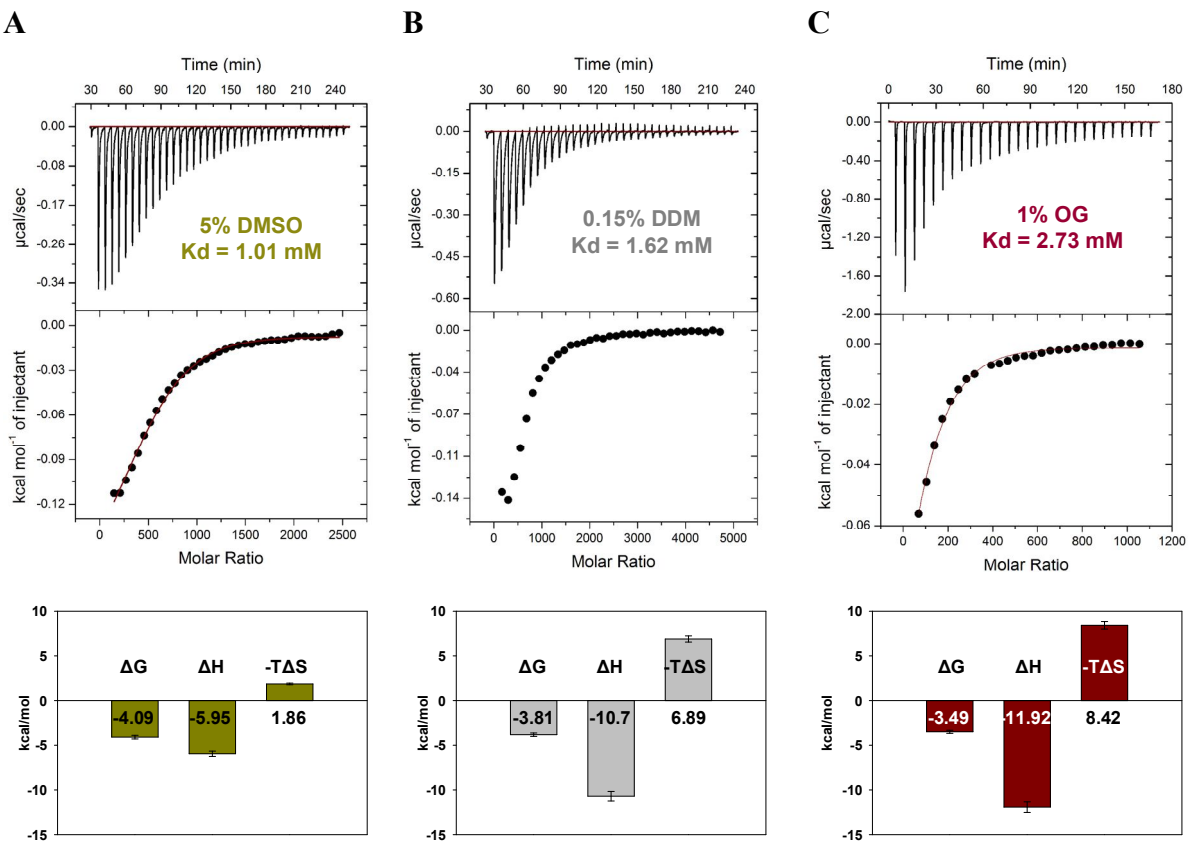

Figure 5-12: Effect of microenvironment on thermodynamic settings of Na^+ binding to *I. tartaricus* wild-type c-ring at pH 5.4. Upper panel: Raw data and integrated heats of a binding experiment titrating 50 mM NaCl into 2.24 µM of wild-type c-ring in 10 mM MES pH 5.4 and 5% DMSO (A), 0.15% DDM (B) or 1% OG (C) at 25°C. In hydrophilic microenvironment made by DMSO, Na^+ binding is stronger in comparison to DDM or OG detergent microenvironments. Lower panel: Thermodynamic signature of Na^+ binding to *I. tartaricus* wild-type c-ring evaluated in different chemical microenvironments. The 6.6 kcal/mol difference in apparent energy contributions was observed between DMSO and OG microenvironments and can be attributed to large entropy/enthalpy (S/H) or enthalpy/entropy (H/S) compensation upon Na^+ binding to the c-ring. Despite large difference in ΔH and –TΔS energies, the energy compensation mechanism is directed to compensate the changes in energies contributions and allows to end up with close free energies of Na^+ binding to the c-ring.

5.3.1.5. Effect of the detergent concentration on Na^+ binding to *I. tartaricus* wild-type c-ring

The aim was also to test whether different concentrations of detergent may affect Na^+ binding to the c-ring. Concentration of DDM that has very low critical micelle concentration (cmc) in H_2O (0.0087%) was varied in the reaction mixture and performed the Na^+ binding experiments with *I. tartaricus* wild-type c-ring were performed. The detergent concentration was kept equal in both, sample and ligand solutions. Our data demonstrated that the detergent-to-protein ratio affects Na^+ binding to wild-type c-ring (**Figure 5-13**).

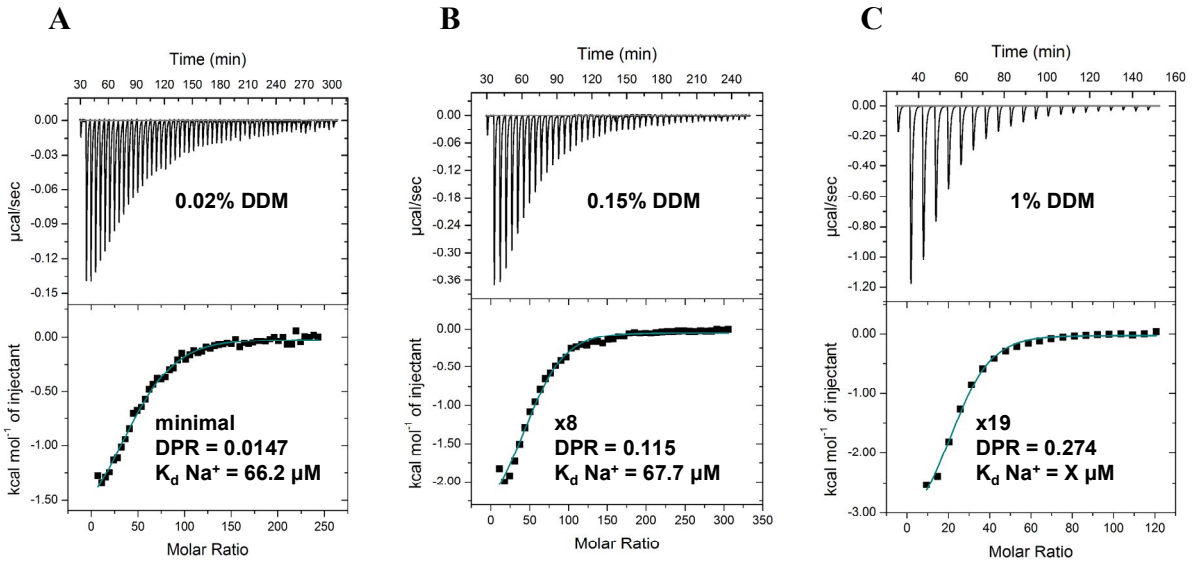

Figure 5-13: Effect of detergent-to-protein ratios (DPR) on Na^+ binding to *I. tartaricus* wild-type c-ring in 10 mM HEPES pH 7.2. When low-cmc DDM detergent was used for solubilization and equilibration of the samples of purified wild-type c-ring, there was a clear effect of detergent-to-protein ratio (% of detergent per µM of protein) on observed K_d (Na^+) values. Very high DPR ratios (≥ 0.32) resulted in higher K_d values for Na^+ binding to wild-type c-ring. (**A**) 0.02% DDM was estimated to be minimal DDM concentration capable to keep 1.4 µM of the wild-type c-ring protein soluble. Wild-type c-ring binds Na^+ with 66.2 µM affinity in 0.02% DDM at pH 7.2. (**B**) 8 times elevated DDM concentration did not affect Na^+ binding to wild-type c-ring. (**C**) 19 times elevated DDM concentration reduces Na^+ binding affinity of wild-type c-ring almost twice. However, normalized DPR ratios allow working even with high DDM concentrations (up to 1%) without changes in Na^+ binding affinities.

It was determined that the gradual elevation of DDM-to-c-ring molar ratio at some point starts

influencing Na^+ association with wild-type c-ring. Therefore, DDM-to-c-ring ratio has to be controlled throughout the experiment. Up to 0.274% of the DDM per each μM of the c-ring can be used without affecting Na^+ binding to wild-type c-ring. This phenomenon has to be taken into account when new surfactant is used for c-ring sample preparation and ligand titration experiments.

5.3.1.6. Contribution of Glu65 carboxyl group deprotonation to observed enthalpies of Na^+ binding

According to available 2.4 Å crystal structure of ion-binding site in *I. tartaricus* wild-type c-ring (Meier et al., 2009), Glu65 residue is involved directly in coordination of Na^+ and is a site of H^+ binding. Moreover, deprotonating Glu65 carboxyl group is essential for Na^+ binding and ion-translocation mechanism and provides the core of ion-coupling mechanism for ATP synthases (see Inroduction, section 2.6.11). Therefore, it was important to define intact protonation state of Glu65 carboxyl group in *I. tartaricus* c-ring and the effect of mutations on Glu65 protonation state. Both reactions (Na^+ binding and mediated H^+ release) have been calorimetrically detected in the detergent-solubilized preparations of wild-type c-ring in buffers with different ionization enthalpies (**Figure 5-14**).

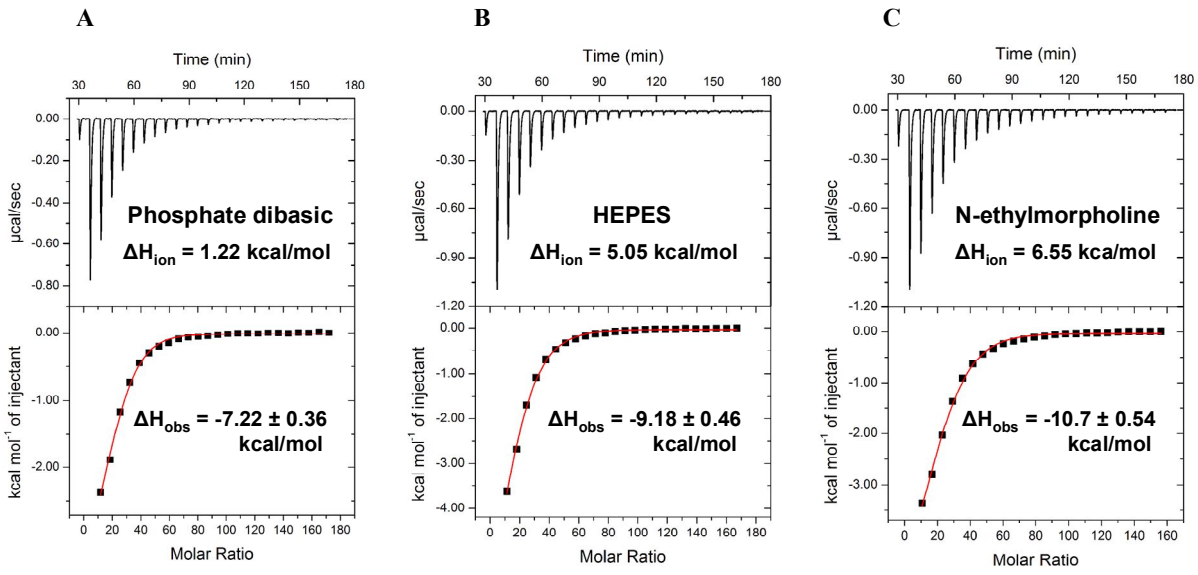

Figure 5-14: Effect of buffers with different heats of ionization on observed enthalpies upon Na^+ binding to *I. tartaricus* wild-type c-ring. Na^+ binding to wild-type c-ring was assessed at pH 7.5 in 0.15% DDM in buffers with different ionization enthalpies (ΔH_{ion}). Use of buffers with high ΔH_{ion} lead to sufficiently increased observed enthalpies of binding indicating clear supplementing effect of released H^+ mediated by Na^+ binding. (**A)** Raw data and plotted heats from Na^+ binding measured in Phosphate dibasic buffer. **(B)** Raw data and plotted heats from Na^+ binding measured in HEPES buffer. For the case of HEPES buffer, switching to buffer with higher ΔH_{ion} increased to a large extent the observed enthalpies. (**C)** Raw data and plotted heats from Na^+ binding measured in N-ethylmorpholine buffer. High ΔH_{ion} of used buffer resulted in a larger observed enthalpy. Differences observed in three used buffers clearly illustrate the involvement of Glu65 carboxylic group deprotonation events in overall measured enthalpy upon binding Na^+.

Figure 5-14 demonstrates the relative differences in enthalpy determined across the experiments using different buffers. To further elucidate the pure heat effect upon Na^+ binding, the obtained data were plotted and re-evaluated as it is described in Methods (Chapter 4.2.6.5). The pure effect of Na^+ binding was dissected from combined effect of H^+ release from Glu65 and Na^+ binding (**Figure 5-15**). Accordingly, the number of protonated Glu65 in the c-ring were determined as a function of observed enthalpies against buffers ionization enthalpies. *I. tartaricus* wild-type c-ring is only partially protonated at tested pH 7.5 (**Figure 5-15**). The 63%

propensity of Glu65 protonation within wild-type c-ring implies pKa for Glu65 > pH 7.5.

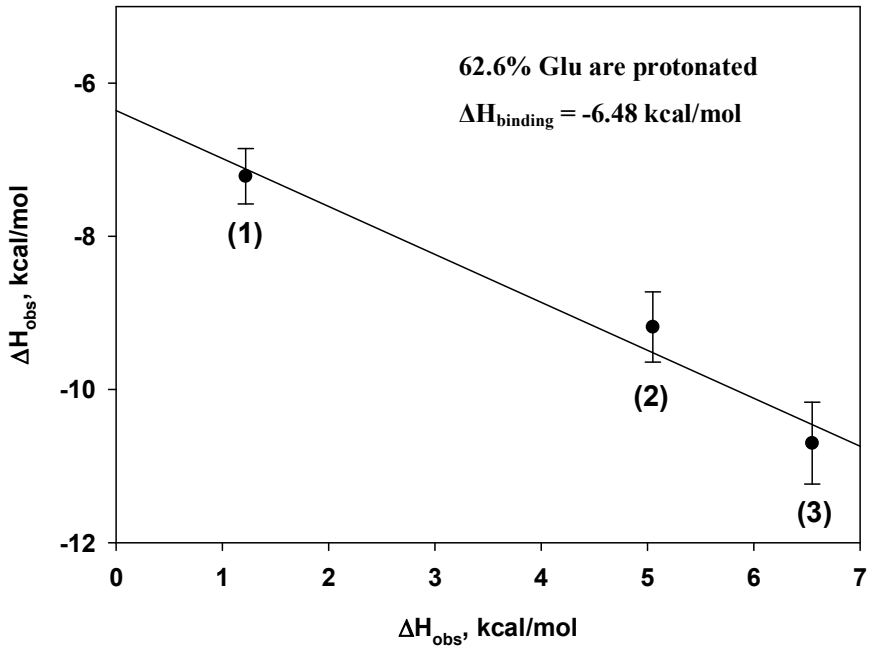

Figure 5-15: Evaluation of contribution from deprotonation of Glu65 to observed enthalpies upon Na^+ binding. ΔH_{obs} were obtained in 3 different buffers and were plotted against buffer ionization enthalpies (ΔH_{ion}): phosphate dibasic buffer with ΔH_{ion}= 1.22 kcal/mol (1); HEPES buffer with ΔH_{ion}= 5.02 kcal/mol (2); N-ethylmorpholine buffer with ΔH_{ion}= 6.55 kcal/mol (3). The negative slope of fitted linear regression function demonstrates that H^+ were released upon Na^+ binding. The calculated value of slope yielded the precise number of H^+ released per each bound Na^+ (0.626). Meaning binding of 11 Na^+ ions to c-ring promotes release of 7 H^+ bound to Glu65.

Knowing the exact Glu65 protonation state at pH 7.5 helped to properly evaluate enthalpy contribution to observed free energy change and correctly extract the entropy change upon Na^+ binding. This further dissection of the free energy change into enthalpy of the binding and entropy revealed insights into thermodynamic settings of Na^+ binding to wild-type c-ring. In the case of wild-type c-ring in DDM, the favorable change of enthalpy (ΔH) is opposed by an unfavorable entropic contribution ($-T\Delta S$) (**Figure 5-16**). This thermodynamic signature constitutes high-affinity Na^+ binding to c-ring, yielding a $\Delta G = -6.48 \pm 0.08$ kcal/mol.

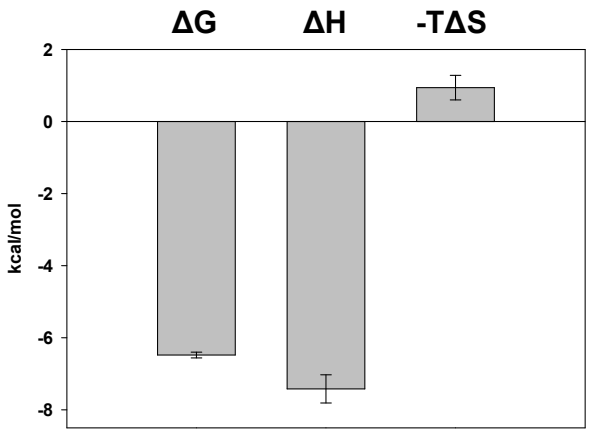

$\Delta G = -6.48 \pm 0.08$ kcal/mol

$\Delta H_{binding} = -7.42 \pm 0.39$ kcal/mol

$-T\Delta S = 0.94 \pm 0.34$ kcal/mol

$\Delta G < 0$, energetically favorable binding

$\Delta H > -T\Delta S$, enthalpy-driven binding

High-affinity Na^+ binding

Figure 5-16: Thermodynamic signature (ΔG, ΔH and –TΔS) of Na^+ binding to *I. tartaricus* wild-type c-ring at pH 7.5. After subtracting the heat effect of Glu65 deprotonation, the complete thermodynamic picture of Na^+ binding to *I. tartaricus* wild-type c-ring was obtained. High-affinity Na^+ binding is favored by large negative enthalpy contribution while entropy term unfavors Na^+ binding.

5.3.1.7. Thermodynamics of Li^+ binding to *I. tartaricus* wild-type c-ring

The *I. tartaricus* wild-type c-ring is capable to bind H^+, Na^+ and Li^+ ions under laboratory conditions (Meier et al., 2003; Krah et al., 2010). With a help of ITC, the aim was to measure in details discriminating properties of Li^+ binding selectivity by wild-type c-ring and the differences that size of the ion may impose to it. In addition, it was important to determine number of H^+ that are released from c-ring upon Li^+ binding and compare it with Na^+.

The properties of Li^+ binding to wild-type c-ring were investigated at pH 7.5 for natively and *E. coli* recombinantly expressed wild-type c-ring. Surprisingly, only measurements in DDM were successful (**Figure 5-17**). Any signals of Li^+ binding were obtained in 1% OG at pH 7.5. The result did not depend on the way the c-ring was expressed and extracted. Natively produced c-ring, as well as c-ring produced recombinantly in *E. coli* DK8 cells, showed no Li^+ binding in1% OG, even when much higher Li^+-to-protein ratios were used. In contrary, for both samples, native and recombinant, Li^+ binding was attainable in 0.15% DDM and showed comparable values for K_d (Li^+) and ΔH parameters.

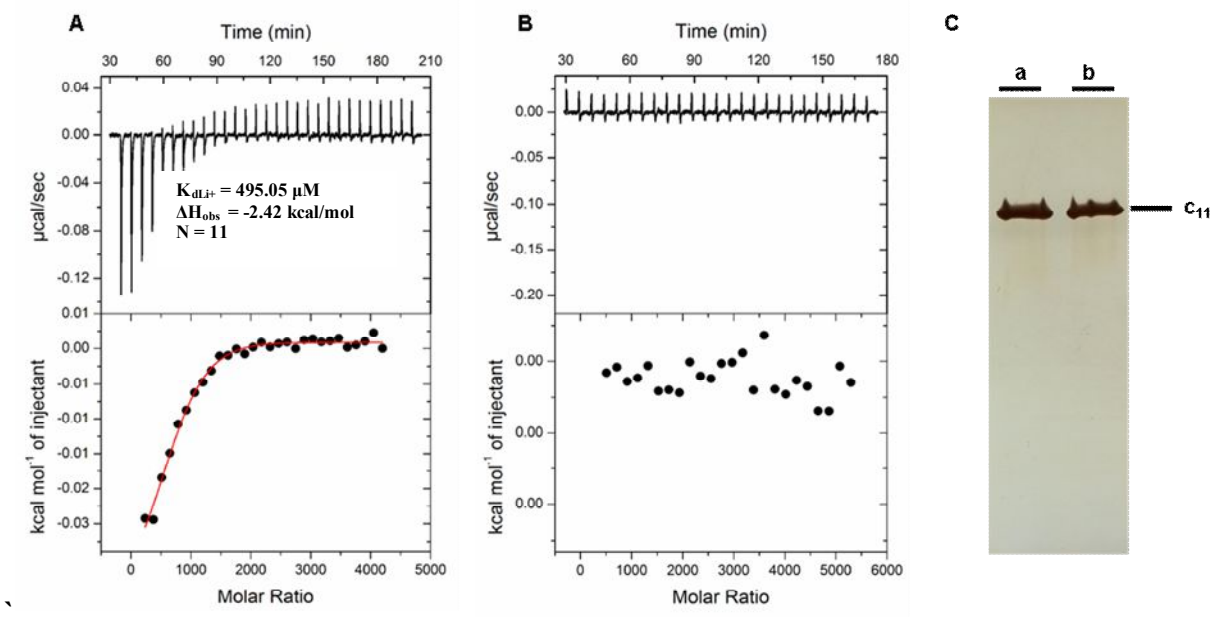

Figure 5-17: Effect of detergent on Li^+ binding to *I. tartaricus* wild-type c-ring recombinantly produced in *E. coli* DK8 cells. For the case of wild-type c-ring, we observe strict discrepancy in ability to bind Li^+ depending on taken detergent microenvironment (short alkyl-chain length OG or long alkyl-chain length DDM). For this experiment, wild-type c-ring was expressed as a part of entire ATP synthase complex and purified from *E. coli* DK8 cells. Measurements were done in 10 mM HEPES pH 7.5 with addition of 0.15% DDM or 1% OG. (**A)** Li^+ binding can be assessed in 0.15% DDM at starting Li^+-to-protein ratio of 238 (45 mM LiCl). Li^+ binding at this condition gives K_d (Li^+) value of 495.05 µM and ΔH_{obs} of -2.42 kcal/mol. Data were fitted with one-site binding model and evaluated with 1:1 stoichiometry of binding (11 Li^+ ions per 1 c-ring molecule). (**B)** High excess of Li^+ over protein (MR of 352; 55 mM LiCl) do not allow Li^+ binding to occur in 1% OG. (**C)** SDS-PAGE of wild-type c-ring protein samples in 0.15% DDM (a) and 1% OG (b) after ITC titrations shows that wild-type c-ring after ITC measurements still keep its oligomeric composition.

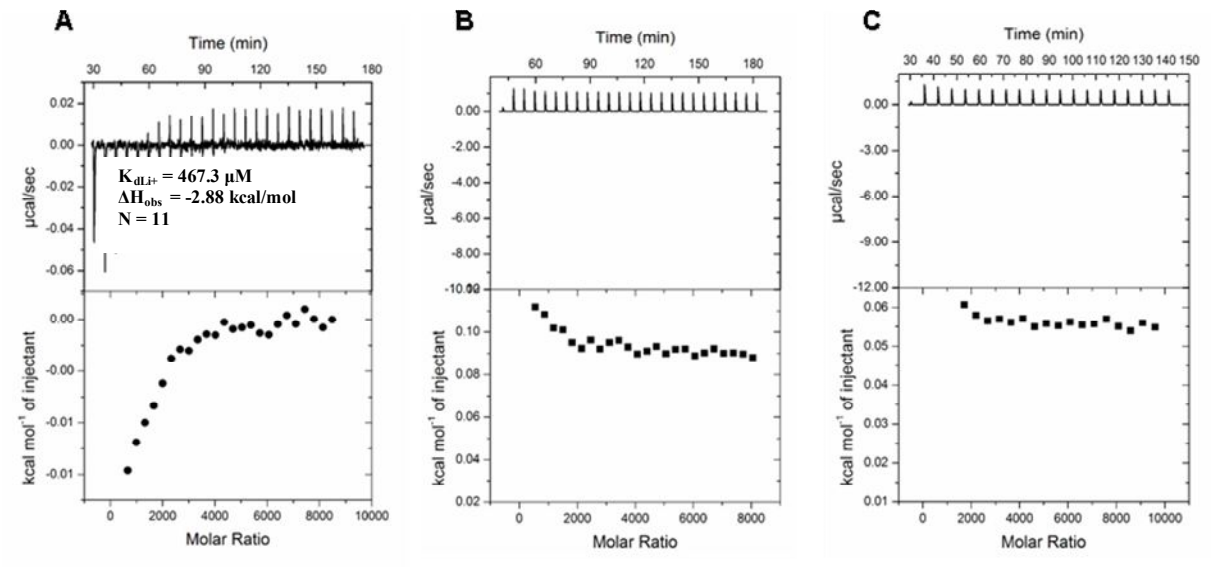

Figure 5-18: Effect of detergent on Li^+ binding to wild-type c-ring natively produced in *I. tartaricus* cells. For the case of natively produced *I. tartaricus* wild-type c-ring, the same strict discrepancy in ability to bind Li^+ depending on taken detergent microenvironment (short alkyl-chain length OG or long alkyl-chain length DDM) was observed. Wild-type c-ring was extracted from natively produced *I. tartaricus* ATP synthase and showed same difference in ability to bind Li^+ depending on taken detergent. (**A)** Li^+ binding was assessed in 0.15% DDM at Li^+-to-protein ratio of 663 (55 mM LiCl) and measured K_d (Li^+) value was 467.3 µM with a ΔH_{obs} = -2.88 kcal/mol. Data were fitted with one-site binding model and evaluated with a fixed stoichiometry of 11 (recalculated per µM of the c-ring). (**B)**, (**C)** no signals of Li^+ binding were observed in 1% OG, even when high excess of Li^+ over protein (MR of 760, 85 mM LiCl) was used.

At the next step, we compared enthalpies of Li^+ binding obtained in buffers with different ionization enthalpies in 0.15% DDM. The difference, if observed, can indicate involvement of Glu65 deprotonation or protonation events in the process of Li^+ binding to *I. tartaricus* wild-type c-ring (**Figure 5-19**). According to obtained data, Li^+ binding at pH 7.5 was accompanied with deprotonation of the Glu65 carboxyl groups in the c-ring. Data correlates with the same conclusion done for the Na^+ binding to the c-ring under similar conditions (**chapter 5.3.1.6**). For the case of Li^+ binding, observed differences in enthalpy were even more prominent and included both, increased ΔH_{obs} for the buffers with higher ΔH_{ion} and increased signal-to noise ratio due to large enhancement of the signals by heats evolved by Glu65 deprotonation.

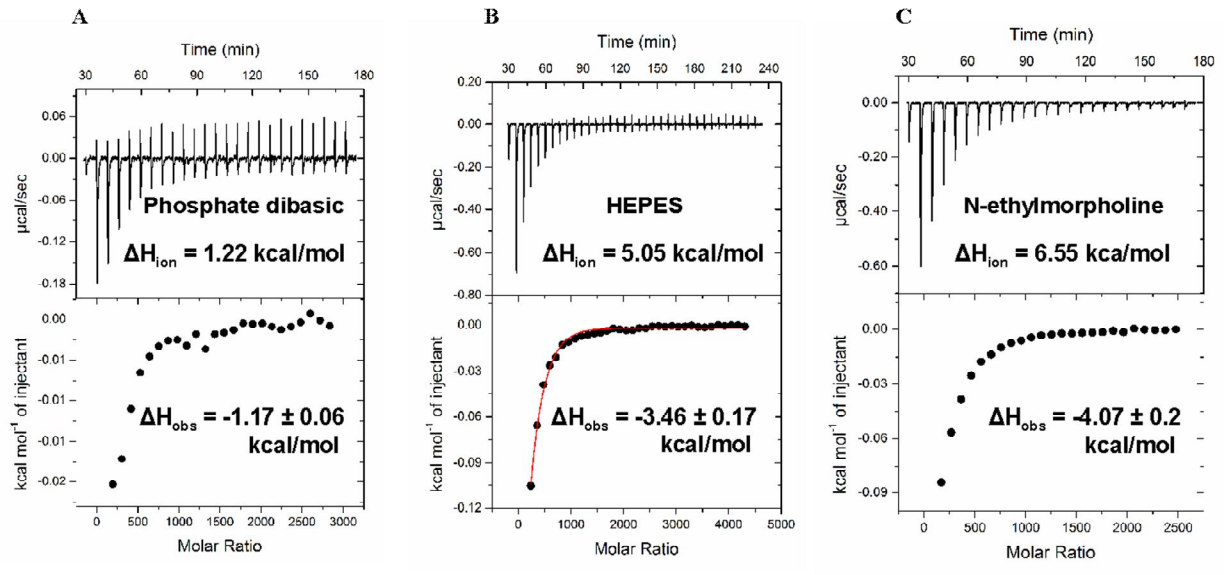

Figure 5-19: Effect of buffers with different heats of ionization on observed enthalpies upon Li^+ binding at pH 7.5. Li^+ binding to wild-type c-ring was assessed at pH 7.5 in 0.15% DDM in buffers with different ionization enthalpies (ΔH_{ion}). Use of buffers with high ΔH_{ion} leads to much increased enthalpies and signal-to-noise ratios indicating clear effect of released H^+ upon Li^+ binding to wild-type c-ring. **(A)** Raw data and plotted heats from Li^+ binding measured in Phosphate dibasic buffer. The low ΔH_{ion} of the buffer results in low signal-to-noise ratio due to small buffer contribution to overall enthalpy upon Li^+ binding. **(B)** Raw data and plotted heats from Li^+ binding measured in HEPES buffer. Switching to buffer with higher ΔH_{ion} increases to a large extent the observed enthalpies upon Li^+ binding. **(C)** Raw data and plotted heats from Li^+ binding measured in N-ethylmorpholine buffer. High ΔH_{ion} of used buffer results in a larger observed enthalpy and good signal-to-noise quality of the obtained thermogram for Li^+ binding. Likewise for the Na^+ binding to wild-type c-ring, observed dependency indicates involvement of Glu65 deprotonation reactions in overall measured heat of the reaction.

For the case of Li^+ binding to *I. tartaricus* wild-type c-ring at pH 7.5, 7 protons were detected to be released upon binding of 11 Li^+ ions. Accordingly, the protonation propensity for Glu65 residues in the wild-type c-ring was evaluated to be ~59% (**Figure 5-20**). There is a good agreement between two independent evaluations of the protonation state for wild-type c-ring at pH 7.5 (59% protonation measured by Li^+ mediated H^+ release and 63% protonation measured by Na^+ mediated H^+ release) that validates the thermodynamic ITC-based approach for evaluation of the protonation state of the ionisable groups within the protein.

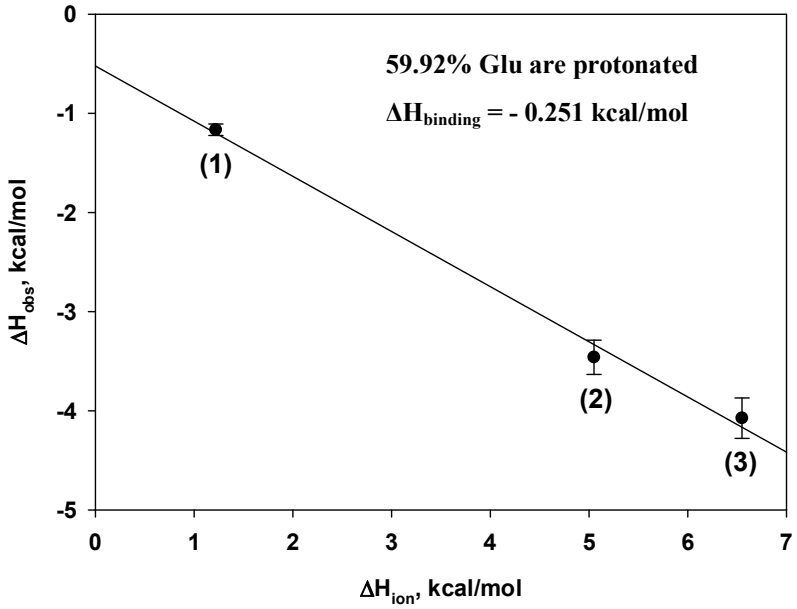

Figure 5-20: Dissection of the heats of Li^+-mediated deprotonation of Glu65 from overall observed enthalpies upon Li^+ binding. ΔH_{obs} were plotted as a function of ΔH_{ion} of the used buffers. Data were reliably fitted with linear regression function (continuous line). Obtained slope has a negative sign and equals to a number of released H^+ per bound Li^+ (0.59). The –X intercept equals to $\Delta H_{binding}$ of the Li^+ (-0.251 kcal/mol).

Figure 5-21 represents properly evaluated energy profile of Li^+ binding to *I. tartaricus* wild-type c-ring at pH 7.5 after subtracting enthalpy term of Glu65 deprotonation events. Energy profile illustrates modest-affinity binding of Li^+ ($\Delta G < 0$) to wild-type c-ring.

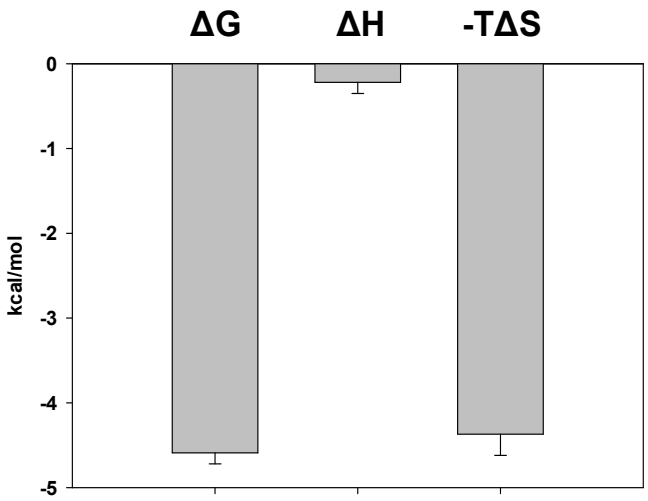

$\Delta G = -4.59 \pm 0.13$ kcal/mol

$\Delta H_{binding} = -0.22 \pm 0.13$ kcal/mol

$-T\Delta S = -4.37 \pm 0.25$ kcal/mol

$\Delta G < 0$, energetically favorable binding

$-T\Delta S > \Delta H$, entropy-driven binding

Modest-affinity Na^+ binding

Figure 5-21: Energy profile of Li^+ binding to *I. tartaricus* wild-type c-ring. After subtracting the contribution of Glu65 deprotonation to observed enthalpy of Li^+ binding, the data obtained in different buffers were averaged and plotted. Obtained energy profile shed light on thermodynamic differences underlying Na^+ and Li^+ binding (is discussed below in more details). Li^+ binding to wild-type c-ring possess modest affinity (-4.59 kcal/mol) and is entropy-driven. Both, enthalpy and entropy have negative sign and contribute favorably to free energy of Li^+ binding to wild-type c-ring.

5.3.1.8. Comparing the thermodynamic signatures of Na^+ and Li^+ binding to *I. tartaricus* wild-type c-ring

In a context of apparent and relative to pH cation-binding selectivity of *I. tartaricus* wild-type c-ring, it was important to compare the energy signatures for Na^+ and Li^+ cations that can competitively replace H^+ from the binding site (**Figure 5-22)**. According to evaluated data, Li^+ binding to *I. tartaricus* wild-type c-ring is 1.89 kcal/mol less favorable in comparison to Na^+ binding (sections 5.3.1.6 and 5.3.1.7). The main difference concerns the contributions from enthalpy and entropy energy terms. Li^+ binding is the entropy-driven reaction, where both, enthalpy and entropy contribute favorably to Li^+ binding. The resulting binding affinity is modest in comparison to Na^+ affinity.

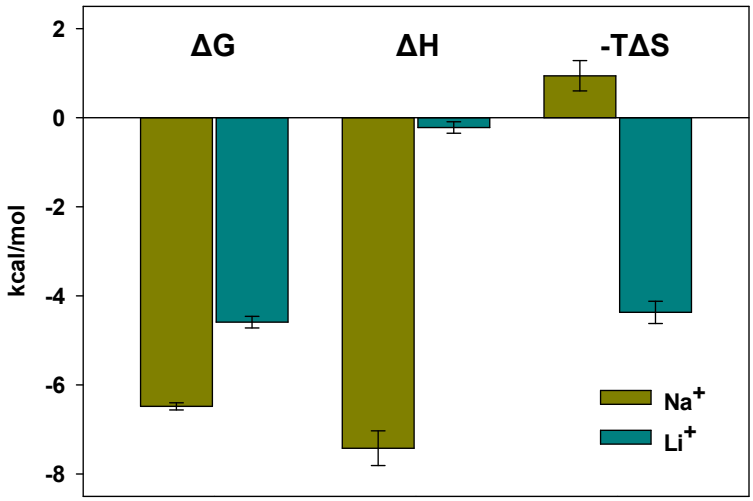

Figure 5-22: Comparison of energy profiles for Na^+ and Li^+ binding to *I. tartaricus* wild-type c-ring at pH 7.5. Li^+ binding to c-ring is 1.89 kcal/mol less favorable and is driven by entropy term. In contrast, Na^+ binding to c-ring is enthalpy-driven with a positive contribution from entropy term that limits the binding from being extremely tight.

The observed differences in energy profiles concern not only the values of contributing enthalpy and entropy energies, but also their sign. For the case of lower affinity Li^+ binding, the binding is dictated by favoring negative contribution from entropy. Meantime, the Na^+ binding is enthalpy-driven interaction.

5.3.2. Effect of mutations on apparent Na^+ binding affinity of *I. tartaricus* c-ring

At the next step, we checked how mutations of the residues that compose the ion-binding site in *I. tartaricus* c-ring affect its apparent Na^+-binding affinity. For that purpose, comparative measurements with *I. tartaricus* wild-type and mutant c-rings were performed in 0.15% DDM at pH 7.5. Analyzed T67S, G25A, T67G and Y70F mutant c-rings were tested to be stable at pH 7.5. Under the given experimental conditions, T67S, T67G, G25A, Y70F and E65D mutant c-rings afforded Na^+ binding (**Figure 5-23).** All recorded Na^+/c-ring interactions were exothermic (reactions released heat upon Na^+ binding).

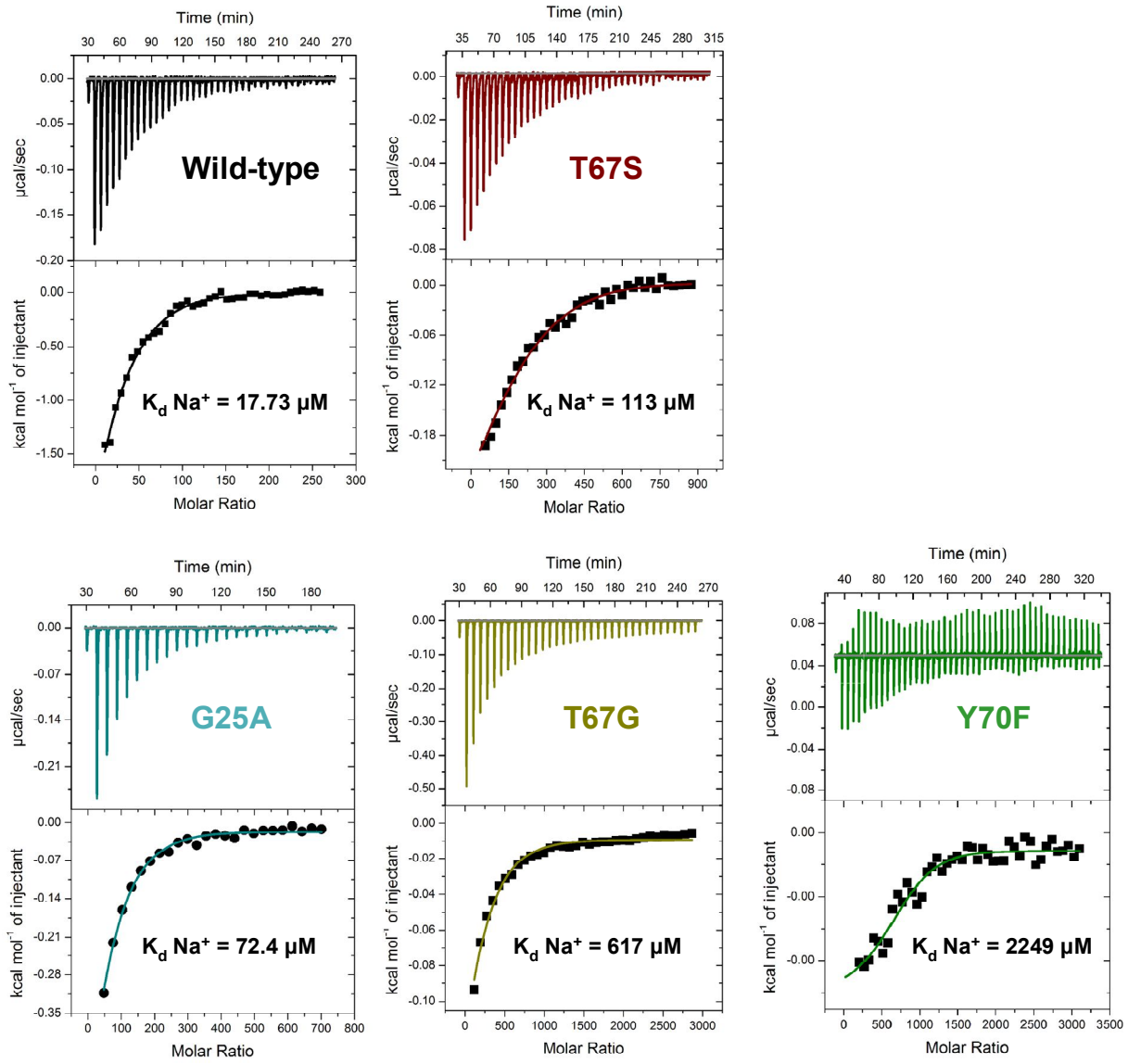

Figure 5-23: Representative thermograms of Na^+ binding to wild-type and mutant forms of *I. tartaricus* c-ring at pH 7.5. In addition to wild-type c-ring, four ion-binding site mutants showed signals for specific Na^+ binding. Presented Na^+ binding thermograms for wild-type (black), T67S (red), G25A (cyan), T67G (yellow) and Y70F (green) mutants demonstrate reduced apparent Na^+-binding affinities of mutant c-rings. Most impaired Na^+ binding affinity was introduced by Y70F substitution.

In the case of the G25A, T67S, T67G and Y70F mutants, the apparent and relative to pH 7.5 Na^+-binding affinity is decreased 4-, 6-, 35- and 127-fold, respectively. Y70F mutant shows the

lowest apparent Na^+-binding affinity among measured mutants. Accordingly, there were calculated differences in free energy change upon Na^+ binding ($\Delta\Delta G$ (Na^+)): Na^+ binds 0.88, 1.47, 2.06 and 2.95 kcal/mol less favorable to G25A, T67S, T67G and Y70F mutant c-rings, respectively (**Table 5-8**). Obtained reduction in Na^+-binding affinity of mutant c-rings correlates with reduced Na^+ protection of Glu65 carboxyl group from DCCD modification (section 5.2.4).

Table 5-8: Mutant specific differences in Na^+-binding affinities and ΔG (Na^+) values

Mutant	**K_d (Na^+), µM**	**ΔG (Na^+), kcal/mol**
Wild-type	17.7 ± 2.5	-6.48 ± 0.08
G25A	72.4 ± 3.6	-5.65 ± 0.08
T67S	113.0 ± 5.7	-5.01 ± 0.11
T67G	617.0 ± 31.0	-4.42 ± 0.08
Y70F	2249.0 ± 390.0	-3.53 ± 0.40

The initial excess of free Na^+ over H^+ (apparent Na^+ concentration versus H^+ concentration at taken pH) required to promote Na^+ binding to *I. tartaricus* c-ring was used as a parameter to describe competitive Na^+/H^+ binding to c-ring (**Table 5-9**). According to our data, *I. tartaricus* wild-type c-ring requires 5-orders of magnitude higher concentration of Na^+ over H^+ for each µM of the protein to replace H^+ from Glu65 carboxyl group in the c-ring. In case of the c-ring mutants, 4-90 times higher excess of Na^+ over H^+ was required to trigger Na^+ binding to c-ring. Among presented five single mutants, Y70F mutation introduces the chemical environment for much worse competitive binding of Na^+ against H^+.

Table 5-9: Molar excess of Na^+ over H^+ required to promote Na^+ binding to mutant c-rings at pH 7.5

Mutant	$[Na^+]/[H^+]/\mu M$ protein $x10^5$
Wild-type	1.6
G25A	6.3
T67G	17.4
T67S	18.0
E65D	50.6
Y70F	137.5

Both, Q32A and S66A/Y70F mutant c-rings did not show any signals of Na^+ binding when samples were intensively screened with different NaCl concentrations at pH range 6.5-8.0. Screening was performed with 30-250 mM solutions of NaCl with 1% OG, 0.02-0.15% DDM and 5% DMSO. Up to 2500:1 molar excess of Na^+ over protein (0.81×10^8 excess of Na^+ over H^+ for each μM of the protein) did not lead to signals of Na^+ binding to Q32A and S66A/Y70F mutant c-rings **(Figure 5-24**, shown for 0.15% DDM). However, performed DCCD modification of Glu65 carboxyl group in Q32A and S66A/Y70F mutant c-rings in presence of NaCl showed that Na^+ is competing with H^+ for binding to c-ring under particular conditions. Therefore, Q32A and S66A/Y70F mutant c-rings are weak Na^+ binders, affinity of which cannot be measured due to limitations of ITC instrumentation, that does not allow measure very weak interactions (K_d> 10 mM). Hence, the conclusion on Na^+ binding affinity for Q32A and S66A/Y70F mutants were done with other biochemical techniques (sections 5.2.4 and 5.4.5).

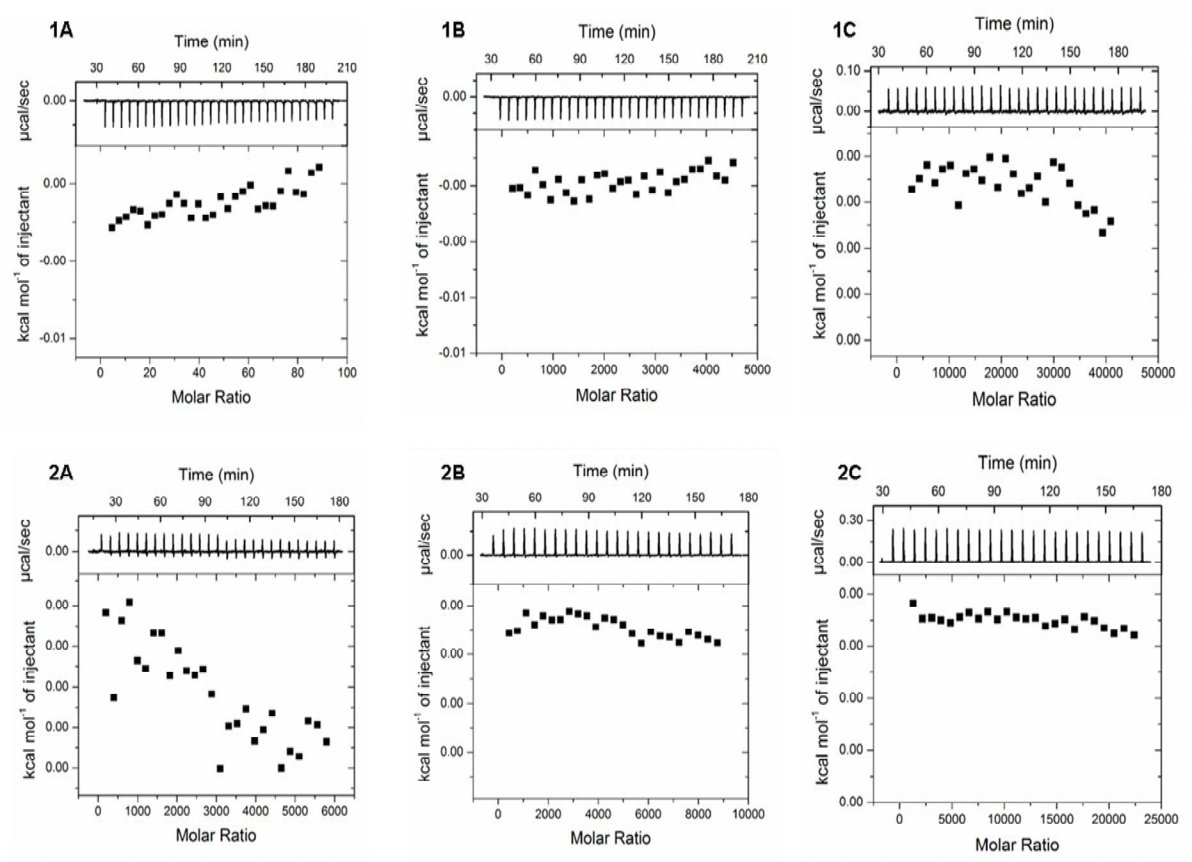

Figure 5-24: Titration of Q32A and S66A/Y70F mutant c-rings with different concentrations of NaCl. Q32A and S66A/Y70F mutant c-rings were titrated with different concentrations of NaCl at pH 7.5. Upper panel: Titrations of Q32A mutant c-ring with 30 mM NaCl (**1A**, MR ~ 5), 60 mM NaCl (**1B**, MR ~ 259) and 120 mM NaCl (**1C**, MR ~ 2569) do not show any signals for Na^+ binding. Lower panel: Titrations of S66A/Y70F mutant c-ring with 40 mM NaCl (**2A**, MR ~ 396), 100 mM NaCl (**2B**, MR ~ 434) and 250 mM NaCl (**2C**, MR ~ 1309) did not lead to any binding respond.

Q32A/Y70F mutant c-ring was thoroughly screened with ITC technique for conditions that can promote Na^+ binding to Q32A/Y70F c-ring. Q32A/Y70F c-ring did not show signals of Na^+ binding at pH range 5.4 – 9.0 in different microenvironments (1% OG, 0.02-0.15% DDM and 5% DMSO) and at different NaCl concentrations (the MRs up to 3800 were tested) (**Figure 5-25**).

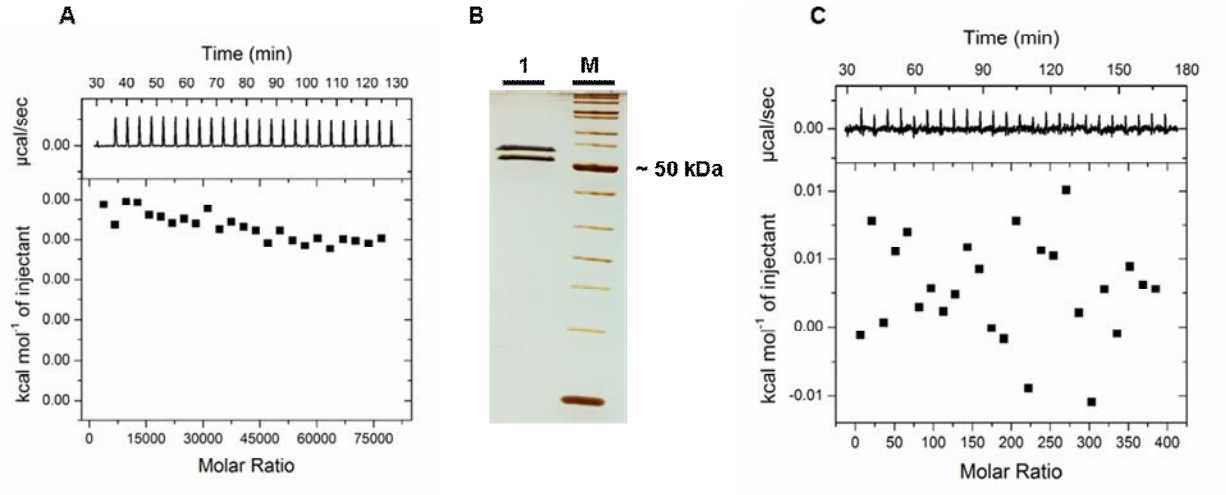

Figure 5-25: Titration of Q32A/Y70F mutant c-ring with different concentrations of NaCl. **(A)** ITC thermogram of titrating 250 mM NaCl into solution of Q32A/Y70F mutant c-ring at pH 7.5 shows no signals for Na^+ binding at molar ratio exceeding 3800. **(B)** SDS-PAGE of Q32A/Y70F c-ring after NaCl titration confirms integrity of the c-ring after ITC titration experiment (lane 1). (**C**) No signals of Na^+ binding were detected for the Q32A/Y70F mutant c-ring prepared and equilibrated in 5% DMSO at pH 9.0.

Q32A/Y70F mutant c-ring did not possess the Na^+ binding selectivity. Observed results correlate with data obtained in DCCD modification experiments: Previously, DCCD modification assay showed that Na^+ is not capable to compete with H^+ for binding to Q32A/Y70F mutant c-ring (section 5.2.4). However, the finalizing conclusions on the cation binding selectivity of Q32A/Y70F mutant were done after the catalytic cation selectivity for complete Q32A/Y70F ATP synthase were verified (see section 5.4.5).

5.3.3. Evaluation of protonation states for Glu65 carboxyl groups in mutant c-rings

Glu65 carboxyl groups in mutant c-rings were evaluated in their protonation state in DDM microenvironment at pH 7.5. In order to do so, we compared the emitted heats upon Na^+ binding in buffers with different ionization enthalpies and quantified the number of released H^+ per each bound Na^+ (details are described in section 4.2.6.5 of Methods). According to obtained data (**Table 5-10**), there is no changes in protonation of Glu65 for a series of T67S, T67G, G25A and

Y70F mutants.

Table 5-10: Protonation state of Glu65 carboxyl group at pH 7.5 depending on mutation

Mutant	*n* of 11 sites that are protonated in the c-ring
Wild-type	7
G25A	8
T67S	7
T67G	7
Y70F	7
Q32A	n/a
S66A/Y70F	n/a
Q32A/Y70F	n/a

n/a – not attainable

Na^+ binding was not attainable for Q32A and S66A/Y70F mutant c-rings at pH 7.5 (section 5.3.2) and therefore, it was not possible to evaluate promptly the number of protonated c-subunits in Q32A and S66A/Y70F c-rings at pH 7.5.

5.3.4. Differences in thermodynamic settings of Na^+ binding to mutant c-rings

Performed dissection of Glu65 deprotonation heats from the total observed enthalpy upon Na^+ binding allowed proper evaluation of the enthalpy and entropy terms of Na^+ binding to mutant c-rings (**Figure 5-26**). Wild-type and T67S c-rings demonstrated enthalpy-driven Na^+ binding with positive contribution from entropy. For the case of G25A and T67G mutant c-rings, both enthalpy and entropy contribute favorably to Na^+ binding. Y70F mutant demonstrated the lowest affinity and different to wild-type thermodynamic settings of Na^+ binding in which only entropy term favors Na^+ binding.

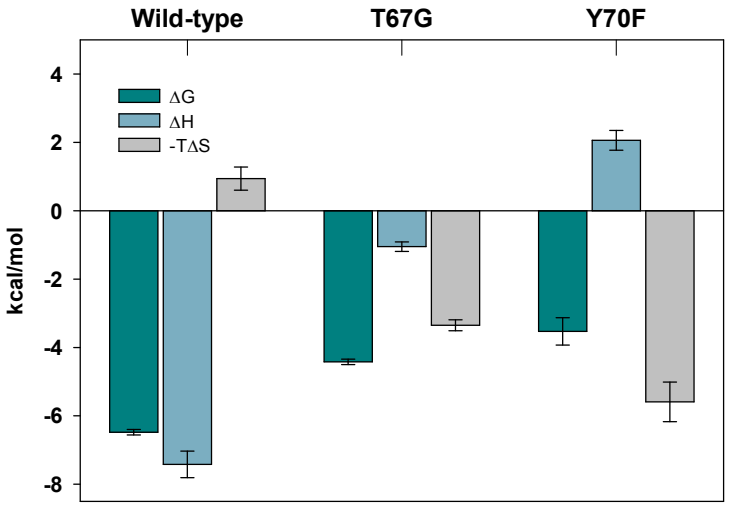

Mutant	ΔH vs -TΔS
Wild-type	ΔH > -TΔS
G25A	ΔH < -TΔS
T67S	ΔH > -TΔS
T67G	ΔH < -TΔS
Y70F	ΔH < -TΔS

Figure 5-26: Different thermodynamic settings of Na^+ binding to *I. tartaricus* c-ring depending on chemical oscillation of the ion-binding site. Wild-type, T67G and Y70F mutant c-rings represent three different thermodynamic settings for Na^+ binding that are accompanied with high- (cyan), middle- (blue) and low- (grey) affinity Na^+ binding, respectively.

In the case of the *I. tartaricus* wild-type c-ring, favorable enthalpy contribution is largely dominating over entropy contribution (~87% of total free energy change of Na^+ binding). For the case of T67G and G25A mutant c-rings, enthalpy contributes less than 30% to the total Na^+ binding free energy change (24% for T67G and 26% for G25A mutants). For the case of Y70F mutant, binding is dictated by favoring entropy change and unfavourable enthalpy contribution only for ~37%.

5.3.5. Grouping of the *I. tartaricus*c-ring mutants depending on the thermodynamic signature of Na^+ binding

Further grouping of the mutant c-rings was carried out based on results of ITC experiments (**Table 5-11**). From thermodynamic point of view, the main restrictions to Na^+ binding concerned the contributions from the enthalpy and entropy terms. Only enthalpy-driven Na^+ binding resulted in high affinity association (shown for wild-type and T67S mutant). The unfavorable entropy contribution prevents Na^+ binding from being extremely tight (μM not nm

range affinities) and makes it reversible. For the case, binding is entropy-driven, favorable negative enthalpy contribution allows binding to occur with middle affinity (shown for T67G and G25A mutants). For the case the entropy-driven biding is counterbalanced with energetically unfavorable contribution from enthalpy, the low affinity binding is detected (Y70F mutant).

Table 5-11: Grouping of c-ring mutants depending on ITC data

Group	**Mutant**	**Thermodynamic properties of Na^+ binding**
I.: High Na^+ affinity	*I. tartaricus* wild-type and T67S	Enthalpy-driven Na^+ binding
II.: Middle Na^+ affinity	T67 and G25A	Entropy-driven Na^+ binding
III.: Low Na^+ affinity	Y70F	Entropy-driven Na^+ binding with unfavorable enthalpy contribution
IV.: Very low Na^+ affinity (K_d>> 10 mM at pH 7.5)	Q32A and S66A/Y70F	H^+ were not replaceable with Na^+ at pH 7.5
V.: No Na^+ affinity	*S. platensis* wild-type and Q32A/Y70F	Non-selective for Na^+

As ITC measurements indicated, particular mutations can restrict Na^+ binding affinity. Namely, we identified Q32A/Y70F mutation in the ion-binding site that restricts Na^+ binding while maintaining the H^+ binding selectivity. The question on whether the same functional principle holds also for the catalytic selectivity of the complete Q32A/Y70F ATP synthase was elucidated further in functional studies (section 5.4.5).

5.3.6. Estimation of the pKa values for Glu65 by combining ITC and DCCD data

Ionisable carboxyl group of Glu65 residue in *I. tartaricus* wild-type c-ring binds H^+ and is directly involved in Na^+ coordination. Carboxylate of Glu65 plays an essential role in H^+ and Na^+ translocation across membrane (Vik and Antonio 1994; Junge et al., 1997; Dimroth 2000;

Fillingame and Dmitriev, 2002; Pogoryelov et al., 2010; Allegretti et al., 2015). The key to Glu65 function lies in its pKa that is determined by the intrinsic state of protonation of the Glu65 carboxyl group in the c-ring and the fine-tuning of the pKa can be essential for defining cation-binding selectivity of the rotor c-rings. Therefore, our next step was to study how the pKa of Glu65 in the *I. tartaricus* c-ring was changed upon different mutations.

Since DCCD reacts only with protonated carboxyl groups, an apparent pKa for Glu65 carboxyl group was estimated indirectly from the DCCD reaction rate as a function of pH (Kluge and Dimroth, 1993; Velazquez et al., 1997; Valiyaveetil et al., 2002). In particularly, pH-dependent DCCD modification of Glu65 in the c-ring follows pH-dependent deprotonation of Glu65 carboxyl group and should progress more rapidly for Na^+-selective c-rings (as Na^+ replaces H^+ from the binding site). Thus, The 50% protonation of carboxyl group (pKa) can be determined from the pH-profile of DCCD modification (details in Methods, Chapter 4.2.7.6).

As follows from estimated pKa values for Glu65 in wild-type c-ring, the local structural environment of ion-binding site in the wild-type c-ring gives rise to apparent pKa of Glu65 ~ pH 7.8 (**Table 5-12**). A perturbed apparent pKa for Glu65 was detected with either a Q32A, S66A/Y70F mutations (pKa ~ pH 8.3) or Q32A/Y70F mutation (pKa ~ pH 9.3), but no effect on the apparent pKa for Glu65 was detected in the E65D, T67G, T67S and Y70F mutant c-rings. None of the analyzed mutations decreased the pKa of Glu65. Meaning the pKa of Glu65 in *I. tartaricus* c-ring shows its own shifted behaviour in correspondence to the local structural situation within or near the ion-binding site in the c-ring and can be modulated by hydrophobic mutations (**Table 5-12, graph 2)**

Table 5-12: **Estimated apparent pKa values and deprotonation energies for Glu65 in wild-type and mutant c-rings**

Mutant	pKa	ΔG_{depr}, kcal/mol	Protonation state, pH 7.5
Wild-type	7.8	-10.16 ± 0.508	7/11
G25A	n/a	n/a	8/12
E65D	7.8	-10.16 ± 0.508	n/a
T67G	7.8	-10.16 ± 0.508	7/11
T67S	7.8	-10.16 ± 0.508	7/11
Y70F	7.8	-10.16 ± 0.508	7/11
S66A/Y70F	8.3	-10.81 ± 0.541	n/a
Q32A	8.3	-10.81 ± 0.541	n/a
Q32A/Y70F	9.3	-12.12 ± 0.606	n/a

n/a – not attainable

The obtained pKa values were represented in a form of energy required to deprotonate Glu65 group (see Introduction, section 2.10). Equation $\mathbf{\Delta G' = -\ 2.3RTpKa}$ was used to transform the data. According to obtained values of deprotonation energy for Glu65, three mutant c-rings (Q32A, S66A/Y70F and Q32A/Y70F) demonstrate 0.65-1.96 kcal/mol energetically more favorable stronger binding of H^+ to Glu65 (**Table 5-12, graph 3**).

The open remained question on actual protonation state of Glu65 carboxyl groups in *I. tartaricus* wild-type and mutant c-rings and its relation to determined pKa values. This question was addressed to ITC measurements. With a help of ITC technique we determined the apparent protonation state of Glu65 in wild-type, T67S, T67G, Y70F and G25A mutant c-rings at pH 7.5. The quantified protonation of the Glu65 carboxyl groups in the wild-type and T67S, T67G, Y70F corresponds to 7 protonated c-subunits within c_{11}-ring and 8 protonated c-subunits within c_{12}-ring of G25A mutant (**Table 5-12, graph 4**). By this data, we show that the estimated pKa values fit to estimated apparent protonation state of Glu65 in *I. tartaricus* wild-type and mutant c-ring.

5.3.7. Summary of ITC experiments

The interaction of *I. tartaricus* wild-type c-ring with different cations such as Na^+, Li^+ and H^+ was investigated by ITC using a MicroCal VP-ITC instrument at 25°C.ITC method was successfully implemented in defining apparent and absolute Na^+ binding and H^+ binding affinities of *I. tartaricus* wild-type c-ring. Performed experiments indicate that *I. tartaricus* wild-type c-ring is originally 637 times more selective to H^+ than to Na^+. However, depending on taken $[Na^+]/[H^+]$ molar ratio apparent Na^+ binding affinity of wild-type c-ring differs.

ITC was also used to describe the thermodynamics of how individual amino acids contribute to the Na^+ binding process by characterizing a panel of mutants. For the set of G25A, T67S, T67G and Y70F mutant c-rings it was shown that apparent Na^+ binding affinity was decreased 4-, 6-, 35- and 127-fold due to introduced mutations in or near the ion binding site. Moreover, G25A, T67G and Y70F mutant c-rings displayed different from wild-type entropy-driven thermodynamic signatures of Na^+ binding.

Release of H^+ from protonated Glu65 carboxyl group during Na^+ binding to c-ring was examined by ITC in different buffer systems. Na^+ binding mediated H^+ release was calorimetrically estimated in wild-type and G25A, T67S, T67G and Y70F mutant c-rings and was used to define protonation state of Glu65 carboxyl group in the c-rings at pH 7.5. According to obtained data, 7 out of 11 c-subunits in the wild-type, T67S, T67G and Y70F mutant c-rings and 8 out of 12 c-subunits in G25A mutant c-ring are protonated at pH 7.5.

5.4. Functional characterization of wild-type and mutant forms of *I. tartaricus* ATP synthase

I. tartaricus F-type bacterial ATP synthase is involved in energy-transduction processes of the cell and hence, characterization of its activity is of high interest. Studying the contributions of hydrophobic/hydrophilic interactions in promoting Na^+-coupled ATP synthesis activity is pre-eminently one of the key steps in understanding the emergence of the cation-binding selectivity of rotary ATP synthases. Some aspects of how wild-type and mutant forms of *I. tartaricus* ATP synthase convert chemical energy by using different cations during ATP synthesis were addressed in this thesis by functional studies. The biochemical analysis of wild-type and mutant c-rings was performed first, followed by functional characterization of the same mutations incorporated into the ATP synthase complex.

5.4.1. Functional insights into cation-coupled ATP synthesis of *I. tartaricus* ATP synthase

5.4.1.1. Heterologous expression and purification of *I. tartaricus* wild-type ATP-synthase

To carry out experiments with purified ATP synthase, we initially tested two types of expression constructs designed for metal affinity purification of *I. tartaricus* ATP synthase. A His-tag on membrane embedded a-subunit resulted in up to 97% assembled *I. tartaricus* wild-type ATP synthase, if judge by ATP hydrolysis activity (**Figure 5-27** and section 5.4.3). In contrast, for the second construct with His-tag on water-soluble β-subunit, the assembly was lower (< 60% coupled ATP hydrolysis activity) due to larger portion of F_o domain detached during affinity chromatography step. Therefore, to guarantee a high degree of complete assembly of *I. tartaricus* ATP synthase, the expression constructs had an N-terminal His-tag at the membrane embedded a-subunit.

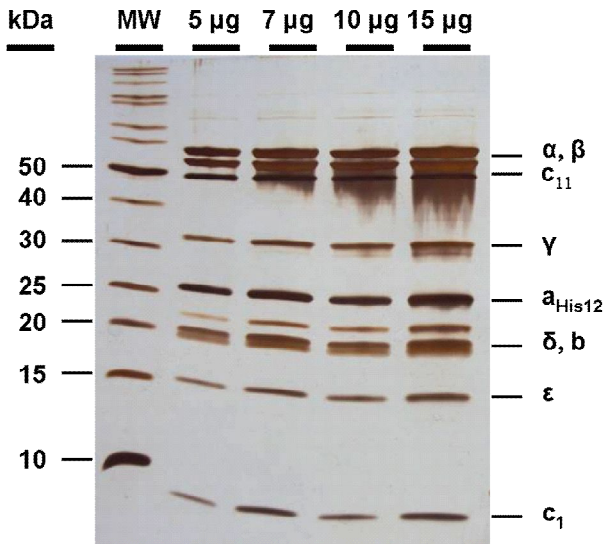

Figure 5-27: Representative SDS-PAGE of purified *I. tartaricus* wild-type ATP synthase heterologously expressed in *E. coli* DK8 cells. The lanes represent different µg amounts of a preparation of wild-type ATP synthase that was recombinantly expressed and purified to high purity from *E. coli* DK8 cells. SDS-PAGE confirms appropriate presence of eight subunits forming ATP synthase complex: α, β, γ, δ, ε, a, b and c-ring. The c-ring runs at the expected level that corresponds to wild-type c_{11}-ring (Meier et al., 2003; Hakulinen et al., 2012).

5.4.1.2. Cation selectivity of *I. tartaricus* wild-type ATP synthase and kinetic of ATP synthesis depending on applied ion-driving force

Samples of purified *I. tartaricus* wild-type ATP synthase were used for reconstitution in ETLE lipid vesicles for subsequent functional studies. As it was difficult to determine directly the concentration of protein incorporated in lipid vesicles, we measured the coupled ATP hydrolysis activity of enzyme before and after reconstitution, and made coupled activity-based determination of remaining protein in the proteoliposomes. Usually, not more than 30-40% of the protein was lost during reconstitution steps.

In the experiments it was revealed that for efficient ATP synthesis turnover, *I. tartaricus* ATP synthase requires its catalytic substrate, ADP, and also a gradient of one of its ion-coupling substrate, H^+, Na^+ or under laboratory conditions Li^+. With each of these three cation-gradients (H^+, Na^+ and Li^+), Michaelis-Menten behaviour (hyperbolic saturation kinetics) was observed

(**Figure 5-28, Table 5-13**). In a series of these experiments, combination of up to -129 mV of ion gradient and up to 135 mV of $\Delta\psi$ was imposed to proteoliposomes. Gradients of other monovalent cations (e.g., K^+, Cs^+ and Rb^+) were not capable to drive ATP synthesis of *I. tartaricus* wild-type ATP synthase (**Table 5-14**).

Table 5-13: Ion-motive forces tested for generation of ATP synthesis by *I. tartaricus* ATP synthase

Ion-motive force	Maximal used mV	ATP synthesis
Rubidium-motive force	-264	no
Caesium-motive force	-264	no
Potassium-motive force	-264	no
Sodium-motive force	-264	yes
Lithium-motive force	-264	yes
Proton-motive force	-264	yes

In order to characterize the ATP synthesis activity of ATP synthase, we used the V_i parameter, s^{-1}, which describes the unimolecular rate of how fast one ATP synthase complex is able to synthesize one molecule of ATP. The V_{max} (k_{cat}) parameter, measured as s^{-1}, was also used to describe the maximum catalytic rate that a single ATP synthase molecule can execute under conditions where it is saturated with ADP and P_i. However, for some of the recorded ATP synthesis activity curves, the classic saturation with substrate ADP was not observed due to irreversible linear activation of luciferase by certain components of the buffer. The luciferase assay was used in this study because of its high femtomolar sensitivity to ATP. However, in some cases, even after a few minutes of ATP synthesis, the maximal rate of ATP synthesis could not be reached and the signal continued to increase due to activation of luciferase. It was challenging to determine the maximal rate of ATP synthesis at the breakpoints of such unsaturatable activity curves. Therefore, for these cases, the maximum of the activity was attributed to the part of the curve, which showed maximal constant V_i/V_{max} ratio. In the case of *I. tartarcius* wild-type ATP synthase, we observed different V_i and V_{max} values for ATP synthesis driven by different ion-motive forces (**Figure 5-28**).

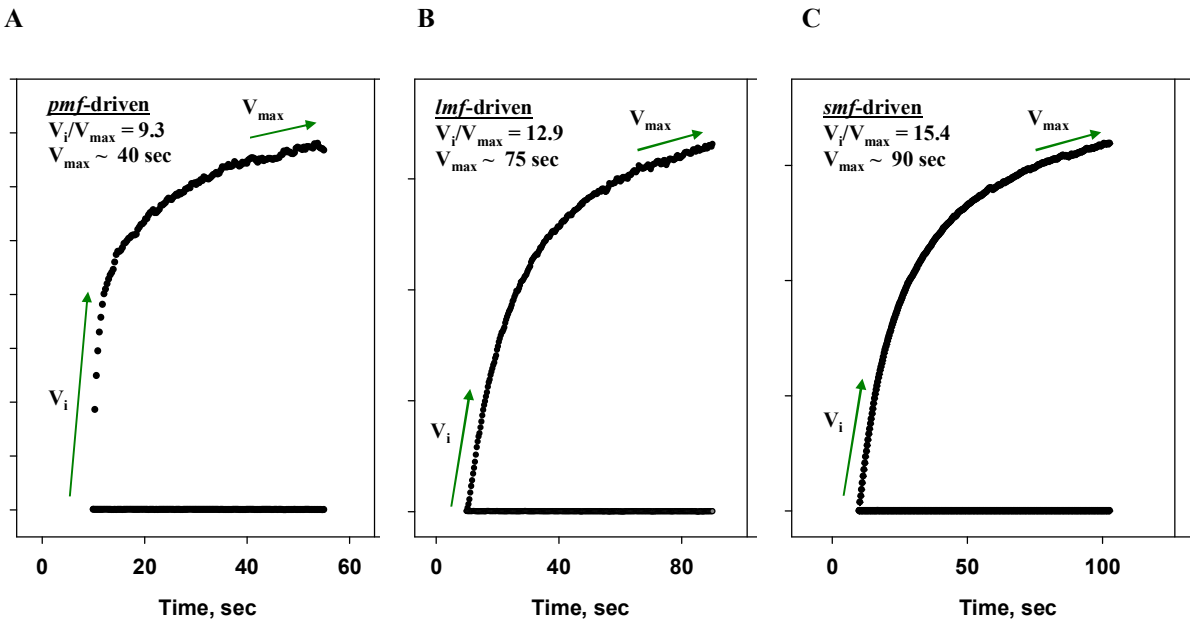

Figure 5-28: ATP synthesis of *I. tartaricus* wild-type ATP synthase driven by different ion-motive forces. Typical time-courses of ATP generation in ETLE proteoliposomes containing reconstituted *I. tartaricus* wild-type ATP synthase. The slope of the first 15 sec of recorded activity curves was used to calculate V_i values. The V_{max} values were evaluated at the point where the activity curves had maximum curvature. We used the V_i/V_{max} ratio to characterize differences in ATP synthesis driven by particular ion-motive forces: The largest V_i/V_{max} ratio and accordingly the largest ATP production was observed for *smf*-driven ATP synthesis. In addition, there was a clear effect of applied ion-motive force on time-dependency for saturation of wild-type ATP synthase with ADP: (**A**) *pmf*-driven ATP synthase becomes saturated with ADP after 40 sec of catalytic activity. (**B**) 75 sec is needed for *lmf*- and (**C**) 90 sec is needed for *smf*-driven ATP synthase to become saturated with ADP. Differences in saturation kinetic with ADP we attribute to faster dissipation of proton gradient as lipid vesicles are leakier to H^+. According to our experiments, the time of ATP synthase saturation by its catalytic substrate ADP appeared to be at least partially a property of the lipid vesicles that tend to be leakier for H^+. The magnitudes of applied ion-motive forces are described in Methods (sections 4.2.8.3-4.2.8.6).

At the next step, we had a closer look on the requirements of ATP synthase for ATP synthesis driven by different ion-motive forces.

5.4.1.3. Requirements of *I. tartaricus* wild-type ATP synthase for *pmf*-driven ATP synthesis

A thorough optimization of conditions for *pmf*-driven ATP synthesis by *I. tartaricus* wild-type

ATP synthase was carried out in order to find out conditions under which good signal-to-noise ratio for ATP synthesis activity can be obtained (**Table 5-14**). It was identified that the *pmf*-driven ATP synthesis of *I. tartaricus* ATP synthase requires strict conditions to be carried out. The main determinants of observed *pmf*-driven activity were the proper pH-acidification and $\Delta\psi$-energization of the proteoliposomes, low Na^+ concentration (< 1 mM) and samples of ATP synthase containing proteoliposomes that are initially highly coupled in ATP hydrolysis (> 50%).

Table 5-14: Optimization of conditions for *pmf*-driven ATP synthesis by *I. tartaricus* wild-type ATP synthase

pH jump	150 mM sucrose (as osmolite)	Incubation time, min	Activity
2.5 (5.0→7.5)	+	6	no
3.5 (4.5→8.0)	no	6	no
4.0 (4.0→8.0)	no	0.5	+
4.0 (4.0→8.0)	no	5	+++
4.0 (4.0→8.0)	no	6	+++
4.0 (4.5→8.5)	+/-	5	+++
4.4 (4.5→8.9)	+	5	++++
4.5 (4.0→8.5)	no	6	no
4.9 (4.0→8.9)	+	5	++++

"++++" - high signal-to-noise ratio for ATP synthesis activity,
"+++" - lower signal-to-noise ratio for ATP synthesis activity,
"+" – ATP synthesis activity is detectable but signal-to-noise ratio is low

Firstly, the effect of Δψ-energization on observed activity of *I. tartaricus* ATP synthase at different external KCl concentrations (50-400 mM) was tested and revealed that Δψ-energization was an indispensable requirement for *pmf*-driven ATP synthesis.Namely,*pmf*-driven ATP synthesis activity was observed only when ≥ 135 mV of Δψ was applied. At the next step, it was determined that pH range 4.0-8.9 can be used for ΔpH generation across proteoliposomes. Formed pH-jump (pH 4.0→ pH 8.9) was suitable to generate ATP synthesis signals of sufficient intensity to be measured by luminometer device (**Table 5-15**). Out of this pH range, the poor stability and high aggregation properties of ATP synthase in proteoliposomes was observed. In addition, the time required to acidify the interior of proteoliposomes was examined. Short acidification of proteoliposomes (~ 30 sec) resulted only in small activity signals even at high pH difference (4 pH units). Only combination of long incubation time (5 min) together with large pH

difference (4 pH units) yielded high signals of ATP synthesis activity. Further increment of incubation time did not lead anymore to increased activity indicating complete acidification of the proteoliposomes' interior after 5 min. Indeed, 6 min incubation of proteoliposomes but with smaller total pH jump (2.5-3.5 pH units) was not enough to drive ATP synthesis. Further increase of pH difference above 4.5 pH units did not result in ATP synthesis activity probably due to increased ion-leakage of the proteoliposomes. Inclusion of 150 mM sucrose as an osmolite in reconstitution buffer helped to solve the osmolarity problem and proteoliposomes could be energized by up to 4.9 pH units difference.

The stability issues of *I. tartaricus* ATP synthase and rates of dissipation of the applied potentials was considered and assigned following conditions to be best suited to generate *pmf* across the proteoliposomes and measure ATP synthesis activity of wild-type ATP synthase:

$\Delta\psi$ = 135 mV,

pH-jump = 4 pH units (4.5 → 8.5)

Acidification time = 5 min

Additionally, the ATP synthesis activity of *E. coli* H^+-selective ATP synthase was tested under the same conditions (**Figure 5-29**). *E. coli* wild-type ATP synthase was expressed in pFV2 plasmid (Ishmukhametov et al., 2005), purified and reconstituted in ETLE vesicles following the established protocol (details in Methods, Chapter 4.2.8.2). With this experiment, the aim was to show that used pH/$\Delta\psi$-energization conditions are generally suitable to drive *pmf*-driven ATP synthesis of different ATP synthases. As a result, the *pmf*-driven ATP synthesis activity was detected when $\Delta\psi$ of 135 mV and pH-jump of 4 pH units were imposed to proteoliposomes with *E. coli* ATP synthase.

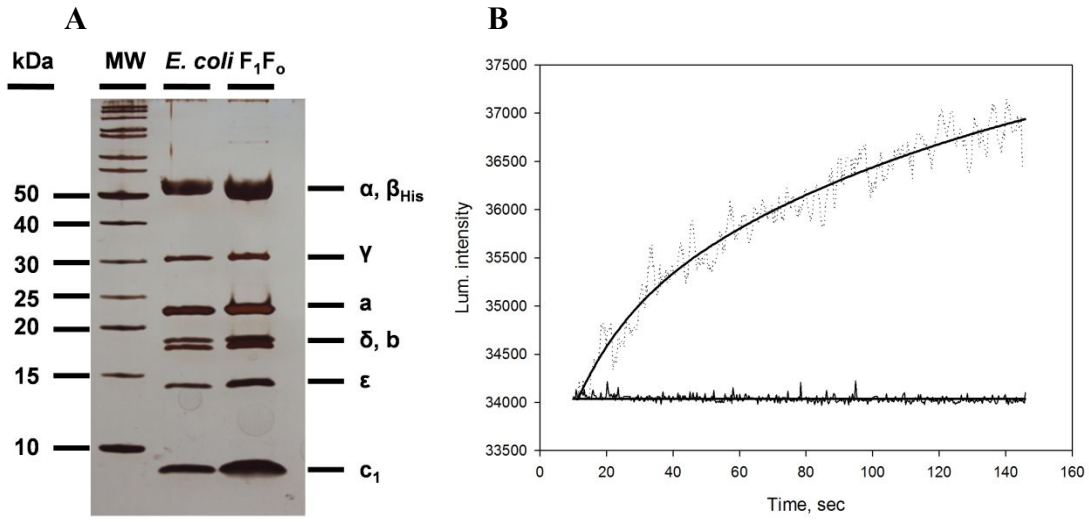

Figure 5-29: ATP synthesis by H^+-selective *E. coli* wild-type ATP synthase. (**A**) SDS-PAGE of purified *E. coli* ATP synthase. Sample of purified *E. coli* ATP synthase showed 2.8 U/mg ATP hydrolysis activity with 96% of coupling and was used for reconstitution in lipids. (**B**) Lipid-reconstituted *E. coli* ATP synthase (6.3 U/ml and 92% coupled ATP hydrolysis activity) showed *pmf*-driven ATP synthesis generated with established procedure.

5.4.1.4. Requirements of *I. tartaricus* wild-type ATP synthase in membrane potential (Δψ) for ATP synthesis

ATP synthesis is an energy demanding process that can be performed only if sufficient driving force (=transembrane electrochemical gradient, in mV) is imposed. The transmembrane electrochemical gradient combines contributions from membrane potential (Δψ) and ion concentration gradient (see Introduction, section 2.1.). Regarding the type of ion gradient implemented in energy transduction, three driving forces are assigned to sodium-, lithium- and proton-motive forces (*smf*, *lmf* and *pmf*). The aim was to test how different are the requirements in total driving force and its components for ATP synthesis by *I. tartaricus* wild-type ATP synthase. According to current experiments, wild-type ATP synthase has evident differences in requirements in Δψ for ATP synthesis depending on imposed ion gradient (**Figures 5-30** and **5-31**). The large ΔpNa (≥ -118 mV) is capable to drive ATP synthesis activity without any contribution from Δψ. In contrast, the *pmf*- and *lmf*-driven ATP synthesis activities were

observed only when ion (proton- or lithium-) gradient was supplemented by a membrane potential. For the case of *pmf*-driven ATP synthesis, contribution from Δψ had to be rather large (~135 mV).

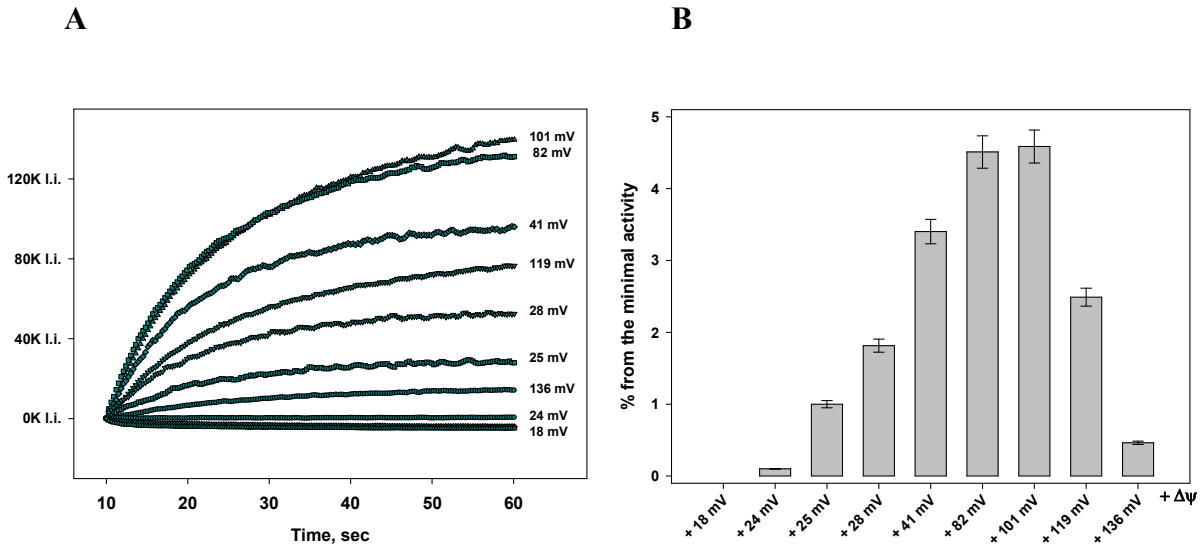

Figure 5-30: Requirements of *I. tartaricus* wild-type ATP synthase in Δψ for *lmf*-driven ATP synthesis. ATP synthesis activity of reconstituted wild-type ATP synthase was monitored at ΔpLi = -120 mV and upon artificially imposed Δψ of different magnitude (18 → 136 mV). (**A**) – Raw data shows curves of ATP synthesis activity driven by combination of fixed ΔpLi and variable Δψ. (**B**) Relative changes in slopes for first 15 sec of observed activity were plotted against imposed Δψ. At taken phosphate potential (Q = 0.32), ATP synthesis activity was observed only after at least 24 mV of Δψ was applied. Further elevation of Δψ from 24 mV up to 82 mV leads to sufficient increase in initial rates of ATP synthesis activity. No difference in activity was observed after subsequent increase of Δψ up to 101 mV suggesting saturation. When Δψ was increased to higher values (119 and 136 mV) activity became much reduced probably due to hyperosmotic conditions caused by high KCl concentrations outside the vesicles.

The ion-driven ATP synthesis activity of *I. tartaricus* wild-type ATP synthase was also checked in presence of different ionophores: a protonophore, carbonylcyanide m-chlorophenylhydrazone (CCCP) and sodium-proton exchanger monensin (Pressman, 1976). Monensin collapses sodium gradient across liposome membrane by exchanges with H^+ and CCCP collapses the formed proton gradient to prevent the further activity driven by H^+. Performed measurements showed

that the *pmf*-driven and *lmf*-driven ATP synthesis could be dissipated or prevented by single addition of 20 μM CCCP (**Figure 5-31A**). This strongly suggests a pivotal role of membrane potential in observed *lmf*- and *pmf*-driven activities. However, to prevent the *smf*-driven ATP synthesis combination of both, monensin and CCCP was required.

A

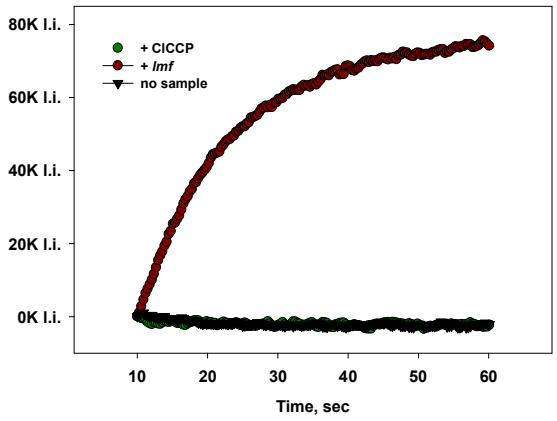

B

	pmf	***lmf***	***smf***
Q ratio	0.32	0.32	0.32
Δp_, mV	-248	-118	-118
Δψ, mV	135	≥ 24	≥ 0
Ionophores	CCCP	CCCP	Monensin + CCCP

Figure 5-31: Requirements of *I. tartaricus* wild-type ATP synthase for ATP synthesis depending on applied ion-motive force. (**A**) Effect of proton-ionophore CCCP on *lmf*-driven ATP synthesis of wild-type ATP synthase: -150mV of applied *lmf* was enough to drive ATP synthesis (shown with red). Observed activity could be easily dissipated by simple addition of CCCP indicating pivotal role of Δψ in observed activity (shown in green)**.** (**B**) Summary of parameters required for ATP synthesis of wild-type ATP synthase and ionophores required to prevent observed activity. Only *smf*-driven ATP synthesis could not be dissipated singly by CCCP. Combination of two ionophores (CCCP and monensin) has to be applied simultaneously.

The origin of observed difference in the requirements of Δψ is unclear. Possibly, it could be related to differences in the parameters of ion binding/release during ion-translocation across the membrane. Additional experiments are required to elucidate this issue.

5.4.1.5. The *pmf*-driven ATP synthesis of hybrid *I. tartaricus* ATP synthase harboring the H^+-selective *Spirulina platensis* c-ring

Spirulina platensis harbors an ATP synthase that was shown to be only H^+-selective (Bakels et al., 1993; Pogoryelov et al., 2009). The c-ring from *S. platensis* ATP synthase has been solved by X-ray crystallography at 2.1 Å (Pogoryelov et al., 2009). The structure shows in atomic detail how H^+ can reversibly bind to this c-ring (Introduction, section 2.6.7.). Therefore, next aim was to test the functional properties of *S. platensis* c-ring when it is incorporated in the Na^+/H^+-selective*I. tartaricus* ATP synthase. As a result, a hybrid TP synthase was constructed in which the c-ring of *I. tartaricus* was replaced by c-ring of *S. platensis* but the remaining protein consisted of *I. tartaricus* ATP synthase subunits (**Figure 5-32A**). This hybrid ATP synthase was used as a reference system to study the potential H^+-selective mutant forms of *I. tartaricus* ATP synthase.

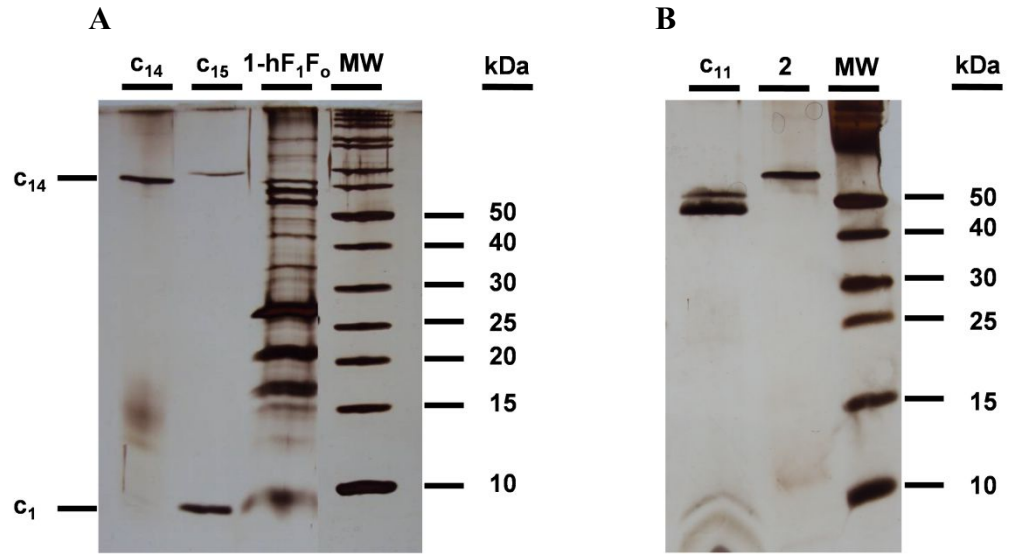

Figure 5-32: SDS-PAGE of a hybrid H^+-selective *S. platensis* c-ring/*I. tartaricus* ATP synthase. (**A**) Hybrid ATP synthase was expressed and extracted from recombinant *E. coli* DK8 expression system. **1 -** Fraction of extracted hybrid ATP synthase on SDS-PAGE illustrates expected subunit composition. According to in-gel electrophoretic mobility of the constructed hybrid ATP synthase, its c-ring possesses higher molecular mass in respect to intact c_{11}-ring of *I. tartaricus* ATP synthase. The mass of this c-ring corresponds to larger c-ring from *S. platensis*. Two other c-rings that correspond to c_{14} and c_{15}-rings were used as reference. (**B**) *S. platensis* c-ring extracted from hybrid ATP synthase (lane 2) runs much slower from *I. tartaricus* wild-type c_{11}-ring on SDS-PAGE.

The hybrid ATP synthase was extracted and reconstituted in pre-formed *E. coli* total lipid extract (ETLE) vesicles similarly to *I. tartaricus* wild-type synthase. The final yield of hybrid ATP synthase (~0.5 mg/ml) was lower than for *I. tartaricus* wild-type ATP synthase but it was still feasible for functional studies as outlined here. The c-ring expressed in a hybrid ATP synthase complex migrated significantly slower from intact *I. tartaricus* c_{11}-ring, as it was expected for *S. platensis* c-ring (**Figure 5-32B**) and showed correct mass of the c-subunits (Pogoryelov et al., 2005) (**Figure 5-33**).

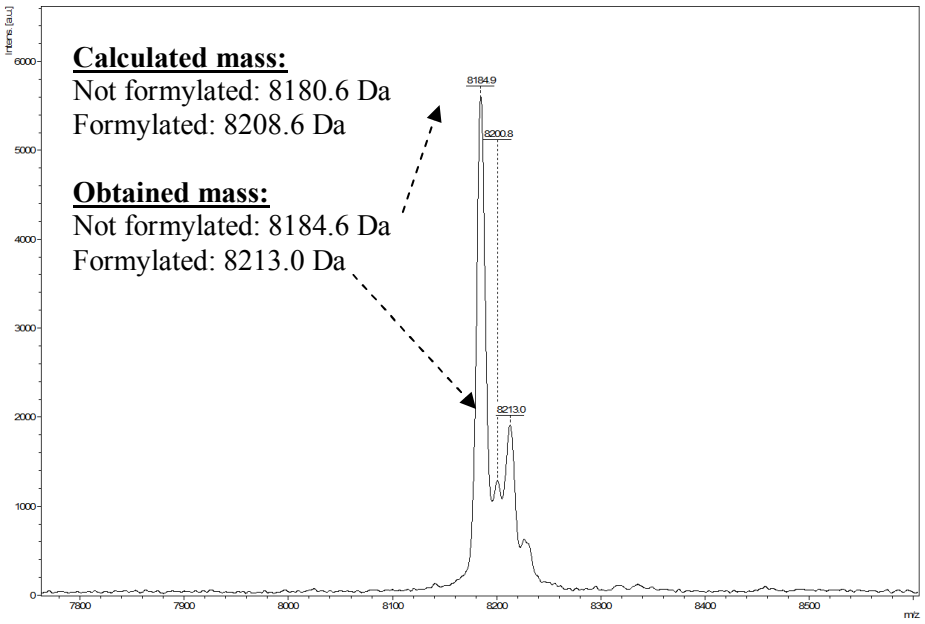

Figure 5-33: MALDI-MS spectra of extracted c-subunits of *S. platensis* c-ring produced recombinantly in *E. coli* DK8 cells as a part of *I. tartaricus* hybrid ATP synthase. MALDI-MS analysis of extracted *S. platensis* c-ring confirmed correct molecular mass for its c-subunits. The large portion of the *S. platensis* c-monomers was formylated. Formylation was detectable through increase in the c-monomer molecular mass (+28 Da shift in the mass).

The isolated hybrid ATP synthase was capable to drive both, ATP hydrolysis and *pmf*-driven ATP synthesis. ATP hydrolysis activity was Na^+- and Li^+-independent. As expected, no detectable signals for *smf*- and *lmf*-driven ATP synthesis was detected as well. This result concurs with previous data showing that the *S. platensis* c-ring binds exclusively H^+ (Krah et al., 2010). After the only *pmf*-selective nature of the hybrid *S. platensis* c-ring/*I. tartaricus* ATP synthase was confirmed, the effect of different concentrations of Na^+ and Li^+ on *pmf*-driven ATP synthesis of hybrid ATP synthase was checked. The range of 1-500 mM NaCl and 1-500 mM LiCl was checked on its ability to compete with H^+ for binding to hybrid ATP synthase during ATP synthesis. According to obtained NaCl- and LiCl-inhibition patterns, only high concentrations of NaCl and LiCl can partially block *pmf*-driven ATP synthesis of hybrid ATP synthase (**Figure 5-34**). Moreover, NaCl- and LiCl-inhibition patterns become very similar at concentrations higher from 200 mM. The observed inhibition effect is due to unspecific binding

of Na^+ and Li^+ to other subunits of hybrid ATP synthase. However, LiCl and NaCl at the range of 1-50/100 mM had little or no effect on *pmf*-driven ATP synthesis and therefore these concentrations were assumed to be useful to investigate H^+ against Na^+ (or Li^+) competition for binding to c-ring in *I. tartaricus* ATP synthase.

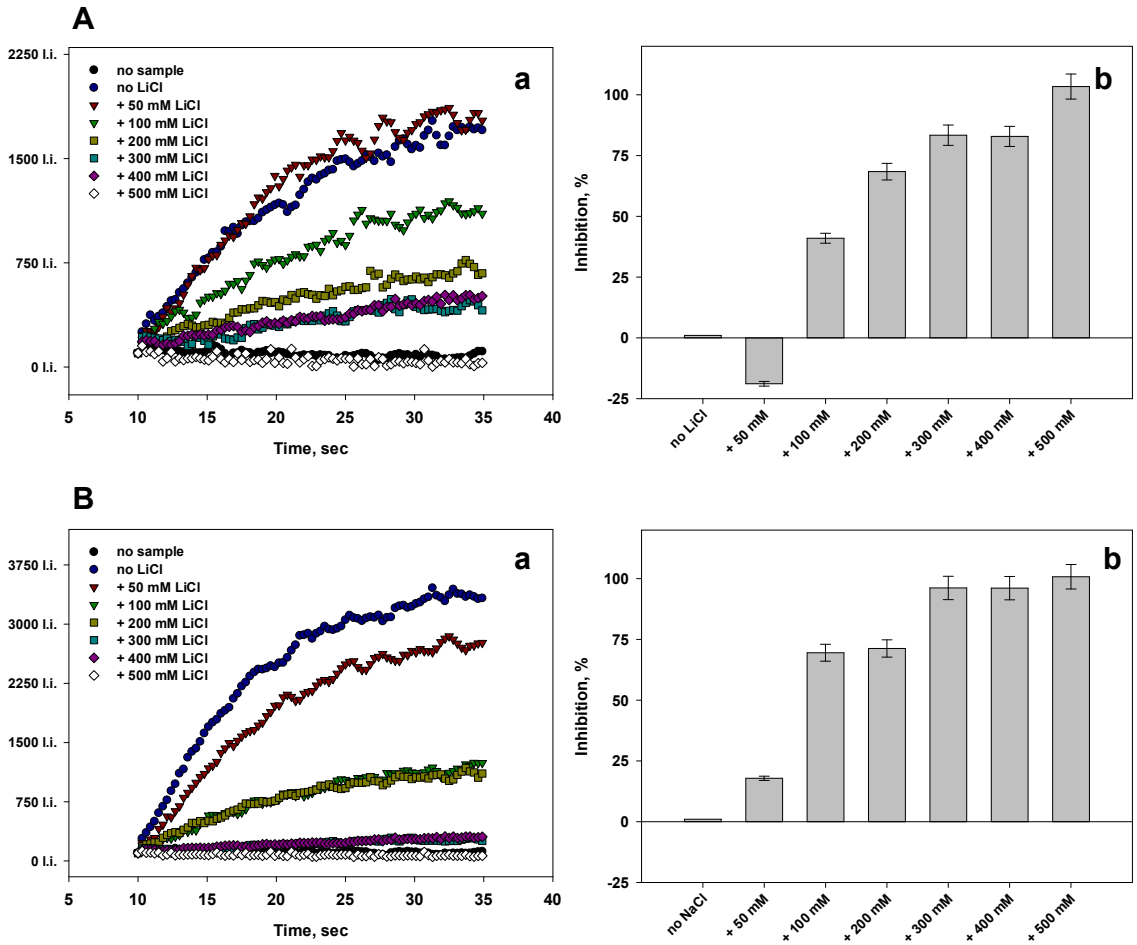

Figure 5-34: NaCl- and LiCl-mediated unspecific inhibition of *pmf*-driven ATP synthesis of hybrid *S. platensis/I. tartaricus* ATP synthase. (**A**) Effect of different concentrations of NaCl on *pmf*-driven ATP synthesis of hybrid ATP synthase. (a) Raw profile for *pmf*-driven ATP synthesis activity at different NaCl concentrations and (b) plotted slopes for NaCl-mediated inhibition show that up to 100 mM NaCl in the reaction mixture did not inhibit *pmf*-driven ATP synthesis of hybrid ATP synthase. (**B**) Effect of different concentrations of LiCl on *pmf*-driven ATP synthesis of hybrid ATP synthase. (a) Raw profile for *pmf*-driven ATP synthesis activity at different LiCl concentrations and (b) plotted slopes for LiCl-mediated inhibition show that up to 50 mM LiCl in the reaction mixture did not inhibit *pmf*-driven ATP synthesis of hybrid ATP synthase. However, we observed ~41% reduction of the original ATP synthesis activity at 100 mM LiCl and no activity at 500 mM LiCl. In general, patterns of NaCl and LiCl inhibition show comparable inhibition at high concentrations of LiCl and NaCl due to similar mode of unspecific binding of Li^+ and Na^+ at and above 100 mM concentration.

The presented results show that *S. platensis* H^+-selective c-ring can functionally replace the

$Na^+/Li^+/H^+$-selective c-ring in *I. tartaricus* ATP synthase and determines the only *pmf*-driven nature of formed hybrid ATP synthase.

5.4.2. Heterologous expression and purification of *I. tartaricus* ATP synthase with mutations in the c-ring

The main intention was to gather experimental evidence that the subtle tuning of the original binding site in *I. tartaricus* c-ring is capable to covert monovalent cation-selectivity of entire *I. tartaricus* ATP synthase. At the first step, we checked whether mutant c-rings can assemble in complete ATP synthase complex, if expressed in and purified from *E. coli* DK8 cells. For that purpose, a total of 12 mutant ATP synthases containing wild-type and mutant c-rings (G25A, G25S, Q32A, E65D, S66A, T67G, T67M, T67S, T67Q, Y70F, S66A/Y70F and Q32A/Y70F) were produced and purified by metal affinity chromatography as it is described in the Methods (Chapter 4.2.3). Next, the migration properties of purified ATP synthases on SDS-PAGE were analyzed. Samples were examined for the presence of 8 subunits forming the complex: α, β, γ, a, b, δ, ε, c-rings and/or c-monomers for the case of (SDS-)unstable c-rings ((SDS-)stable and (SDS-)unstable c-rings are characterized in **Section 5.1.1**). According to obtained migration profiles on SDS-PAGE, mutant ATP synthases retain similar to wild-type subunit composition (**Figure 5-35**). Furthermore, in all 12 mutant ATP synthases the (SDS-)stable c-rings (G25A, Q32A, E65D, T67G, T67S, Y70F, S66A/Y70F and Q32A/Y70F) or the c-monomers of (SDS-)unstable c-rings (G25S, S66A, T67M and T67Q mutants) were detectable. Only G25A mutant c-ring in ATP synthase was shown to assemble with c_{12}-ring stoichiometry instead of originally inherent for wild-type c_{11}-ring stoichiometry (**Figure 5-35B)** (Pogoryelov et al., 2012). Rest of the SDS-stable c-ring mutants run on the level of wild-type c_{11}-ring.

In addition, it was shown that assembly properties of γ/ε-E65D mutant c-ring complex are better when c-ring is expressed and purified as a part of complete ATP synthase (modification of the expression procedure is described in Methods, Chapter 4.2.3). Previously it was shown that E65D mutant c-ringis not capable to bind to γ/ε subcomplex when expressed as a single gene and purified directly from *E. coli* membranes (section 5.1.2). However, incorporation of E65D c-ring in complete ATP synthase allowed improving the assembly properties for E65D mutant ATP

synthase. By this experiment, the possibility of mutant c-rings to assemble in *E.coli* cells within complete ATP synthase complex was confirmed and at the functional characterisation of mutant ATP synthases was performed.

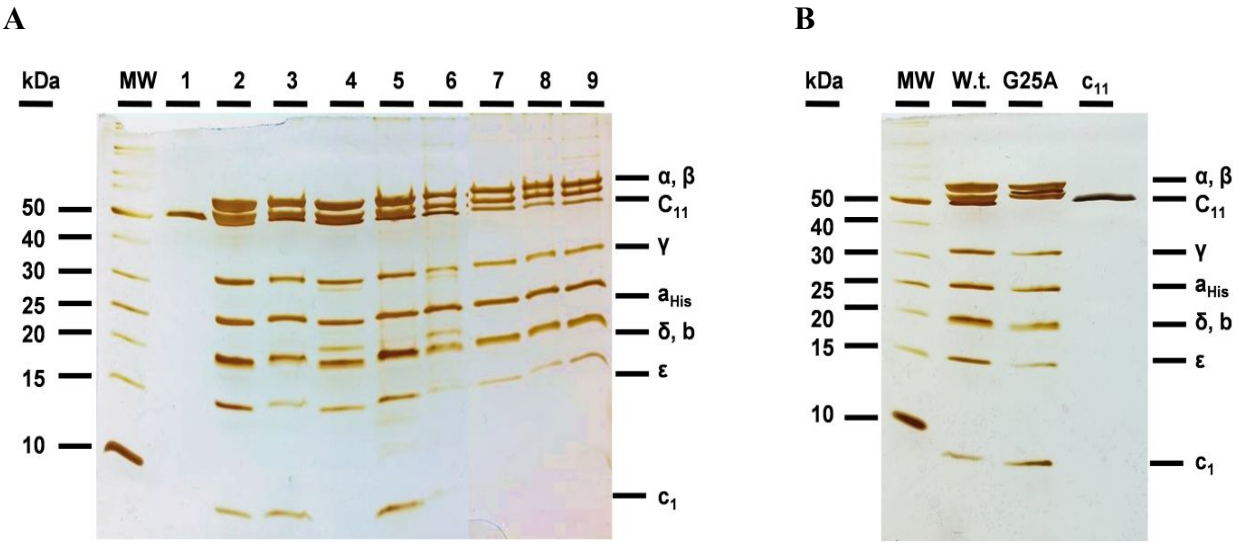

Figure 5-35: Comparative SDS-PAGE of extracted wild-type and mutant ATP synthases expressed recombinantly in *E. coli* DK8 cells. (**A**) ATP synthases of wild-type (1), Q32A (2), Y70F (3), Q32A/Y70F (4), S66A/Y70F (5), T67S (6), T67G (7) and E65D (8) mutants showed high level of purity and assembling when extracted from *E. coli* membranes. Presented set of ATP synthases contain mutant c-rings with unaltered oligomeric state: We clearly detect SDS-stable c-rings of Q32A, Y70F, Q32A/Y70F, S66A/Y70F, T67S, T67G and E65D mutant ATP synthases. The good assembly properties made these mutant ATP synthases useful for further functional studies. (**B**) Comparative SDS-PAGE of wild-type and G25A mutant ATP synthases shows slower in-gel migration of larger G25A c_{12}-ring in respect to wild-type c_{11}-ring.

5.4.3. Coupled ATP hydrolysis activity of wild-type and mutant forms of *I. tartaricus* ATP synthase

After the *I. tartaricus* wild-type and mutant ATP synthases were purified, all samples were checked for their ATP hydrolysis activity and its inhibition by the F_1 specific inhibitor NaN_3 and F_o specific inhibitor DCCD (Fillingame 1975; Negrin et al, 1980; Sebald et al., 1980; Murataliev et al., 1991; Pogoryelov et al., 2010). Based on the NaN_3 and DCCD inhibition of the ATP hydrolysis activity the coupling ratio for each ATP synthase form was evaluated. The so-called coupling ratio for ATP hydrolysis reflects the F_1/F_o assembly and was used to assess how much F_1part was detached from the ATP synthase during purification procedure. The ability to perform coupled ATP hydrolysis was an important step of verification of functionality for mutant ATP synthases.ATP hydrolysis measurements were performed in detergent solution. All analysed mutant ATP synthases were expressed and purified at sufficient levels to give detectable function (≥ 1 mg/ml). According to the measurements presented in this thesis, the *I. tartaricus* wild-type ATP synthase demonstrated the highest rate of specific ATP hydrolysis activity (μM ATP/mg protein/min) - 11 U/mg (**Table 5-15**). The double mutant S66A/Y70F and the mutant T67Q ATP synthases showed comparably high, close to wild-type, ATP hydrolysis activities (7.5 and 7.7 U/mg). In the case of G25A, T67G, Y70F and Q32A/Y70F mutant ATP synthases, the rates of ATP hydrolysis were reduced and varied in a range of 1.9-3.3 U/mg. The remaining Q32A, E65D, S66A, T67S mutant and *S. platensis* c-ring/*I. tartaricus* hybrid ATP synthases showed activities lower than 1.3 U/mg.

Table 5-15: Specific ATP hydrolysis activity of *I. tartaricus* wild-type and mutant ATP synthases

Mutant	Activity, U/mg	Coupling, %
Wild-type	11.0 ± 0.55	97.6 ± 4.9
G25A	2.2 ± 0.11	61.3 ± 3.1
G25S	-	n/d*
Q32A	1.3 ± 0.07	42.1 ± 2.1
E65D	0.4 ± 0.02	44.8 ± 2.2
S66A	0.8 ± 0.04	n/d
T67G	1.9 ± 0.09	n/d
T67M	-	n/d
T67Q	7.5 ± 0.38	n/d
T67S	0.6 ± 0.03	19.0 ± 0.9
Y70F	2.6 ± 0.13	53.6 ± 2.7
Q32A/Y70F	3.3 ± 0.17	60.8 ± 3.0
S66A/Y70F	7.7 ± 0.39	84.4 ± 4.2
c_{15}/*Ilyobacter* hybrid	0.6 ± 0.03	n/d

n/d* – Not detectable DCCD inhibition when 5 min incubation with 50-200 μM DCCD was used

The activities were next inhibited by NaN_3 and DCCD and the coupling ratios were calculated. According to the calculated coupling ratios, the wild-type and S66A/Y70F ATP synthases were the best coupled ATP synthases, with their highly (SDS-)stable c-rings (97.6 and 84.4%, respectively). G25A, Y70F and Q32A/Y70F mutant ATP synthases were less well coupled but still more than 50% of F_1 and F_o subcomplexes were attached to each other. Remaining T67S, E65D and Q32A mutant ATP synthases were coupled only by 19-44.8%. The group of S66A, T67G, T67M, T67Q and c_{15}/*I. tartaricus* hybrid ATP synthases were not inhibited by 50-200 μM DCCD, hence they showed no coupling at all under the conditions tested. Obviously, longer incubation with higher concentration of DCCD is needed for sufficient inhibition of ATP hydrolysis activity of these ATP synthases. Nevertheless, higher concentrations of DCCD (> 200 μM) were not tried as above these concentrations DCCD starts to inhibit F_1 domain (Pougeois et al., 1979; Yoshida et al. 1983).

Conclusions from these experiments are: A reduced coupling ratio for ATP hydrolysis was often

characteristic for the less stable c-rings (S66A, T67G and G25A). The stable c-rings (wild-type, S66A/Y70F and Q32A/Y70F) did not have problems to assemble efficiently in ATP synthase complex. In addition, we showed that poorly assembled (< 10%) or not assembled ATP synthases are not suited to operate in either directions, hydrolysing or synthesizing ATP and therefore, appropriate samples were excluded for this study.

5.4.4. Incorporation of *I. tartaricus* wild-type and mutant ATP synthases in lipid vesicles: The ATP hydrolysis activity in reconstituted ATP synthases is enhanced

At the next step, it was important to make sure that obtained ATP synthases can be incorporated in sufficient amount (few molecules of ATP synthase per vesicle) in lipid vesicles without loss in their coupled ATP hydrolysis activity. Firstly, purified wild-type and mutant ATP synthases were incorporated in pre-formed lipid vesicles made by *E. coli* total lipid extract, ETLE. The efficiency of incorporation was confirmed by freeze fracture electron microscopy (**Figure 5-36**).

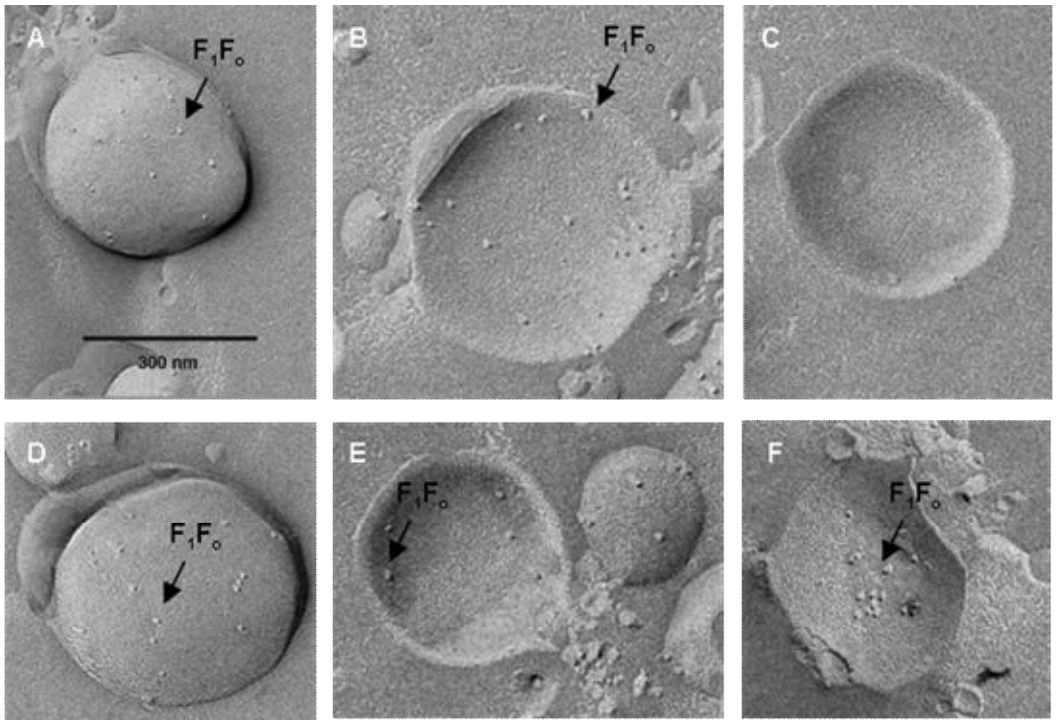

Figure 5-36: Representative freeze fracture electron microscopy of *I. tartaricus* wild-type and mutant ATP synthases incorporated in pre-formed lipid vesicles composed of ETLE. Presented is the freeze fracture electron microscopy of reconstituted *I. tartaricus* wild-type (A), S66A/Y70F (B), no (C), G25A (D), Q32A/Y70F (E) and T67S (F) ATP synthases. The arrows point to the dots that represent water-soluble F_1 domain of ATP synthase. Micrographs confirm successful and efficient incorporation of wild-type and mutant forms of *I. tartaricus* ATP synthase in lipid vesicles.

At the next step, the activity of reconstituted ATP synthases was checked. ATP hydrolysis activity became increased almost 5 times for wild-type and S66A/Y70F ATP synthases after reconstitution (**Table 5-16**). Moreover, the coupling ratio (> 96% for both, wild-type and S66A/Y70F mutant ATP synthases) shows that proteoliposomes contain perfectly intact F_1F_o complexes. Meaning the reconstitution in ETLE vesicles further improved the quality of the samples. The assumption is that during the proper reconstitution procedure the detached protein subcomplexes were removed and only assembled F_1F_o stayed in the proteoliposomes. Freeze fracture electron microscopy analysis also confirms good incorporation of wild-type and S66A/Y70F ATP synthases into pre-formed lipid vesicles (**Figures 5-36A and 5-36B**). In

addition, the detected sticking out dense dots that represent F_1 domains, confirm that ATP synthase molecules were incorporated into the liposomes in an inside-out orientation. Main distribution for the vesicle size was in a range of 200-300 nm with few molecules of ATP synthase inside each. As a control, if no protein was used, the vesicles stayed empty (**Figure 5-36C**).

Table 5-16: Rates of specific ATP hydrolysis activity of *I. tartaricus* wild-type and mutant ATP synthases incorporated in vesicles

Mutant	ATP hydrolysis, U/mg	Coupling, %
Wild-type	57.8 ± 2.89	96.3 ± 4.8
G25A	2.2 ± 0.11	61.3 ± 3.1
G25S	1.0 ± 0.05	n/d*
Q32A	9.2 ± 0.46	81.4 ± 4.1
E65D	1.4 ± 0.07	16.7 ± 0.8
S66A	1.4 ± 0.07	62.7 ± 3.1
T67G	4.7 ± 0.24	81.7 ± 4.1
T67M	0.9 ± 0.04	n/d
T67Q	7.5 ± 0.38	n/d
T67S	1.9 ± 0.09	87.5 ± 4.4
Y70F	11.2 ± 0.56	87.6 ± 4.4
Q32A/Y70F	9.1 ± 0.46	67.3 ± 3.4
S66A/Y70F	43.8 ± 2.19	97.2 ± 4.9
c_{15}/*I. tartaricus* hybrid	0.6 ± 0.03	11.9 ± 0.6

n/d – Not detectable DCCD inhibition when 5 min incubation with 50-200 μM DCCD was used

For Q32A, T67Q, Q32A/Y70F, Y70F and T67G mutant ATP synthases we detected 2.5-7 times increased specific ATP hydrolysis activity upon incorporation in lipids. Same ATP synthases showed good coupling of ATP hydrolysis (67-88%) as well. Remaining G25A, G25S, E65D, S66A, T67M, T67S and c_{15}/*I. tartaricus* hybrid ATP synthases showed improved but lower from 3 U/mg specific ATP hydrolysis activities. Except for E65D and c_{15}/*I. tartaricus* hybrid ATP synthases, coupling ratios were higher from 60%. ATP synthases in proteoliposomes that showed

high rates of coupled ATP hydrolysis activity were feasible for further ATP synthesis measurements.

5.4.5. Characterization of the cation selectivity by lipid-reconstituted *I. tartaricus* mutant ATP synthases

The performed set of experiments imply that *I. tartaricus* wild-type c-ring exhibits a range of relative to pH cation binding affinities, from strong H^+ and Na^+ binding affinities to weaker Li^+ binding affinity (**sections 5.2-5.3**). In this chapter, it was verified whether ATP synthesis activity of *I. tartaricus* wild-type ATP synthase is coupled to gradients of Na^+, Li^+ or H^+ ions depending on applied conditions. The previously obtained data also suggest that the activity by certain mutant ATP synthases is coupled not only to Na^+ but at the same time also to H^+ transport. Thus, these ATP synthases should also depend on the *pmf* and/or *smf*. To explore this possibility, the reconstituted mutant ATP synthases were checked on ability to drive ATP synthesis if an artificial *pmf* and *smf* are imposed (see details in Methods, Chapters 4.2.8.4 and 4.2.8.5). The ATP synthesis activity was determined at RT by continuously recording for 7-15 min ATP formation in the luminometer. From the set of the 13 analyzed mutant ATP synthases only 5 were capable to work solely on *pmf* – E65D, G25S, T67M, T67Q and Q32A/Y70F mutant ATP synthases. The rest of mutant ATP synthases were shown to work on both *smf* and *pmf* depending on applied conditions (**Figure 5-37**). In addition, the *lmf*-driven ATP synthesis activity of mutant ATP synthases was tested. Only Q32A and T67S mutant ATP synthases demonstrated *lmf*-driven ATP synthesis. The Li^+-coupled ATP synthesis activity for the rest of the mutants was not observed (summarizing **Table 5-17**).

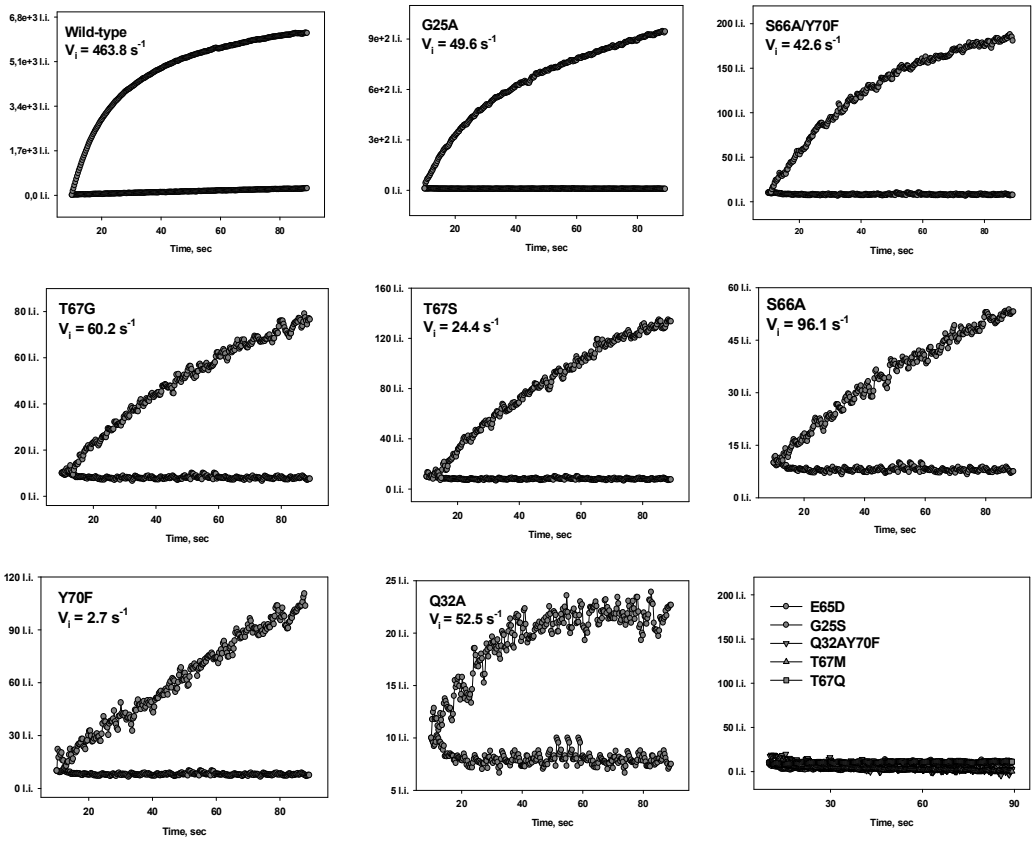

Figure 5-37: Verification of *smf*-driven ATP synthesis activity of *I. tartaricus* wild-type and mutant ATP synthases reconstituted in lipids. Obtained proteoliposomes containing mutant ATP synthases were examined in their ability to drive ATP synthesis using imposed *smf* (-118 mV of ΔpNa and 36 mV of ΔΨ). G25A, S66A/Y70F, T67G, T67S, S66A, Y70F and Q32A mutant ATP synthases showed detectable but sufficiently reduced in comparison to wild-type *smf*-driven ATP synthesis activities (all activity curves are presented in relation to baseline level). Important parameter describing the initial velocity of observed activity (V_i) was determined accounting the ATP production signals (luminescent intensity, l.i., per nM of ATP) and amount of incorporated protein (nM). According to V_i parameter, Y70F mutant ATP synthase demonstrated apparent difficulties for *smf*-driven ATP synthesis. E65D, G25S, Q32A/Y70F, T67M and T67Q mutant ATP synthases showed no signals for *smf*-driven ATP synthesis, even when larger *smf* was imposed (-129 mV of ΔpNa and 135 mV of ΔΨ). These mutants lost the ability to use sodium gradient due to constraints in Na^+ binding (G25S, Q32A/Y70F, T67M and T67Q mutant c-rings) or constraints in Na^+ transport (E65D mutant ATP synthase).

Table 5-17: Coupling of ATP synthesis to different monovalent cations by wild-type and mutant forms of *I. tartaricus* ATP synthase

Mutant	Coupling ion for ATP synthesis
Wild-type	$H^+/Na^+/Li^+$
Q32A	$H^+/Na^+/Li^+$
T67S	$H^+/Na^+/Li^+$
G25A	H^+/Na^+
Y70F	H^+/Na^+
S66A	H^+/Na^+
T67G	H^+/Na^+
S66A/Y70F	H^+/Na^+
E65D	H^+
G25S	H^+
T67M	H^+
T67Q	H^+
Q32A/Y70F	H^+
***S. platensis*/*I. tartaricus* hybrid**	H^+

Additional experiments were further carried out in order to assign biochemical parameters of ATP synthesis of wild-type and mutant ATP synthases. In particularly, ATP synthesis activity was analyzed and compared in a context of turnover rates (V_i and V_{max}), binding affinity for Na^+ (K_M (Na^+) values) and efficiency of ATP synthesis ($k_{cat}/K_M=V_{max}/K_M$ parameter). The mentioned parameters are described in sections below.

5.4.6. Effect of Na^+ on *pmf*-driven ATP synthesis of *I. tartaricus* wild-type and mutant ATP synthases

As it follows from the performed experiments (**section 5.4.3**), analyzed mutant ATP synthases retained the capability to drive *pmf*-energized ATP synthesis at particular conditions, i.e. typically low Na^+ concentration (< 1 mM), large pH-jump (4 pH-units) and large membrane potential (135 mV). These data are in a good agreement with biochemical experiments based on

pH-dependent modification of Glu65 residue in the c-ring (section 5.2.3) that showed H^+ binding affinity to be intact property of the mutant c-rings. Nevertheless, the open remained a question on how different is the *pmf*-driven ATP synthesis of mutant ATP synthases in respect to wild-type. Therefore, the aim was to investigate the competitive binding of Na^+ against H^+ during *pmf*-driven ATP synthesis through Na^+ inhibition of the observed *pmf*-driven activity. As it is presented in **Figure 5-38,** were observed both, the Na^+-dependent and Na^+-independent *pmf*-driven ATP synthesis of mutant ATP synthases. Particularly, among the 12 mutant ATP synthases, only the eight contribute to Na^+-dependent ATP synthesis driven by *pmf*, whereas the function of the remaining four mutant ATP synthases (G25S, T67M, T67Q, Q32A/Y70F) remains Na^+-independent. The Na^+-dependent/independent *pmf*-driven ATP synthesis exhibits Michaelis-Menten dependence, i.e. demonstrate typical hyperbolic saturatable shape of the activity curve with a maximum rate of ATP synthesis activity after 40 sec. The patterns of Na^+-inhibition of *pmf*-driven ATP synthesis in a context of different saturation properties of the wild-type and mutant binding sites in the c-rings were next analyzed. Namely, the slopes at the steepest part of the curves were used to evaluate Na^+-inhibition effect (in %) depending on used concentration of NaCl (in mM). Obtained Na^+ inhibition values (in %) were plotted as a function of NaCl concentration (in mM) in order to evaluate K_M (Na^+) values.

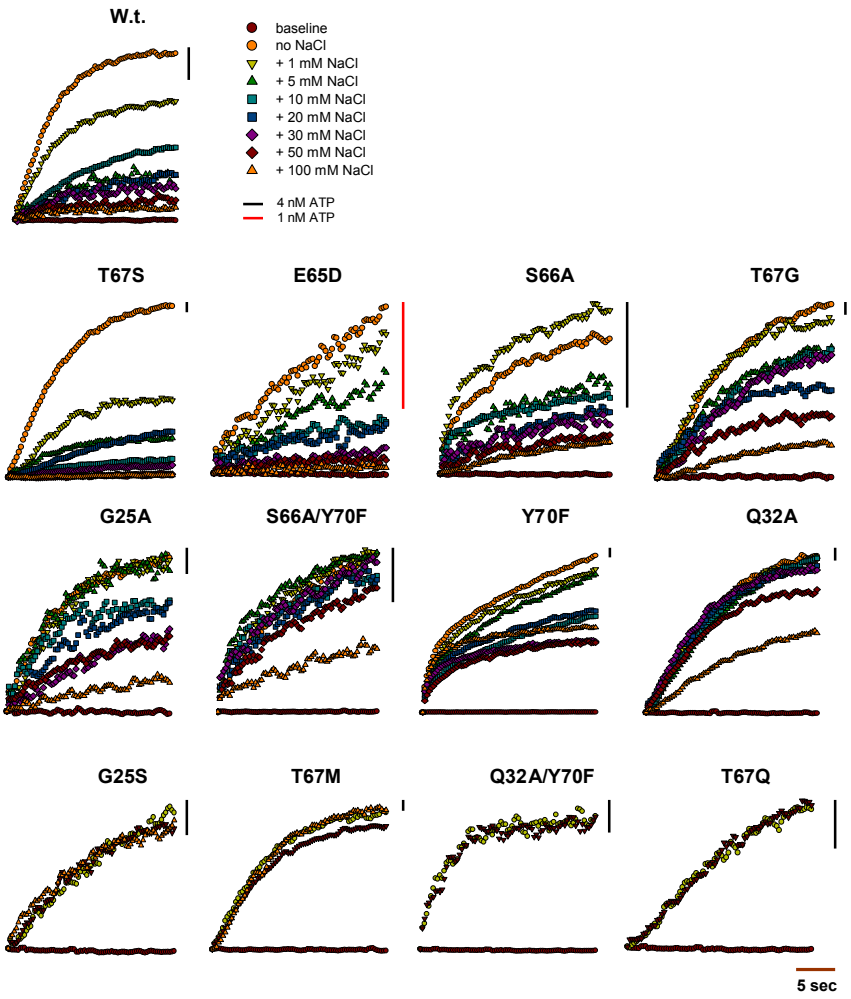

Figure 5-38: Na^+-inhibition of *pmf*-driven ATP synthesis of *I. tartaricus* wild-type and mutant ATP synthases. Proteoliposomes containing wild-type and mutant ATP synthases were examined on their ability to run *pmf*-driven ATP synthesis at different concentrations of NaCl. To test the Na^+ effect lipid vesicles were pre-incubated for 5 min at 4°C before the assay with acidic buffer containing NaCl varying from 1 to 100 mM NaCl. The same NaCl levels were also present in the assay buffer. **Upper panel:** Nonlinear relationship between increase in NaCl concentration and inhibition of *pmf*-driven ATP-synthesis was observed for wild-type and the set of T67S, E65D, S66A, T67G, G25A, S66A/Y70F, Y70F and Q32Amutant ATP synthases. **Lower panel:** For remaining G25S, T67M, Q32A/Y70F and T67Q mutant ATP synthases there was no effect of Na^+ on *pmf*-driven ATP synthesis. These mutant ATP synthases are the only H^+-coupled with lost capability of doing both, bind and transport Na^+. Interestingly, E65D mutant ATP synthase showed Na^+-dependent inhibition of *pmf*-driven ATP synthesis, although ATP synthesis by E65D ATP synthase is coupled only to H^+. This phenomenon can be a consequence of present Na^+-binding properties and deteriorated or lost Na^+-transporting properties.

5.4.7. Estimation of K_M values for Na^+ binding to *I. tartaricus* wild-type and mutant ATP synthases

The data on Na^+-inhibition of *pmf*-driven ATP synthesis in the form of hyperbolic Michaelis-Mentel data (% of the Na^+ inhibition as a function of NaCl concentration) were linearized by Lineweaver-Burk transformation and further used to extrapolate the K_M (Na^+) values (**Figure 5-39**).

A

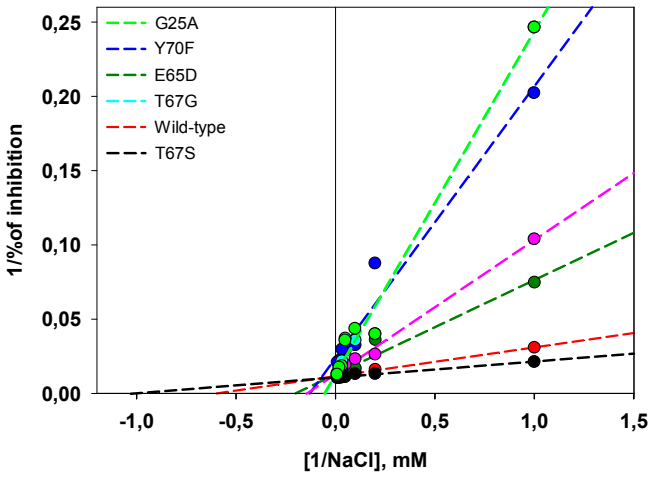

B

Mutant	K_M (Na^+), mM
T67S	0.97
Wild-type	1.71
E65D	5.08
S66A	6.94
Y70F	7.75
G25A	18.87
T67G	19.42
Q32A	> 19.42
S66A/Y70F	> 19.42

Figure 5-39: Lineweaver–Burk plots for Na^+ binding to the c-rings in the wild-type and mutant ATP synthases. (**A**) Linewear-Burk transformation of the data: Reciprocal of the Na^+-inhibition of *pmf*-driven ATP synthesis in % was plotted as ordinates and reciprocal of appropriate NaCl concentrations were plotted as abscissae. The obtained data were fit with linear equation (dashed straight lines). The Lineweaver-Burk plot yields a straight line in case of saturatable specific binding of the ligand with the intercept on the x-axis that equals to $-1/K_M$. The plots for most of the mutant ATP synthases were linear and intersected the 1/NaCl axis at the different points indicating different K_M values for Na^+ binding to c-ring. (**B**) Extrapolated K_M values were mutant specific and lay in a range of 0.97-19.42 mM. Na^+ binding to Q32A and S66A/Y70F mutant ATP synthases was difficult to interpret by the Lineweaver–Burk plot alone and therefore, K_M values were not estimated for these two mutants.

Obtained K_M (Na^+) are apparent for the taken H^+ concentration. According to obtained data, at [H^+] = 31.62 µM, Na^+ competitively binds to *I. tartaricus* ATP synthase with K_M 0.97-19.42 mM

depending on introduced mutation (**Figure 5-39B**). Polar-to-polar T67S replacement is the only mutation that increased the apparent Na^+ binding affinity in the c-ring at tested pH 4.5.

5.4.8. Maximal Na^+ occupancy of ion binding sites in *I. tartaricus* wild-type and mutant ATP synthases

The estimation of the Na^+ binding capacities [B_{max} (Na^+) values] for ATP synthases as maximum inhibition of the *pmf*-driven ATP synthesis at 100 mM NaCl under conditions of full saturation of Na^+ inhibition was done. These values are defined by maximal occupancy of the c-ring ion-binding sites by Na^+ at taken pH (maximal % of the binding sites within c-ring that could be occupied by Na^+). Almost full inhibition of *pmf*-driven ATP synthesis by wild-type, E65D and T67S ATP synthases at 100 mM NaCl was observed (**Figure 5-40**). The B_{max} (Na^+) values for wild-type, E65D and T67S ATP synthases exceed 90%. For other mutant ATP synthases, Na^+ inhibition of *pmf*-driven ATP synthesis activity was only partial (< 80%) due to reduced Na^+ binding capacities of mutant c-rings. The most dramatic effect we observed for Y70F mutant ATP synthase that was characterized with twice-reduced B_{max} (Na^+) value in respect to wild-type ATP synthase. The effect can be associated with low-affinity Na^+ binding to Y70F c-ring with different from wild-type thermodynamic settings through which Na^+ seems to be flexible in the formed Na^+-c-ring complex (see sections 5.3.2-5.3.3)

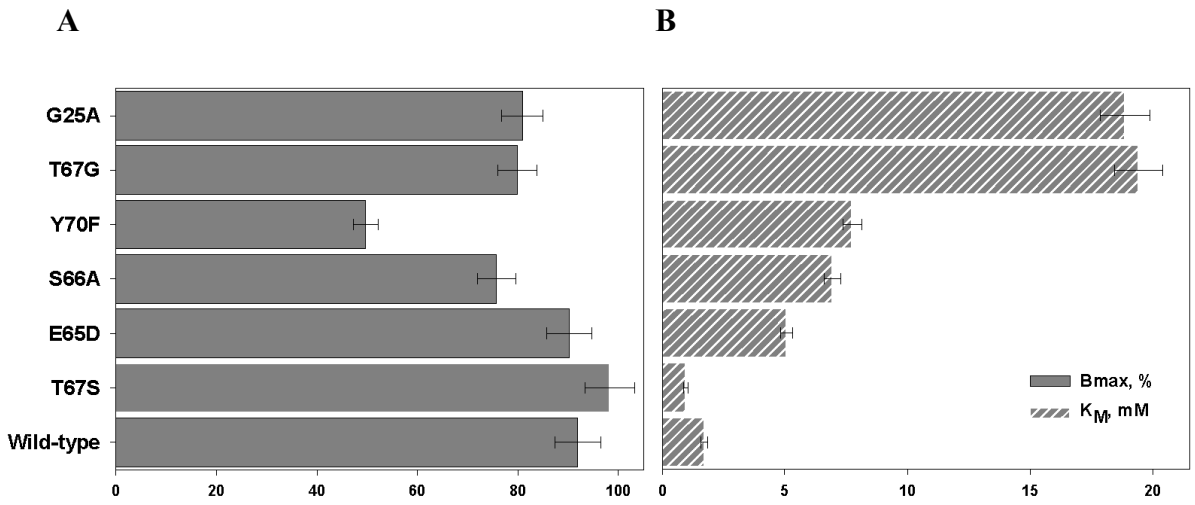

Figure 5-40: Comparison of the kinetic equilibrium constants K_M (Na^+) and B_{max} (Na^+) for the ATP synthases with wild-type and mutant c-rings. (**A**) The calculated K_M (Na^+) values for *I. tartaricus* ATP synthase c-rings (wild-type and mutants). ATP synthases containing wild-type, T67S or E65D c-rings show almost full Na^+-inhibition of *pmf*-driven ATP synthesis due full saturation of ion-binding sites by Na^+ at tested pH 4.5. The *pmf*-driven ATP synthesis activity by other mutant ATP synthases (G25A, T67G, Y70F and S66A) was only partially inhibited by the high NaCl concentration. The high residual *pmf*-driven ATP synthesis activity under conditions of saturated Na^+ binding at high NaCl concentration is due to reduced occupancy of the mutant c-rings by Na^+ at low pH and illustrates the decrease in Na^+ against H^+ binding potency by mutant c-rings. (**B**) Calculated B_{max} (Na^+) for the ATP synthases (wild-type and mutant) c-rings. In the case of G25A, T67G, Y70F, S66A and E65D mutants, the decrease in B_{max} (Na^+) values correlates with increase in K_M (Na^+) values).

Importantly, the c-rings with high Na^+-binding capacities (wild-type, T67S and E65D mutant c-rings) show that acidic pH (= high H^+ concentration) effectively decreases the apparent affinity (but not capacity) of Na^+ binding to c-rings. This means that despite full protonation of Glu65 carboxyl group at pH close to 4.5, Na^+ is still capable to replace H^+ in the ion-binding site at particular $[Na^+]/[H^+]$ ratios. Interestingly, it seems that both, polar-to-polar and charge-to-charge replacements (T67S and E65D) did not affect much the capacity of Na^+ binding. The data are in a good agreement with ITC data that showed only small changes in thermodynamics of Na^+ binding upon introducing T67S mutation in the *I. tartaricus* c-ring (section 5.3.3). For other mutants (particularly polar-to-hydrophobic replacements, i.e. T67G mutation) acidic pH

decreases both, the Na^+-binding affinity and Na^+-binding capacity as well. According to the obtained differences in the B_{max} and K_M values for Na^+, the wild-type and mutant ATP synthases were grouped into:

Group I.: WT-like high capacity of Na^+ binding correlates with decreased affinity of Na^+ binding (T67S and E65D mutant ATP synthases)

Group II.: reduced capacity of Na^+ binding correlates with decreased affinity of Na^+ binding (G25A, S66A, T67G and Y70F mutant ATP synthases)

Group III.: no or very low capacity of Na^+ binding correlates with no or very low affinity of Na^+ binding (Q32A, S66A/Y70F, Q32A/Y70F mutant ATP synthases and hybrid *S. platensis*/*I. tartaricus* hybrid ATP synthase)

5.4.9. Verification of the binding model describing Na^+ binding to *I. tartaricus* wild-type and mutant ATP synthases

In the next step, the working hypothesis that saturation of *I. tartaricus* wild-type and mutant binding sites with Na^+ follows one-binding site model was tested. The calculated kinetic constants B_{max} (Na^+) and K_M (Na^+) were used to fit the data on Na^+ binding to the one-site saturation binding (hyperbola) model from the classic equation list (Sigma plot version 10) (**Figure 5-41**). Obtained plot is a complementary representation of the raw data (**Figure 5-38**). The quality of obtained fit confirms the Na^+-inhibition of *pmf*-driven ATP synthesis is due to competitive binding of Na^+ against H^+ to the binding sites in the c-ring.

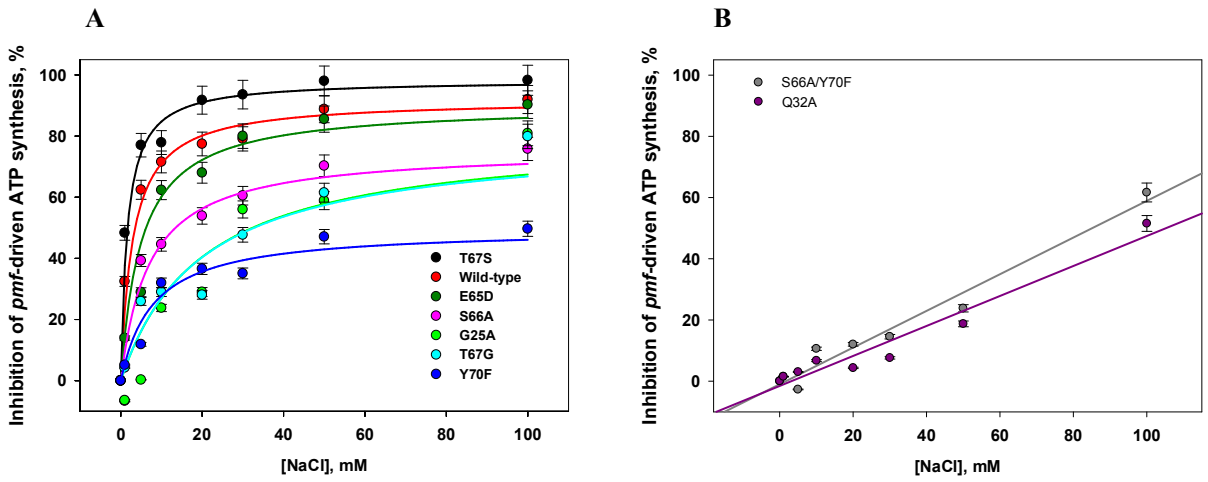

Figure 5-41: Patterns of Na^+-dependent inhibition of *pmf*-driven ATP synthesis fitted to one-site binding model. (**A**) The data on Na^+-inhibition of *pmf*-driven ATP synthesis were fitted with one-site saturation equation using the estimated B_{max} (Na^+) and K_M (Na^+) values for T67S (black), E65D (dark green), S66A (pink), G25A (green), T76G (cyan), Y70F (blue) and wild-type (red) ATP synthases. The chi-square goodness-of-fit test confirmed different saturation properties of the ion-binding site depending on introduced mutation. These curves yielded half-saturation (K_M) values at 0.97-19.42 mM depending on the mutation. (**B**) Patterns of Na^+ inhibition of *pmf*-driven ATP synthesis for Q32A (dark pink) and S66A/Y70F (dark grey) mutant ATP synthases were best fitted with a linear regression function: For the case of Q32A and S66A/Y70F ATP synthases there was no apparent saturation kinetics within the measured range of 1-100 mM NaCl. Therefore, no K_M (Na^+) values can be estimated for Q32A and S66A/Y70F mutant c-rings at pH 4.5.

5.4.10. Verification of cooperativity in Na^+ binding to *I. tartaricus* wild-type and mutant ATP synthases

As *I. tartaricus* c-ring has 11 (in the case of G25A: 12) ion binding sites (=number of c-subunits in the c-ring) (Meier et al., 2009; Pogoryelov et al., 2012), more than one Na^+ is simultaneously involved in binding to a c-ring. Therefore, the analysis of cooperativity in Na^+ binding based on Hill coefficient (*h*) was applied to wild-type and mutants. To do so, the patterns of competitive Na^+ binding to ATP synthases at five different Na^+ concentrations were used to determine the *h* coefficients. In case of *I. tartaricus* wild-type ATP synthase, the Hill coefficient of Na^+ binding

did not exceed 1 (**Figure 5-42A**). The derivation assumes a noncooperative independent binding reaction between Na^+ and distinct ion-binding sites within c-ring. Na^+-response of T67S, E65D, S66A, Y70F, G25A, T67G, Q32A and S66A/Y70F mutant ATP synthases were also analyzed by means of Hill coefficient (**Figure 5-42B)**. The obtained *h* values were in a close proximity to 1 and therefore, no cooperativity is assumed for the Na^+ binding to mutant c-rings as well. The individual binding sites in the wild-type and mutant c-rings bind Na^+ independently and thus, one-site binding model can be applied when K_d and K_M values for Na^+ are estimated.

A

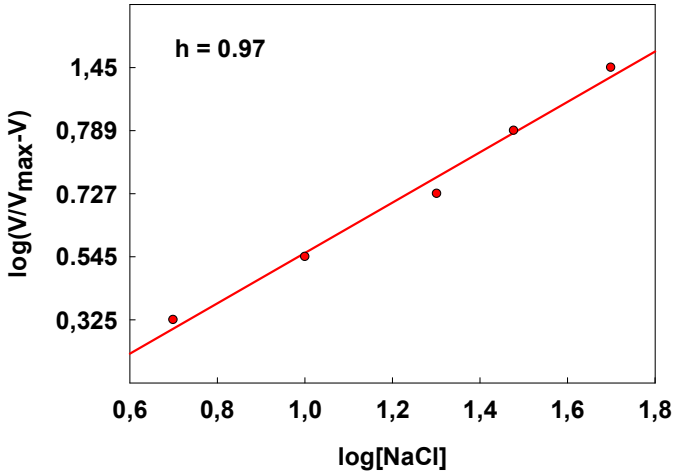

B

Mutant	*h*	Cooperativity
T67S	1.13 ± 0.38	no
Wild-type	0.97 ± 0.11	no
E65D	1.03 ± 0.24	no
S66A	1.01 ± 0.13	no
Y70F	1.19 ± 0.34	no
G25A	1.21 ± 0.14	no
T67G	0.93 ± 0.07	no
Q32A	0.77 ± 0.07	no
S66A/Y70F	1.00 ± 0.08	no

Figure 5-42: Estimation of cooperativeness of Na^+ binding to *I. tartarcius* ATP synthase containing wild-type and mutant c-rings. (**A**) Patterns of competitive Na^+ binding to wild-type ATP synthase were fitted to Hill equation. The increased slope of the Hill plot shows concentration-dependent binding of Na^+ to wild-type c-ring and yields Hill coefficient *h* of 0.97, indicating noncooperative binding of Na^+. This means each binding site accommodates 1 Na^+ ion independently on the occupancy of the neighbouring binding sites. (**B**) The analysis of cooperativity based on the Hill coefficient was applied to mutant ATP synthases. Evaluated *h* coefficients for Na^+ binding to mutant ATP synthases are in the range of 0.77-1.21. Therefore, it was concluded that none of the mutations affected the independent mode of Na^+ binding to ATP synthase.

5.4.11. Li^+-inhibition of *pmf*-driven ATP synthesis by *I. tartaricus* wild-type and mutant ATP synthases

We next aimed to verify whether the presence of Li^+ has a similar effect on the binding of H^+ to *I. tartaricus* ATP synthase. To do so, the influence of different concentrations of Li^+ on *pmf*-driven ATP synthesis by *I. tartaricus* wild-type ATP synthase was investigated. The experiments were performed in the similar way that the Na^+-inhibition of *pmf*-driven ATP synthesis (details in Methods). The result of this study was that the initial rates of *pmf*-driven ATP synthesis in the presence of up to 100 mM LiCl. Hence, we did not detect the competitive binding of Li^+ to ATP synthase in the range 1-100 mM LiCl at pH 4.5 (**Figure 5-43**). The initial rates of *pmf*-driven ATP synthesis start to decrease, however, from 200 mM LiCl and above it. This decrease in activity is due to unspecific binding of Li^+ to ATP synthase. The same LiCl-inhibition effect we observed for hybrid H^+-selective *S. platensis*/ *I.tartaricus* ATP synthase (section 5.4.1.5).

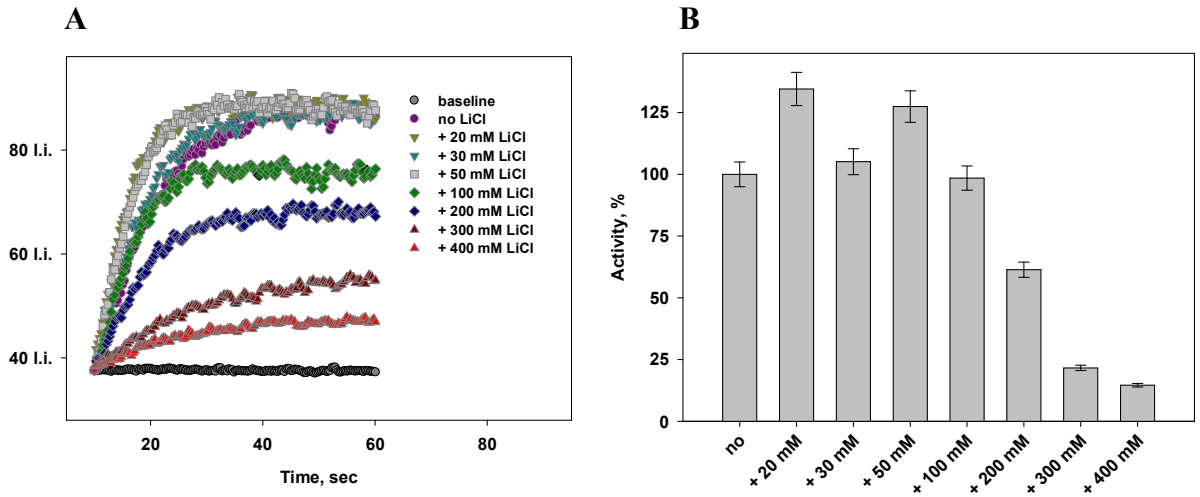

Figure 5-43: Unspecific Li^+-inhibition of *pmf*-driven ATP synthesis of *I. tartaricus* wild-type ATP synthase. (**A**) The raw data illustrate effect of different concentrations of LiCl on *pmf*-driven activity of *I. tartaricus* wild-type ATP synthase. Only unspecific effect of high concentrations of LiCl was observed at ≥ 200 mM LiCl. (**B**) The initial rates of *pmf*-driven ATP synthesis at different LiCl concentrations were calculated and plotted to illustrate the effect of LiCl on *pmf*-driven ATP synthesis. No Li^+-inhibition within range 1-100 mM was observed.

According to the obtained data, for the case of *I. tartaricus* wild-type ATP synthase, the selectivity is limited to H^+ and Na^+ at high H^+ concentration (pH 4.5). It was not possible to quantify the Li^+ inhibition of *pmf*-driven ATP synthesis at low pH range due to very high preference toward H^+. Only at high (alkaline) pH range where the concentration of H^+ is much lower, it was shown that the selectivity of wild-type ATP synthase for monovalent cations can have broader variability (H^+, Na^+ and Li^+) (see sections 5.3.1.1 and 5.3.1.7).

In addition to experiments with wild-type ATP synthase, it was tested whether Li^+ can compete with H^+ for binding to Q32A and T67S mutant ATP synthases. Q32A and T67S mutant ATP synthases were shown to use *lmf* for ATP synthesis and therefore, evidently can bind and transport Li^+ (section 5.4.5). According to performed tests, *pmf*-driven ATP synthesis of Q32A and T67S mutant ATP synthases was not affected by 100 mM LiCl (**Figure 5-44)**. For the case of Q32A and T67S ATP synthases, Li^+ is not capable to compete with H^+ for binding to c-ring at tested pH due to much lower Li^+ binding affinity. Presented data corroborates generally low Li^+ binding selectivity of mutant ATP synthases.

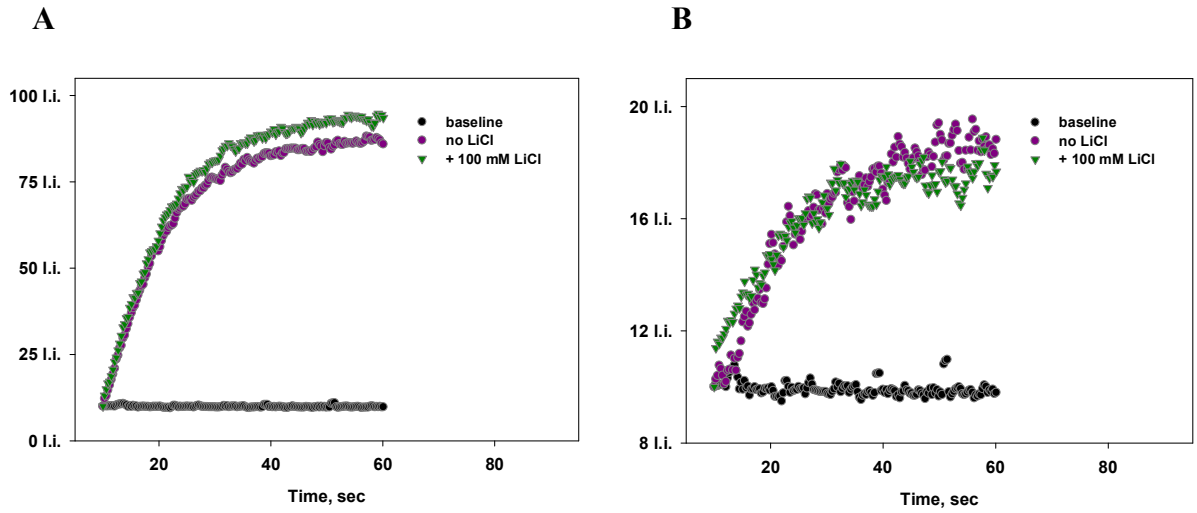

Figure 5-44: *pmf*-driven ATP synthesis of mutant ATP synthases at high LiCl concentration. The *pmf*-driven ATP synthesis by *I. tartaricus* mutant ATP synthases was monitored in the presence of different LiCl concentrations. High concentration of LiCl shows no inhibition effect on *pmf*-driven ATP synthesis of Q32A (**A**) and T67S (**B**) mutant ATP synthases.

5.4.12. Effect of mutations on initial rates (V_i) of cation-driven ATP synthesis

Previously with the help of pH-dependent modification of conserved Glu65 residue in the c-ring it was shown that the H^+-binding affinity is the inherent property of the rotary c-rings as far as the negatively charged Glu/Asp65 residue is not replaced form the ion-binding site (see section 5.2.3). The concomitant ability of *I. tartaricus* mutant ATP synthases to bind and translocate H^+ across membrane under particular conditions was also shown (section 5.4.5). The *pmf*-driven activity of mutant ATP synthases was evaluated and compared. The majority of the mutations did not impair or even improved the velocities of *pmf*-driven ATP synthesis by *I. tartaricus* ATP synthase (**Table 5-18**). Namely, Q32A, T67G and S66A mutations in the c-ring and their combination with Y70F replacement lead to 1.5-7.2-fold improved velocities of *pmf*-driven ATP synthesis. The mutations of T67 residue in the c-ring also increased the turnover numbers in comparison to wild-type ATP synthase. The only mutations that did not improve the velocities of *pmf*-driven ATP synthesis were the G25A and G25S mutations near the binding site and E65D mutation in the binding site. E65D mutant ATP synthase was characterized with the lowest

turnover rates for *pmf*-driven ATP synthesis. The reduction in turnover rates of E65D mutant ATP synthase can be related to reduced assembly of F_1 and F_o domains in ATP synthase.

Table 5-18: Initial and maximal velocities of ATP synthesis driven by different monovalent cation-motive forces

Mutant	*pmf*-driven V_i, s^{-1}	*pmf*-driven V_{max}, s^{-1}	*smf*-driven V_i, s^{-1}	*lmf*-driven V_i, s^{-1}
Wild-type	76.1 ± 11.4	26.7 ± 4.0	463.8 ± 32.5	64.6 ± 5.2
G25A	73.3 ± 11.0	32.9 ± 4.9	49.6 ± 3.5	no
G25S	82.4 ± 6.6	68.6 ± 5.5	no*	no
Q32A	492.4 ± 24.6	492.4 ± 24.6	52.5 ± 3.7	32.1 ± 2.6
E65D	35.8 ± 5.4	20.5 ± 3.1	no	no
S66A	148.7 ± 11.9	53.5 ± 4.3	96.1 ± 6.7	no
T67G	544.7 ± 27.2	309.4 ± 15.5	60.2 ± 4.2	no
T67M	478.3 ± 23.9	211.1 ± 10.6	no	no
T67Q	154.3 ± 7.7	106.7 ± 5.3	no	no
T67S	234.7 ± 11.7	103.8 ± 5.2	24.4 ± 1.7	11.2 ± 0.9
Y70F	816.1 ± 40.8	294.5 ± 14.7	2.7 ± 0.2	no
Q32A/Y70F	253.6 ± 12.7	74.6 ± 3.7	no	no
S66A/Y70F	117.3 ± 9.4	52.5 ± 4.2	42.6 ± 3.0	no
***S. platensis*/*I. tartaricus* hybrid**	1590.9 ± 79.5	685.7 ± 34.3	no	no

*- no ATP synthesis was observed driven by marked ion-motive force and marked ATP synthase

Interestingly, the mutations that increased turnover rates for *pmf*-driven ATP synthesis had reciprocal effect on initial velocities of *smf*-driven ATP synthesis. *I. tartaricus* wild-type ATP synthase appeared to be best tuned to work on *smf*. High rates of *smf*-driven ATP synthesis were related to high F_1/F_o assembly and high Na^+-binding affinity of the c-ring in ATP synthase. Among the mutations that did not restrict the ability to use *smf*, Y70F mutation had a very pronounce effect on *smf*-driven ATP synthesis. This polar-to-aromatic mutation decreased more than 170 times the initial velocity of *pmf*-driven ATP synthesis. Combination of Y70F mutation with any other polar-to-hydrophobic substitution (e.g., Q32A and S66A mutations) lead to

complete inability of ATP synthase to bind and transport Na^+ (Q32A/Y70F mutant) or lead to much reduced Na^+ binding and transporting properties (S66A/Y70F mutant). On the other hand, the V_i of *pmf*-driven ATP synthesis of Y70F ATP synthase increased more than 10 times in respect to wild-type ATP synthase. The essential changes in V_i displayed by the mutant ATP synthases were linked to changes in K_M (Na^+) values.

5.4.13. Efficiency of *smf*-driven ATP synthesis, V_{max}/K_d parameter

V_{max}/K_M ratio is an important parameter that describes the efficiency of enzyme. The low efficiency for mutant ATP synthases can become lethal phenotypes on the cellular level. Therefore, it was crucial to evaluate how mutations affected the efficiency of *smf*-driven ATP synthesis pivotal for *I. tartaricus* cells. Efficiency for performed ATP synthesis was gained by examining the ratio between V_{max} (maximal velocity when enzyme is saturated by its catalytic substrate ADP) and K_d (parameter that describes half maximal concentration of ion-coupling substrate (H^+, Na^+ or Li^+) to reach the maximal catalytic velocity). The V_{max}/K_d parameter depends on $[Na^+]/K_d$ ratio (Eisenthal et al., 2015). Therefore, the efficiency of wild-type and mutant ATP synthases was analysed under conditions of different concentrations of Na^+ present in the medium. Wild-type and mutant ATP synthases were catalytically active at pH 7.5 and thus suitable for V_{max}/K_d evaluation and comparison. The V_{max} values were obtained from kinetic curves of *smf*-driven ATP synthesis recorded at pH 7.5. The apparent K_d (Na^+) values were taken from ITC measurements of Na^+ binding to wild-type and mutant c-rings at pH 7.5. The calculated intact efficiency of *smf*-driven ATP synthesis of *I. tartaricus* wild-type ATP was used for comparison with mutant ATP synthases. **Figure 5-45** schematically illustrates the relative changes in efficiency of *smf*-driven ATP synthesis of wild-type ATP synthase after selected mutations were introduced in its c-ring.

In the first case, the efficiencies of *smf*-driven ATP synthesis were considered when both parameters V_{max} and K_d are crucial in defining efficiency of ATP synthase (**Figure 5-45A**). It is important that the baseline Na^+ concentration have to be low enough to make affinity parameter crucial: $[Na^+]/K_d < 1$. Under these conditions, the majority of the efficiencies of mutant ATP synthases are 2-3-orders of magnitude reduced. Only G25A mutant ATP synthase displays 3%

level of initial efficiency of wild-type ATP synthase. For the second case, we considered a situation when the baseline Na^+ concentration exceeds half saturation Na^+ concentration for the c-ring: $[Na^+]/K_d > 1$ (**Figure 5-45B**). In this case, V_{max} is a parameter that best describes the efficiency. In this situation the efficiencies of *smf*-driven ATP synthesis are 1-order of magnitude reduced. G25A and T67G mutant ATP synthases would be the most efficient among the mutant ATP synthases at this condition. For the latter case was considered a situation when ATP synthase is working at conditions of very low baseline Na^+ concentration: $[Na^+]/K_d <<< 1$ (**Figure 5-45C**). In this case, the K_d (Na^+) values are determinative for efficiencies of *smf*-driven ATP synthesis. In this case, G25A mutant ATP synthase would be just 4-times less efficient than wild-type ATP synthase.

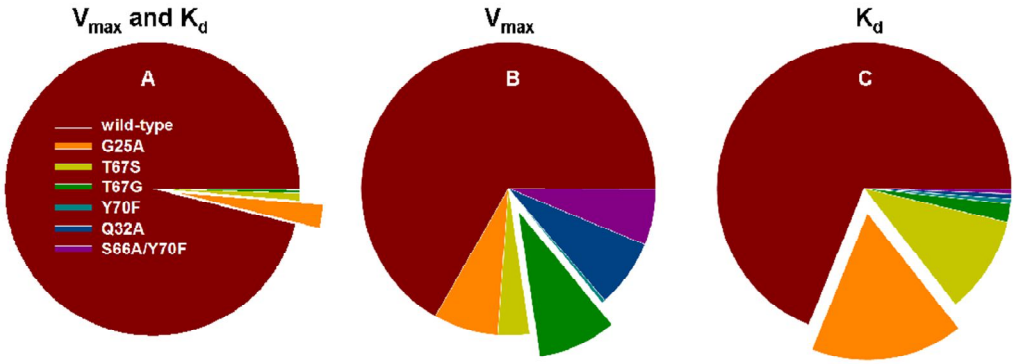

		A $[Na^+]/K_d<1$	B $[Na^+]/K_d>1$	C $[Na^+]/K_d<<<1$
	Wild-type	100.00	100.00	100.00
	G25A	2.62	10.69	24.45
	T67S	0.82	5.26	15.66
	T67G	0.37	12.98	2.87
	Y70F	0.01	0.58	0.79
	E65D	x	x	x
	Q32A	0.09	11.32	0.79
	S66A/Y70F	0.07	9.18	0.79

Figure 5-45: Relative changes in efficiencies of *smf*-driven ATP synthesis by mutant ATP synthases. (**A**) $[Na^+]/K_d< 1$: Both parameters, V_{max} and K_d, define the efficiency of ATP synthesis driven by *smf*. In this case, G25A mutant (exploded slice) possesses closest to wild-type efficiency of ATP synthesis (only 3% of the intact efficiency of wild-type ATP synthase). Rest of mutants show 2-orders of magnitude lower efficiencies (< 1% of the intact wild-type efficiency). (**B**) $[Na^+]/K_d> 1$: The main determinant of the efficiency is the velocity of catalysis (V_{max}). ATP synthesis occurs at conditions close to half saturation of the most mutant binding sites with Na^+. For this case, 1-order of magnitude difference in efficiency is observed. Namely, T67G mutant (exploded slice), G25A and Q32A mutant ATP synthases display 10.7-12.9% of the original wild-type efficiency. Y70F mutant ATP synthase will have the lowest efficiency among mutant ATP synthases. (**C**) $[Na^+]/K_d<<< 1$: The main determinant of the efficiency is Na^+ affinity. In this case, the V_{max} velocities are negligible and binding of Na^+ occurs at conditions where K_d values are pivotal. In this case, G25A mutant (exploded slice) will have only 4-times reduced efficiency of *smf*-driven ATP synthesis compared to wild-type ATP synthase.

Independently on the parameter that is determining for the efficiency of ATP synthesis (V_{max} or

K_d), wild-type ATP synthase will remain the most powerful *smf*-driven catalyst independently on $[Na^+]/K_d$ ratio and the efficiency of *smf*-driven ATP synthesis of Y70F mutant ATP synthase is the most impaired for all analyzed cases.

5.4.14. Summary of functional studies

The following questions were addressed in this chapter:

(i) How would the substitution of conserved residues in the ion binding site affect the assembly and activity of *I. tartaricus* ATP synthase

(ii) Are the distant conserved residues (Gln25) functionally important as well?

With respect to question (i): In total 12 mutant ATP synthases were checked for their assembly and further analyzed in their ability to use *smf*, *pmf* and *lmf* to drive ATP synthesis reaction. ATP synthesis by G25S, T67M, T67Q, E65D and Q32A/Y70F mutant ATP synthases was driven only by *pmf*. For the case of G25S, T67M, T67Q and Q32A/Y70F mutant ATP synthases it was additionally shown that *pmf*-driven ATP synthesis is not affected by high (≤ 100 mM) NaCl concentrations and therefore, these ATP synthases are not Na^+-selective. For the rest of the mutant ATP synthases, the K_M (Na^+) values were determined and compared. If compare to wild-type, K_M (Na^+) values decreased 3-, 4-, 4.5-, 11- and 11.5-time for the E65D, S66A, Y70F, G25A and T67G mutant ATP synthases.

Concerning (ii), the example of G25A and G25S mutant ATP synthases showed that Na^+-selectivity of ATP synthases is additionally modulated by residues that are not a part of defined ion binding site but are situated in a close proximity (~5 Å) to affect Na^+ binding and related *smf*-driven ATP synthesis. Substitution of Gln25 to Ala (G25A mutant) or to Ser (G25S mutant) in the c-ring of *I. tartaricus* ATP synthase restricted its ion selectivity to H^+/Na^+ and to H^+, respectively. Meanwhile, for the case of both mutant ATP synthases, G25A and G25S, the initial rates of *pmf*-driven ATP synthesis (V_i, s^{-1}) were not affected, the *smf*-driven ATP synthesis by G25A ATP synthase was almost 10-times slower from wild-type ATP synthase. In addition to changes in rates of *smf*-driven ATP synthesis by G25A ATP synthase, the change in Na^+ binding affinity was also detected for G25A mutant ATP synthase. Namely, the K_M (Na^+) was 11-times higher for G25A ATP synthase in respect to wild-type. In addition, the lower Na^+ binding

capacity for G25A mutant ATP synthase was detected as well.

5.5. 3D crystallization of Q32A/Y70F mutant c-ring

5.5.1. Extraction and 3D crystallization of Q32A/Y70F mutant c-ring

Q32A/Y70F mutant c-ring was particularly interesting for structural investigation as experiments with the purified Q32A/Y70f mutant c-ring and Q32A/Y70F mutant ATP synthase indicated its exclusive H^+-selectivity. Two approaches were used for purification of Q32A/Y70F mutant c-ring. In the first approach, Q32A/Y70F mutant c-ring was extracted from purified Q32A/Y70F mutant ATP synthase (**Figure 5-46A**, lane 2). By the second approach, Q32A/Y70F mutant was expressed as a single *atpE* gene in *E. coli* BL21 cells and extracted directly from membranes. This sample had a population of aggregated (or misfolded) protein (**Figure 5-46A**, lane 4). This aggregated/misfolded protein brake down to monomers (**Figure 5-46A**, lane 5) after treatment with 12% Trichloroacetic acid (TCA). Moreover, this fraction was shown to re-assemble *in vitro* into the λ/ε/c-ring rotor part of *I. tartaricus* ATP synthase (**Figure 5-46B**).

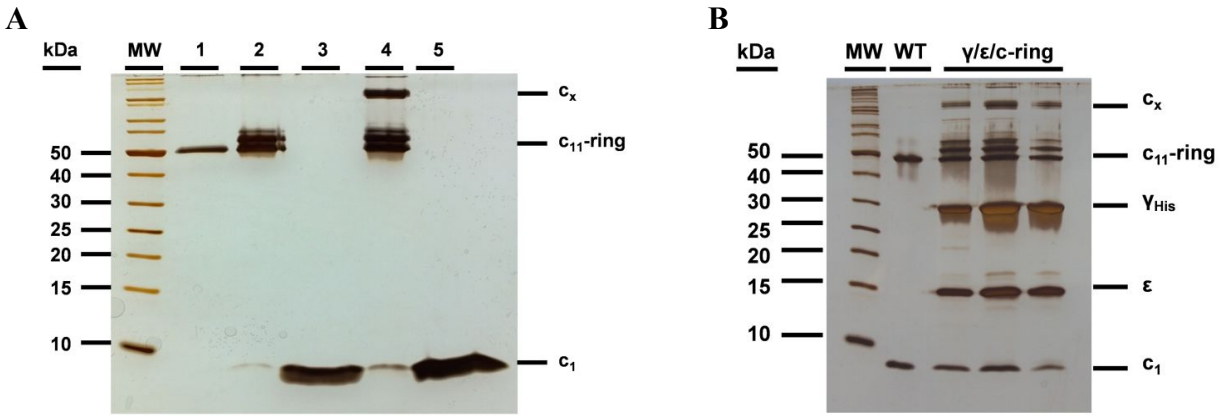

Figure 5-46: Q32A/Y70F mutant c-ring purified by two different approaches. (A) SDS-PAGE of Q32A/Y70F mutant c-ring. **(1)** – wild-type c_{11}-ring reference. (**2)** – Q32A/Y70F mutant c-ring extracted from Q32A/Y70F mutant ATP synthase and (**3**) its monomers after TCA treatment. (**4) -** Q32A/Y70F mutant c-ring, which was produced singly and extracted directly from *E. coli* membranes, contains portion of aggregated/misfolded protien. (**5**) Q32A/Y70F mutant c-ring and its aggregated/misfolded fraction can be monomerized by TCA treatment. (**B**) SDS-PAGE of Q32A/Y70F mutant c-ring (fraction 4 at panel A) is re-assembled in λ/ε/c-ring rotor part.

The aggregated/misfolded fraction of Q32A/Y70F mutant c-ring was removed by 2 rounds of sucrose density centrifugation and MonoQ anion exchange chromatography (**Figure 5-47**)

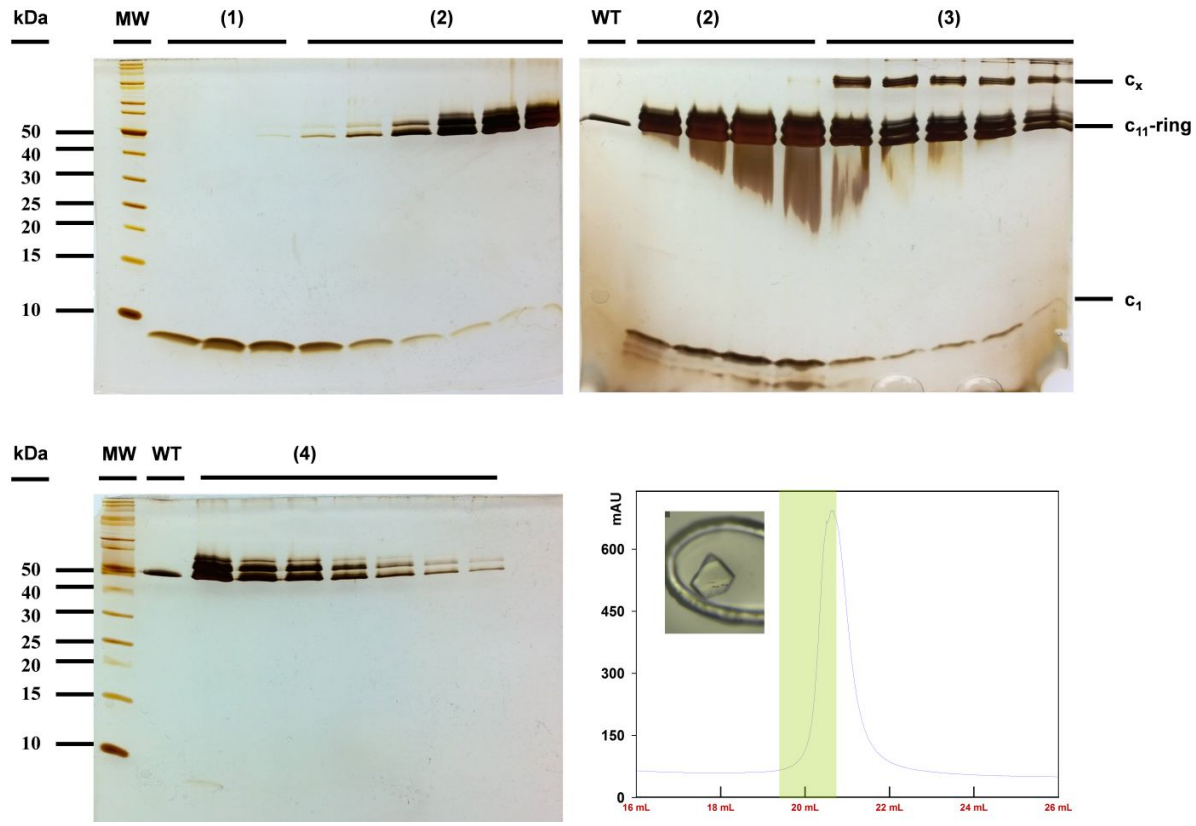

Figure 5-47: Refining sample for further crystallization. Upper panel: Extracted Q32A/Y70F mutant c-ring after HAP chromatography was run through first 5-35% sucrose density gradient made in 20 mM Tris pH 8.0, 100 mM NaCl and 0.05% DDM. SDS-PAGE shows distribution of proteins from top (low sucrose concentration) to bottom (high sucrose concentration) of the tube after 14 hours of centrifugation. First sucrose density centrifugation of sample helped to remove partially monomers (**1,** 5-15% fraction of sucrose gradient) and aggregated/misfolded protein (**3,** 30-35% fraction of sucrose gradient). Main fraction (**2,** 20-25% fraction of sucrose gradient) contained Q32A/Y70F mutant c-ring. **Lower panel:** To further improve quality of the sample, the second subsequent 5-35% sucrose density gradient made in 20 mM Ammonium Acetate pH 6.9, 0.05% DDM was used to run through Q32A/Y70F mutant c-ring (fraction 2 of first sucrose gradient). This step more properly separated remaining Q32A/Y70F c-subunits and Q32A/Y70F c-ring. Obtained sample with only oligomeric protein (**4**) was additionally subjected to MonoQ anion exchange chromatography (right corner). Resulting homogeneous sample (indicated in green on a sample running profile) was used for 3D crystallization setups. Example of obtained crystal mounted in nylon loop is shown.

Improved in purity sample after extensive (few days) dialysis was used for 3D crystallization by vapour diffusion in hanging drop 24-well and 96-sitting drop well plate format. Multiple crystal

forms were obtained for Q32A/Y70f mutant c-ring and tested (**Figure 5-48 and Figure 5-49**).

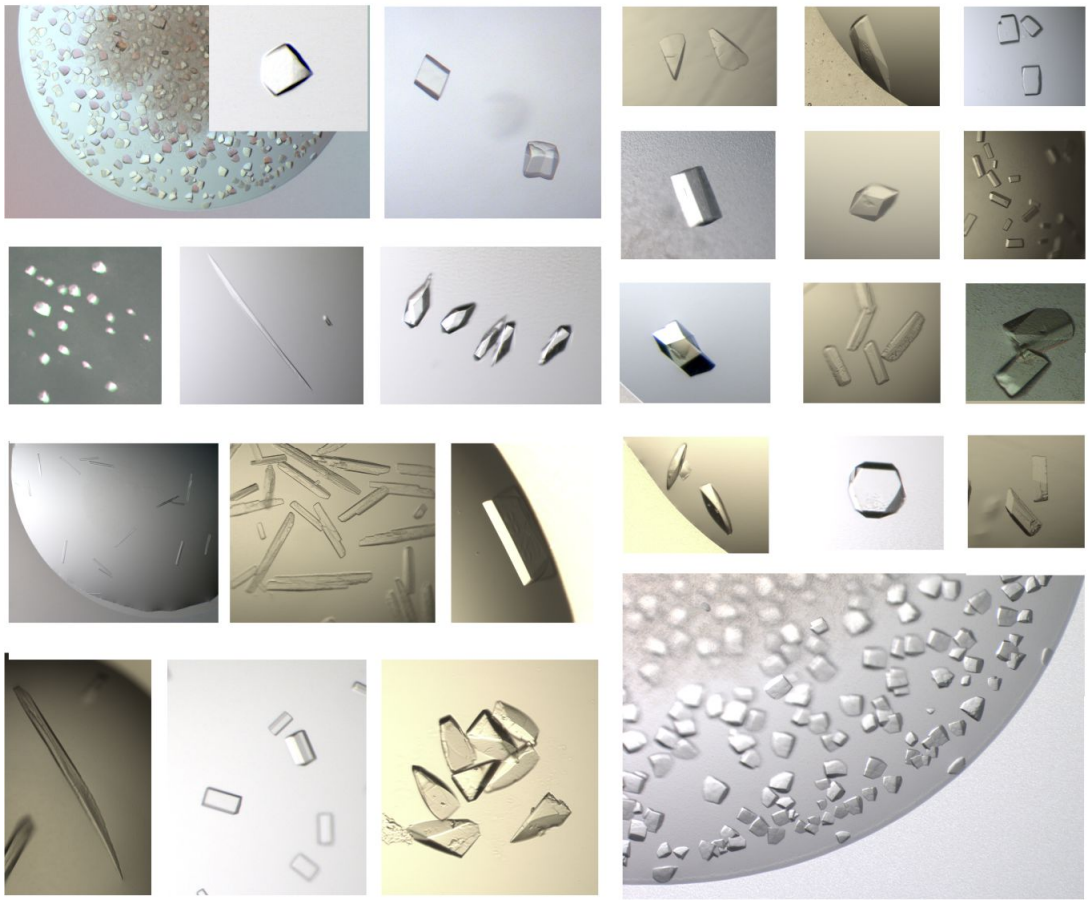

Figure 5-48: Crystals of Q32A/Y70F mutant c-ring. Presented is a panel of crystal forms obtained for Q32A/Y70F mutant c-ring. Crystals were obtained by vapour diffusion method at 18°C in 24-well hanging drop format plates.

Despite multiple obtained crystal forms, further variations in purification and crystallization protocol (e.g., use of different detergents for sample preparation, pre-crystallization treatment of sample, use of different temperatures and crystallization screens for growing the crystals), obtained crystals belonged to triclinic space group P_1 and were anisotropic. Therefore, it was decided to have a closer look on a stoichiometry of the complex and verify whether multiple oligomer forms are present in the sample, which would explain problems with packing of protein in crystal.

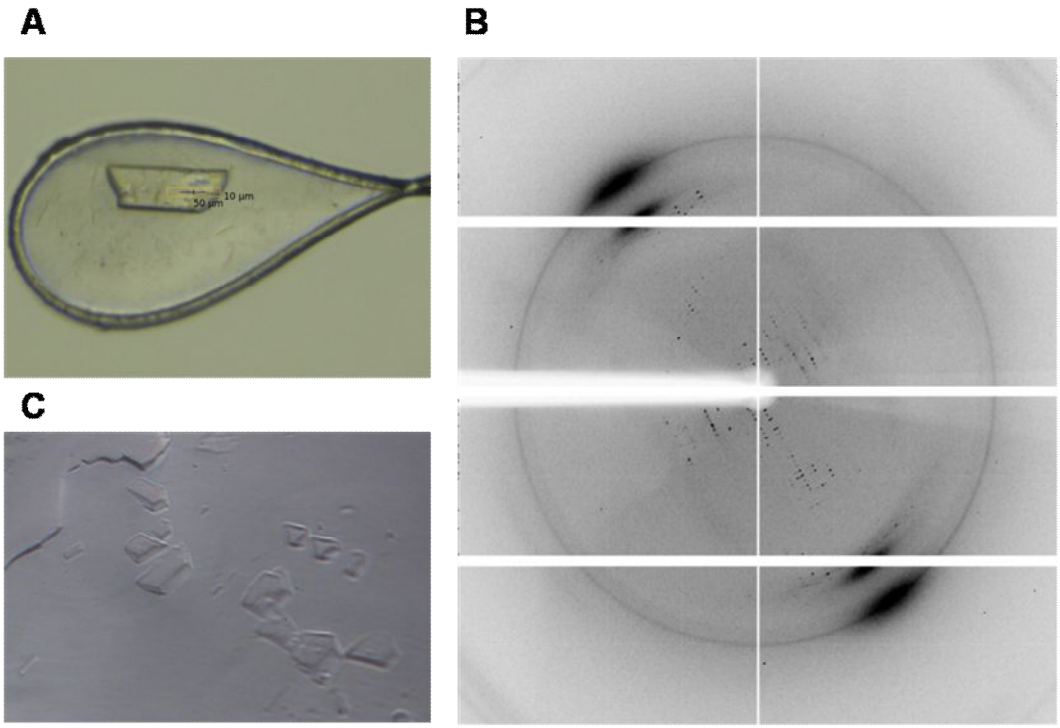

Figure 5-49: Example of diffraction pattern for one of the obtained crystal forms of Q32A/Y70F mutant c-ring. (**A**) Crystal grown by vapour diffusion method was mounted in 0.1-0.2 mm nylon loop and flash frozen in liquid nitrogen before testing. (**B**) Protein crystal exhibits diffraction anisotropy. (**C**) As alternative, lipidic cubic phase (LCP) method was used for growing the crystals of Q32A/Y70F mutant c-ring. Presented is an example of one of the obtained 3D crystals.

5.5.2. Electroelution of Q32A/Y70F mutant c-ring from SDS-PAGE and its 3D crystallization

Q32A/Y70F mutant c-ring, when extracted and purified to homogeneity, showed two protein bands in SDS-PAGE. One of the protein bands corresponded to size of wild-type c_{11}-ring and other protein band run slower from wild-type c_{11}-ring. Slower in-gel running behaviour can correspond to higher stoichiometry (>11) of the part of Q32A/Y70F mutant c-ring. In order to test this working hypothesis, the two factions of Q32A/Y70F were electroeluted from SDS-PAGE and analysed (**Figure 5-50** and **Figure 5-51**).

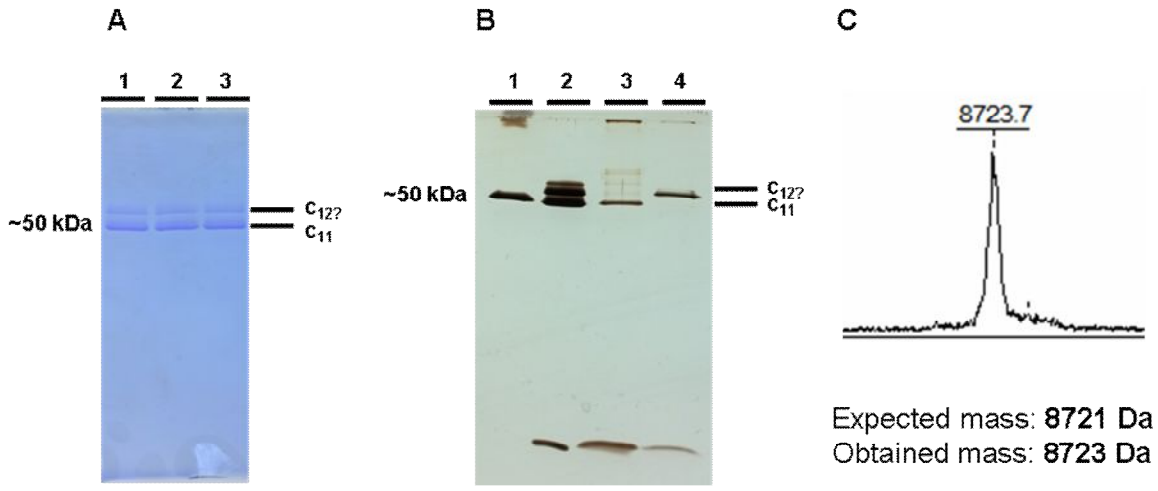

Figure 5-50: Electroelution of Q32A/Y70F c-ring from SDS-PAGE stained with Coomassie brilliant blue R-250 dye. As a first proof of principles, two fractions of Q32A/Y70F mutant c-ring were excised and electroeluted from SDS-PAGE stained with Coomassie brilliant blue R-250 dye. (**A**) Q32A/Y70F sample extracted directly from *E. coli* membranes was run for 4 hours on SDS-PAGE and stained with Coomassie brilliant blue R-250 dye. Two protein bands are clearly seen (lanes 1, 2 and 3). **(B)** Comparison of original sample and samples after electroelution on SDS-PAGE. (**1**) –wild-type c_{11}-ring reference. (**2**) – Q32A/Y70F mutant c-ring before electroelution. (**3**) – electroeluted lower band of Q32A/Y70F mutant c-ring corresponds to size of wild-type c_{11}-ring. (**4**) – electroeluted upper band of Q32A/Y70F mutant c-ring migrates slower from wild-type c_{11}-ring. (**C**) Electroeluted sample that corresponds to upper band of Q32A/Y70F mutant c-ring (lane 4 in section B) was subjected to mass spectrometry analysis. The shortcut of obtained MALDI-MS spectrogram shows that electroeluted fraction consists of the c-subunits of one molecular weight (8723 Da). The mass of these c-subunits corresponds to the mass of Q32A/Y70F mutant c-subunits (8721 Da).

Q32A/Y70F mutant possess comparably high SDS-stability and therefore can stand long run on SDS-PAGE and subsequent electroelution. First electroelution trials were done for the SDS gels stained with Coomassie Brilliant blue R-250. Two oligomers could be separated and analyzed. Unfortunately, Coomassie staining appeared to be hardly reversible and required very harsh destroying conditions to remove completely the stain (few days of dialysis in methanol-containing distaining buffer). Therefore, in order to perform biochemical and crystallization tests, the staining and electroelution procedure was changed. Instead of Coomassie brilliant blue R-250 dye was used easily reversible negative $CuCl_2$-based staining. Changing the gel staining procedure has improved both, efficiency and quality of electroelution.

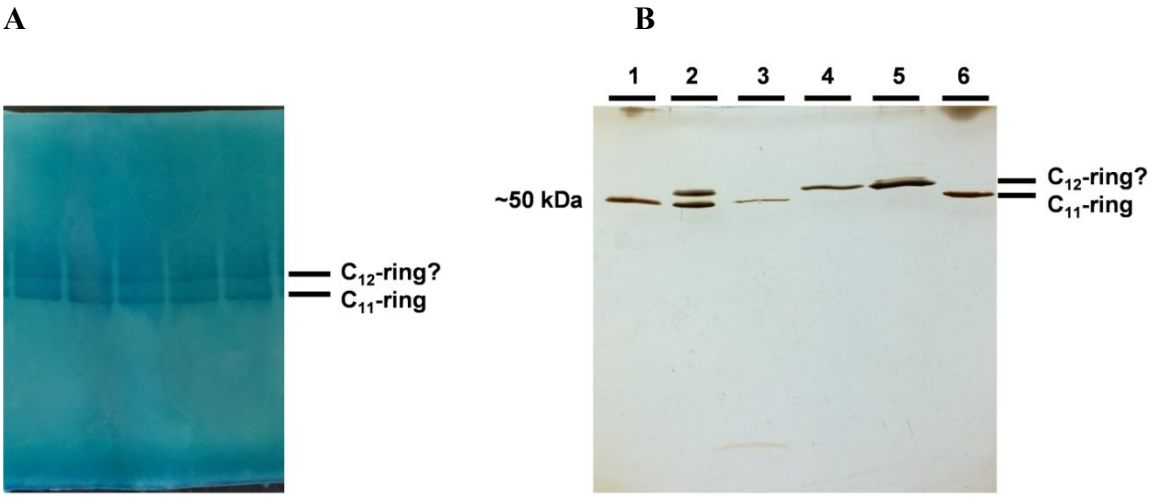

Figure 5-51: Electroelution of Q32A/Y70F c-ring from SDS-PAGE negatively stained with $CuCl_2$. (**A**) Visualization of Q32A/Y70F sample in the SDS-PAGE was done by 5 min incubation in 0.3 M $CuCl_2$ solution. Colorless protein bands were excised from gel and electroeluted. (**B**) SDS-PAGE compares samples before and after electrolution. As a reference was used wild-type c_{11}-ring (lanes 1 and 6). Before electroelution there are two clear protein bands in Q32A/Y70F sample (lane 2). Electroelution allows to extract protein from each of the excised protein-containing gel slices (lanes 3, 4 and 5).

Separated fractions were subjected to dialysis against 20 mMTris pH 8.0 and after supplemented with 2% of DM orNM detergents. Unfortunately, the resolution of such crystals (these crystals diffracted only up to ~ 9 Å) did not allow refine the data and clarify the open question on stoichiometry of upper band in Q32A/Y70F sample. Further improvement of sample quality and/or crystallization conditions is highly required.

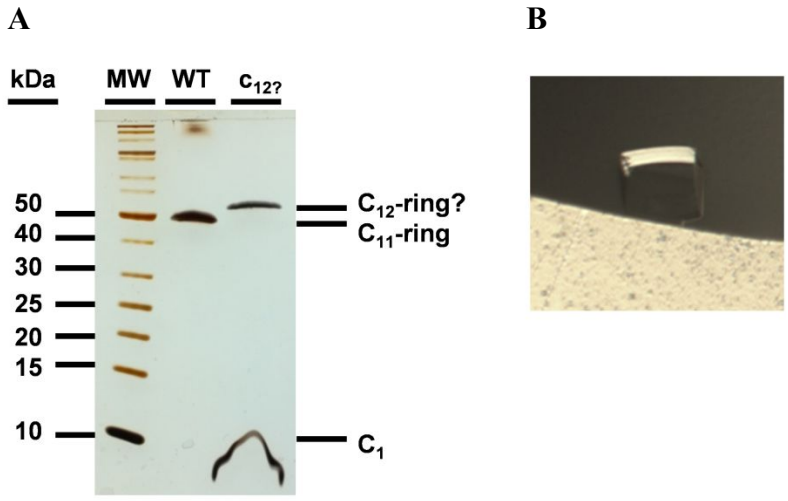

Figure 5-52. Electroeluted and prepared for crystallization probable c_{12}-oligomer of Q32A/Y70F mutant. (A) SDS-PAGE of electroeluted and prepared for crystallization c_{12}-oligomer of Q32A/Y70F mutant. Sample was stable and feasible for further crystallization trials. **(B)** Sample was crystallized in 3D in 2% DM. Diffraction pattern showed best points up to 7 Å.

5.6. Summary of all obtained results

The ion binding site of *I. tartaricus* c-ring was studied by mutagenesis approach. In this regard, 12 *I. tartaricus* c-ring mutants were recombinantly produced in and purified from *E. coli* cells in quantity and quality suitable for further biochemical analysis (e.g. large amounts, milligram scale, of pure and homogeneous target proteins).

Biochemical characterization of obtained mutants was initiated by performing DCCD modification of target Glu65 carboxyl group in wild-type and mutant c-rings under different pH and salt conditions:

1. DCCD modification of target Glu65 carboxyl group at different pH points revealed deprotonation of Glu65 carboxyl group in both, wild-type and mutant c-rings under exposure to a pH greater than 6.5.
2. The pKa = 7.8 was evaluated for Glu65 carboxyl group in wild-type, E65D, T67G, T67S and Y70F mutant c-rings based on the pH-dependency of Glu65 deprotonation. The up-shifted pKa = 8.3 was evaluated for Glu65 carboxyl group in Q32A and S66A/Y70F mutant c-rings and pKa = 9.3 was evaluated for the Glu65 carboxyl group in Q32A/Y70F mutant c-ring.
3. The pH-dependent Na^+ protection of Glu65 carboxyl group against DCCD modification was observed for the case of T67G, T67S, E65D, Y70F, S66A/Y70F and Q32A mutant c-rings. No Na^+ protection against DCCD modification was observed for the case of Glu65 carboxyl group in Q32A/Y70F mutant c-ring.
4. The intact specific rate of Glu65 carboxyl group modification by DCCD was reduced in T67S, T67G, Y70F, S66A/Y70F, Q32A, Q32A/Y70F but not in E65D mutant c-ring.

In order to characterize the thermodynamics that defines the interaction of c-ring with Na^+, ITC experiments have been carried out in the present study:

1. It has been found that the binding of Na^+ to *I. tartaricus* wild-type c-ring is exothermic in nature and is governed by favourable enthalpic contribution.
2. Affinity of Na^+binding to wild-type c-ring (K_d (Na^+)) is relative to pH and depends on

appropriate $[Na^+]/[H^+]$ ratio.

3. The Na^+ binding to G25A, T67S, T67G and Y70F mutant c-ring was found to be also exothermic.
4. G25A, T67S, T67G and Y70F mutant c-rings were shown to bind Na^+ with lower Na^+ affinity (shown by K_d (Na^+) values) and Q32A, S66A/Y70F and Q32A/Y70F mutant c-rings did not show signals of Na^+ binding at tested pH and NaCl range.
5. For the case of G25A, T67G and Y70F mutant c-rings the thermodynamic settings of Na^+ binding were different from wild-type c-ring. Main contribution from entropy term was detected.
6. Na^+ binding to wild-type and mutant c-rings showed significant protonation effects at pH ≤ 7.5.

The same residues were also mutated within entire *I. tartaricus* ATP synthase. At this final step, the set of c-ring mutants was tested for ability to assemble in ATP synthase and perform coupled ATP hydrolysis and ATP synthesis driven by different ion-motive forces:

1. Obtained 12 mutant c-rings were shown to assemble in complete ATP synthase complex and catalyze coupled ATP hydrolysis in detergent solution and when incorporated in lipid (ETLE) vesicles.
2. Mutant ATP synthases reconstituted in lipid vesicles showed reduced specific ATP hydrolysis activity with respect to wild-type ATP synthase. The only exception wasS66A/Y70F mutant ATP synthase for which similar to wild-type ATP hydrolysis rates were recorded.
3. ATP synthesis measurements revealed that E65D, G25S, T67M, T67Q and Q32A/Y70F mutant ATP synthases can use only *pmf* to drive ATP synthesis, meanwhile ATP synthesis by G25A, Y70F, S66A, T67G and S66A/Y70F mutant ATP synthases can be driven by *smf* and *pmf*. Only for the case ofwild-type, Q32A and T67S mutant ATP synthases the *smf*-, *pmf*- and *lmf*-driven ATP synthesis was detected depending on applied ion-motive force.
4. The clear tendency was observed for mutants: the rates of *pmf*-driven ATP synthesis were elevated and the rates of *smf*- and *lmf*-driven ATP synthesis were reduced in comparison

to wild-type.

5. The efficiency of *smf*-driven ATP synthesis was sufficiently reduced for the case of mutant ATP syntheses.

Taken together, obtained results indicate that apparent Na^+ binding affinity of *I. tartaricus* c-ring depends on molar ratio between H^+, Na^+ and Li^+ in the environment. The defined values of absolute binding affinities for H^+(0.0124 μM) and for Na^+(7.9 μM) indicate that *I. tartaricus* c-ring is originally more selective to H^+ than to Na^+. The performed mutagenesis study shows that H^+ selectivity is intact property of the c-ring as far as ionisable Glu/Asp residue is not removed from the ion binding site. It was shown that both, Na^+ and H^+ binding affinities of the c-ring can be influenced by specific mutations in the ion binding site. For the particular set of obtained mutants, the H^+ binding affinity was increased and Na^+ binding affinity was either reduced or eliminated. Namely, the set of Q32A, S66A/Y70F and Q32A/Y70F mutants possess pronounce increases in H^+ binding affinities expressed as pKa values. The set of G25A, T67S, T67G and Y70F mutant c-rings have reduced Na^+ binding affinities expressed as K_d (Na^+) values. The same mutations but incorporated into entire ATP synthase lead to drastic changes in ATP synthesis driven by corresponding ion-motive force. In total 4 mutations were identified (G25S, T67M, T67Q and Q32A/Y70F) that are linked to losses in Na^+ binding affinity of corresponding mutant c-ring and *smf*-driven ATP synthesis by corresponding mutant ATP synthase. In general, the obtained data was used to understand and later discuss what makes *I. tartaricus* c-ring selective to Na^+ under physiological conditions and which principles underlie relative cation selectivity of corresponding ATP synthases.

.

6. Discussion

In the current thesis, the representative selected ATP synthase of *I. tartaricus* that display the principles of relative competitive $Na^+/H^+/Li^+$ monovalent cation selectivity was explored. An intriguing question of what determines the cation selectivity of this particular ATP synthase was addressed. In this chapter the design principles for competitive Na^+/Li^+ and/or H^+ selectivity of several rotary ATP synthases are discussed on the a basis of the results obtained in this work on *I. tartaricus* ATP synthase, c-ring and their mutants.

6.1. The pKa values of ionisable chemical groups in proteins

Ionisable chemical groups (ICG) are the groups of atoms of a molecule that change their charge due to protonation/deprotonation reactions, due to changes in chemical environment, typically, because of pH changes and/or changes in their local electrostatic environment (Goh et al. 2014). In proteins, seven amino acids (Arg, Asp, Cys, Glu, His, Lys and Tyr) of the twenty standard amino acids, contain ICG in their side chains.Namely, carboxylic acid group of aspartic and glutamic acids, imidazole group of histidine, thiol group of cysteine, hydroxyl group of tyrosine and amino group of lysine, that ionize between pH 1.0 and 14.0 (Pace et al. 2009, Gunner and Baker 2016). The pH, at which the protonation (or deprotonation) probability of ICG is 50%, is called pKa or $pK_{1/2.}$ The pKa parameter is used to describe the ionization behaviour of all types of ICG. The charge of ICG in proteins depends on pH of the solvent and on details of the protein scaffold around ICG (Bombarda and Ullmann 2010).In a protein environment, some ICG can have substantially perturbed pKa values, in respect to the ICG pKa´s of corresponding free amino acids in aqueous solution, due to:

1) dehydration and burial in hydrophobic environment (Born effect),
2) charge-charge interactions (Coulombic effect),
3) charge dipole interactions (hydrogen bonding effect) (Harris and Turner 2002, Pace, et al. 2009).

For example, Glu and Asp carboxylic groups in proteins often do have relatively high pKa values compared with the pKa = 3.9 and pKa = 4.3, respectively, for corresponding Glu and Asp carboxylic groups in aqueous solution (Gutteridge and Thornton 2005, Platzer et al. 2014). Thus,

pKa values of Glu and Asp carboxylic groups can be up shifted by as much as 6 pH units in some extreme cases (Isom, et al. 2010, Isom et al. 2011). For example, the values ranging from 0.5 up to 12.0 have been reported for the Asp (Anderson et al. 1990, Chivers et al. 1997, Dyson et al. 1997, Giletto and Pace 1999, Zscherp et al. 1999, Grimsley et al. 2009) and values ranging from 2.1 to 8.8 have been reported for the Glu residue (Dwyer et al. 2000), for details see **Table 6-1**.

Table 6-1: The extreme pKa values of Asp and Glu residues reported for folded proteins

Residue	pKa	Protein	Reference
Asp70	0.5	T4 lysozyme	(Anderson, et al. 1990)
Asp76	0.5	RNase T1	(Giletto and Pace 1999)
Asp26	9.2	Thioredoxin	(Karp et al. 2007)
Asp96	11.4-12.0	Bacteriorhodopsin	(Zscherp, et al. 1999)
Glu73	2.1	Barnase	(Schreiber et al. 1997)
Glu(V66E)	8.8	SNase	(Dwyer, et al. 2000)

The Coulombic effect, because of charge-charge interactions with other amino acids (Arg and Lys), seems to be the cause of extremely low pKa of Asp70 in the T4 lysozyme and Glu73 in Glu73 of barnase. In another case, strong hydrogen bonding of Asp76 with nearby hydrogen donors and acceptors determine low pKa of Asp76 carboxylic group in RNase T1. The Born effect (high dielectric constant of the environment) due to the hydrophobic vicinity (Asp96 in bacteriorhodopsin, unphotolyzed state) and desolvation of the charged group when it is buried in a hydrophobic environment (V66E mutant of staphylococcal nuclease (SNase)) are the dominant factors determining the high pKa of these Asp and Glu residues (Zscherp, et al. 1999, Garcia-Moreno et al. 2002).

Significantly perturbed, but nevertheless functionally tuned pKa values of ICG are also found in active sites of proteins such as multidrug transporter EmrE (Yerushalmi and Schuldiner 2000), tetracycline efflux pump TetA(B) (Tamura et al. 2001), solute transporter lactose permease LacY (Kaback et al. 2001, Abramson et al. 2003, Kaback 2005), melibiose carrier MelB (Zani et al.

1993), in bacteriorhodopsin (PebayPeyroula et al. 1997, Luecke et al. 1998), rhodopsin (Periole et al. 2004) and cytochrome c oxidase (Iwata et al. 1995). These ICG are often buried in more hydrophobic environments in proteins and are essential for biochemical catalysis (Warshel and Aqvist 1991, Cannon and Benkovic 1998, Harris and Turner 2002), binding and translocation of ligands, stability of protein, for ion homeostasis and pH regulation of cells (Doyle et al. 1998, Jiang and Fillingame 1998, Murtazina et al. 2001, Hunte et al. 2005), for light-activated processes (PebayPeyroula, et al. 1997, Luecke, et al. 1998) and are necessary for H^+ and Na^+ transmembrane transport (Abrahams, et al. 1994, Meier, et al. 2005, Murata, et al. 2005, von Ballmoos, et al. 2009). Namely, in biomolecules involved in H^+ transport, the pKa values of carboxylic groups are up-shifted either to enhance their ability to cage H^+ or to change electrostatic environment around the active site (Fersht 1999, Gunner and Alexov 2000, Forsyth et al. 2002, Harris and Turner 2002).

Experimental and computational methods are used to determine the pKa of the ICG in proteins. A number of direct and indirect experimental methods, such as: nuclear magnetic resonance spectroscopy (NMR), ultra-high resolution (>1.2 Å) X-ray crystallography, infrared spectroscopy (FTIR), pH-metric, UV-metric, solubility, capillary electrophoresis, conductometry, voltammetry, calorimetry, fluorimetry, polarimetry and kinetic methods have been employed for determination of pKa values of ICG in proteins (Reijenga et al. 2013). However, the experimental determination of pKa values of ICG is a nontrivial task and remains extremely challenging because of sample restriction (lack of pH-stability, sample impurities, overlapping pKa‘s), measurements in the extremes of the pH scale and because of insufficient precision (Dwyer, et al. 2000, Isom, et al. 2010, Reijenga, et al. 2013). The accuracy of pKa computation is also not optimal due X-ray model quality, computational model inconsistency and confines deviation of up to 1 pH unit from experimental pKa values (Antosiewicz et al. 1996, Schutz and Warshel 2001, Ho and Coote 2010, Kilambi and Gray 2012).

6.1.1. The pKa values of Glu/Asp carboxyl groups in the ion-binding site of the c-rings

The carboxyl group of the conserved Glu or Asp residues (**Figure 6-1**) in the ion-binding sites of the rotor-ring is conserved and is the important ICG of the c(K)-ring determining the ion-translocation properties of the ATPase.

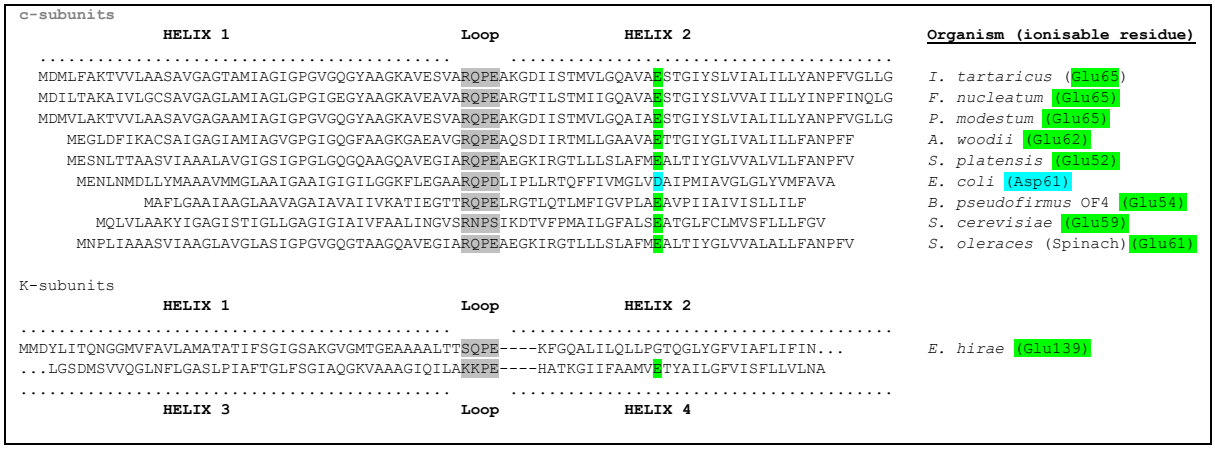

Figure 6-1: Multiple sequence alignment of c(K)-subunits from different species. In color are shown the ionisable Glu (green) or Asp (blue) residues in the c(K)-ring of different species involved in ion coordination and transport across membrane. Presented are the c(K)-subunits of species for which the protonation state/pKa of Glu/Asp in the c(K)-ring was probed experimentally. The c-subunits have two-helix topology (indicated as helixes 1-2) with one ionisable Glu/Asp in C-terminal α-helix. The distinctive property of K-subunit is its four-helix topology (indicated as helixes 1-4) with one ionisable Glu/Asp in C-terminal α-helix. The indicated numbering of Glu/Asp residues is kept according to amino acid numbering in original sequences of c(K)-subunits.

The determination of the c(K)-ring ICG pKa has been attempted by various following direct and indirect methods on various rotary ATP synthases/ases (**Figure 6-2** and **Table 6-2**):

Direct method: Solution ^{1}H NMR of the *E. coli* c-subunits in the organic solvents leads to the determination of the pKa of Asp61 in the single c-subunits with high accuracy (Assadi-Porter and Fillingame 1995, Forsyth, et al. 2002, Castaneda et al. 2009, Farrell et al. 2010, Reijenga, et al. 2013). However, the pKa values were obtained for the Asp61 carboxyl group placed in the non-relevant environment (non-oligomeric protein environment and in organic solvent).

Therefore, to justify the physiological meaning of the obtained pKa values the measurements have to be performed with the c-ring and in lipidic/aqueous environment.

Indirect methods:

(1) Rate of DCCD modification of the protonated Glu/Asp residues in the c-rings as a function of pH detected by (i) MALDI-MS, (ii) ESI-MS and (iii) HPLC (Kluge and Dimroth 1993, Meier et al. 2003, Pogoryelov, et al. 2010, Mizutani, et al. 2011). Due to covalent binding of the DCCD to protonated carboxyl group, the obtained rates of DCCD modification are not reflecting equilibrium of protonation and deprotonation reactions of target ICG, and therefore, the DCCD labeling methods can be used in approximation for net protonation state of ICG. In addition, MALDI-MS detection method does not account for isotope distribution of sample and therefore, has disadvantage of being less precise and reproducible then ESI-MS (Strupat 2005). From other side, ESI-MS is slower, more sensitive to the sample buffer composition and is not suited to high-throughput experiments (Signor and Boeri Erba 2013).

(2) Estimation of pKa based on inhibition of ATPase activity by specific inhibitor DCCD as a function of pH (Valiyaveetil et al. 2002). This method has a same problem of being non-equilibrium reaction (described in p1). Moreover, apart from the c-ring, ATPase F_1 domain has additional ICG that can be modified with DCCD (Pougeois, et al. 1979).

(3) Competitive $^{22}Na^+/H^+$ binding/release assay based on $^{22}Na^+$ radioactivity. This method is only applicable for Na^+ binding c-rings (Murata, et al. 2008). Reproducibility of this wash-based assay is compromised because of strong binding of Na^+ to the filter support and dependency of results on washing steps and used volumes of washing buffers.

(4) Determination of pKa values *in silico* by computational approaches based on 3D structure of c(K)-ring (**Table 6-2**, column 4) (Vollmar et al. 2009, Symersky, et al. 2012). Lack of computational models that account for all explicitly effects of local neighbourhood in the surrounding of ICG makes computation of pKa values still challenging.

The methodological problems mentioned above hamper choice of method for pKa estimation in c-rings and imply careful validation of obtained pKa values.

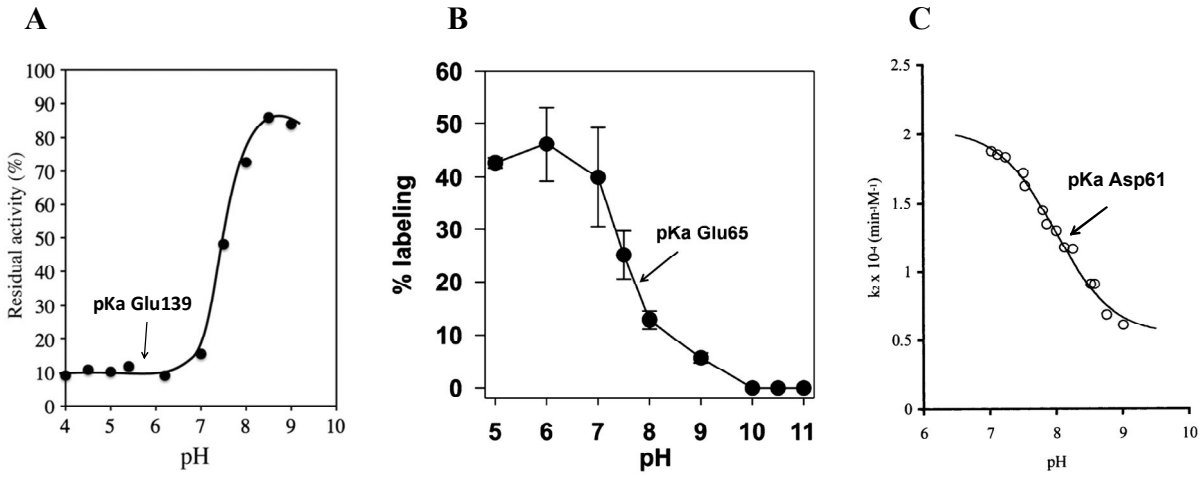

Figure 6-2: Examples of indirect assays used for estimation of pKa values for ionisable Glu/Asp residues in the c-rings/ATP synthases from different species. (**A**) The pH-dependent DCCD inhibition of Na^+ binding to purified Na^+-K-ring of *E. hirae* was used to estimated pKa = 5.5 for Glu139 carboxyl group (modified form (Mizutani, et al. 2011)). (**B**) The pH-dependent DCCD modification of Na^+-c-ring of *I. tartaricus* ATP synthase was used to estimated pKa = 7.5 for Glu65 carboxyl group (from (von Ballmoos and Dimroth 2007)). (**C**) The pH-dependent DCCD inhibition of *E. coli* ATPase activity was used to estimate pKa = 8.0 for Asp61 carboxyl group (modified from (Valiyaveetil, et al. 2002)).

The published estimates of the pKa of Glu/Asp in the c(K)-rings are presented in **Table 6-1**. The listed pKa values for Glu/Asp in the c-rings range from 5.5 (Glu139 in *E. hirae* K-ring) to 8.0 (Glu54 in *B. pseudofirmus* OF4 c-ring) (**Table 6-2**). The majority of determined pKa values for Glu/Asp residues in the rotor rings lie in alkaline pH region. This observation on different pKa values of Glu/Asp residues in c(K)-rings can be related to the Born, Coulombic and hydrogen bonding effects as it was described in section 6.1 and proposed by (Harris and Turner 2002). Only for Glu139 in the Na^+ binding K-ring of *E. hirae* the pKa was estimated to be in acidic range (pKa ~ 5.5) (Murata, et al. 2008, Mizutani, et al. 2011, Ueno et al. 2014).

Table 6-2: Estimates of pKa values of ionisable Glu/Asp residues in the c-rings/c-subunits/ATP synthases of different species in respect to their ion-binding selectivity

Organism	Ion selectivity	pKa	Technique
Glu139 ***E. hirae* K-ring**	$H^+/Na^+/Li^+$	5.5 (K_{10}-ring) ~ 5.5 (K_{10}-ring)	Radioactive assay of competitive $^{22}Na^+/H^+$ binding/release (Murata, et al. 2008); Kinetic of DCCD inhibition of Na^+ binding to K-ring at different pH in 0.05% DDM (Mizutani, et al. 2011)
Glu65 ***P. modestum* c-ring**	$H^+/Na^+/Li^+$	~ 7.0 (c_{11}-ring in ATPase)	pH-dependent kinetic of DCCD inhibition of ATP hydrolysis by ATP synthase in 0.05-0.1% Triton X-100 (Kluge and Dimroth 1993)
Glu65 ***I. tartaricus* c-ring**	$H^+/Na^+/Li^+$	6.7 (c_{11}-ring) 7.5 (c_{11}-ring)	MALDI-MS with c/m extracted and HPLC purified c-subunits after pH-dependent DCCD modification of c-ring in 1% OG (Meier, et al. 2003); MALDI-MS with c/m extracted c-subunits after pH-dependent DCCD modification of c-ring in ATP synthase (von Ballmoos and Dimroth 2007);
Asp61 ***E. coli* c-ring**	H^+	7.1(c_1) 8.0 (c_{10}-ring in ATPase)	Solution NMR with c-subunits (Assadi-Porter and Fillingame 1995); pH-dependent DCCD inhibition of ATP hydrolysis activity of ATP synthase in 0.5% Na-cholate/0.5% Na-deoxycholate (Valiyaveetil, et al. 2002)
Glu59 **Yeast chloroplast,** ***S. cerevisiae* c-ring**	H^+	$\leq$ 7.1 (c_{10}-ring)	Estimation based on available three 3D X-Ray structures of c-ring obtained at pH 5.5, 6.1 and 8.3-(Symersky, et al. 2012)
Glu61 **Spinach chloroplast,** ***S. oleracea* c-ring**	H^+	7.3 (c_{14}-ring)	3D X-Ray structure-based computing (Vollmar, et al. 2009)
Glu54 ***B. pseudofirmus* OF4 c-ring**	H^+	7.7 (c_1) ~ 8.0 (c_{13}-ring)	Solution NMR with c-subunits (Rivera-Torres et al. 2004); pH-dependent DCCD modification in 0.05% DDM (Preiss, et al. 2014)
Glu62 ***S. platensis* c-ring**	H^+	$\geq$ 9.3 (c_{15}-ring)	pH-dependent DCCD modification in 0.05% DDM (current study)

The differences in between used techniques, and in between sample conditions and in between sample preparation methods (**Table 6-2**, column 4) make obtained pKa values difficult to compare. For instance, NMR technique was used to determine pKa = 7.1 of Asp61 for *E. coli* c-subunit in $CHCl_3$:CH_3OH:H_2O (4:4:1) mixture (Assadi-Porter and Fillingame 1995), meanwhile DCCD inhibition of *E. coli* ATPase activity gave the pKa value of 8.0 for Asp61 (Valiyaveetil, et al. 2002) (**Table 6-1**, **Figure 6-2 C**). Observed 1 pH-unit discrepancy in pKa estimation can lead to prediction of the wrong protonation state of Glu/Asp and results in errors in the binding free energy for H^+ on the order of 1-3 kcal/mol (Liptak et al. 2002, Jensen 2015). Therefore, in order to figure out the functional implication of different pKa values of Glu/Asp in c-ring of ATP synthases/ases, the same reliable pKa estimation approach (equilibrium, precise, quantitative and reproducible) has to be employed for c(K)-rings prepared using the same sample preparation protocol. In the current thesis, the same pKa estimation approach was used as well as the same sample preparation protocol for *I. tartaricus* c-ring and set of its ion binding site mutants was employedin order to justify which factors determine pKa of Glu65 carboxyl group and its functional implication.

6.1.2. High pKa of Glu65 carboxyl group in *I. tartaricus* wild-type c-ring

The *I. tartaricus* c-subunit has only one membrane-embedded charged residue, namely, Glu65, which plays a central role in H^+ and Na^+ binding and translocation by ATP synthase (Meier, et al. 2005, Meier, et al. 2009). In the current study, the two indirect approaches were employed to evaluate the apparent pKa value of Glu65 carboxyl group in the ion-binding site of *I. tartaricus* c-ring.By the first approach, the pKa of Glu65 carboxyl group in *I. tartaricus* wild-type c-ring was determined by evaluating the protonation state-dependent DCCD modification of Glu65 carboxyl group(sections 5.3.6 and 6.1.1**).** It was measured that Glu65 carboxyl group has pKa of ~ 7.8 in the wild-type c-ring of *I. tartaricus* ATP synthase. In the second approach, the pKa value obtained by DCCD modification method was justified by an ITC method based on Na^+-induced deprotonation of Glu65 carboxyl group in detergent-solubilized preparation of *I. tartaricus* wild-type c-ring (section 5.3.1.6). The essential correlation between determined pKa value (7.8, corresponds to 50% protonation) and the protonation state value of Glu65 carboxyl

group in *I. tartaricus* c-ring determined at pH 7.5 and pH 9.0 was found. Namely, at pH = 7.5 (pH < pKa) 62.6% of carboxylic groups (7 out of 11) in the c-ring were protonated and at pH = 9.0 (pH >> pKa) the carboxylic groups of Glu65 in the c-ring were fully deprotonated. The consistent results obtained by both approaches indicate relevant applicability of two above-mentioned methods when measurements are performed with equivalent samples in similar conditions.The obtained pKa value of 7.8 is comparable with the range of already published values for pKa of Glu65 in *I. tartaricus* c-ring (6.5 and 7.5) (Meier, et al. 2003, von Ballmoos and Dimroth 2007) (**Table 6-1**). The variables in obtained values indicate that pKa of Glu65 carboxyl group is very sensitive to variations in sample environment used for the measurements (detergents, salt concentration).

Surprisingly, the range of the indicated pKa values (7.5-7.8) for Glu65 carboxyl group in *I. tartaricus* c-ring is in odd with the acidic pKa value (5.5) obtained for Glu139 in the $Na^+/Li^+/H^+$ binding site of *E. hirae* K-ring (**Table 6-1**) in the comparable detergent (DDM) and salt conditions. The pKa of 5.5 for Glu139 in *E. hirae* K-ring predicts deprotonated, negatively charged state of the side chain at pH 7.0. The pKa of 7.5-7.8 for Glu65 in *I. tartaricus* c-ring suggests that this side chain should be protonated and, therefore, neutral under physiological conditions within the pH 6.0-7.0 range. It is not obvious from the structure of *E. hirae* and *I. tartaricus* c(K)-rings which effects and elements of the protein environment lead to such different pKa. The question arises, why two physiologically Na^+-selective c(K)-rings can have large difference in pKa of ionisable Glu residues? This difference can be related to physiological role of *E. hirae* V-ATPase, which is an exclusive ATP-driven Na^+ pump in *E. hirae* cells (Ikegami et al. 1999, Ueno, et al. 2014). The pKa value of 5.5 for Glu139 results in constantly deprotonated carboxylic groups at physiological pH and can help V-ATPase to pump Na^+ from cytosol more efficiently as it was first proposed by (Murata, et al. 2001).

In contrast to *E. hirae,* it was shown in this work that purified *I. tartaricus* ATP synthase is capable to catalyze both, ATP hydrolysis and ATP synthesis using one of the applied ion-motive forces (*smf*, *pmf* or *lmf*) (section 5.4.1). However, the ATP synthesis driven by *pmf* can be detected *in vitro* only under low Na^+ concentration and large pH gradient (sections 5.4.1.3 and 5.4.6). The relatively high pKa values of Glu65 in *I. tartaricus* wild-type c-ring is not surprising: Many of the internal Glu and Asp ICG that act as H^+ donor groups in proteins that function

optimally at neutral pH have near neutral pKa values (Coutinho and Henrissat 1999, Nielsen and McCammon 2003, Isom et al. 2008). However, it is not clear whether *I. tartaricus* cells need to rely on H^+ binding and transport properties of *I. tartaricus* ATP synthase cells under particular conditions. The explanation and better understanding of problem of the pKa in the c-rings of ATP synthease/ases require additional experimental and computational work. Therefore, in the current thesis, the panel of *I. tartaricus* c-ring mutants was used to study the effects that determine the pKa of Glu in c-rings. The Na^+/H^+ selective ATP synthase of *I. tartaricus* was used as a model system to assign a role of Glu65 pKa for *pmf*-driven ATP synthesis under particular conditions.

6.1.3. Functional implication of high pKa values of the Glu/Asp in *I. tartaricus* mutant ATP synthases

As H^+-selectivity of rotary ATP synthases results from protonation/deprotonation of ionisable Asp/Glu residues in their c-rings, it seems reasonable that pKa values of ionisable Glu/Asp residues in the ion-binding sites of the c-rings should be tuned with respect to their ion-binding selectivity. The reported pKa values of many of the carboxylates responsible for H^+ translocation by secondary-active transporters and primary H^+ pumps are unusually high (Rastogi and Girvin 1999, Yerushalmi and Schuldiner 2000, Checover et al. 2001, Kaback, et al. 2001, Abramson, et al. 2003, Periole, et al. 2004). Indeed, as it was already mentioned before in section 6.2, the high pKas of Glu/Asp were estimated also for the only H^+-selective c-rings. Traditionally, the caveat of c-subunit Glu/Asp pKa determination was that these values were measured in the monomeric, isolated form of the c-subunit, without a neighbouring network of amino acid residues ("*microenvironment*") and the measurements were done in chloroform/methanol. Nevertheless, the pKa = 8.0 was determined for Glu54 in *B. pseudofirmus* OF4 H^+ binding c-ring and pKa = 8.0 was determined for Asp61 in *E. coli* H^+ binding c-ring. It was previously suggested that such a high pKa of ionisable Glu/Asp residues is needed for better H^+ acquisition/retention during rotation of the c-ring (Liu et al. 2009). In the current work, the aim was to check functional implication of high pKa values of the Glu/Asp carboxyl group in rotor c-ring of ATP synthase. To do so, the complex biochemical and functional analysis of *I. tartaricus* c-ring and ATP

synthase mutants was done.

The data obtained in this work show that the pKa value of Glu65 carboxyl group in *I. tartaricus* wild-type c-ring (pKa = 7.8) is up-shifted by 0.5-1.5 units in the mutant c-rings with Q32A, S66A/Y70F and Q32A/Y70F polar-to-hydrophobic substitutions (section 5.3.6). This is equivalent to the 0.65-1.96 kcal/mol tighter H^+ binding to Glu65 in Q32A, S66A/Y70F and Q32A/Y70F mutants of *I. tartaricus* c-rings (section 5.3.6) (**Figure 6-3**). ATP synthases with the same Q32A, S66A/Y70F and Q32A/Y70F polar-to-hydrophobic mutations in the c-ring showed 1.5-6.5 higher turnover rates of *pmf*-driven ATP synthesis, respectively (section 5.4.12) (**Figure 6-3**). Moreover, Q32A, S66A/Y70F and Q32A/Y70F mutant ATP synthases had lower or no Na^+ inhibition of the *pmf*-driven ATP synthesis, pointing to changes in Na^+*versus* H^+ binding affinity of corresponding c-rings (section 5.4.5).

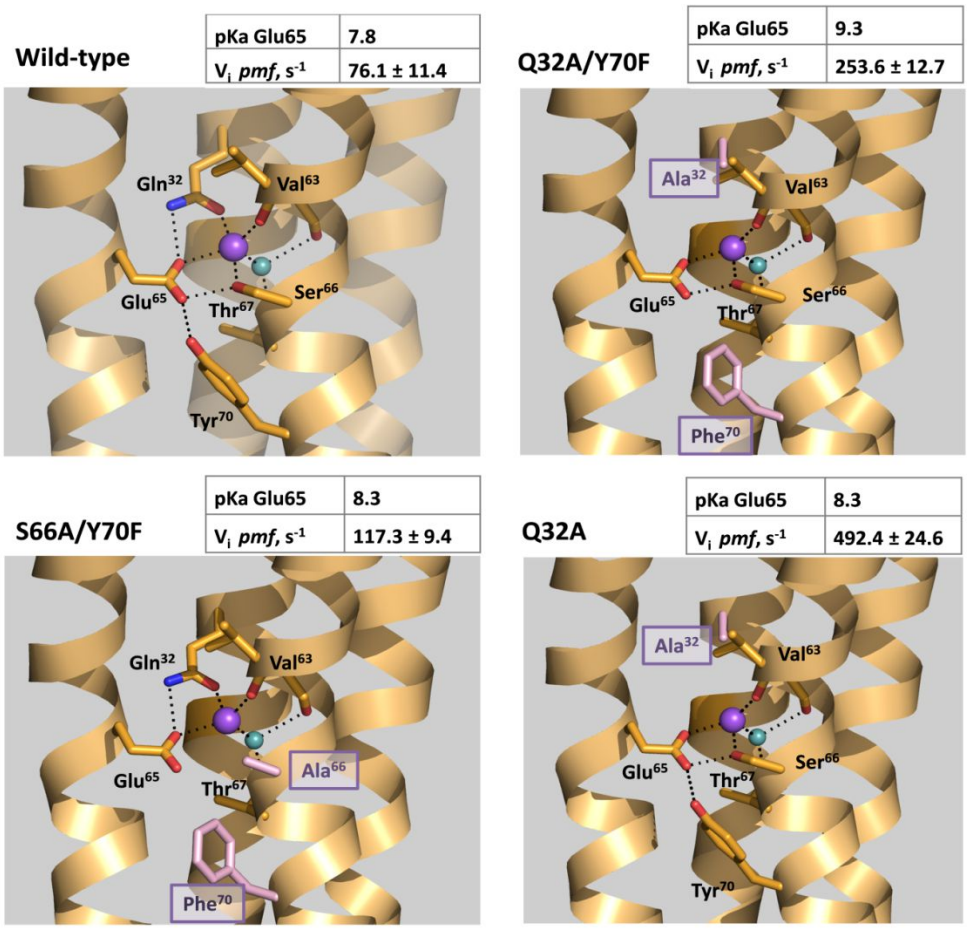

Figure 6-3: pKa of Glu65 carboxyl group in *I. tartaricus* wild-type and mutant c-rings and its effect on rates of *pmf*-driven ATP synthesis. Three polar residues from ion binding site in *I. tartaricus* c-ring (Gln32, Ser66 and Tyr70) were replaced with hydrophobic residues (Ala32, Ala66 and Phe70). Using the crystal structure of the Na^+-bound c-ring of *I. tartaricus* (Meier et al., 2005, 2009), three-dimensional structural models of ion binding site in Q32A, S66A/Y70F and Q32A/Y70F mutant c-rings were generated using PyMOL (Na^+ ion in modelled mutant ion binding sites is shown as sphere in violet and water molecule is depicted by cyan sphere). Obtained Q32A, S66A/Y70F and Q32A/Y70F mutant c-rings demonstrated up-shifted pKas for Glu65 carboxyl group. Stronger H^+ binding due to mutationally increased hydrophobicity of *I. tartaricus* ion-binding site (Born effect) correlates with significantly higher V_i values of *pmf*-driven ATP synthesis of Q32A, S66A/Y70F and Q32A/Y70F mutant ATP synthases than those of wild-type. Stronger H^+ binding (expressed in pKa values of Glu65 in corresponding mutant c-rings) and higher turnover rates of *pmf*-driven ATP synthesis by Q32A, S66A/Y70F and Q32A/Y70F reflect improved efficiency of the *pmf*-driven ATP synthesis. The efficiency was estimated as a ratio between maximal velocity of *pmf*-driven ATP synthesis of corresponding ATP synthase (V_{max}) and H^+ binding affinity of the c-ring (pKa of Glu65).

Taken together, presented data state, that high pKa values of the Glu/Asp residues in the c-ring have functional implication by providing the physical basis for more efficient catalytic *pmf*-driven function of corresponding ATP synthases and thus is a good adaptation for H^+-selective ATP synthases.

6.1.4. Factors that determine high pKa and H^+ selectivity of Glu/Asp residue in the c-rings

It is known that the pKa values of ionisable residues in folded proteins can be strongly influenced by the local microenvironment through the Born, Coulombic and hydrogen bonding effects (McIntosh et al. 1996, Chivers, et al. 1997, Dwyer, et al. 2000, Harris and Turner 2002). Therefore, hydrophobic residues tend to raise the pKa of acidic residues in many enzymes by providing a non-polar environment (Gutteridge and Thornton 2005). In our work, exploring a panel of ion binding site mutants, we showed that the hydrophobicity (Born effect) plays the dominant role in establishing high pKa and accordingly high H^+-binding affinity of Glu/Asp carboxyl group in the rotary c-rings. Namely, Q32A, S66A/Y70F and Q32A/Y70F mutant c-rings demonstrate that hydrophobicity of the ion binding site contributes strongly to high pKa of target Glu65 carboxyl group.

Another question is whether hydrophobicity also contributes to higher H^+ selectivity of c-rings. In computational work by Krah et al. (Krah, et al. 2010) the H^+ selectivity of *I. tartaricus* c-ring was estimated to be ~2-3 kcal/mol in wild-type c-ring and enlarged in mutant c-rings with higher hydrophobicity of residues forming ion-binding site. For comparison, the only H^+-binding c-ring of *S. platensis* was estimated to have $\geq$ 13 kcal/mol H^+-selectivitiy and 10-100 orders of magnitude higher H^+ binding affinity with respect to *I. tartaricus* wild-type c-ring. In our experimental work, Q32A/Y70F mutant of *I. tartaricus* c-ring with two polar-to-hydrophobic substitution that enlarged hydrophobicity of the ion binding site was characterized by a much higher affinity for H^+ and no affinity for Na^+ (sections 5.2.4, 5.3.2 and 5.4.5). Other two mutants, Q32A and S66A/Y70F were characterized by higher affinity for H^+ and much lower affinity for Na^+. Therefore, we can conclude that hydrophobicity (Born effect) is one of the factors that enlarge not only H^+ binding affinity but also H^+ selectivity of the rotor c-rings. The example of Q32A/Y70F mutant of *I. tartaricus* ATP synthase supports hypothesis that the transition between

the Na^+/H^+- and H^+-selective ATP synthases can be achieved by gains and losses of the hydrophobic residues, which are involved in ion binding and which modulate the pKa of ionisable Glu/Asp residues without loss of intact ATP synthase *pmf*-driven functionality.

6.2. Principles that underlie high Na^+ binding affinity and selectivity of the proteins

The binding of two molecules can be viewed as a reversible and rapid process in an equilibrium (Kastritis and Bonvin 2013). Ligand-protein binding association has two important defining characteristics:
(i) ***Selectivity***, which distinguishes the highly specific binding partner from less specific binding partners (selectivity refers to differences in absolute binding affinity between ligands);
(ii) ***Affinity***, which describes the probability of finding a ligand molecule bound to the receptor for a given ligand (Jones, et al. 1998, Demchenko 2001).

In the current study, the binding affinity was considered as the strength of the interaction between molecules that bind reversibly (interact). The binding affinity was translated into physico-chemical terms in the dissociation constant (K_d), which is the concentration of the free ligand that occupies half of the overall sites of the protein at equilibrium (Kastritis and Bonvin 2013). High affinity interaction is characterized by a low K_d values.
A variety of physical phenomena is thought to contribute to the binding affinity of an interaction established by a ligand to a protein (Olsson et al. 2008) and therefore, in particularly, Na^+ association with c-ring can be analyzed on the basis of the different forces involved in the process of Na^+-c-ring complex formation process. The examples of the LeuT secondary active transporter, the GluR5 kainate receptor and numerous Na^+ channels point to some general principles that underlie cation selectivity in proteins (Dudev and Lim 2014). It is assumed that the protein selectivity to bind and transport a particular cation is achieved by combination of certain structural and physicochemical principles. The main determinants of preferential Na^+ selectivity in proteins are the following:

1. Architecture of the protein that provides cavities or selectivity filters for cations;
2. Size, rigidity and geometry of the ion-binding site (Yu et al. 2010, Thomas et al. 2013,

Dudev and Lim 2014);

3. Atomic composition of the ion-binding site (e.g., number of coordinating ligands and their chemical and physical properties) (Berneche and Roux 2001, Noskov et al. 2004, Noskov and Roux 2006, Bostick and Brooks 2007, Thomas et al. 2007, Varma and Rempe 2007, Dixit et al. 2009). This also include strong charge donating ability of the protein such as Asp/Glu carboxylate or backbone carbonyl groups in the binding site or negatively charged/polar groups placed along the ion path in order to compensate the positive charge of cation (Yu, et al. 2010);
4. Kinetics of ion-protein binding (K_{on} and K_{off} parameters). Molecular determinants of binding kinetics are binding site accessibility, conformational fluctuations, electrostatics and hydrophobicity (Pan et al. 2013);
5. Thermodynamic factors (e.g., more favorable energetic compensation of dehydration upon ion binding to the ion binding site and the free energy landscapes of ion entrance and translocation; solvent exposure of the binding site) (Yu, et al. 2010).

Na^+ selective proteins very often are characterized by presence of conserved Na^+ binding motifs in their sequences. Conserved Na^+-binding motifs are highly distributed among different protein families and reflect highly tuned binding selectivity toward Na^+. For instance, three residues (Asn-Asp-Gln) form NDQ motif that are thought to be characteristic of Na^+-pumping rhodopsins, NaRs (Inoue, et al. 2013, Inoue et al. 2015, Kato et al. 2015). Another Na^+-binding motif (SNT motif) is formed by Ser-Asn-Thr residues that make up the cation binding site among SLC13 family members of which perform electrogenic Na^+-coupled sulphate/carboxylate transport (Mancusso et al. 2012, Schlessinger et al. 2014). The ion binding selectivity of *I. tartaricus* ATP synthase is encoded by Na^+-binding motif that is conserved among Na^+-motive ATP synthases. At least three residues (Gln/Glu-Glu/Asp-Ser/Thr) in the c-ring compose this conserved Na^+-binding motif (Meier, et al. 2009).

In this study, the focused was set on a few factors that contribute to the Na^+ selectivity and binding affinity of rotary ATP synthases and may be characteristic for other Na^+-selective proteins. The characterization was done for the intact ion binding site of *I. tartaricus* ATP synthase that represents Na^+ binding motif conserved across Na^+-c-rings and (i) explored

influence of microenvironment of different polarity on binding of Na^+ to c-ring, (ii) assigned the role of atomic composition with particular thermodynamic mechanism of interaction, (iii) match in cavity size and (iv) presence of ionisable Glu65 for attaining high Na^+ binding affinity by *I. tartaricus* c-ring.

6.2.1. Determined Na^+ binding affinity and selectivity of *I. tartaricus* wild-type c-ring

In our study we evaluated that in the case *I. tartaricus* wild-type c-ring is solubilized in 0.02-0.15% DDM the K_d (Na^+) = 7.9 μM at [H^+] = 0 (section 5.3.1.3). We showed that Na^+ binds to c-ring with equivalent affinity only at conditions of low H^+ concentration ([H^+] = 0.001 μM) and full deprotonation of Glu65, when no cation competition for binding is observed (section 5.3.1.3). Comparing the data obtained in DDM, the *I. tartaricus* wild-type c-ring possesses close to, or slightly higher, binding affinity for Na^+ in comparison to the *E. hirae* Na^+-K-ring (**Table 6-2,** graph 1). However, in terms of total ion selectivity (calculated as K_d (Na^+)/K_d (H^+)), *I. tartaricus* wild-type c-ring possesses a much lower selectivity towards Na^+ in comparison to *E. hirae* (**Table 6-2,** graph 3). The reason for this discrepancy we see in higher intact H^+ binding affinity of *I. tartaricus* c-ring. Both, evaluated K_d (H^+) values and pKa values for ionisable Glu residues support our statement (**Table 6-3**).

Table 6-3: Na^+ binding affinity and ion selectivity of the c-rings of different species

Organism	**K_d (Na^+), μM at [H^+] = 0**	**K_d (H^+), μM at [Na^+] = 0**	**pKa of Glu**	**K_d (Na^+)/K_d (H^+)**
I. tartaricus (this work)	7.9 ± 0.4	0.0124 ± 0.001	7.8	637
E. hirae	12 ±3*	3.5*	5.5**	3.5

* - (Murata, et al. 2008), ** - (Mizutani, et al. 2011)

As is was already discussed in section 6.1.2., much higher selectivity towards Na^+ in *E. hirae* K-

ring can be an evolutionary adaptation of *E. hirae* V-ATPase to its exclusive ATP-dependent Na^+ pumping activity that results in generation of Na^+ gradient across membrane. Meanwhile, *I. tartaricus* ATP synthase was shown to operate as efficient ATP synthase using imposed *smf* at pH 6-7 (sections 5.4.1.2 and 5.4.13).

6.2.2. Effect of microenvironment on Na^+ binding to *I. tartaricus* wild-type c-ring

The microenvironment is defined to be the local neighbourhood around the protein in which its structure and function exists. Detergents, lipids and small molecules (e.g., DMSO) of different nature create microenvironment of different polarity in which ligand/protein interaction occurs. In this work it is shown that affinity of Na^+-protein interaction differs in different microenvironments (lipidic, detergent micelles or organic solvent=strongly dipolar solvent) and may occur as a general phenomenon among membrane proteins. When *I. tartaricus* wild-type c-ring is solubilized in 1% OG detergent the K_d (Na^+) value at $[H^+] = 0$ is inconsistent with data obtained in DDM (Leone et al., 2015) (**Table 6-4**). We also show that *I. tartaricus* wild-type c-ring is not able to bind Li^+ in 1% OG (section 5.3.1.7).

Table 6-4: Na^+ and Li^+ binding to *I. tartaricus* wild-type c-ring in different microenvironments

Property	DDM-solubilized	OG-solubilized	DMSO-solubilized
K_d Na^+ at $[H^+] = 0$	7.9 μM	290 μM**	n/e
K_d H^+ at $[Na^+] = 0$	0.0124 μM	0.28 μM**	n/e
K_d (Na^+)/K_d (H^+)	637	1025**	n/e
H/S compensation	Yes	Yes	yes
Li^+ binding	Yes	n/d	yes
Coupling of enzyme	Yes	No	n/e

n/e – not evaluated, n/d – not detected

** - condition of $[H^+] = 0$ is theoretical (section 5.3.1.3)

** - (Leone, et al. 2015)

The present study exemplifies the influence of detergents on the ion binding affinity of membrane proteins, namely c-ring of *I. tartaricus* ATP synthase: The variations in microenvironment of the c-ring promoted enthalpy/entropy (H/S) compensation. Indeed, it was calorimetrically observed different interplay between entropy and enthalpy directed to attain close free energy change upon Na^+ binding in these different microenvironments (details in section 5.3.1.4). The suggestion is that the large difference between the enthalpies of Na^+ binding to OG-, DDM- and DMSO-solubilized *I. tartaricus* c-ring is ascribed to H/S compensation due to water (solvation) effects upon Na^+-c-ring interaction. In order to clarify the issue of plausible differences in solvation upon Na^+ binding in different microenvironments, additional biochemical experiments are required. In particularly, calorimetrically estimated heat capacity coefficients (ΔC_p) for Na^+ binding in DDM, OG and DMSO can answer the question on altered water effects for Na^+ binding to *I. tartaricus* c-ring.

H/S compensation is not unique phenomena and has been observed in many biological systems after relatively minor perturbations to the system. It was observed during protein-metal interactions (Kuroki et al. 1992, Blasie and Berg 2004), cAMP receptor protein variants and RNA polymerase binding (Krueger et al. 2003), peptides binding to the Src Homology 2 domain of the Src kinase (Davidson et al. 2002), carbohydrate binding to lectins (Lemieux et al. 1991, Schwarz et al. 1993) and antibodies (Herron et al. 1986, Sigurskjold and Bundle 1992, Brummell et al. 1993) as well as ligands binding to cyclodextrin variants (Rekharsky and Inoue 1998, Houk et al. 2003). However, H/S compensation was never detected so far for ligand binding to c-rings.

Origin of H/S compensation is still controversial. However, the structure and thermodynamic properties of solvent are considered to be important contributors to the H/S compensation phenomenon (Breiten et al. 2013, Portman et al. 2014, Ryde 2014, Du et al. 2016). In particularly, hydrogen-bonded water molecules in the active site of protein, hydrogen bonded water surrounding ligand in the solution and water molecules associated with a bound ligand molecule in a protein-ligand complex can be the sources of compensating changes in enthalpy and entropy (Breiten, et al. 2013, Portman, et al. 2014). The loss in enthalpy upon ligand binding to the binding site of a protein due to stripping off the surface-bound water plays a major role in energetics of ligand-protein binding in salt-water environment. Hence, a linear relationship in entropy-enthalpy compensation is attributed to the solvent displacement when binding

interactions occur in aqueous solution (Lemieux, et al. 1991, Brummell, et al. 1993, Gilson and Zhou 2007, Dam et al. 2008). This compensation comprises nearly equal and opposite changes in -TΔS and ΔH usually of 1−2 kcal/mol, resulting in only minimal differences in the overall ΔΔGwhen comparing the binding of different complexes (Sharp 2001).

Detergents were already shown to affect ligand binding affinity and ligand binding thermodynamics for membrane proteins (Amin et al. 2015). For instance, loss of entropy upon ligand binding can happen due to restricted conformational dynamic of protein if detergent interacts tightly with a protein. As a result, K_d value for ligand binding is increased (Amin, et al. 2015). Detergent micelles can also affect the ligand binding stoichiometry and activity of proteins (Quick et al. 2009). Even in detergent-free environment (e.g., for protein reconstituted in lipidic vesicles) the detergent that was used for solubilization of protein may play an essential role for its activity (Quick, et al. 2009).In particularly, for the case of wild-type LeuT transporter, the effect of DDM and OG detergents on ligand and Na^+ binding to protein was observed. Namely, 1.17% OG-solubilized Leu-T protein demonstrated two times reduced stoichiometry of ^{3}H-Leu binding in comparison to 0.05% DDM-solubilized LeuT-protein for which both, S1 and S2 substrate binding sites demonstrate high affinity substrate binding in presence of DDM. However, for the case the concentration of DDM was elevated to ≥ 0.175%, the molar binding stoichiometry of Leu substrate was also reduced. Inability of S2 site to bind Leu molecule in presence of OG remains unresolved. Effect of detergent on Na^+-dependent activity was even more drastic. In particularly, no Na^+-dependent ^{3}H-Ala transport was observed for wild-type Leu-T protein reconstituted in proteoliposomes after OG-solubilization of enzyme (Quick, et al. 2009).

In the other case, H^+, Na^+ or Li^+/galactosides symporter melibiose permease from *Salmonella typhimurium* ($MelB_{St}$) solubilized in lauryl maltose neopentyl glycol (MNG-3) showed 5.6-fold reduction in entropy of melibiose binding to MelBSt that results in 2.6 higher K_d value for melibiose binding in respect to other detergent, *n*-undecyl-*β*-D-maltoside (UDM) (**Figure 6-4**) (Amin, et al. 2015).

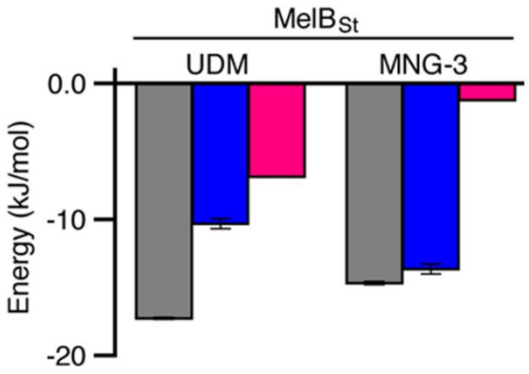

Figure 6-4: Effect of detergent on energetics of melibiose binding by $MelB_{St}$. MNG-3-solubilized MelBSt showed reduced conformational entropy and accordingly higher K_d values for melibiose binding in respect to UDM-solubilised MelBSt (from (Amin, et al. 2015)).

The finding here of a requirement for a particular microenvironment for a purified c-ring for association with Na^+ or Li^+underlines that entropy and enthalpy terms should not be compared on absolute scale but only relative to each other, when different microenvironments are used for cation binding measurements. Particular care should be taken for choosing the detergent and its concentration for solubilization of membrane proteins in order to retain their full and unaffected binding and transport activities.

6.2.3. Thermodynamic principles that underlie Na^+ binding affinity and selectivity of *I. tartaricus* wild-type and mutant c-rings

It was shown in this study that mutation of one or two residues in or near the ion binding site of *I. tartaricus* c-ring produced decreases in the apparent affinity for Na^+ (shown by K_d and K_M values for Na^+) or restricts Na^+ binding (sections 5.3.2 and 5.4.7). Indeed, 4 mutant c-rings (Q32A/Y70F, G25A, T67M and T67Q) lost its Na^+ binding, retained its native H^+-binding properties, and were present in assembled functional ATP synthases.

The polar and nonpolar chemical groups contribute differently to Na^+ binding affinity and cation selectivity through attained differences in thermodynamic signatures of Na^+ binding to c-ring. Thermodynamically speaking, the binding process involves two parameters, enthalpy and

entropy. In this work, the proportions to which enthalpy and entropy contribute to Na^+-c-ring binding in order to explore thermodynamic principles that underlie high Na^+ binding and transport affinity of rotary ATP synthases were looked at. The study indicates that a proportion to which the binding enthalpy and entropy contribute to Na^+ binding and their sign are important to attain high Na^+ binding affinity. There is a large number of potential enthalpic and entropic contributions to the binding affinity of ligand (Irudayam and Henchman 2009). Obtained ITC data point to the fact that distal effects (demonstrated by mutations of Gly25 residue), stabilizing effects (demonstrated by mutation of Tyr70 residue) and hydrogen bonding patterns with Na^+ and with water molecule (representative are mutations of Gln32, Ser66 and Thr67 residues) contribute sufficiently to Na^+ binding affinity of *I. tartaricus* c-ring (**Figure 6-5**).

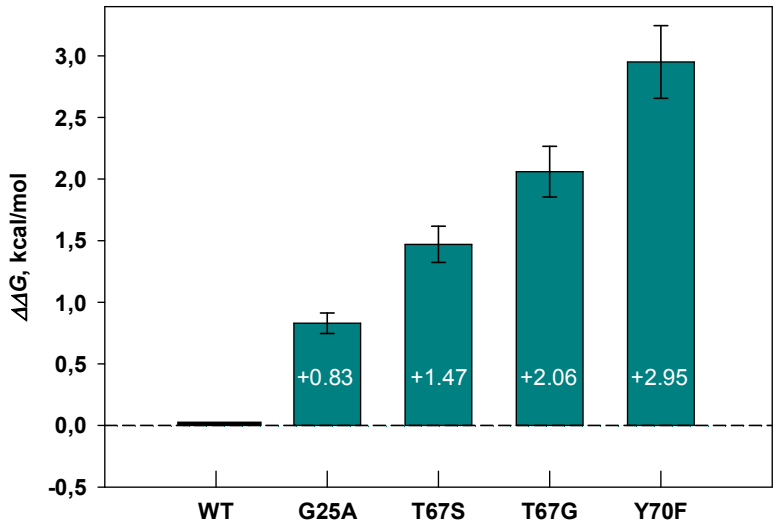

Figure 6-5: Differences in free energy change of Na^+ binding (ΔΔG) between *I. tartaricus* wild-type and mutant c-rings. Mutagenesis study on atomic composition of the ion-binding site in *I. tartaricus* c-ring showed that most of the intended mutations decrease free energy change of Na^+ binding to c-ring (details in section 5.3.2). Replacement of Gly25 to Ala renders distal (~5 Å proximity to the ion-binding site) effect on Na^+ binding, which amounts to 0.8 kcal/mol. Mutation of Tyr70 residue to Phe unfavors Na^+ binding by 2.95 kcal/mol, although Tyr70 is not involved directly in Na^+ coordination but indirectly by forming an important hydrogen bond with the Glu65 carboxylate. It plays a crucial role in stabilization of Glu65 residue in Na^+-bound state (Meier et al., 2009). Replacement of Thr67 to hydrophobic Ser and Gly unfavors Na^+ binding by 1.5-2 kcal/mol.

The analysis was performed for the *I. tartaricus* wild-type c-ring and T67S mutant c-ring with polar-to-polar substitution that provide enthalpy-driven Na^+ association with a c-ring. The enthalpy-driven binding is based on specific protein-ligand interactions that include directed van der Waals interactions, salt bridges, hydrogen bonding and electrostatic complementarity (Chang et al. 2007, Irudayam and Henchman 2009). Typically, the specificity between interacting molecules is achieved enthalpically through van der Waals and/or hydrogen bonding contacts (Chothia and Janin 1975). Strong enthalpic interactions (e.g., strong hydrogen bonds established by polar groups) are characterized with stringent distance and angle constraints that significantly contribute to the binding enthalpy (Kawasaki and Freire 2011) and can improve selectivity even if they do not contribute to an improvement in binding affinity (Kawasaki and Freire 2011). Experimentally, the best way to identify strong hydrogen bonds is by directly measuring the binding enthalpy by ITC. The experimental approach is much faster and more accurate than any available structure-based computational algorithm (Wiseman, et al. 1989, Holdgate 2001, Ladbury 2001). The best location for the hydrogen bond donor in binding site of protein is immediately detected by a more favorable enthalpy. The drop in binding enthalpy will confirms that the best functionality at that location is a hydrogen bond donor (Ruben, et al. 2006, Freire 2008). For instance, for the case of T67S mutation, there were no large changes in enthalpy and overall thermodynamic signature of Na^+ binding to c-ring in respect to wild-type (section 5.3.4).
In case of both, wild-type and T67S c-rings, Na^+-c-ring interaction has a small entropic penalty in energy binding landscape (< 15% of total free energy change upon Na^+-c-ring binding). In general, high nano- and picomolar binding affinity of the ligand requires favorable both, enthalpic and entropic contributions (Kawasaki and Freire 2011). There are few examples of ligands that bind with nanomolar affinity to subunits of rotary ATPases/ATPsynthases. For instance, macrolide antibiotic bafilomycin binds to V-ATPases with 0.1-5 nM binding affinity (Bowman et al. 1988, Drose and Altendorf 1997). Another example is the catalytic β subunit in F_1 subcomplex of *E. coli* ATP synthase that has high-affinity (nanomolar) site for MgADP (Weber et al. 1993, Mao and Weber 2007). We assume that the detected small entropy penalty prevents Na^+ binding from being more tight [K_d (Na^+) << 7.9 μM]. The observed small entropic penalty in strong enthalpic interaction could be attributed to low residual mobility of Na^+ in the bound state (Ladbury, et al. 2010, Klebe 2015). Another high affinity Na^+-selective c-rings (e.g.,

K-ring of *E. hirae*) lacks the full thermodynamic description of their Na^+-bound states. Therefore, it is not clear whether a similar energetic contribution underlie high-affinity Na^+- K-ring interaction.

It was estimated that the stabilizing contribution of Tyr70 in terms of free energy change of Na^+ binding to wild-type c-ring is roughly ~ 3 kcal/mol (section 5.3.2). The thermodynamic settings of Na^+ interaction with Y70F c-ring (polar-to-hydrophobic substitution) have consistent mechanistic perturbation if compare with wild-type c-ring (**Figure 6-6**). The changes in thermodynamic settings of Na^+ binding that we observed for Y70F mutation impairs to a large extent the original *smf*-driven ATP synthesis activity of *I. tartaricus* wild-type ATP synthase (section 5.4.12, **Figure 6-6B**). The turnover number of *smf*-driven ATP synthase activity for the purified *I. tartaricus* wild-type ATP synthase (463.8 ± 32.5 s^{-1}), determined at $\Delta\Psi$ = 36 mV and ΔpNa = -118 mV, was relatively high compared with previously published values, however, reflects physiological conditions with high ATP synthesis rates (>70–200 ATP/s) (Burzik et al. 2003, von Ballmoos, et al. 2009). This data mean that to achieve a desired biological effect, the c-ring binding site requires cations with particular mode of action and thus requires distinct thermodynamic binding profile.

The binding and transport affinity for H^+(studied here as a resulting *pmf*-driven activity) remains unaffected for Y70F mutant c-ring (shown by functional studies in sections 5.4.5 and 5.4.12). The Y70F mutation does not change the original deprotonation energy for Glu65 carboxylate, meaning Tyr70 residue is more crucial for proper Na^+ but not H^+ binding and translocation. This conclusion is consistent with functional studies with Y70F ATP synthase: Y70F ATP synthase is operational and demonstrates high turnover rates of ATP synthesis when driven by *pmf* (**Figure 6-6B**).

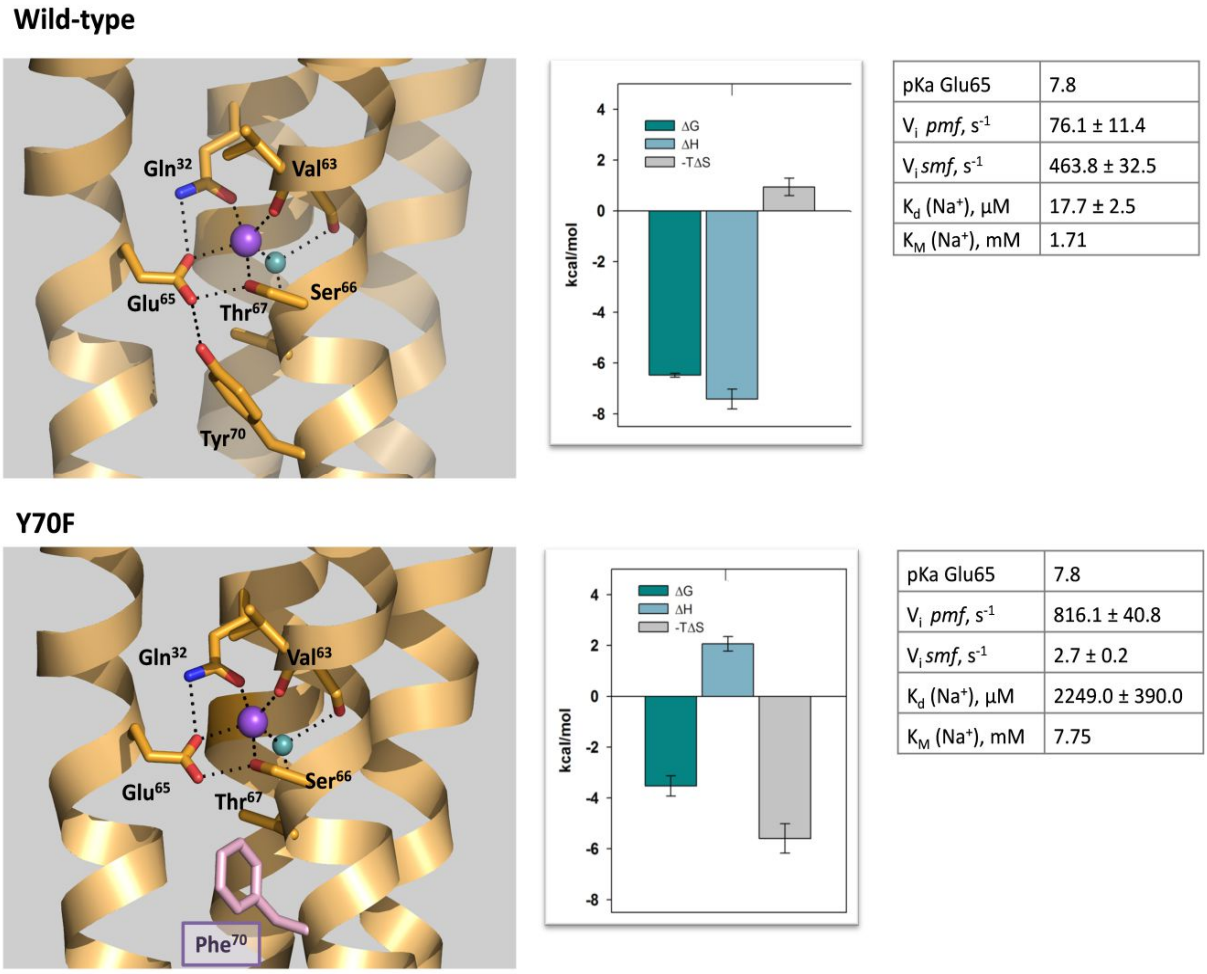

pKa Glu65	7.8
V_i *pmf*, s^{-1}	76.1 ± 11.4
V_i *smf*, s^{-1}	463.8 ± 32.5
K_d (Na^+), μM	17.7 ± 2.5
K_M (Na^+), mM	1.71

pKa Glu65	7.8
V_i *pmf*, s^{-1}	816.1 ± 40.8
V_i *smf*, s^{-1}	2.7 ± 0.2
K_d (Na^+), μM	2249.0 ± 390.0
K_M (Na^+), mM	7.75

Figure 6-6: Effect of Y70F (polar-to-hydrophobic) mutation. Shown is a contrasting Na^+ binding thermodynamics for the wild-type and Y70F mutant c-rings with respect to the known structure of wild-type ion binding site and modelled structure of ion binding site in Y70F mutant (Na^+ ion is shown as sphere in yellow and water molecule is depicted by red sphere). Upon Y70F mutation, the low-affinity entropy-driven Na^+ binding is observed. Obvious differences have been reported in the enzyme properties of Y70F versus wild-type ATP synthase. The Y70F mutation has clear impairing effect on *smf*-driven ATP synthesis, although the rate of *pmf*-driven ATP synthesis is not reduced. The determined K_d values of Na^+ binding to c-rings and K_M values of Na^+ binding to ATP synthases show decrease in Na^+ binding affinity of Y70F mutant.

Interestingly, Tyr70 residue is not always assigned as a part of conserved Na^+ binding motif. Combination of Glu/Asp-Glu-Ser/Thr or Glu/Asp-Glu-Ser/Thr-Tyr residues are assigned as

Na^+binding motifs in c-rings, especially when rotor c(K)-rings from F- and V/A-type ATP synthases are compared (Meier, et al. 2005, Ferguson et al. 2006, Pisa, et al. 2007, Dibrova, et al. 2010). Nevertheless, the tyrosine on the second α-helix of the c-ring is quite often present among both, H^+- and Na^+-selective ion-binding sites in c-rings (Pogoryelov, et al. 2009, Schulz, et al. 2013, Matthies, et al. 2014). In few cases, for instance, in archaeal genus *Methanosarcina*, tyrosine is substituted to phenylalanine in the ion-binding site of K-ring. In a good agreement presented in this work, these ion-binding sites are indicated to be H^+-selective or simultaneously selective to both, Na^+ and H^+ (Schlegel, et al. 2012, Schlegel and Muller 2013). Therefore, it is suggested that stabilization of Glu65 through Tyr70 in Na^+-bound state is important for formation of strong interaction to Na^+, as shown in (Meier, et al. 2005).

It was next showed that replacing the residues directly involved in Na^+ and water coordination to more hydrophobic one was evidenced primarily in the enthalpic cost to Na^+ binding (see section 5.3.4). A gain in entropy for Na^+ binding to G25A and T67G mutant c-rings was observed. The entropy-driven binding is based on nonspecific lipophilic (hydrophobic) interactions (Chang, et al. 2007, Irudayam and Henchman 2009) where the water-related effects are one of the main origins of the entropic driving force (Setny et al. 2010). When an enthalpic interaction such as a hydrogen bond or a salt bridge is lost, motional freedom of bound ligand should increase. As a result, a certain amount of entropy should be gained (Brummell, et al. 1993, Dam, et al. 2008). It can be expected that the entropic control of the Na^+ binding process in mutants indicates that hydrophobic interactions play a predominant role in establishing middle low millimolar range Na^+-binding affinity and/or one hydrogen bond was lost upon introduced mutation (**Figure 6-7**).

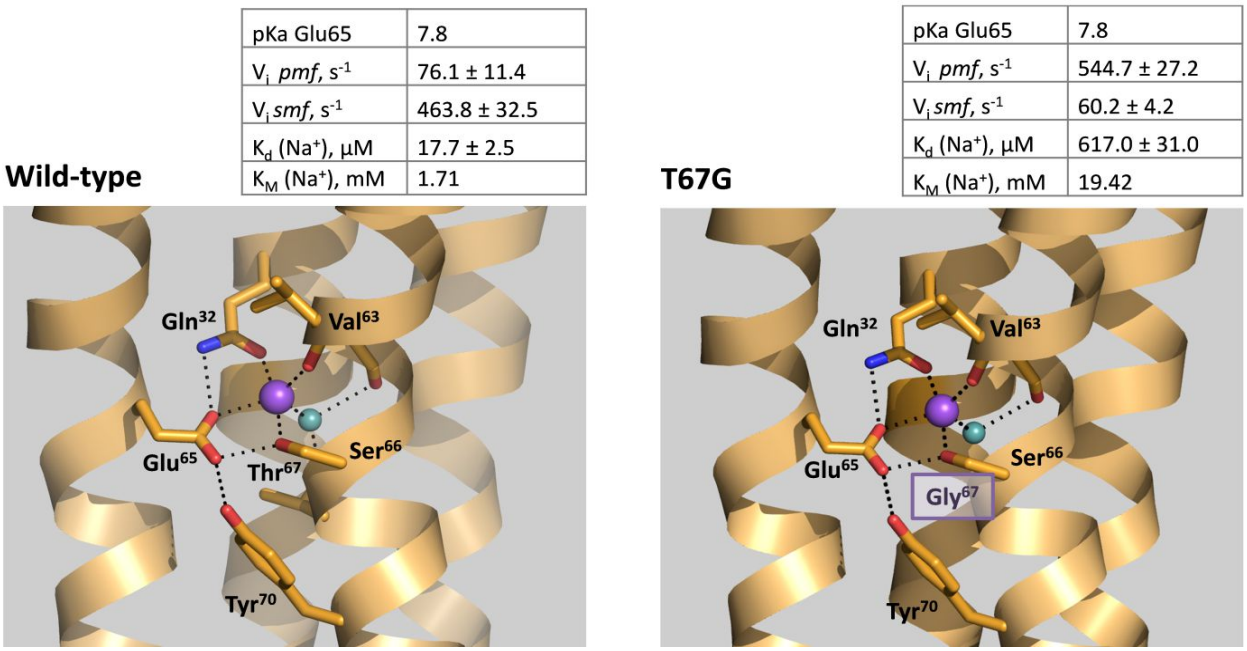

Figure 6-7: Effect of T67G (polar-to-hydrophobic) mutation. Shown is a structure of wild-type ion binding site in respect to homology model of ion binding site in T67G mutant c-ring. Thermodynamic changes in Na^+ binding by T67G mutant c-ring allow presuming loss of one hydrogen bond in Na^+ coordination sphere (Na^+ ion is shown as sphere in yellow and water molecule is depicted by red sphere). The K_d and K_M constants for Na^+ in mutant T67G versus *I. tartaricus* wild-type were compared. For the case of T67G mutant, large changes in both, K_d (Na^+) and K_M (Na^+) values were estimated. The detected decrease in Na^+ binding affinity correlated to lower turnover numbers for *smf*-driven ATP synthesis by T67G ATP synthase.

The observed mutagenic effects on Na^+-binding thermodynamics provide to the conclusion on different thermodynamic settings that underlie tight and loose Na^+-binding affinities. After analysing the thermodynamic aspects of Na^+ binding to *I. tartaricus* wild-type and mutant c-ringsthree types of interactions were manifested for the binding of Na^+ to c-ring depending on determined changes in partition (%) of enthalpy and entropy in binding free energy change of Na^+ binding (section 5.3.4):

(i) High-affinity, enthalpy-driven Na^+ interaction with a c-ring (low µM range);

(ii) Middle- affinity, entropy-driven Na^+ interaction with a c-ring (high µM range);

(iii)Low-affinity, only entropy-driven Na^+ interaction with a c-ring (mM range).

6.2.4. Match of the size of the ion-binding site

The cavity size of *I. tartaricus* c-ring binding pocket matches well to the ion size of Na^+ and Li^+, but not to larger K^+ or Cs^+ (see section 5.3.1.1). It was well known that Na^+-coupled ATP synthases usually also recognize Li^+ but with lower affinities. For instance, Na^+-translocating F-type ATP synthase from *P. modestum* transports Li^+ with a 10-fold lower affinity than Na^+ (Kaim, et al. 1997). Indeed, the rotor ring of *E. hirae* V-type ATPase (K-ring) binds Li^+ with only 5-fold lower affinity than Na^+ (Murata, et al. 2008).In the current study, it was demonstrated that *I. tartaricus* c-ring binds Li^+ with almost 30-times lower relative binding affinity under closely to physiological conditions (section 5.3.1.7).

The cavity size is thought to be one of the key factors involved for cation selectivity and is important particularly for distinguishing between cations (Harding 2001, Gouaux and Mackinnon 2005). With respect to the ion-binding site of *I. tartarcius* c-ring, the size restriction caused by mutations was not shown to be crucial and necessary for stronger selectivity toward H^+ (Krah, et al. 2010). However, restricting the size of the ion-binding site could be one of the factors limiting selectivity toward Na^+ (Krah, et al. 2010).

6.2.5. Importance of water molecule in the ion binding site of c-ring (T67M and T67Q mutations)

Molecular dynamic simulations on *I. tartaricus* wild-type c-ring predicts that water molecule that was found in the structure of *I. tartaricus* c-ring in the ion binding site plays an important role in the exit of Na^+ selectivity (Meier et al., 2009; Krah et al., 2010). The set of T67L, T67I, T67M and T67Q mutations were designed to distort hydrogen bonding network with water molecule in the ion-binding site of *I. tartaricus* c-ring (Krah, et al. 2010). The consequence of T67 mutations should be the absence of the bound structural water in the ion-binding site of *I. tartaricus* c-ring (Krah et al. 2010). In particular, molecular dynamic simulations showed that the S66A/T67L double mutant reproduces the configuration of H^+-bound state of *S. platensis* c-ring (Krah et al. 2010).

In the current experimental work, it was found out that introducing Leu and Iso instead of Thr67

in the ion-binding site of *I. tartaricus* c-ring has a large impact on stability of the c-ring: T67L, T67I replacements and their combination with other point mutations impair the ability of c-monomers to assemble in the c-ring (section 5.1.1). Thus, for the Thr67 mutations described here (T67L, T67I, T67A, T67G, T67S and T67M and T67Q mutations), their structural effect divides into those with an obvious negative effect on oligomer stability of the c-ring (e.g., T67L, T67I and T67A mutations), and those without or with little effect on oligomer stability of the c-ring (T67G, T67S, T67Q and T67M) (section 5.1.1).

T67M and T67Q mutant ATP synthases exhibited sufficient expression in *E. coli* cells to be studied in detail. In presented work, T67M and T67Q mutant ATP synthases were extracted and functionally characterized (section 5.4). The functional analysis of corresponding mutant ATP synthases showed that T67M and T67Q mutations restrict *smf*- and *lmf*-driven ATP synthesis by assembled *I. tartaricus* ATP synthase, although keeping the *pmf*-driven ATP synthesis activity intact. At the same time, the measured *pmf*-driven activity by T67M and T67Q ATP synthases was Na^+-insensitive and hence, the ion coupling was restricted only to H^+ (sections 5.4.4, 5.4.6 and 5.4.12) (**Table 6-5**).

Table 6-5: Effect of T67M and T67Q mutations on activity of *I. tartaricus* ATP synthase

ATP synthase	**DCCD inhibition of ATP hydrolysis**	**Na^+ sensitivity of *pmf*-driven ATP synthesis**	**V_i*pmf*, s^{-1}**
Wild-type	yes	Yes	76.1 ± 11.4
T67M	no	No	478.3 ± 23.9
T67Q	no	No	154.3 ± 7.7

The detected insensitivity of T67M and T67Q mutant ATP synthases to DCCD inhibition (5 min incubation at 100 μM DCCD was used) can be attributed to very low specific rate of Glu65 modification by DCCD due to very tight H^+ binding and thus, lower accessibility of Glu65 carboxyl group for modification. However, the high resolution structures of T67M and T67Q c-rings are required to answer the question on presence of water molecule in the ion binding site of these two exclusively H^+ coupled ATP synthases.

6.2.6. Importance of the negatively charged carboxylic group for Na^+ transport by rotary ATPases (E65D mutation)

To clarify the role of the ionisable Glu65 carboxyl group in Na^+ binding and ATP synthesis, wild-type c-ring/ATP synthase was compared with E65D mutant c-ring/ATP synthase in which the Glu65 was substituted by one carbon atom shorter aspartic acid. It was shon that mutation of Glu65 in *I. tartaricus* wild-type c-ring to Asp65 restricts *smf*-driven ATP synthesis, although keeping reduced Na^+-binding affinity by its c-ring (sections 5.4.5-5.4.7) (**Figure 6-8**). This result points to a role of Glu65 in the catalytic mechanism of c-ring in addition to direct binding of the H^+. The *smf*-driven ATP synthesis activity of the E65D mutant could not be rescued at any of applied driving forces, showing that the loss of activity caused by the substitution of the shorter side chain is due to specific stereochemical requirements of the carboxylate in the Na^+ transport process.

Parameter	Wild-type	E65D
Reactivity of Glu65	++++	++++
pKa of Glu65	7.8	7.8
Na^+ protection against DCCD modification	yes	yes
Coupling ion for ATP synthesis	$H^+/Na^+/Li^+$	H^+
V_i pmf, s^{-1}	76.1 ± 11.4	35.8 ± 5.4
V_i smf, s^{-1}	463.8 ± 32.5	no
K_M (Na^+), mM	1.71	5.08

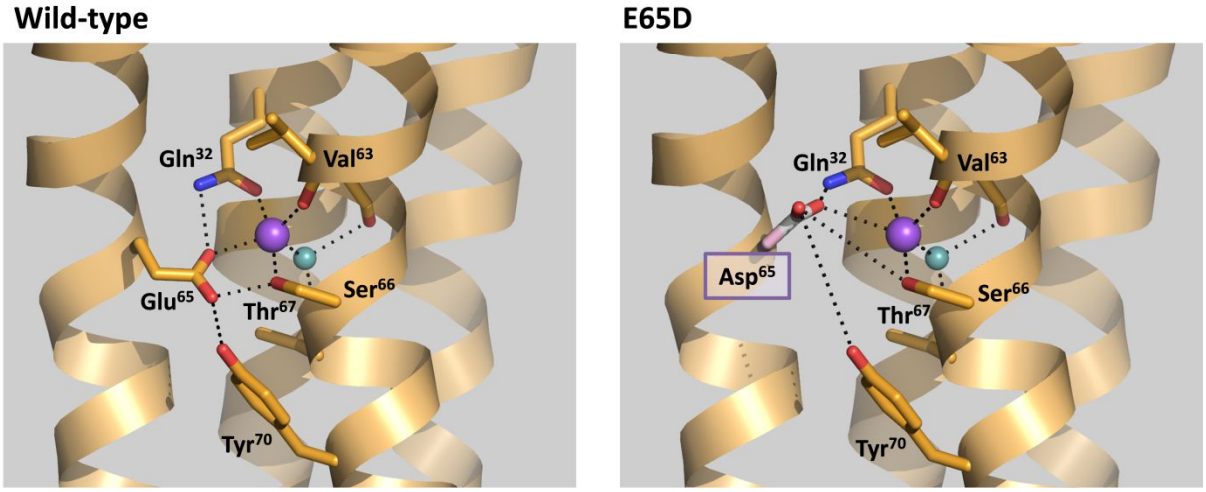

Figure 6-8: Effect of E65D (charge-to-charge) mutation: Biochemical analysis revealed that E65D mutation did not change the H^+ binding properties of carboxyl group in E65D mutant. Namely, the reactivity of Asp65 carboxyl group toward DCCD modification and its pKa did not change in comparison to wild-type c-ring. However, the Na^+ binding properties of E65D c-ring and functional operation of corresponding mutant ATP synthase differed from wild-type: ATP synthesis activity by E65D ATP synthase was not observed when *smf* and *lmf* was applied. Moreover, the evaluated K_M (Na^+) value of E65D ATP synthase was lower than one of wild-type.

On the other hand, experiments revealed that Glu→Asp substitution does not change the H^+-binding affinity expressed in terms of residue-specific pKa of carboxylic group in the ion-binding site of *I. tartaricus* c-ring. However, Glu→Asp mutation caused a reduction in the V_{max} of *pmf*-driven ATP synthesis by E65D ATP synthase (section 5.4.12) (**Table 6-5**). Reasons for this disparity between the binding and functional data can be due to observed instability of rotor

complex with E65D mutant c-ring (section 5.1.2). There is currently no structural explanation for the E65D mutant phenotype. It will be necessary to carry out a more detailed analysis of the functional effects of the Glu→Asp replacement.

To understand the functional implication of carboxylic group, the conserved Glu/Asp in c-ring subunits were mutated. In a good agreement with current data, it was experimentally shown that in general, the removal (=neutralization) of the conserved Glu/Asp from the ion-binding site is crucial for both, H^+ and Na^+ coupling of ATP synthases (Hoppe and Sebald 1980, Hoppe et al. 1982, Kawano-Kawada, et al. 2011, Kawano-Kawada, et al. 2012) and is believed to be related to its partitioning in the ion-translocation mechanism. For instance, mutations of Asp61 to Asn or Gly in the H^+ selective c-ring of *E. coli* ATP synthase abolish H^+ translocation and neutralization of Glu139 in H^+/Na^+ selective K-ring of *E. hirae* decreases the affinity for Na^+ and release the bound Na^+ ion (Hoppe et al. 1980, 1982). It is believed that Glu139 residue determines the binding affinity toward cation, and other residues that form the ion binding site are required to maintain a rigid conformation of the cation-binding site (Kawano-Kawada et al. 2011, 2012). Therefore, the conservation of the Glu139 residue of the *E. hirae* K-ring of V-ATPase is thus important for the physiology of organism in adapting to a saline environment (Kawano-Kawada et al. 2011).

Not only c-rings require ionisable Glu/Asp for Na^+ coordination and transport (**Figure 6-9**). From the available crystal structures deposited to Protein Data Bank (PDB) follows that Na^+ coordination usually requires five to six ligands and one of them usually include direct coordination from negatively charged Asp or Glu residues with an average Na^+ to ligand distance of 2.35 Å (Noskov and Roux 2008, Loo et al. 2013). There are few examples for the important role of evolutionary conserved negatively charged Glu/Asp in establishing high selectivity towards Na^+ ion for both, ion dependent transporters and channels. One of the convincing examples is the LeuT transporter. LeuT is a Na^+/leucine symporter from the neurotransmitter/sodium symporter (NSS) family (Yamashita et al. 2005) that has two binding sites for $Na^+$with different Na^+-binding affinity: Na1 and Na2 (Gouaux and Mackinnon 2005). In the Na1 binding site of the LeuT dehydrated Na^+ is coordinated directly by 6 oxygen atoms including one carboxylate from the bound leucine molecule. It is believed that thestrong electrostatic field provided by the negatively charged carboxylate of leucine ligand is used to

attain high inherent selectivity towards Na^+ in the site Na1 while the site Na2 with neutral ligands becomes Na^+-selective due to the local geometric force imposed by hydrogen-bond network (Gouaux and Mackinnon 2005, Yamashita, et al. 2005, Noskov and Roux 2008, Yu, et al. 2010).

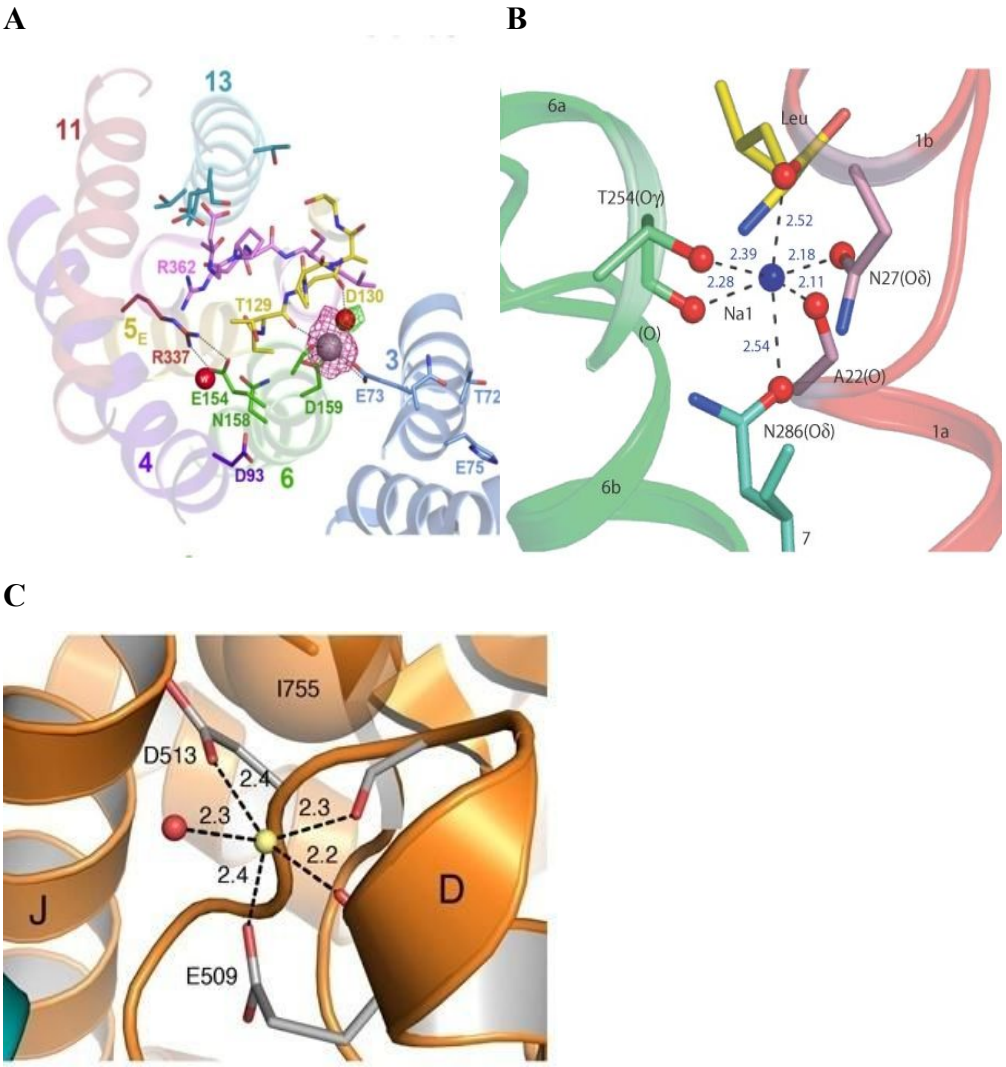

Figure 6-9: Na^+ coordination involving negative charge in different transporters. (**A**) 3.15 Å resolution structure of the substrate ion binding site of Na^+/H^+ antiporter PaNhaP from *Pyrococcus abyssii* (from (Wohlert et al. 2014)), where ion-binding site for Na^+ involves acidic side chains of Glu73 and Asp159. Crystals were soaked in thallium acetate and identified by anomalous scattering in order to get information on ion coordination in Na^+/H^+ antiporter. Ti^+ coordination that mimics Na^+ coordination directly involves Glu73 and Asp159 residues. (**B**) LeuT Na1 binding site with six coordinating ligands includes one carboxylate from leucine substrate (from (Yamashita, et al. 2005)). (**C**) 1.72 Å resolution structure of Na^+ binding site in GluR6 kainate receptor. Na^+ binding site in GluR6 kainate receptor is composed of 5 ligands including two side chain carboxylate groups of Asp513 and Glu59 (taken from (Plested et al. 2008).

Another example is GluK1-K3 kainate-sensitive ionotropic glutamate receptor (previously known as GluR5-R7kainate receptors): GluK1-K3 kainate receptors are the functional class of glutamate receptor ion channels (iGluRs) thatmodulate neurotransmitter release (Chittajallu et al. 1999) and mediate excitatory synaptic transmission in the brain of vertebrates (Madden 2002, Mayer and Armstrong 2004, Mayer 2006). GluK1 and GluK2 kainate receptors (previously known as GluR5 and GluR6 subtypes, respectively) contain a pair of cation binding sites capable of binding Na^+, which are involved in stabilization of protein dimer interface and play an essential role in receptor function (Plested, et al. 2008, Chaudhry et al. 2009, MacLean et al. 2011). In the cation-binding site, Na^+ is 5-fold coordinated and interacts directly with two side chain carboxylate groups of Asp513 and Glu590 in GluK1 kainate receptor (Plested et al. 2008) (**Figure 6-7C**). These two acidic residues in the GluK1 kainate receptor metal-binding site favors Na^+ binding over other cations (Vijayan et al. 2009). E493Q and D497A mutations of equivalent GluK2 receptor lead to desensitization and reduced ability to discriminate between cations (Plested et al. 2008).

The determinants of Na^+ selectivity in Na^+ channels also include strong electrostatic field provided by the negatively charged amino acids (Dudev and Lim 2014). For instance, negatively charged carboxylates of Asp/Glu in the DEKA selectivity filter of the eukaryotic voltage-gated Na^+ channels can significantly increase the Na^+/K^+ selectivity of the pore (Terlau et al. 1991, Heinemann et al. 1992, Yamashita, et al. 2005, Noskov and Roux 2008). The bacterial Na^+ channel NavAb from *Arcobacter butzleri* also has four ionisable glutamic side chains (EEEE motif) at the similar position (Payandeh et al. 2012). These carboxylates coordinates Na^+ in selectivity filter (Chakrabarti et al. 2013) and are the key determinants of ion selectivity in this channel (Heinemann, et al. 1992, Yang et al. 1993, Ellinor et al. 1995, Chen et al. 1996, Favre et al. 1996).

In current study, it is additionally emphasized the crucial role of the negatively charged Glu/Asp residue in the ion-binding motif of the c-ring in establishing high Na^+ binding and transport affinity of rotary ATP synthases. For E65D mutant, the affinity for H^+ was not, or only mildly, affected while the affinity for Na^+ was selectively reduced, with significant weakening of the activities of ATP hydrolysis and ATP synthesis, suggesting that the Glu65 plays an essential role in Na^+ binding and transport across membrane.

6.3. Comparison of K_d (Na^+) and K_M (Na^+) values obtained for *I. tartaricus* c-ring and ATP synthase

K_d value is a measure of ligand-protein affinity. High affinity interaction is characterized by a low K_d values. The K_M value represents the affinity of the enzyme for the substrate and is defined by the substrate concentration required to approach its half-maximum rate (1/2 V_{max}). Smaller values of K_M indicate that the enzyme and substrate are tightly bound. For simple enzymes and rapid equilibrium reaction K_M is similar to K_d. (Ellis et al., 1991; Engel 1981). However, K_M is not generally equal to the K_d. If the binding of one substrate to the enzyme affects the binding of the other substrate and cooperativity in enzyme activity is observed, then this relationship of K_d to K_M would not be expected to hold (Sanker et al. 2001).

The question raises, how in general the K_d (Na^+) value determined by ITC for the Na^+-c-ring interaction correlate with K_M (Na^+) value determined for Na^+-ATP synthase interaction from functional studies. For the case of Na^+-selective K-ring of *E. hirae*, it was evidently shown that K_d (Na^+) and K_M (Na^+) values corresponds to each other in DDM. Indeed, the K_d value of Na^+ binding to K-ring was 12 ± 3 μM and was similar to K_M value of Na^+ binding to purified whole ATPase complex [K_M (Na^+) = 15 ± 5 μM] (Murata, et al. 2000). In our study, we showed that at [H^+] ≤ 4 μM the K_d and K_M values of Na^+ binding to *I. tartaricus* c-ring and ATP synthase correspond to each other. K_d (Na^+) = 1616 ± 80.8 μM determined for the c-ring solubilized in DDM (section 5.3.1.2) corresponds to K_M (Na^+) = 1710 ± 85.5 μM determined for the ATP synthase solubilized in DDM and further reconstituted in lipid vesicles (section 5.4.7). This means that K_M (Na^+) value for *I. tartaricus* ATP synthase is only determined by its c-ring Na^+ binding affinity. However, detected impact of microenvironment on apparent values of enthalpy of Na^+ binding does not allow comparing K_M (Na^+) and K_d (Na^+)values obtained in different detergents (e.g., OG and DDM).

6.4. Summary and outlook

By applying a combination of biochemical and biophysical approaches, new insights into cation selectivity of rotary ATP synthases were gained. Presented data confirmed presence of competitive $H^+/Na^+/Li^+$ selectivity in the c-ring of *I. tartaricus*ATP synthase. The absolute binding affinity of the c-ring solubilized in DDM was estimatedtobe 0.0124 μMfor H^+ and 7.9 μM for Na^+. Thus, the *I. tartaricus* c-ring is originally more specific to H^+than to Na^+. The generated and analysed panel of mutant c-rings allowed to shed light on how the cation selectivity is determined and how high H^+ and Na^+ affinities are achieved in the c-rings. The H^+ selectivity of the c-rings is determined by ionisable Glu65 residue present in the ion binding site motif. The high H^+ binding affinity relates to hydrophobicity of the residues that compose ion binding site in *I. tartaricus* c-ring. The Na^+ selectivity of the c-ring is determined by combination of several factors among which the number and polarity of ligands that contribute hydrogen bonds to Na^+ and stabilization of Na^+ in the bound state were shown to be crucial. For attaining high Na^+ binding affinity the atomic composition and solvent environment that allow enthalpy-driven strong but reversible Na^+ binding were shown to be important.

The ATP synthesis activity of *I. tartaricus* was shown to be very sensitive to changes in the H^+/Na^+ selectivity of its c-ring. Namely, the higher H^+ binding affinity of the c-ring (pKa of Glu65 carboxyl group in the c-rings was carefully calculated and compared) allowed to catalyze *pmf*-driven ATP synthesis by corresponding ATP synthase at much higher turnover rates compared to intact enzyme. The changes in Na^+ binding affinity of the c-rings in ATP synthases led to decreased rates of *smf*-driven ATP synthesis or no observed *smf*-driven activity. The latter case was in particularly interesting as showed that one or two substitutions in or near the ion binding site may restrict Na^+ binding affinity of the c-ring and *smf*-driven activity of corresponding ATP synthase, although H^+ binding affinity and *pmf*-driven activity of corresponding ATP synthase remain. It would be therefore of a great interest to solve thehigh-resolution structures of these c-rings. Preliminary crystallization gave the first diffracting 3D crystals for Q32A/Y70F mutant c-ring. The crystallization in lipidic cubic phase can be a method of choice for further optimization of diffraction resolution.

7. Appendix

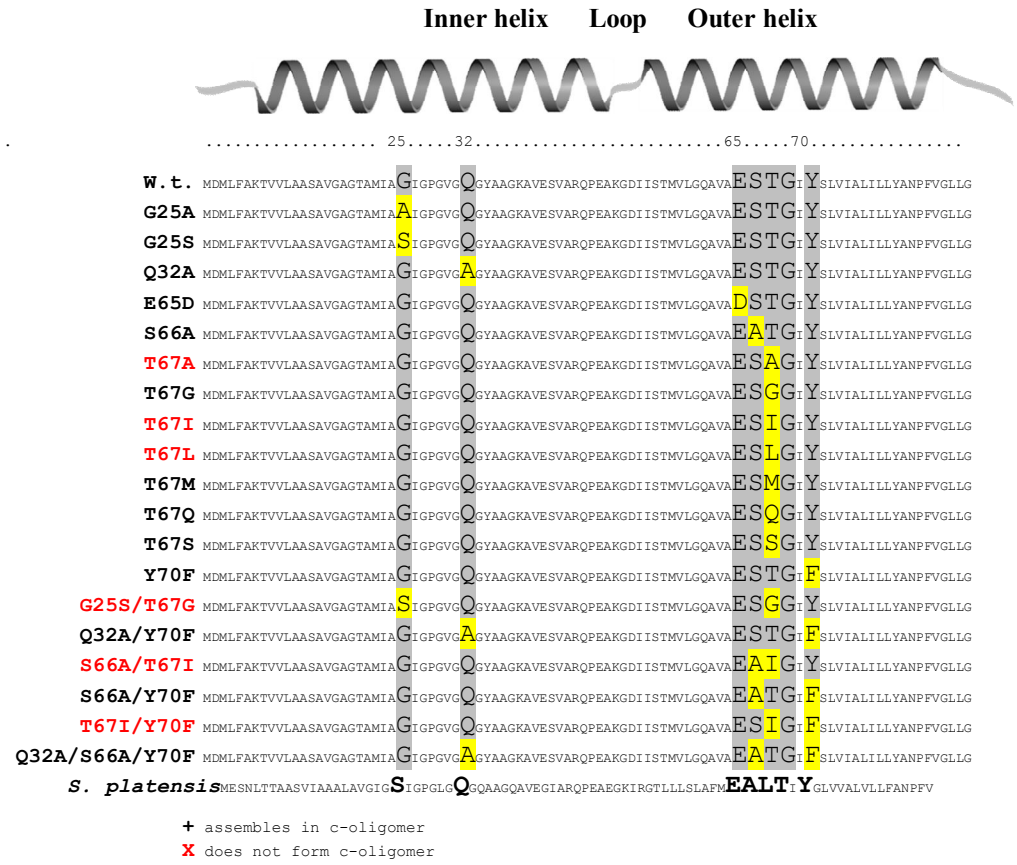

Figure 7-1: Sequence alignment of *I. tartaricus*and *S. platensis*wild-type c-subunits and *I. tartaricus* c-subunits with mutations. Residues shown in yellow replaced the conserved residuesinvolved in ion binding (Gln32, Glu65, Ser66, Thr67, Gln68 and Tyr70 residues, shown in grey) and one belonging to helix packing motif (Gln25 residue, shown in grey).

Wild-type:

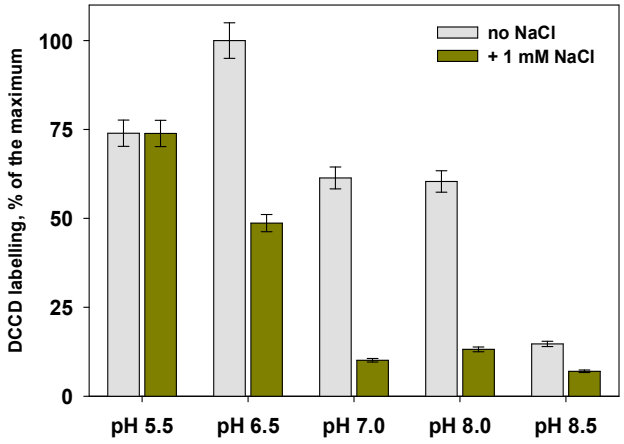

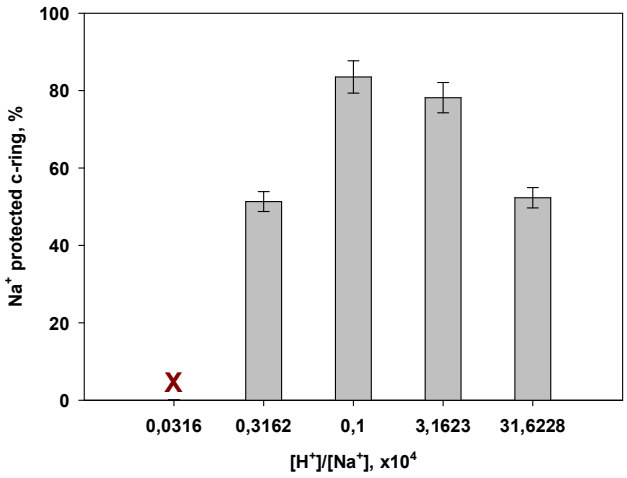

$[Na^+][H^+]$ x10^4	Na^+ protection, %
0.0316	x
0.3162	51.33 ± 2.6
1.0	83.53 ± 4.2
10.0	78.18 ± 3.9
31.6228	52.31 ± 2.6

Figure 7-2: pH-dependent and Na^+-protected DCCD modification of the wild-type c-ring. Upper panel: Presented is a DCCD modification profile of Glu65 carboxyl group in *I. tartaricus*wild-type c-ring at different pH and NaCl conditions. **Lower panel:** The Na^+ protection of Glu65 carboxyl group against DCCD modification (% of the non-labelled c-subunits) was calculated at taken Na^+-to-H^+ molar ratios (known pH and Na^+ concentrations were used to obtain these values).

Q32A mutant:

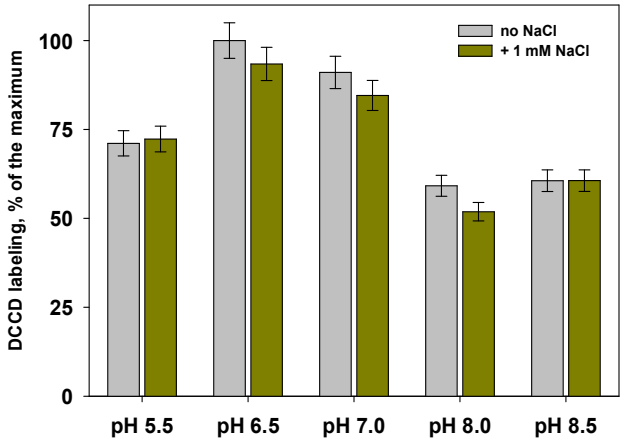

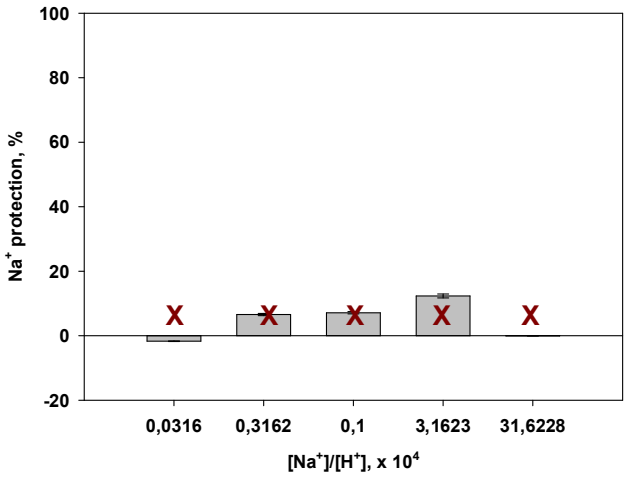

$[Na^+][H^+]$ x10^4	Na^+ protection, %
0.0316	x
0.3162	x
1.0	x
10.0	x
31.6228	x

Figure 7-3: pH-dependent DCCD-modification of Q32A mutant. Upper panel: Presented is a DCCD modification profile of Glu65 carboxyl group in *I. tartaricus* Q32A mutant c-ring at different pH and NaCl conditions. **Lower panel:** The Na^+ protection of Glu65 carboxyl group against DCCD modification (% of the non-labelled c-subunits) was calculated at taken Na^+-to-H^+ molar ratios (known pH and Na^+ concentrations were used to obtain these values).

T67G mutant:

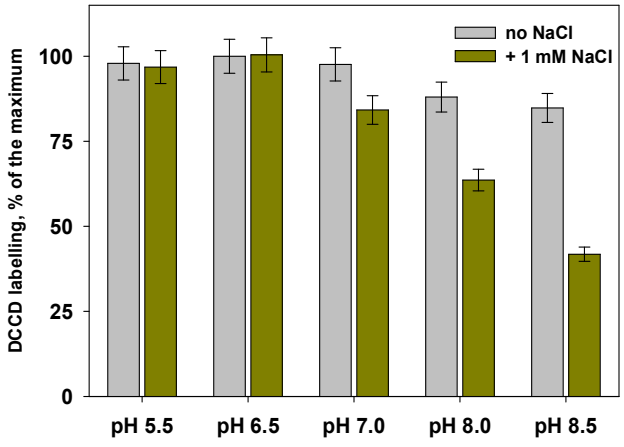

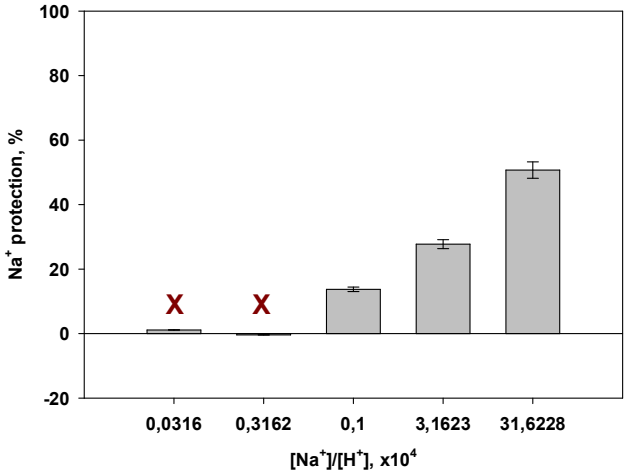

$[Na^+][H^+]$ x10^4	Na^+ protection, %
0.0316	x
0.3162	x
1.0	13.73 ± 0.7
10.0	27.73 ± 1.4
31.6228	50.71 ± 2.5

Figure 7-4: pH-dependent and Na^+-protected DCCD modification of T67G mutant.Upper panel: Presented is a DCCD modification profile of Glu65 carboxyl group in *I. tartaricus* T67G mutant c-ring at different pH and NaCl conditions. **Lower panel:** The Na^+ protection of Glu65 carboxyl group against DCCD modification (% of the non-labelled c-subunits) was calculated at taken Na^+-to-H^+ molar ratios (known pH and Na^+ concentrations were used to obtain these values).

S66A/Y70F mutant:

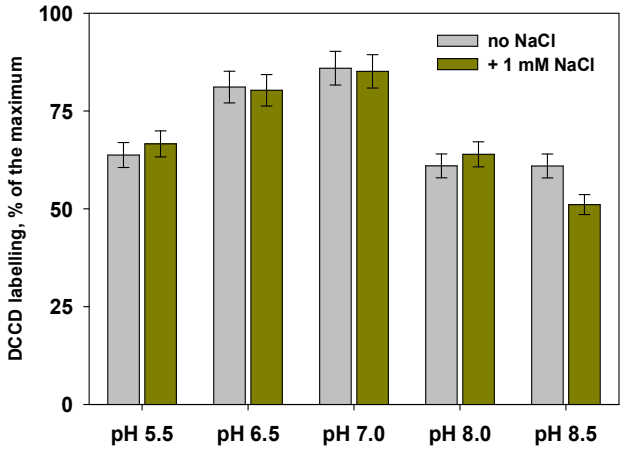

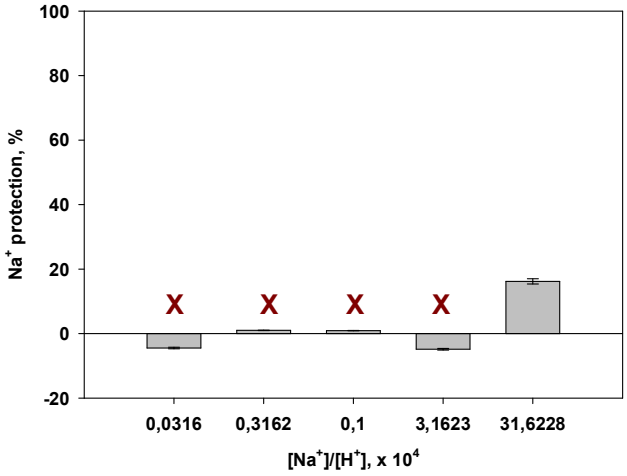

$[Na^+][H^+]$ x10^4	Na^+ protection %
0.0316	x
0.3162	x
1.0	x
10.0	x
31.6228	16.20 ± 0.8

Figure 7-5: pH-dependent and Na^+-protected DCCD modification of S66A/Y70F mutant. Presented is a DCCD modification profile of Glu65 carboxyl group in *I. tartaricus* S66A/Y70F mutant c-ring at different pH and NaCl conditions. **Lower panel:** The Na^+ protection of Glu65 carboxyl group against DCCD modification (% of the non-labelled c-subunits) was calculated at taken Na^+-to-H^+ molar ratios (known pH and Na^+ concentrations were used to obtain these values).

Q32A/Y70F mutant:

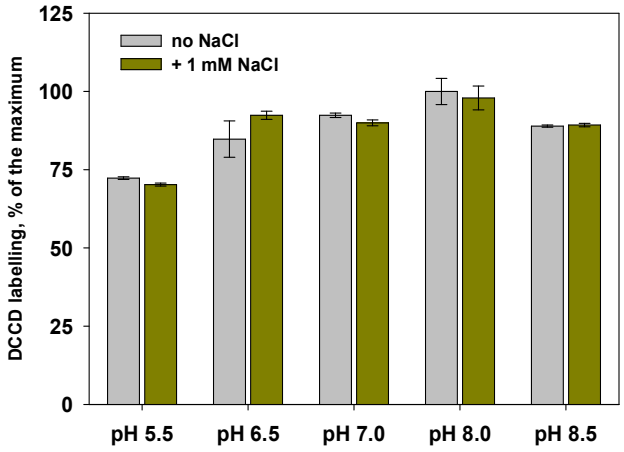

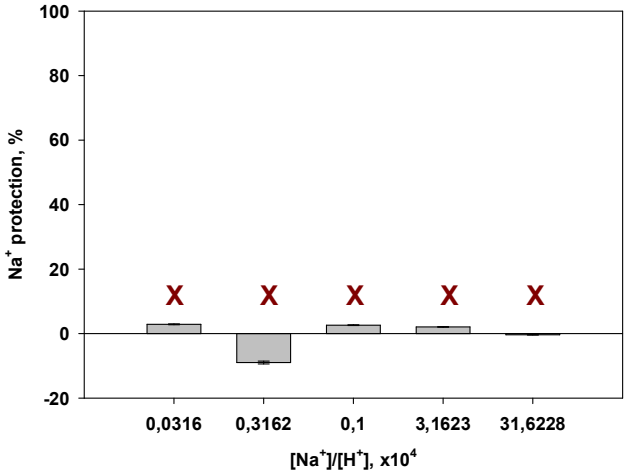

$[Na^+][H^+]$ x10^4	Na^+ protection, %
0.0316	x
0.3162	x
1.0	x
10.0	x
31.6228	x

Figure 7-6: pH-dependent DCCD-modification of Q32A/Y70F mutant. Presented is a DCCD modification profile of Glu65 carboxyl group in *I. tartaricus* Q32A/Y70F mutant c-ring at different pH and NaCl conditions. **Lower panel:** The Na^+ protection of Glu65 carboxyl group against DCCD modification (% of the non-labelled c-subunits) was calculated at taken Na^+-to-H^+ molar ratios (known pH and Na^+ concentrations were used to obtain these values).

Y70F mutant:

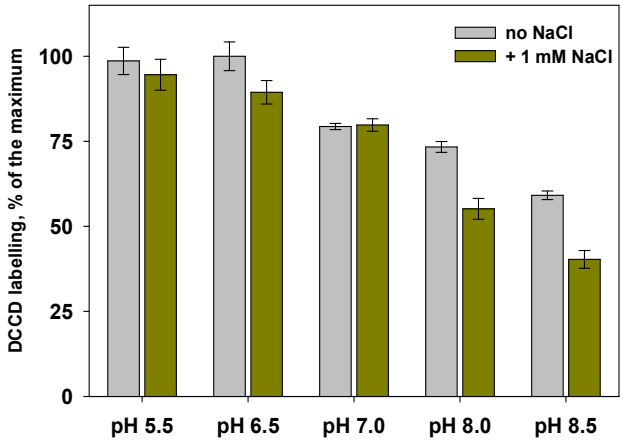

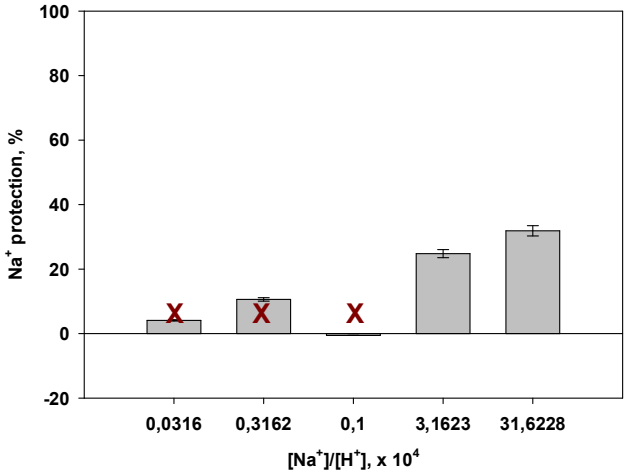

$[Na^+][H^+]$ x10^4	Na^+ protection, %
0.0316	x
0.3162	10.60 ± 0.5
1.0	x
10.0	24.80 ± 1.2
31.6228	31.90 ± 1.6

Figure 7-7: pH-dependent and Na^+-protected DCCD modification of Y70F mutant. Presented is a DCCD modification profile of Glu65 carboxyl group in *I. tartaricus* Y70F mutant c-ring at different pH and NaCl conditions. **Lower panel:** The Na^+ protection of Glu65 carboxyl group against DCCD modification (% of the non-labelled c-subunits) was calculated at taken Na^+-to-H^+ molar ratios (known pH and Na^+ concentrations were used to obtain these values).

T67S mutant:

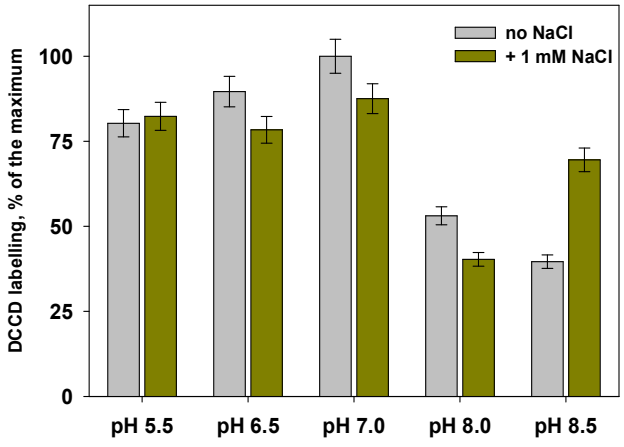

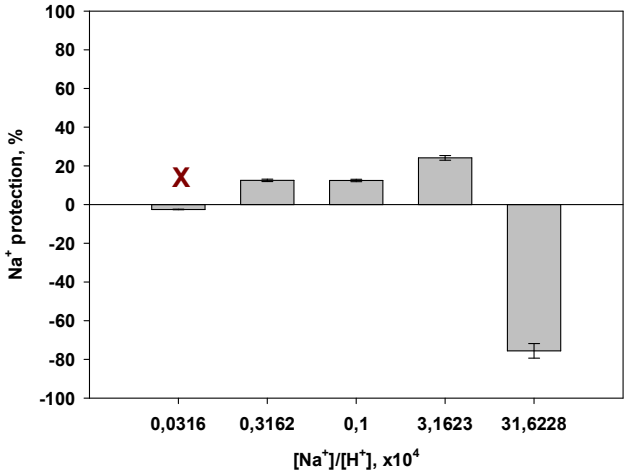

$[Na^+][H^+]$ x10^4	Na^+ protection, %
0.0316	x
0.3162	12.50 ± 0.6
1.0	12.50 ± 0.6
10.0	24.10 ± 1.2
31.6228	x

Figure 7-8: pH-dependent and Na^+-protected DCCD modification of T67S mutant. Presented is a DCCD modification profile of Glu65 carboxyl group in *I. tartaricus* T67G mutant c-ring at different pH and NaCl conditions. **Lower panel:** The Na^+ protection of Glu65 carboxyl group against DCCD modification (% of the non-labelled c-subunits) was calculated at taken Na^+-to-H^+ molar ratios (known pH and Na^+ concentrations were used to obtain these values).

8. Acknowledgments

I would like to acknowledge Prof. Dr. Thomas Meier for giving me the unique opportunity to be a part of his group, first as a post diploma practical student and latter as a PhD student. It was a great time and place to practice and develop research skills.

I am thankful to people in the MPI of Biophysics who supported me and motivated all these years: Dr. Denys Pogoryelov for direct supervision, Dr. Julian Langer for performing MALDI-MS measurements, Friederike Joos for performed freeze fracture electron microscopy and Dr. Ernst Grell for all time he has invested into maintenance of ITC facility in perfect operational state and for all his help in design of ITC experiments and in the discussion/interpretation of obtained data. It was a good experience to be a part of such big team of highly motivated and erudite people.

Хочу поблагодарить мою сестру и моего отца за поддержку все эти году.

9. Curriculum Vitae

Born October 24, 1986, Odessa, Ukraine

Education:

1. PhD student, Max-Planck Institute of Biophysics, Department of Structural Biology, Laboratory of Thomas Meier, Frankfurt am Main, Germany, 2012-2018
2. Post diploma practicum, Max-Planck Institute of Biophysics, Department of Structural Biology, Laboratory of Thomas Meier, Frankfurt am Main, Germany, 2009-2011
3. M.Sc. and B.Sc., Odessa I.I.Mechnikov National University, Department of Genetics and Molecular Biology, Odessa, Ukraine, laboratory of Vladlen Totskiy, 2008-2009
4. Study of Genetics and Molecular biology at Odessa I.I.Mechnikov National University, Department of Genetics and Molecular Biology, Odessa, Ukraine, laboratory of Vladlen Totskiy, 2005-2007
5. High School, Ruchelieu lyceum, Odessa, Ukraine

Publications:

1. Pogoryelov D, Klyszejko AL, **Krasnoselska GO**, Heller E-M, Leone V, Langer JD, Vonck J, Muller DJ, Faraldo-Gómez JD, Meier T (2012) Engineering rotor ring stoichiometries in the ATP synthase. *PNAS* 109: E1599-1608
2. **Krasnoselska GO**, Meier T. (2018) Purification and reconstitution of *Ilyobacter tartaricus* ATP synthase. *Methods Molecular Biology*. Vol 1805: 978-1-4939-8554-8

References

Abrahams JP, Leslie AGW, Lutter R et al. (1994) Structure at 2.8-Angstrom Resolution of F1-Atpase from Bovine Heart-Mitochondria. *Nature* **370**(6491): 621-628.

Abramson J, Smirnova I, Kasho V et al. (2003) Structure and mechanism of the lactose permease of Escherichia coli. *Science* **301**(5633): 610-615.

Adachi K, Oiwa K, Nishizaka T et al. (2007) Coupling of rotation and catalysis in F-1-ATPase revealed by single-molecule imaging and manipulation. *Cell* **130**(2): 309-321.

Adachi K, Yasuda R, Noji H et al. (2000) Stepping rotation of F-1-ATPase visualized through angle-resolved single-fluorophore imaging. *Proceedings of the National Academy of Sciences of the United States of America* **97**(13): 7243-7247.

Alberty RA (2003) Thermodynamics of the hydrolysis of adenosine triphosphate as a function of temperature, pH, pMg, and ionic strength. *Journal of Physical Chemistry B* **107**(44): 12324-12330.

Allegretti M, Klusch N, Mills DJ et al. (2015) Horizontal membrane-intrinsic alpha-helices in the stator a-subunit of an F-type ATP synthase. *Nature* **521**(7551): 237-240.

Amin A, Hariharan P, Chae PS et al. (2015) Effect of Detergents on Galactoside Binding by Melibiose Permeases. *Biochemistry* **54**(38): 5849-5855.

Anderson DE, Becktel WJ and Dahlquist FW (1990) pH-induced denaturation of proteins: a single salt bridge contributes 3-5 kcal/mol to the free energy of folding of T4 lysozyme. *Biochemistry* **29**(9): 2403-2408.

Angevine CM, Herold KAG, Vincent OD et al. (2007) Aqueous access pathways in ATP synthase subunit a - Reactivity of cysteine substituted into transmembrane helices 1, 3, AND 5. *Journal of Biological Chemistry* **282**(12): 9001-9007.

Antosiewicz J, Briggs JM, Elcock AH et al. (1996) Computing ionization states of proteins with a detailed charge model. *Journal of Computational Chemistry* **17**(14): 1633-1644.

Arai HC, Yukawa A, Iwatate RJ et al. (2014) Torque Generation Mechanism of F-1-ATPase upon NTP Binding. *Biophysical Journal* **107**(1): 156-164.

Ariga T, Muneyuki E and Yoshida M (2007) F1-ATPase rotates by an asymmetric, sequential mechanism using all three catalytic subunits(vol 14, pg 841, 2007). *Nature Structural & Molecular Biology* **14**(10): 984-984.

Assadi-Porter FM and Fillingame RH (1995) Proton-translocating carboxyl of subunit c of F1Fo H(+)-ATP synthase: the unique environment suggested by the pKa determined by 1H NMR. *Biochemistry* **34**(49): 16186-16193.

Ausubel FM, Brent R and Kingston RE (2002) Current Protocols in Molecular Biology. *John Wiley & Sons Inc., New York, NY* **2**(
Axe DD and Bailey JE (1995) Transport of Lactate and Acetate through the Energized Cytoplasmic Membrane of Escherichia-Coli. *Biotechnology and Bioengineering* **47**(1): 8-19.

Azzi A, Casey RP and Nalecz MJ (1984) The Effect of N,N'-Dicyclohexylcarbodiimide on Enzymes of Bioenergetic Relevance. *Biochim Biophys Acta* **768**(3-4): 209-226.

Balsera M, Buey RM and Li XD (2011) Quaternary Structure of the Oxaloacetate Decarboxylase Membrane

Complex and Mechanistic Relationships to Pyruvate Carboxylases. *Journal of Biological Chemistry* **286**(11): 9457-9467.

Batista AP, Marreiros BC and Pereira M (2012) The role of proton and sodium Ions in energy transduction by respiratory complex I. *Febs Journal* **279**(8-9.

Beattie DS and Clejan L (1982) The Binding of Dicyclohexylcarbodiimide to Cytochrome-B of Complex-Iii Isolated from Yeast Mitochondria. *Febs Letters* **149**(2): 245-248.

Becher B, Muller V and Gottschalk G (1992) The Methyl-Tetrahydromethanopterin - Coenzyme-M Methyltransferase of Methanosarcina Strain Go1 Is a Primary Sodium-Pump. *Fems Microbiology Letters* **91**(3): 239-244.

Berneche S and Roux B (2001) Energetics of ion conduction through the K+ channel. *Nature* **414**(6859): 73-77.

Biegel E and Muller V (2010) Bacterial Na+-translocating ferredoxin: NAD(+) oxidoreductase. *Proceedings of the National Academy of Sciences of the United States of America* **107**(42): 18138-18142.

Blasie CA and Berg JM (2004) Entropy-enthalpy compensation in ionic interactions probed in a zinc finger peptide. *Biochemistry* **43**(32): 10600-10604.

Borders CL, Jr., Chan VW, Miner LA et al. (1989) Inactivation of human thrombin by water-soluble carbodiimides. The essential carboxyl has a pKa of 5.6 and is one other than Asp-189. *Febs Letters* **255**(2): 365-368.

Bostick DL and Brooks CL (2007) Selectivity in K+ channels is due to topological control of the permeant ion's coordinated state. *Proceedings of the National Academy of Sciences of the United States of America* **104**(22): 9260-9265.

Bott M, Pfister K, Burda P et al. (1997) Methylmalonyl-CoA decarboxylase from Propionigenium modestum--cloning and sequencing of the structural genes and purification of the enzyme complex. *Eur J Biochem* **250**(2): 590-599.

Bowler MW, Montgomery MG, Leslie AG et al. (2007) Ground state structure of F1-ATPase from bovine heart mitochondria at 1.9 A resolution. *Journal of Biological Chemistry* **282**(19): 14238-14242.

Bowman EJ, Siebers A and Altendorf K (1988) Bafilomycins: a class of inhibitors of membrane ATPases from microorganisms, animal cells, and plant cells. *Proc Natl Acad Sci U S A* **85**(21): 7972-7976.

Boyer PD (1975) A model for conformational coupling of membrane potential and proton translocation to ATP synthesis and to active transport. *Febs Letters* **58**(1): 1-6.

Boyer PD (1993) The binding change mechanism for ATP synthase--some probabilities and possibilities. *Biochim Biophys Acta* **1140**(3): 215-250.

Boyer PD (2000) Catalytic site forms and controls in ATP synthase catalysis. *Biochimica Et Biophysica Acta-Bioenergetics* **1458**(2-3): 252-262.

Boyer PD, Kohlbrenner, W.E. (1981) The present status of the binding-change mechanism and its relation to ATP formation by chloroplasts. *In Energy Coupling in Photosynthesis, B.R. Selman and S. Selman-Reimer, eds. (Amsterdam: Elsevier)*: 231-240.

Breiten B, Lockett MR, Sherman W et al. (2013) Water networks contribute to enthalpy/entropy compensation in protein-ligand binding. *J Am Chem Soc* **135**(41): 15579-15584.

Brummell DA, Sharma VP, Anand NN et al. (1993) Probing the combining site of an anti-carbohydrate antibody by saturation-mutagenesis: role of the heavy-chain CDR3 residues. *Biochemistry* **32**(4): 1180-1187.

Buchner J (1996) Supervising the fold: Functional principles of molecular chaperones. *Faseb Journal* **10**(1): 10-19.

Buckel W (2001) Sodium ion-translocating decarboxylases. *Biochimica Et Biophysica Acta-Bioenergetics* **1505**(1): 15-27.

Buckel W and Thauer RK (2013) Energy conservation via electron bifurcating ferredoxin reduction and proton/Na(+) translocating ferredoxin oxidation. *Biochim Biophys Acta* **1827**(2): 94-113.

Burzik C, Kaim G, Dimroth P et al. (2003) Charge displacements during ATP-hydrolysis and synthesis of the Na+-transporting FoF1-ATPase of Ilyobacter tartaricus. *Biophysical Journal* **85**(3): 2044-2054.

Cain BD and Simoni RD (1989) Proton Translocation by the F1f0-Atpase of Escherichia-Coli Mutagenic Analysis of the Alpha-Subunit. *Journal of Biological Chemistry* **264**(6): 3292-3300.

Cannon WR and Benkovic SJ (1998) Solvation, reorganization energy, and biological catalysis. *Journal of Biological Chemistry* **273**(41): 26257-26260.

Carbonell T and Freire E (2005) Binding thermodynamics of statins to HMG-CoA reductase. *Biochemistry* **44**(35): 11741-11748.

Castaneda CA, Fitch CA, Majumdar A et al. (2009) Molecular determinants of the pKa values of Asp and Glu residues in staphylococcal nuclease. *Proteins-Structure Function and Bioinformatics* **77**(3): 570-588.

Chakrabarti N, Ing C, Payandeh J et al. (2013) Catalysis of Na+ permeation in the bacterial sodium channel Na(V)Ab. *Proceedings of the National Academy of Sciences of the United States of America* **110**(28): 11331-11336.

Chan VWF, Jorgensen AM and Borders CL (1988) Inactivation of Bovine Thrombin by Water-Soluble Carbodiimides - the Essential Carboxyl Group Has a Pka of 5.51. *Biochem Biophys Res Commun* **151**(2): 709-716.

Chang CEA, Chen W and Gilson MK (2007) Ligand configurational entropy and protein binding. *Proceedings of the National Academy of Sciences of the United States of America* **104**(5): 1534-1539.

Chaudhry C, Weston MC, Schuck P et al. (2009) Stability of ligand-binding domain dimer assembly controls kainate receptor desensitization. *Embo Journal* **28**(10): 1518-1530.

Checover S, Marantz Y, Nachliel E et al. (2001) Dynamics of the proton transfer reaction on the cytoplasmic surface of bacteriorhodopsin. *Biochemistry* **40**(14): 4281-4292.

Chen LQ, Santarelli V, Horn R et al. (1996) A unique role for the S4 segment of domain 4 in the inactivation of sodium channels. *Journal of General Physiology* **108**(6): 549-556.

Chittajallu R, Braithwaite SP, Clarke VR et al. (1999) Kainate receptors: subunits, synaptic localization and function. *Trends Pharmacol Sci* **20**(1): 26-35.

Chivers PT, Prehoda KE, Volkman BF et al. (1997) Microscopic pKa values of Escherichia coli thioredoxin. *Biochemistry* **36**(48): 14985-14991.

Chothia C and Janin J (1975) Principles of protein-protein recognition. *Nature* **256**(5520): 705-708.

Cingolani G and Duncan TM (2011) Structure of the ATP synthase catalytic complex (F(1)) from Escherichia coli in an autoinhibited conformation. *Nature Structural & Molecular Biology* **18**(6): 701-707.

Coutinho PM and Henrissat B (1999) Carbohydrate-active enzymes: An integrated database approach. *Recent Advances in Carbohydrate Bioengineering* 246): 3-12.

Cox GB, Jans DA, Fimmel AL et al. (1984) Hypothesis. The mechanism of ATP synthase. Conformational change by rotation of the beta-subunit. *Biochim Biophys Acta* **768**(3-4): 201-208.

Cross RL and Muller V (2004) The evolution of A-, F-, and V-type ATP synthases and ATPascs: reversals in function and changes in the H+/ATP coupling ratio. *Febs Letters* **576**(1-2): 1-4.

Dahinden P, Auchli Y, Granjon T et al. (2005) Oxaloacetate decarboxylase of Vibrio cholerae: purification, characterization, and expression of the genes in Escherichia coli. *Arch Microbiol* **183**(2): 121-129.

Dam TK, Torres M, Brewer CF et al. (2008) Isothermal titration calorimetry reveals differential binding thermodynamics of variable region-identical antibodies differing in constant region for a univalent ligand. *Journal of Biological Chemistry* **283**(46): 31366-31370.

Dautant A, Velours J and Giraud MF (2010) Crystal Structure of the Mg center dot ADP-inhibited State of the Yeast F(1)c(10)-ATP Synthase. *Journal of Biological Chemistry* **285**(38): 29502-29510.

Davidson JP, Lubman O, Rose T et al. (2002) Calorimetric and structural studies of 1,2,3-trisubstituted cyclopropanes as conformationally constrained peptide inhibitors of Src SH2 domain binding. *J Am Chem Soc* **124**(2): 205-215.

DeLeon-Rangel J, Ishmukhametov RR, Jiang WR et al. (2013) Interactions between subunits a and b in the rotary ATP synthase as determined by cross-linking. *Febs Letters* **587**(7): 892-897.

Demchenko AP (2001) Recognition between flexible protein molecules: induced and assisted folding. *Journal of Molecular Recognition* **14**(1): 42-61.

Devenish RJ, Prescott M and Rodgers AJW (2008) The structure and function of mitochondrial F(1)F(0)-ATP synthases. *International Review of Cell and Molecular Biology, Vol 267* **267**(1-+.

Di Berardino M and Dimroth P (1995) Synthesis of the oxaloacetate decarboxylase Na+ pump and its individual subunits in Escherichia coli and analysis of their function. *Eur J Biochem* **231**(3): 790-801.

Dibrova DV, Galperin MY, Koonin EV et al. (2015) Ancient Systems of Sodium/Potassium Homeostasis as Predecessors of Membrane Bioenergetics. *Biochemistry (Mosc)* **80**(5): 495-516.

Dibrova DV, Galperin MY and Mulkidjanian AY (2010) Characterization of the N-ATPase, a distinct, laterally transferred Na+-translocating form of the bacterial F-type membrane ATPase. *Bioinformatics* **26**(12): 1473-1476.

Dickson VK, Silvester JA, Fearnley IM et al. (2006) On the structure of the stator of the mitochondrial ATP synthase. *Embo Journal* **25**(12): 2911-2918.

Dimroth P (1980) A new sodium-transport system energized by the decarboxylation of oxaloacetate. *Febs Letters* **122**(2): 234-236.

Dimroth P (1982) The generation of an electrochemical gradient of sodium ions upon decarboxylation of oxaloacetate by the membrane-bound and Na+-activated oxaloacetate decarboxylase from Klebsiella aerogenes. *Eur J Biochem* **121**(2): 443-449.

Dimroth P (1987) Sodium ion transport decarboxylases and other aspects of sodium ion cycling in bacteria. *Microbiol Rev* **51**(3): 320-340.

Dimroth P (1992) Structure and function of the Na(+)-translocating ATPase of Propionigenium modestum. *Acta Physiol Scand Suppl* **607**(97-103.

Dimroth P (1994) Bacterial sodium ion-coupled energetics. *Antonie Van Leeuwenhoek* **65**(4): 381-395.

Dimroth P (1997) Primary sodium ion translocating enzymes. *Biochim Biophys Acta* **1318**(1-2): 11-51.

Dimroth P and Hilpert W (1984) Carboxylation of Pyruvate and Acetyl Coenzyme-a by Reversal of the Na+ Pumps Oxaloacetate Decarboxylase and Methylmalonyl-Coa Decarboxylase. *Biochemistry* **23**(22): 5360-5366.

Dimroth P, Jockel P and Schmid M (2001) Coupling mechanism of the oxaloacetate decarboxylase Na(+) pump. *Biochim Biophys Acta* **1505**(1): 1-14.

Dimroth P and Schink B (1998) Energy conservation in the decarboxylation of dicarboxylic acids by fermenting bacteria. *Arch Microbiol* **170**(2): 69-77.

Dimroth P and Thomer A (1983) Subunit composition of oxaloacetate decarboxylase and characterization of the alpha chain as carboxyltransferase. *Eur J Biochem* **137**(1-2): 107-112.

Dimroth P, von Ballmoos C and Meier T (2006) Catalytic and mechanical cycles in F-ATP synthases. Fourth in the Cycles Review Series. *EMBO Rep* **7**(3): 276-282.

Dixit PD, Merchant S and Asthagiri D (2009) Ion Selectivity in the KcsA Potassium Channel from the Perspective of the Ion Binding Site. *Biophysical Journal* **96**(6): 2138-2145.

Doyle DA, Cabral JM, Pfuetzner RA et al. (1998) The structure of the potassium channel: Molecular basis of K+ conduction and selectivity. *Science* **280**(5360): 69-77.

Driessen AJM, vandeVossenberg JLCM and Konings WN (1996) Membrane composition and ion-permeability in extremophiles. *Fems Microbiology Reviews* **18**(2-3): 139-148.

Drose S and Altendorf K (1997) Bafilomycins and concanamycins as inhibitors of V-ATPases and P-ATPases. *J Exp Biol* **200**(Pt 1): 1-8.

Du X, Li Y, Xia YL et al. (2016) Insights into Protein-Ligand Interactions: Mechanisms, Models, and Methods. *International Journal of Molecular Sciences* **17**(2).

Dudev T and Lim C (2014) Competition among Metal Ions for Protein Binding Sites: Determinants of Metal Ion Selectivity in Proteins. *Chemical Reviews* **114**(1): 538-556.

Dumon-Seignovert L, Cariot G and Vuillard L (2004) The toxicity of recombinant proteins in Escherichia coli: a comparison of overexpression in BL21(DE3), C41(DE3), and C43(DE3). *Protein Expr Purif* **37**(1): 203-206.

Duncan TM, Bulygin VV, Zhou Y et al. (1995) Rotation of Subunits during Catalysis by Escherichia-Coli F1-Atpase. *Proceedings of the National Academy of Sciences of the United States of America* **92**(24): 10964-10968.

Duncan TM, Duser MG, Heitkamp T et al. (2014) Regulatory conformational changes of the epsilon subunit in single FRET-labeled FoF1-ATP synthase. *Proc SPIE Int Soc Opt Eng* **8948**(89481J.

Dunn SD, Kellner E and Lill H (2001) Specific heterodimer formation by the cytoplasmic domains of the b and b' subunits of cyanobacterial ATP synthase. *Biochemistry* **40**(1): 187-192.

Duser MG, Zarrabi N, Cipriano DJ et al. (2009) 36 degrees step size of proton-driven c-ring rotation in FoF1-ATP synthase. *EMBO J* **28**(18): 2689-2696.

Dwyer JJ, Gittis AG, Karp DA et al. (2000) High apparent dielectric constants in the interior of a protein reflect water penetration. *Biophysical Journal* **79**(3): 1610-1620.

Dyson HJ, Jeng MF, Tennant LL et al. (1997) Effects of buried charged groups on cysteine thiol ionization and reactivity in Escherichia coli thioredoxin: structural and functional characterization of mutants of Asp 26 and Lys 57. *Biochemistry* **36**(9): 2622-2636.

Ellinor PT, Yang J, Sather WA et al. (1995) Ca2+ Channel Selectivity at a Single-Locus for High-Affinity Ca2+ Interactions. *Neuron* **15**(5): 1121-1132.

Elston T, Wang H and Oster G (1998) Energy transduction in ATP synthase. *Nature* **391**(6666): 510-513.

Espindola FS, Espreafico EM, Coelho MV et al. (1992) Biochemical and immunological characterization of p190-calmodulin complex from vertebrate brain: a novel calmodulin-binding myosin. *J Cell Biol* **118**(2): 359-368.

Farrell D, Miranda ES, Webb H et al. (2010) Titration_DB: storage and analysis of NMR-monitored protein pH titration curves. *Proteins-Structure Function and Bioinformatics* **78**(4): 843-857.

Favre I, Moczydlowski E and Schild L (1996) On the structural basis for ionic selectivity among Na+, K+, and Ca2+ in the voltage-gated sodium channel. *Biophysical Journal* **71**(6): 3110-3125.

Ferguson SA, Keis S and Cook GM (2006) Biochemical and molecular characterization of a Na+-translocating F1Fo-ATPase from the thermoalkaliphilic bacterium Clostridium paradoxum. *J Bacteriol* **188**(14): 5045-5054.

Ferry JG (2011) Fundamentals of methanogenic pathways that are key to the biomethanation of complex biomass. *Current Opinion in Biotechnology* **22**(3): 351-357.

Fersht A (1999) Structure and Mechanism in Protein Science.

Fillingame RH (1975) Identification of the dicyclohexylcarbodiimide-reactive protein component of the adenosine 5'-triphosphate energy-transducing system of Escherichia coli. *J Bacteriol* **124**(2): 870-883.

Fillingame RH and Dmitriev OY (2002) Structural model of the transmembrane F-o rotary sector of H+-transporting ATP synthase derived by solution NMR and intersubunit cross-linking in situ. *Biochimica Et Biophysica Acta-Biomembranes* **1565**(2): 232-245.

Forgac M (2007) Vacuolar ATPases: rotary proton pumps in physiology and pathophysiology. *Nature Reviews Molecular Cell Biology* **8**(11): 917-929.

Forsyth WR, Antosiewicz JM and Robertson AD (2002) Empirical relationships between protein structure and carboxyl pK(a) values in proteins. *Proteins-Structure Function and Bioinformatics* **48**(2): 388-403.

Frater R (1971) Reactivity of Carboxyl Groups in Modified Proteins. *Febs Letters* **12**(4): 186-&.

Freire E (2008) Do enthalpy and entropy distinguish first in class from best in class? *Drug Discovery Today* **13**(19-20): 869-874.

Fukada H and Takahashi K (1998) Enthalpy and heat capacity changes for the proton dissociation of various buffer components in 0.1 M potassium chloride. *Proteins-Structure Function and Genetics* **33**(2): 159-166.

Gabellini N, Gao Z, Eckerskorn C et al. (1988) Purification of the H+-Atpase from Rhodobacter-Capsulatus, Identification of the F1f0 Components and Reconstitution of the Active Enzyme. *Biochim Biophys Acta* **934**(2): 227-234.

Garcia-Moreno B, Fitch C, Karp D et al. (2002) Experimental pKa values of buried residues: Analysis with continuum electrostatic methods and assessment of contributions by water penetration. *Biophysical Journal* **82**(1): 300a-300a.

Gething MJ and Sambrook J (1992) Protein Folding in the Cell. *Nature* **355**(6355): 33-45.

Giletto A and Pace CN (1999) Buried, charged, non-ion-paired aspartic acid 76 contributes favorably to the conformational stability of ribonuclease T1. *Biochemistry* **38**(40): 13379-13384.

Gilson MK and Zhou HX (2007) Calculation of protein-ligand binding affinities. *Annual Review of Biophysics and Biomolecular Structure* **36**(21-42.

Goh GB, Laricheva EN and Brooks CL, 3rd (2014) Uncovering pH-dependent transient states of proteins with buried ionizable residues. *J Am Chem Soc* **136**(24): 8496-8499.

Gopal B, Swaminathan CP, Bhattacharya S et al. (1997) Thermodynamics of metal ion binding and denaturation of a calcium binding protein from Entamoeba histolytica. *Biochemistry* **36**(36): 10910-10916.

Gottschalk G and Thauer RK (2001) The Na(+)-translocating methyltransferase complex from methanogenic archaea. *Biochim Biophys Acta* **1505**(1): 28-36.

Gouaux E and Mackinnon R (2005) Principles of selective ion transport in channels and pumps. *Science* **310**(5753): 1461-1465.

Granjon T, Maniti O, Auchli Y et al. (2010) Structure-function relations in oxaloacetate decarboxylase complex. Fluorescence and infrared approaches to monitor oxomalonate and Na(+) binding effect. *PLoS One* **5**(6): e10935.

Grimsley GR, Scholtz JM and Pace CN (2009) A summary of the measured pK values of the ionizable groups in folded proteins. *Protein Sci* **18**(1): 247-251.

Grodberg J and Dunn JJ (1988) ompT encodes the Escherichia coli outer membrane protease that cleaves T7 RNA polymerase during purification. *J Bacteriol* **170**(3): 1245-1253.

Gruber G, Manimekalai MS, Mayer F et al. (2014) ATP synthases from archaea: the beauty of a molecular motor. *Biochim Biophys Acta* **1837**(6): 940-952.

Gunner MR and Alexov E (2000) A pragmatic approach to structure based calculation of coupled proton and electron transfer in proteins. *Biochim Biophys Acta* **1458**(1): 63-87.

Gunner MR and Baker NA (2016) Continuum Electrostatics Approaches to Calculating pKas and Ems in Proteins. *Methods Enzymol* **578**(1-20.

Gutteridge A and Thornton JM (2005) Understanding nature's catalytic toolkit. *Trends Biochem Sci* **30**(11): 622-629.

Hakulinen JK, Klyszejko AL, Hoffmann J et al. (2012) Structural study on the architecture of the bacterial ATP

synthase Fo motor. *Proc Natl Acad Sci U S A* **109**(30): E2050-2056.

Harding MM (2001) Geometry of metal-ligand interactions in proteins. *Acta Crystallogr D Biol Crystallogr* **57**(Pt 3): 401-411.

Harold FMMPC (1996) Energy transduction by ion currents. *American Society for Microbiology*: 283–306.

Harris TK and Turner GJ (2002) Structural basis of perturbed pKa values of catalytic groups in enzyme active sites. *Iubmb Life* **53**(2): 85-98.

Hase CC and Barquera B (2001) Role of sodium bioenergetics in Vibrio cholerae. *Biochim Biophys Acta* **1505**(1): 169-178.

Hase CC, Fedorova ND, Galperin MY et al. (2001) Sodium ion cycle in bacterial pathogens: evidence from cross-genome comparisons. *Microbiol Mol Biol Rev* **65**(3): 353-370, table of contents.

Hassinen IE and Vuokila PT (1993) Reaction of dicyclohexylcarbodiimide with mitochondrial proteins. *Biochim Biophys Acta* **1144**(2): 107-124.

Hatch LP, Cox GB and Howitt SM (1995) The Essential Arginine Residue at Position-210 in the Alpha-Subunit of the Escherichia-Coli Atp Synthase Can Be Transferred to Position-252 with Partial Retention of Activity. *Journal of Biological Chemistry* **270**(49): 29407-29412.

Heinemann SH, Teriau H, Stuhmer W et al. (1992) Calcium-Channel Characteristics Conferred on the Sodium-Channel by Single Mutations. *Nature* **356**(6368): 441-443.

Hemsworth GR, Henrissat B, Davies GJ et al. (2014) Discovery and characterization of a new family of lytic polysaccharide monooxygenases. *Nat Chem Biol* **10**(2): 122-126.

Hermanson GT (1996) In Bioconjugate chemistry. *Academic Press: San Diego*: 169–173.

Hermolin J and Fillingame RH (1989) H+-Atpase Activity of Escherichia-Coli F1f0 Is Blocked after Reaction of Dicyclohexylcarbodiimide with a Single Proteolipid (Subunit-C) of the F0 Complex. *Journal of Biological Chemistry* **264**(7): 3896-3903.

Herrmann RG, Steppuhn J, Herrmann GS et al. (1993) The Nuclear-Encoded Polypeptide Cfo-Ii from Spinach Is a Real, 9th Subunit of Chloroplast Atp Synthase. *Febs Letters* **326**(1-3): 192-198.

Herron JN, Kranz DM, Jameson DM et al. (1986) Thermodynamic Properties of Ligand-Binding by Monoclonal Anti-Fluorescyl Antibodies. *Biochemistry* **25**(16): 4602-4609.

Hille B (2001) Ion channels of excitable membranes. *Third edition Sinauer Associates, Sunderland, MA*: 1-814.

Hilpert W and Dimroth P (1983) Purification and characterization of a new sodium-transport decarboxylase. Methylmalonyl-CoA decarboxylase from Veillonella alcalescens. *Eur J Biochem* **132**(3): 579-587.

Hilpert W and Dimroth P (1984) Reconstitution of Na+ transport from purified methylmalonyl-CoA decarboxylase and phospholipid vesicles. *Eur J Biochem* **138**(3): 579-583.

Hirono-Hara Y, Noji H, Nishiura M et al. (2001) Pause and rotation of F-1-ATPase during catalysis. *Proceedings of the National Academy of Sciences of the United States of America* **98**(24): 13649-13654.

Ho JM and Coote ML (2010) A universal approach for continuum solvent pK(a) calculations: are we there yet?

Theoretical Chemistry Accounts **125**(1-2): 3-21.

Ho SN, Hunt HD, Horton RM et al. (1989) Site-Directed Mutagenesis by Overlap Extension Using the Polymerase Chain-Reaction. *Gene* **77**(1): 51-59.

Hoare DG and Koshland DE, Jr. (1967) A method for the quantitative modification and estimation of carboxylic acid groups in proteins. *Journal of Biological Chemistry* **242**(10): 2447-2453.

Holdgate GA (2001) Making cool drugs hot: isothermal titration calorimetry as a tool to study binding energetics. *Biotechniques* **31**(1): 164-166, 168, 170 passim.

Hoppe J, Schairer HU, Friedl P et al. (1982) An Asp-Asn substitution in the proteolipid subunit of the ATP-synthase from Escherichia coli leads to a non-functional proton channel. *Febs Letters* **145**(1): 21-29.

Hoppe J and Sebald W (1980) Amino acid sequence of the proteolipid subunit of the proton-translocating ATPase complex from the thermophilic bacterium PS-3. *Eur J Biochem* **107**(1): 57-65.

Houk KN, Leach AG, Kim SP et al. (2003) Binding affinities of host-guest, protein-ligand, and protein-transition-state complexes. *Angew Chem Int Ed Engl* **42**(40): 4872-4897.

Hunte C, Screpanti E, Venturi M et al. (2005) Structure of a Na+/H+ antiporter and insights into mechanism of action and regulation by pH. *Nature* **435**(7046): 1197-1202.

Ikegami M, Kawano M, Takase K et al. (1999) Enterococcus hirae vacuolar ATPase is expressed in response to pH as well as sodium. *Febs Letters* **454**(1-2): 67-70.

Inoue K, Konno M, Abe-Yoshizumi R et al. (2015) The Role of the NDQ Motif in Sodium-Pumping Rhodopsins. *Angewandte Chemie-International Edition* **54**(39): 11536-11539.

Inoue K, Ono H, Abe-Yoshizumi R et al. (2013) A light-driven sodium ion pump in marine bacteria. *Nature Communications* **4**(
Irudayam SJ and Henchman RH (2009) Entropic Cost of Protein-Ligand Binding and Its Dependence on the Entropy in Solution. *Journal of Physical Chemistry B* **113**(17): 5871-5884.

Ishii TM, Zerr P, Xia XM et al. (1998) Site-directed mutagenesis. *Methods Enzymol* **293**(53-71.

Ishmukhametov R, Hornung T, Spetzler D et al. (2010) Direct observation of stepped proteolipid ring rotation in E. coli F(0)F(1)-ATP synthase. *EMBO J* **29**(23): 3911-3923.

Ishmukhametov R, Hornung T, Spetzler D et al. (2010) Direct observation of stepped proteolipid ring rotation in E. coli FoF1-ATP synthase. *Embo Journal* **29**(23): 3911-3923.

Isom DG, Cannon BR, Castaneda CA et al. (2008) High tolerance for ionizable residues in the hydrophobic interior of proteins. *Proc Natl Acad Sci U S A* **105**(46): 17784-17788.

Isom DG, Castaneda CA, Cannon BR et al. (2011) Large shifts in pKa values of lysine residues buried inside a protein. *Proc Natl Acad Sci U S A* **108**(13): 5260-5265.

Isom DG, Castaneda CA, Cannon BR et al. (2010) Charges in the hydrophobic interior of proteins. *Proc Natl Acad Sci U S A* **107**(37): 16096-16100.

Ito Y and Ikeguchi M (2015) Mechanism of the alphabeta conformational change in F1-ATPase after ATP hydrolysis: free-energy simulations. *Biophysical Journal* **108**(1): 85-97.

Itoh H, Takahashi A, Adachi K et al. (2004) Mechanically driven ATP synthesis by F-1-ATPase. *Nature* **427**(6973): 465-468.

Iwata S, Ostermeier C, Ludwig B et al. (1995) Structure at 2.8-Angstrom Resolution of Cytochrome-C-Oxidase from Paracoccus-Denitrificans. *Nature* **376**(6542): 660-669.

Jagendorf AT and Uribe E (1966) Atp Formation Caused by Acid-Base Transition of Spinach Chloroplasts. *Proceedings of the National Academy of Sciences of the United States of America* **55**(1): 170-+.

Jensen JH (2015) Predicting accurate absolute binding energies in aqueous solution: thermodynamic considerations for electronic structure methods. *Physical Chemistry Chemical Physics* **17**(19): 12441-12451.

Jiang WP and Fillingame RH (1998) Interacting helical faces of subunits a and c in the F1F0 ATP synthase of Escherichia coli defined by disulfide cross-linking. *Proceedings of the National Academy of Sciences of the United States of America* **95**(12): 6607-6612.

Jockel P, Schmid M, Steuber J et al. (2000) A molecular coupling mechanism for the oxaloacetate decarboxylase Na+ pump as inferred from mutational analysis. *Biochemistry* **39**(9): 2307-2315.

Jones MV, Sahara Y, Dzubay JA et al. (1998) Defining affinity with the GABAA receptor. *J Neurosci* **18**(21): 8590-8604.

Jones PC, Hermolin J, Jiang WP et al. (2000) Insights into the rotary catalytic mechanism of F0F1 ATP synthase from the cross-linking of subunits b and c in the Escherichia coli enzyme. *Journal of Biological Chemistry* **275**(40): 31340-31346.

Joullie MM and Lassen KM (2010) Evolution of amide bond formation. *Arkivoc*: 189-250.

Junge W, Lill H and Engelbrecht S (1997) ATP synthase: an electrochemical transducer with rotatory mechanics. *Trends Biochem Sci* **22**(11): 420-423.

Junge W and Nelson N (2005) Structural biology. Nature's rotary electromotors. *Science* **308**(5722): 642-644.

Junge W, Panke O, Cherepanov DA et al. (2001) Inter-subunit rotation and elastic power transmission in F0F1-ATPase. *Febs Letters* **504**(3): 152-160.

Junge W, Sielaff H and Engelbrecht S (2009) Torque generation and elastic power transmission in the rotary F(O)F(1)-ATPase. *Nature* **459**(7245): 364-370.

Kaback HR (2005) Structure and mechanism of the lactose permease. *C R Biol* **328**(6): 557-567.

Kaback HR, Sahin-Toth M and Weinglass AB (2001) The kamikaze approach to membrane transport. *Nat Rev Mol Cell Biol* **2**(8): 610-620.

Kabaleeswaran V, Shen H, Symersky J et al. (2009) Asymmetric structure of the yeast F1 ATPase in the absence of bound nucleotides. *Journal of Biological Chemistry* **284**(16): 10546-10551.

Kaim G and Dimroth P (1998) A triple mutation in the a subunit of the Escherichia coli Propionigenium modestum F1F0 ATPase hybrid causes a switch from Na+ stimulation to Na+ inhibition. *Biochemistry* **37**(13): 4626-4634.

Kaim G and Dimroth P (1999) ATP synthesis by F-type ATP synthase is obligatorily dependent on the transmembrane voltage. *Embo Journal* **18**(15): 4118-4127.

Kaim G, Wehrle F, Gerike U et al. (1997) Molecular basis for the coupling ion selectivity of F1F0 ATP synthases: Probing the liganding groups for Na+ and Li+ in the c subunit of the ATP synthase from Propionigenium modestum. *Biochemistry* **36**(30): 9185-9194.

Kandori H, Furutani Y and Murata T (2015) Infrared spectroscopic studies on the V-ATPase. *Biochimica Et Biophysica Acta-Bioenergetics* **1847**(1): 134-141.

Kane PA (2006) The where, when, and how of organelle acidification by the yeast vacuolar H+-ATPase. *Microbiology and Molecular Biology Reviews* **70**(1): 177-+.

Karp DA, Gittis AG, Stahley MR et al. (2007) High apparent dielectric constant inside a protein reflects structural reorganization coupled to the ionization of an internal Asp. *Biophysical Journal* **92**(6): 2041-2053.

Kashket ER (1987) Bioenergetics of Lactic-Acid Bacteria - Cytoplasmic Ph and Osmotolerance. *Fems Microbiology Letters* **46**(3): 233-244.

Kastritis PL and Bonvin AMJJ (2013) On the binding affinity of macromolecular interactions: daring to ask why proteins interact. *Journal of the Royal Society Interface* **10**(79).

Kato HE, Inoue K, Abe-Yoshizumi R et al. (2015) Structural basis for Na+ transport mechanism by a light-driven Na+ pump. *Nature* **521**(7550): 48-U347.

Kawano-Kawada M, Iwaki T, Hosaka T et al. (2012) Mutagenesis of the residues forming an ion binding pocket of the NtpK subunit of Enterococcus hirae V-ATPase. *J Bacteriol* **194**(17): 4546-4549.

Kawano-Kawada M, Takahashi H, Igarashi K et al. (2011) Significance of the glutamate-139 residue of the V-type Na+-ATPase NtpK subunit in catalytic turnover linked with salt tolerance of Enterococcus hirae. *J Bacteriol* **193**(14): 3657-3661.

Kawasaki Y and Freire E (2011) Finding a better path to drug selectivity. *Drug Discovery Today* **16**(21-22): 985-990.

Kayalar C, Rosing J and Boyer PD (1977) An alternating site sequence for oxidative phosphorylation suggested by measurement of substrate binding patterns and exchange reaction inhibitions. *Journal of Biological Chemistry* **252**(8): 2486-2491.

Khorana HG (1953) The Chemistry of Carbodiimides. *Chemical Reviews* **53**(2): 145-166.

Kilambi KP and Gray JJ (2012) Rapid Calculation of Protein pK(a) Values Using Rosetta. *Biophysical Journal* **103**(3): 587-595.

Kinosita K, Adachi K and Itoh H (2004) Rotation of F-1-ATPase: How an ATP-driven molecular machine may work. *Annual Review of Biophysics and Biomolecular Structure* **33**(245-268.

Kinosita K, Jr., Yasuda R, Noji H et al. (2000) A rotary molecular motor that can work at near 100% efficiency. *Philos Trans R Soc Lond B Biol Sci* **355**(1396): 473-489.

Kinosita K, Yasuda R, Noji H et al. (1998) F-1-ATPase: A rotary motor made of a single molecule. *Cell* **93**(1): 21-24.

Klebe G (2015) Applying thermodynamic profiling in lead finding and optimization. *Nat Rev Drug Discov* **14**(2): 95-110.

Klionsky DJ, Brusilow WSA and Simoni RD (1984) Invivo Evidence for the Role of the Epsilon-Subunit as an Inhibitor of the Proton-Translocating Atpase of Escherichia-Coli. *J Bacteriol* **160**(3): 1055-1060.

Kluge C and Dimroth P (1993) Specific Protection by Na+ or Li+ of the F1f0-Atpase of Propionigenium-Modestum from the Reaction with Dicyclohexylcarbodiimide. *Journal of Biological Chemistry* **268**(20): 14557-14560.

Konings WN, Albers SV, Koning S et al. (2002) The cell membrane plays a crucial role in survival of bacteria and archaea in extreme environments. *Antonie Van Leeuwenhoek International Journal of General and Molecular Microbiology* **81**(1-4): 61-72.

Krah A, Pogoryelov D, Langer JD et al. (2010) Structural and energetic basis for H+ versus Na+ binding selectivity in ATP synthase Fo rotors. *Biochim Biophys Acta* **1797**(6-7): 763-772.

Krebs EG and Fischer EH (1955) Phosphorylase activity of skeletal muscle extracts. *Journal of Biological Chemistry* **216**(1): 113-120.

Krieg NR and Holt JG (1984) Bergey's manual of systematic bacteriology, 9th edn, vol 1. . *Williams and Wilkins, Baltimore London*.

Krueger S, Gregurick S, Shi Y et al. (2003) Entropic nature of the interaction between promoter bound CRP mutants and RNA polymerase. *Biochemistry* **42**(7): 1958-1968.

Kull FJ (2000) Motor proteins of the kinesin superfamily: structure and mechanism. *Essays Biochem* **35**(61-73.

Kunkel TA (1985) Rapid and efficient site-specific mutagenesis without phenotypic selection. *Proc Natl Acad Sci U S A* **82**(2): 488-492.

Kuroki R, Nitta K and Yutani K (1992) Thermodynamic changes in the binding of Ca2+ to a mutant human lysozyme (D86/92). Enthalpy-entropy compensation observed upon Ca2+ binding to proteins. *Journal of Biological Chemistry* **267**(34): 24297-24301.

Ladbury JE (2001) Isothermal titration calorimetry: application to structure-based drug design. *Thermochimica Acta* **380**(2): 209-215.

Ladbury JE, Klebe G and Freire E (2010) Adding calorimetric data to decision making in lead discovery: a hot tip. *Nat Rev Drug Discov* **9**(1): 23-27.

Lane N, Allen JF and Martin W (2010) How did LUCA make a living? Chemiosmosis in the origin of life. *Bioessays* **32**(4): 271-280.

Lane N and Martin WF (2012) The Origin of Membrane Bioenergetics. *Cell* **151**(7): 1406-1416.

Lau WCY and Rubinstein JL (2012) Subnanometre-resolution structure of the intact Thermus thermophilus H+-driven ATP synthase. *Nature* **481**(7380): 214-+.

Laubinger W, Deckershebestreit G, Altendorf K et al. (1990) A Hybrid Adenosine-Triphosphatase Composed of F1 of Escherichia-Coli and F0 of Propionigenium-Modestum Is a Functional Sodium-Ion Pump. *Biochemistry* **29**(23): 5458-5463.

Laubinger W and Dimroth P (1988) Characterization of the Atp Synthase of Propionigenium-Modestum as a Primary Sodium-Pump. *Biochemistry* **27**(19): 7531-7537.

Leavitt S and Freire E (2001) Direct measurement of protein binding energetics by isothermal titration calorimetry. *Current Opinion in Structural Biology* **11**(5): 560-566.

Lee LK, Stewart AG, Donohoe M et al. (2010) The structure of the peripheral stalk of Thermus thermophilus H+-ATPase/synthase. *Nature Structural & Molecular Biology* **17**(3): 373-U145.

Lemieux RU, Delbaere LTJ, Beierbeck H et al. (1991) Involvement of Water in Host-Guest Interactions. *Host-Guest Molecular Interactions : From Chemistry to Biology* **158**(231-248.

Lenaz G, Esposti MD and Castelli GP (1982) Dccd Inhibits Proton Translocation and Electron Flow at the 2nd Site of the Mitochondrial Respiratory-Chain. *Biochem Biophys Res Commun* **105**(2): 589-595.

Leone V, Pogoryelov D, Meier T et al. (2015) On the principle of ion selectivity in Na+/H+-coupled membrane proteins: Experimental and theoretical studies of an ATP synthase rotor. *Proceedings of the National Academy of Sciences of the United States of America* **112**(10): E1057-E1066.

Li J, Li C, Xiao W et al. (2008) Site-directed mutagenesis by combination of homologous recombination and DpnI digestion of the plasmid template in Escherichia coli. *Anal Biochem* **373**(2): 389-391.

Lichtenberger O, Woltersdorf J, Hering N et al. (2000) Electron energy loss spectra of carbodiimides. *Zeitschrift Fur Anorganische Und Allgemeine Chemie* **626**(9): 1881-1891.

Lietzan AD and St Maurice M (2014) Functionally diverse biotin-dependent enzymes with oxaloacetate decarboxylase activity. *Archives of Biochemistry and Biophysics* **544**(75-86.

Liptak MD, Gross KC, Seybold PG et al. (2002) Absolute pK(a) determinations for substituted phenols. *J Am Chem Soc* **124**(22): 6421-6427.

Liu GB, Xu H, Zhang L et al. (2011) Fe Binding Properties of Two Soybean (Glycine max L.) LEA4 Proteins Associated with Antioxidant Activity. *Plant and Cell Physiology* **52**(6): 994-1002.

Liu J, Fujisawa M, Hicks DB et al. (2009) Characterization of the Functionally Critical AXAXAXA and PXXEXXP Motifs of the ATP Synthase c-Subunit from an Alkaliphilic Bacillus. *Journal of Biological Chemistry* **284**(13): 8714-8725.

Long JC, Wang S and Vik SB (1998) Membrane topology of subunit a of the F1F0 ATP synthase as determined by labeling of unique cysteine residues. *Journal of Biological Chemistry* **273**(26): 16235-16240.

Loo DDF, Jiang X, Gorraitz E et al. (2013) Functional identification and characterization of sodium binding sites in Na symporters. *Proceedings of the National Academy of Sciences of the United States of America* **110**(47): E4557-E4566.

Luecke H, Richter HT and Lanyi JK (1998) Proton transfer pathways in bacteriorhodopsin at 2.3 Angstrom resolution. *Science* **280**(5371): 1934-1937.

Lymn RW and Taylor EW (1971) Mechanism of adenosine triphosphate hydrolysis by actomyosin. *Biochemistry* **10**(25): 4617-4624.

MacLean DM, Wong AYC, Fay AM et al. (2011) Cations But Not Anions Regulate the Responsiveness of Kainate Receptors. *Journal of Neuroscience* **31**(6): 2136-2144.

Madden DR (2002) The structure and function of glutamate receptor ion channels. *Nat Rev Neurosci* **3**(2): 91-101.

Malinen AM, Belogurov GA, Baykov AA et al. (2007) Na+-pyrophosphatase: a novel primary sodium pump. *Biochemistry* **46**(30): 8872-8878.

Mancusso R, Gregorio GG, Liu Q et al. (2012) Structure and mechanism of a bacterial sodium-dependent dicarboxylate transporter. *Nature* **491**(7425): 622-+.

Mao HZ and Weber J (2007) Identification of the beta(TP) site in the x-ray structure of F-1-ATPase as the high-affinity catalytic site. *Proceedings of the National Academy of Sciences of the United States of America* **104**(47): 18478-18483.

Masaike T, Koyama-Horibe F, Oiwa K et al. (2008) Cooperative three-step motions in catalytic subunits of F(1)-ATPase correlate with 80 degrees and 40 degrees substep rotations. *Nature Structural & Molecular Biology* **15**(12): 1326-1333.

Matthies D, Zhou W, Klyszejko AL et al. (2014) High-resolution structure and mechanism of an F/V-hybrid rotor ring in a Na(+)-coupled ATP synthase. *Nature Communications* **5**(5286.

Mayer F, Leone V, Langer JD et al. (2012) A c subunit with four transmembrane helices and one ion (Na+)-binding site in an archaeal ATP synthase: implications for c ring function and structure. *Journal of Biological Chemistry* **287**(47): 39327-39337.

Mayer F, Lim JK, Langer JD et al. (2015) Na+ transport by the A1AO-ATP synthase purified from Thermococcus onnurineus and reconstituted into liposomes. *Journal of Biological Chemistry* **290**(11): 6994-7002.

Mayer F and Muller V (2014) Adaptations of anaerobic archaea to life under extreme energy limitation. *Fems Microbiology Reviews* **38**(3): 449-472.

Mayer ML (2006) Glutamate receptors at atomic resolution. *Nature* **440**(7083): 456-462.

Mayer ML and Armstrong N (2004) Structure and function of glutamate receptor ion channels. *Annu Rev Physiol* **66**(161-181.

McIntosh LP, Hand G, Johnson PE et al. (1996) The pKa of the general acid/base carboxyl group of a glycosidase cycles during catalysis: a 13C-NMR study of bacillus circulans xylanase. *Biochemistry* **35**(31): 9958-9966.

McMillan DG, Ferguson SA, Dey D et al. (2011) A1Ao-ATP synthase of Methanobrevibacter ruminantium couples sodium ions for ATP synthesis under physiological conditions. *Journal of Biological Chemistry* **286**(46): 39882-39892.

Meier T and Dimroth P (2002) Intersubunit bridging by for the unusual stability Na+ ions as a rationale of the c-rings of Na+-translocating F1F0 ATP synthases. *EMBO Rep* **3**(11): 1094-1098.

Meier T, Krah A, Bond PJ et al. (2009) Complete Ion-Coordination Structure in the Rotor Ring of Na+-Dependent F-ATP Synthases. *J Mol Biol* **391**(2): 498-507.

Meier T, Matthey U, von Ballmoos C et al. (2003) Evidence for structural integrity in the undecameric c-rings isolated from sodium ATP synthases. *J Mol Biol* **325**(2): 389-397.

Meier T, Polzer P, Diederichs K et al. (2005) Structure of the rotor ring of F-type Na+-ATPase from Ilyobacter tartaricus. *Science* **308**(5722): 659-662.

Menz RI, Walker JE and Leslie AG (2001) Structure of bovine mitochondrial F(1)-ATPase with nucleotide bound to all three catalytic sites: implications for the mechanism of rotary catalysis. *Cell* **106**(3): 331-341.

Miroux B and Walker JE (1996) Over-production of proteins in Escherichia coli: Mutant hosts that allow synthesis of some membrane proteins and globular proteins at high levels. *J Mol Biol* **260**(3): 289-298.

Mitchell P (1961) Coupling of phosphorylation to electron and hydrogen transfer by a chemi-osmotic type of mechanism. *Nature* **191**(144-148.

Mitome N, Ono S, Sato H et al. (2010) Essential arginine residue of the F(o)-a subunit in F(o)F(1)-ATP synthase has a role to prevent the proton shortcut without c-ring rotation in the F(o) proton channel. *Biochemical Journal* **430**(1): 171-177.

Mizutani K, Yamamoto M, Suzuki K et al. (2011) Structure of the rotor ring modified with N,N'-dicyclohexylcarbodiimide of the Na+-transporting vacuolar ATPase. *Proc Natl Acad Sci U S A* **108**(33): 13474-13479.

Muench SP, Huss M, Song CF et al. (2009) Cryo-electron microscopy of the vacuolar ATPase motor reveals its mechanical and regulatory complexity. *J Mol Biol* **386**(4): 989-999.

Muench SP, Trinick J and Harrison MA (2011) Structural divergence of the rotary ATPases. *Q Rev Biophys* **44**(3): 311-356.

Mulkidjanian AY, Bychkov AY, Dibrova DV et al. (2012) Origin of first cells at terrestrial, anoxic geothermal fields. *Proceedings of the National Academy of Sciences of the United States of America* **109**(14): E821-E830.

Mulkidjanian AY, Galperin MY, Makarova KS et al. (2008) Evolutionary primacy of sodium bioenergetics. *Biol Direct* **3**(13.

Muller V, Aufurth S and Rahlfs S (2001) The Na(+) cycle in Acetobacterium woodii: identification and characterization of a Na(+) translocating F(1)F(0)-ATPase with a mixed oligomer of 8 and 16 kDa proteolipids. *Biochim Biophys Acta* **1505**(1): 108-120.

Muller V and Gruber G (2003) ATP synthases: structure, function and evolution of unique energy converters. *Cell Mol Life Sci* **60**(3): 474-494.

Muller V, Imkamp F, Biegel E et al. (2008) Discovery of a ferredoxin:NAD+-oxidoreductase (Rnf) in Acetobacterium woodii: a novel potential coupling site in acetogens. *Ann N Y Acad Sci* **1125**(137-146.

Muller V, Lemker T, Lingl A et al. (2005) Bioenergetics of archaea: ATP synthesis under harsh environmental conditions. *J Mol Microbiol Biotechnol* **10**(2-4): 167-180.

Murata T, Igarashi K, Kakinuma Y et al. (2000) Na+ binding of V-type Na+-ATPase in Enterococcus hirae. *Journal of Biological Chemistry* **275**(28): 21780-21780.

Murata T, Kawano M, Igarashi K et al. (2001) Catalytic properties of Na+-translocating V-ATPase in Enterococcus hirae. *Biochimica Et Biophysica Acta-Bioenergetics* **1505**(1): 75-81.

Murata T, Takase K, Yamato I et al. (1997) Purification and reconstitution of Na+-translocating vacuolar ATPase from Enterococcus hirae. *Journal of Biological Chemistry* **272**(40): 24885-24890.

Murata T, Takase K, Yamato I et al. (1999) Properties of the V0V1 Na+-ATPase from Enterococcus hirae and its V-0 moiety. *Journal of Biochemistry* **125**(2): 414-421.

Murata T, Yamato I, Kakinuma Y et al. (2005) Structure of the rotor of the V-type Na+-ATPase from Enterococcus

hirae. *Science* **308**(5722): 654-659.

Murata T, Yamato I, Kakinuma Y et al. (2008) Ion binding and selectivity of the rotor ring of the Na+-transporting V-ATPase. *Proceedings of the National Academy of Sciences of the United States of America* **105**(25): 8607-8612.

Murtazina R, Booth BJ, Bullis BL et al. (2001) Functional analysis of polar amino-acid residues in membrane associated regions of the NHE1 isoform of the mammalian Na+/H+ exchanger. *European Journal of Biochemistry* **268**(17): 4674-4685.

Nakajo K, Komori R, Ishikawa S et al. (2006) Resistance to acidic and alkaline environments in the endodontic pathogen Enterococcus faecalis. *Oral Microbiology and Immunology* **21**(5): 283-288.

Nalecz MJ, Casey RP and Azzi A (1986) Use of N,N'-Dicyclohexylcarbodiimide to Study Membrane-Bound Enzymes. *Methods in Enzymology* **125**(86-108.

Nam K, Pu JZ and Karplus M (2014) Trapping the ATP binding state leads to a detailed understanding of the F-1-ATPase mechanism. *Proceedings of the National Academy of Sciences of the United States of America* **111**(50): 17851-17856.

Negrin RS, Foster DL and Fillingame RH (1980) Energy-transducing H+-ATPase of Escherichia coli. Reconstitution of proton translocation activity of the intrinsic membrane sector. *Journal of Biological Chemistry* **255**(12): 5643-5648.

Neumann S, Matthey U, Kaim G et al. (1998) Purification and properties of the F1F0 ATPase of Ilyobacter tartaricus, a sodium ion pump. *J Bacteriol* **180**(13): 3312-3316.

Nicholls D (2002) Mitochondrial bioenergetics, aging, and aging-related disease. *Sci Aging Knowledge Environ* **2002**(31): pe12.

Nielsen JE and McCammon JA (2003) Calculating pKa values in enzyme active sites. *Protein Sci* **12**(9): 1894-1901.

Nishizaka T, Oiwa K, Noji H et al. (2004) Chemomechanical coupling in F1-ATPase revealed by simultaneous observation of nucleotide kinetics and rotation. *Nature Structural & Molecular Biology* **11**(2): 142-148.

Noji H, Yasuda R, Yoshida M et al. (1997) Direct observation of the rotation of F1-ATPase. *Nature* **386**(6622): 299-302.

Noskov SY, Berneche S and Roux B (2004) Control of ion selectivity in potassium channels by electrostatic and dynamic properties of carbonyl ligands. *Nature* **431**(7010): 830-834.

Noskov SY and Roux B (2006) Ion selectivity in potassium channels. *Biophys Chem* **124**(3): 279-291.

Noskov SY and Roux B (2008) Control of ion selectivity in LeuT: two Na+ binding sites with two different mechanisms. *J Mol Biol* **377**(3): 804-818.

Novy R, Drott D, Yaeger K et al. (2001) Overcoming the codon bias of E. coli for enhanced protein expression. *Innovations* **12**(1-3.

O'Brien R, J. E. Ladbury, Chowdry B. Z. (2001) sothermal titration calorimetry of biomolecules. *In S. E. Harding and B. Z. Chowdry (Eds.) Protein-Ligand Interactions: hydrodynamics and calorimetry. Oxford University Press, Oxford*: 263-286.

Oberfeld B (2006) F1Fo ATP synthase: identification of a plug within the c-ring and heterologous expression of a

sodium-translocating enzyme. *PhD Thesis, ETH Zurich, Switzerland.*

Ohtaka H and Freire E (2005) Adaptive inhibitors of the HIV-1 protease. *Prog Biophys Mol Biol* **88**(2): 193-208.

Okazaki K and Hummer G (2013) Phosphate release coupled to rotary motion of F1-ATPase. *Proc Natl Acad Sci U S A* **110**(41): 16468-16473.

Okuno D, Fujisawa R, Iino R et al. (2008) Correlation between the conformational states of F-1-ATPase as determined from its crystal structure and single-molecule rotation. *Proceedings of the National Academy of Sciences of the United States of America* **105**(52): 20722-20727.

Olsson TSG, Williams MA, Pitt WR et al. (2008) The Thermodynamics of Protein-Ligand Interaction and Solvation: Insights for Ligand Design. *J Mol Biol* **384**(4): 1002-1017.

Oster G and Wang HY (1999) ATP synthase: two motors, two fuels. *Structure with Folding & Design* **7**(4): R67-R72.

Pace CN, Grimsley GR and Scholtz JM (2009) Protein ionizable groups: pK values and their contribution to protein stability and solubility. *Journal of Biological Chemistry* **284**(20): 13285-13289.

Pan AC, Borhani DW, Dror RO et al. (2013) Molecular determinants of drug-receptor binding kinetics. *Drug Discovery Today* **18**(13-14): 667-673.

Payandeh J, El-Din TMG, Scheuer T et al. (2012) Crystal structure of a voltage-gated sodium channel in two potentially inactivated states. *Nature* **486**(7401): 135-U166.

PebayPeyroula E, Rummel G, Rosenbusch JP et al. (1997) X-ray structure of bacteriorhodopsin at 2.5 angstroms from microcrystals grown in lipidic cubic phases. *Science* **277**(5332): 1676-1681.

Peng GH, Bostina M, Radermacher M et al. (2006) Biochemical and electron microscopic characterization of the F1F0 ATP Synthase from the hyperthermophilic eubacterium Aquifex aeolicus. *Febs Letters* **580**(25): 5934-5940.

Pennington RM and Fisher RR (1981) Dicyclohexylcarbodiimide Modification of Bovine Heart Mitochondrial Transhydrogenase. *Journal of Biological Chemistry* **256**(17): 8963-8969.

Periole X, Ceruso MA and Mehler EL (2004) Acid-base equilibria in rhodopsin: Dependence of the protonation state of Glu134 on its environment. *Biochemistry* **43**(22): 6858-6864.

Pisa KY, Huber H, Thomm M et al. (2007) A sodium ion-dependent A(1)A(o) ATP synthase from the hyperthermophilic archaeon Pyrococcus furiosus. *Febs Journal* **274**(15): 3928-3938.

Pisa KY, Weidner C, Maischak H et al. (2007) The coupling ion in the methanoarchaeal ATP synthases: H+ vs. Na+ in the A(1)A(0) ATP synthase from the archaeon Methanosarcina mazei Go1. *Fems Microbiology Letters* **277**(1): 56-63.

Platzer G, Okon M and McIntosh LP (2014) pH-dependent random coil (1)H, (13)C, and (15)N chemical shifts of the ionizable amino acids: a guide for protein pK a measurements. *J Biomol NMR* **60**(2-3): 109-129.

Plested AJR, Vijayan R, Biggin PC et al. (2008) Molecular basis of kainate receptor modulation by sodium. *Neuron* **58**(5): 720-735.

Poehlein A, Schmidt S, Kaster AK et al. (2012) An Ancient Pathway Combining Carbon Dioxide Fixation with the Generation and Utilization of a Sodium Ion Gradient for ATP Synthesis. *PLoS One* **7**(3).

Pogoryelov D, Klyszejko AL, Krasnoselska GO et al. (2012) Engineering rotor ring stoichiometries in the ATP synthase. *Biochimica Et Biophysica Acta-Bioenergetics* **1817**(S21-S21.

Pogoryelov D, Krah A, Langer JD et al. (2010) Microscopic rotary mechanism of ion translocation in the F-0 complex of ATP synthases. *Nat Chem Biol* **6**(12): 891-899.

Pogoryelov D, Yildiz O, Faraldo-Gomez JD et al. (2009) High-resolution structure of the rotor ring of a proton-dependent ATP synthase. *Nature Structural & Molecular Biology* **16**(10): 1068-U1088.

Pogoryelov D, Yu JS, Meier T et al. (2005) The c(15) ring of the Spirulina platensis F-ATP synthase: F-1/F-0 symmetry mismatch is not obligatory. *EMBO Rep* **6**(11): 1040-1044.

Pohorille A and Deamer D (2009) Self-assembly and function of primitive cell membranes. *Research in Microbiology* **160**(7): 449-456.

Portman KL, Long J, Carr S et al. (2014) Enthalpy/Entropy Compensation Effects from Cavity Desolvation Underpin Broad Ligand Binding Selectivity for Rat Odorant Binding Protein 3. *Biochemistry* **53**(14): 2371-2379.

Pougeois R, Satre M and Vignais PV (1979) Reactivity of Mitochondrial F1-Atpase to Dicyclohexylcarbodiimide - Inactivation and Binding-Studies. *Biochemistry* **18**(8): 1408-1413.

Preiss L, Klyszejko AL, Hicks DB et al. (2013) The c-ring stoichiometry of ATP synthase is adapted to cell physiological requirements of alkaliphilic Bacillus pseudofirmus OF4. *Proceedings of the National Academy of Sciences of the United States of America* **110**(19): 7874-7879.

Preiss L, Langer JD, Hicks DB et al. (2014) The c-ring ion binding site of the ATP synthase from Bacillus pseudofirmus OF4 is adapted to alkaliphilic lifestyle. *Molecular Microbiology* **92**(5): 973-984.

Preiss L, Yildiz O, Hicks DB et al. (2010) A New Type of Proton Coordination in an F1Fo-ATP Synthase Rotor Ring. *Plos Biology* **8**(8).

Quick M, Winther AML, Shi L et al. (2009) Binding of an octylglucoside detergent molecule in the second substrate (S2) site of LeuT establishes an inhibitor-bound conformation. *Proceedings of the National Academy of Sciences of the United States of America* **106**(14): 5563-5568.

Rajarathnam K and Rosgen J (2014) Isothermal titration calorimetry of membrane proteins - Progress and challenges. *Biochimica Et Biophysica Acta-Biomembranes* **1838**(1): 69-77.

Rastogi VK and Girvin ME (1999) Structural changes linked to proton translocation by subunit c of the ATP synthase. *Nature* **402**(6759): 263-268.

Rea SL, Graham BH, Nakamaru-Ogiso E et al. (2010) Bacteria, yeast, worms, and flies: exploiting simple model organisms to investigate human mitochondrial diseases. *Dev Disabil Res Rev* **16**(2): 200-218.

Rees DM, Leslie AGW and Walker JE (2009) The structure of the membrane extrinsic region of bovine ATP synthase. *Proceedings of the National Academy of Sciences of the United States of America* **106**(51): 21597-21601.

Rees DM, Montgomery MG, Leslie AGW et al. (2012) Structural evidence of a new catalytic intermediate in the pathway of ATP hydrolysis by F-1-ATPase from bovine heart mitochondria. *Proceedings of the National Academy of Sciences of the United States of America* **109**(28): 11139-11143.

Reijenga J, van Hoof A, van Loon A et al. (2013) Development of Methods for the Determination of pKa Values.

Anal Chem Insights **8**(53-71.

Rekharsky MV and Inoue Y (1998) Complexation thermodynamics of cyclodextrins. *Chemical Reviews* **98**(5): 1875-1917.

Revington M, McLachlin DT, Shaw GS et al. (1999) The dimerization domain of the b subunit of the Escherichia coli F(1)F(0)-ATPase. *Journal of Biological Chemistry* **274**(43): 31094-31101.

Rivera-Torres IO, Krueger-Koplin RD, Hicks DB et al. (2004) pKa of the essential Glu54 and backbone conformation for subunit c from the H+-coupled F1F0 ATP synthase from an alkaliphilic Bacillus. *Febs Letters* **575**(1-3): 131-135.

Rosing J and Slater EC (1972) The value of G degrees for the hydrolysis of ATP. *Biochim Biophys Acta* **267**(2): 275-290.

Roskoski R, Jr. (2015) A historical overview of protein kinases and their targeted small molecule inhibitors. *Pharmacol Res* **100**(1-23.

Roy A, Hutcheon ML, Duncan TM et al. (2012) Improved crystallization of Escherichia coli ATP synthase catalytic complex (F1) by introducing a phosphomimetic mutation in subunit epsilon. *Acta Crystallogr Sect F Struct Biol Cryst Commun* **68**(Pt 10): 1229-1233.

Ruben AJ, Kiso Y and Freire E (2006) Overcoming roadblocks in lead optimization: A thermodynamic perspective. *Chemical Biology & Drug Design* **67**(1): 2-4.

Ruhmann E, Betz M, Fricke M et al. (2015) Thermodynamic signatures of fragment binding: Validation of direct versus displacement ITC titrations. *Biochim Biophys Acta* **1850**(4): 647-656.

Russell MJ, Daniel RM and Hall AJ (1993) On the Emergence of Life Via Catalytic Iron-Sulfide Membranes. *Terra Nova* **5**(4): 343-347.

Russell MJ, Daniel RM, Hall AJ et al. (1994) A Hydrothermally Precipitated Catalytic Iron Sulfide Membrane as a First Step toward Life. *Journal of Molecular Evolution* **39**(3): 231-243.

Russell MJ and Hall AJ (1997) The emergence of life from iron monosulphide bubbles at a submarine hydrothermal redox and pH front. *J Geol Soc London* **154**(3): 377-402.

Russell MJ, Hall AJ, Cairnssmith AG et al. (1988) Submarine Hot Springs and the Origin of Life. *Nature* **336**(6195): 117-117.

Russell MJ, Hall AJ and Turner D (1989) In vitro growth of iron sulphide chimneys: possible culture chambers for origin-of-life experiments. *Terra Nova* **1**(3): 238-241.

Ryde U (2014) A fundamental view of enthalpy-entropy compensation. *Medchemcomm* **5**(9): 1324-1336.

Sambongi Y, Iko Y, Tanabe M et al. (1999) Mechanical rotation of the c subunit oligomer in ATP synthase (F0F1): Direct observation. *Science* **286**(5445): 1722-1724.

Sambrook J, Maccallum P and Russel D (2001) Molecular cloning: A laboratory manual, 3nd ed. *Cold Springs Harbour Press, NY, ISBN 0-87969-577-3*: 1ß2344.

Sanker S, Campbell HA and Kent C (2001) Negative cooperativity of substrate binding but not enzyme activity in wild-type and mutant forms of CTP:glycerol-3-phosphate cytidylyltransferase. *Journal of Biological Chemistry*

276(41): 37922-37928.

Sapra R, Bagramyan K and Adams MWW (2003) A simple energy-conserving system: Proton reduction coupled to proton translocation. *Proceedings of the National Academy of Sciences of the United States of America* **100**(13): 7545-7550.

Saroussi S, Schushan M, Ben-Tal N et al. (2012) Structure and Flexibility of the C-Ring in the Electromotor of Rotary FoF1-ATPase of Pea Chloroplasts. *PLoS One* **7**(9).

Sarver RW, Peevers J, Cody WL et al. (2007) Binding thermodynamics of substituted diaminopyrimidine renin inhibitors. *Anal Biochem* **360**(1): 30-40.

Schink B (1984) Fermentation of Tartrate Enantiomers by Anaerobic-Bacteria, and Description of 2 New-Species of Strict Anaerobes, Ruminococcus-Pasteurii and Ilyobacter-Tartaricus. *Arch Microbiol* **139**(4): 409-414.

Schlegel K, Leone V, Faraldo-Gomez JD et al. (2012) Promiscuous archaeal ATP synthase concurrently coupled to Na+ and H+ translocation. *Proceedings of the National Academy of Sciences of the United States of America* **109**(3): 947-952.

Schlegel K and Muller V (2013) Evolution of Na+ and H+ bioenergetics in methanogenic archaea. *Biochemical Society Transactions* **41**(421-426.

Schlessinger A, Sun NN, Colas C et al. (2014) Determinants of Substrate and Cation Transport in the Human Na+/Dicarboxylate Cotransporter NaDC3. *Journal of Biological Chemistry* **289**(24): 16998-17008.

Schliwa M and Woehlke G (2003) Molecular motors. *Nature* **422**(6933): 759-765.

Schmehl M, Jahn A, Meyer zu Vilsendorf A et al. (1993) Identification of a new class of nitrogen fixation genes in Rhodobacter capsulatus: a putative membrane complex involved in electron transport to nitrogenase. *Mol Gen Genet* **241**(5-6): 602-615.

Schreiber G, Frisch C and Fersht AR (1997) The role of Glu73 of barnase in catalysis and the binding of barstar. *J Mol Biol* **270**(1): 111-122.

Schulz S, Iglesias-Cans M, Krah A et al. (2013) A New Type of Na+-Driven ATP Synthase Membrane Rotor with a Two-Carboxylate Ion-Coupling Motif. *Plos Biology* **11**(6).

Schutz CN and Warshel A (2001) What are the dielectric "constants" of proteins and how to validate electrostatic models? *Proteins-Structure Function and Bioinformatics* **44**(4): 400-417.

Schwarz FP, Puri KD, Bhat RG et al. (1993) Thermodynamics of Monosaccharide Binding to Concanavalin-a, Pea (Pisum-Sativum) Lectin, and Lentil (Lens-Culinaris) Lectin. *Journal of Biological Chemistry* **268**(11): 7668-7677.

Schwem BE and Fillingame RH (2006) Cross-linking between helices within subunit a of Escherichia coli ATP synthase defines the transmembrane packing of a four-helix bundle. *Journal of Biological Chemistry* **281**(49): 37861-37867.

Sebald W, Machleidt W and Wachter E (1980) N,N'-Dicyclohexylcarbodiimide Binds Specifically to a Single Glutamyl Residue of the Proteolipid Subunit of the Mitochondrial Adenosine-Triphosphatases from Neurospora-Crassa and Saccharomyces-Cerevisiae. *Proceedings of the National Academy of Sciences of the United States of America-Biological Sciences* **77**(2): 785-789.

Setny P, Baron R and McCammon JA (2010) How Can Hydrophobic Association Be Enthalpy Driven? *Journal of*

Chemical Theory and Computation **6**(9): 2866-2871.

Shannon RD (1976) Revised Effective Ionic-Radii and Systematic Studies of Interatomic Distances in Halides and Chalcogenides. *Acta Crystallographica Section A* **32**(Sep1): 751-767.

Sharp K (2001) Entropy-enthalpy compensation: Fact or artifact? *Protein Science* **10**(3): 661-667.

Shimabukuro K, Yasuda R, Muneyuki E et al. (2003) Catalysis and rotation of F-1 motor: Cleavage of ATP at the catalytic site occurs in 1 ms before 40 degrees substep rotation. *Proceedings of the National Academy of Sciences of the United States of America* **100**(25): 14731-14736.

Shock E and Canovas P (2010) The potential for abiotic organic synthesis and biosynthesis at seafloor hydrothermal systems. *Geofluids* **10**(1-2): 161-192.

Sielaff H and Borsch M (2013) Twisting and subunit rotation in single FOF1-ATP synthase. *Philosophical Transactions of the Royal Society B-Biological Sciences* **368**(1611).

Signor L and Boeri Erba E (2013) Matrix-assisted laser desorption/ionization time of flight (MALDI-TOF) mass spectrometric analysis of intact proteins larger than 100 kDa. *J Vis Exp* 79).

Sigurskjold BW and Bundle DR (1992) Thermodynamics of Oligosaccharide Binding to a Monoclonal-Antibody Specific for a Salmonella O-Antigen Point to Hydrophobic Interactions in the Binding-Site. *Journal of Biological Chemistry* **267**(12): 8371-8376.

Skulachev VP (1989) The Sodium Cycle - a Novel Type of Bacterial Energetics. *J Bioenerg Biomembr* **21**(6): 635-647.

Skulachev VP (1991) Chemiosmotic Systems in Bioenergetics - H+-Cycles and Na+-Cycles. *Bioscience Reports* **11**(6): 387-444.

Skulachev VP (1992) The Laws of Cell Energetics. *European Journal of Biochemistry* **208**(2): 203-209.

Solioz M (1984) Dicyclohexylcarbodiimide as a Probe for Proton Translocating Enzymes. *Trends Biochem Sci* **9**(7): 309-312.

Solioz M and Davies K (1994) Operon of Vacuolar-Type Na+-Atpase of Enterococcus-Hirae. *Journal of Biological Chemistry* **269**(13): 9453-9459.

Speelmans G, Poolman B, Abee T et al. (1993) Energy Transduction in the Thermophilic Anaerobic Bacterium Clostridium-Fervidus Is Exclusively Coupled to Sodium-Ions. *Proceedings of the National Academy of Sciences of the United States of America* **90**(17): 7975-7979.

Stewart AG, Sobti M, Harvey RP et al. (2013) Rotary ATPases: models, machine elements and technical specifications. *Bioarchitecture* **3**(1): 2-12.

Stock D, Gibbons C, Arechaga I et al. (2000) The rotary mechanism of ATP synthase. *Curr Opin Struct Biol* **10**(6): 672-679.

Stock D, Leslie AGW and Walker JE (1999) Molecular architecture of the rotary motor in ATP synthase. *Science* **286**(5445): 1700-1705.

Strupat K (2005) Molecular weight determination of peptides and proteins by ESI and MALDI. *Methods Enzymol* **405**(1-36.

Studer R, Dahinden P, Wang WW et al. (2007) Crystal structure of the carboxyltransferase domain of the oxaloacetate decarboxylase Na+ pump from Vibrio cholerae. *J Mol Biol* **367**(2): 547-557.

Surin S, Cubonova L, Majernik AI et al. (2007) Isolation and characterization of an amiloride-resistant mutant of Methanothermobacter thermautotrophicus possessing a defective Na+/H+ antiport. *Fems Microbiology Letters* **269**(2): 301-308.

Symersky J, Pagadala V, Osowski D et al. (2012) Structure of the c(10) ring of the yeast mitochondrial ATP synthase in the open conformation. *Nature Structural & Molecular Biology* **19**(5): 485-491, S481.

Takase K, Yamato I and Kakinuma Y (1993) Cloning and sequencing of the genes coding for the A and B subunits of vacuolar-type Na(+)-ATPase from Enterococcus hirae. Coexistence of vacuolar- and F0F1-type ATPases in one bacterial cell. *Journal of Biological Chemistry* **268**(16): 11610-11616.

Tamura N, Konishi S, Iwaki S et al. (2001) Complete cysteine-scanning mutagenesis and site-directed chemical modification of the Tn10-encoded metal-tetracycline/H+ antiporter. *Journal of Biological Chemistry* **276**(23): 20330-20339.

Terlau H, Heinemann SH, Stuhmer W et al. (1991) Mapping the site of block by tetrodotoxin and saxitoxin of sodium channel II. *Febs Letters* **293**(1-2): 93-96.

Thauer RK, Kaster AK, Seedorf H et al. (2008) Methanogenic archaea: ecologically relevant differences in energy conservation. *Nat Rev Microbiol* **6**(8): 579-591.

Thomas M, Jayatilaka D and Corry B (2007) The predominant role of coordination number in potassium channel selectivity. *Biophysical Journal* **93**(8): 2635-2643.

Thomas M, Jayatilaka D and Corry B (2013) An entropic mechanism of generating selective ion binding in macromolecules. *PLoS Comput Biol* **9**(2): e1002914.

Toei M and Noji H (2013) Single-molecule analysis of F0F1-ATP synthase inhibited by N,N-dicyclohexylcarbodiimide. *Journal of Biological Chemistry* **288**(36): 25717-25726.

Toei M, Saum R and Forgac M (2010) Regulation and isoform function of the V-ATPases. *Biochemistry* **49**(23): 4715-4723.

Tsunoda SP, Aggeler R, Noji H et al. (2000) Observations of rotation within the FOFl-ATP synthase: deciding between rotation of the F(O)c subunit ring and artifact. *Febs Letters* **470**(3): 244-248.

Tsunoda SP, Aggeler R, Yoshida M et al. (2001) Rotation of the c subunit oligomer in fully functional F1Fo ATP synthase. *Proc Natl Acad Sci U S A* **98**(3): 898-902.

Uchihashi T, Iino R, Ando T et al. (2011) High-Speed Atomic Force Microscopy Reveals Rotary Catalysis of Rotorless F-1-ATPase. *Science* **333**(6043): 755-758.

Ueno H, Minagawa Y, Hara M et al. (2014) Torque generation of Enterococcus hirae V-ATPase. *Journal of Biological Chemistry* **289**(45): 31212-31223.

Ueno H, Suzuki T, Kinosita K et al. (2005) ATP-driven stepwise rotation of FOF1,-ATP synthase. *Proceedings of the National Academy of Sciences of the United States of America* **102**(5): 1333-1338.

Unemoto T and Hayashi M (1979) Nadh - Quinone Oxidoreductase as a Site of Na+-Dependent Activation in the

Respiratory-Chain of Marine Vibrio-Alginolyticus. *Journal of Biochemistry* **85**(6): 1461-1467.

Valiyaveetil F, Hermolin J and Fillingame RH (2002) pH dependent inactivation of solubilized F1F0 ATP synthase by dicyclohexylcarbodiimide: pK(a) of detergent unmasked aspartyl-61 in Escherichia coli subunit c. *Biochimica Et Biophysica Acta-Bioenergetics* **1553**(3): 296-301.

Valiyaveetil FI and Fillingame RH (1997) On the role of Arg-210 and Glu-219 of subunit a in proton translocation by the Escherichia coli F0F1-ATP synthase. *Journal of Biological Chemistry* **272**(51): 32635-32641.

Valiyaveetil FI and Fillingame RH (1998) Transmembrane topography of subunit a in the Escherichia coli F1F0 ATP synthase. *Journal of Biological Chemistry* **273**(26): 16241-16247.

van de Vossenberg JL, Ubbink-Kok T, Elferink MG et al. (1995) Ion permeability of the cytoplasmic membrane limits the maximum growth temperature of bacteria and archaea. *Molecular Microbiology* **18**(5): 925-932.

Varma S and Rempe SB (2007) Tuning ion coordination architectures to enable selective partitioning. *Biophysical Journal* **93**(4): 1093-1099.

Verkhovsky MI and Bogachev AV (2010) Sodium-translocating NADH:quinone oxidoreductase as a redox-driven ion pump. *Biochim Biophys Acta* **1797**(6-7): 738-746.

Vgenopoulou I, Gemperli AC and Steuber J (2006) Specific modification of a Na+ binding site in NADH : quinone oxidoreductase from Klebsiella pneumoniae with dicyclohexylcarbodiimide. *J Bacteriol* **188**(9): 3264-3272.

Vijayan R, Plested AJ, Mayer ML et al. (2009) Selectivity and cooperativity of modulatory ions in a neurotransmitter receptor. *Biophysical Journal* **96**(5): 1751-1760.

Vik SB and Antonio BJ (1994) A mechanism of proton translocation by F1F0 ATP synthases suggested by double mutants of the a subunit. *Journal of Biological Chemistry* **269**(48): 30364-30369.

Vik SB, Patterson AR and Antonio BJ (1998) Insertion scanning mutagenesis of subunit a of the F1F0 ATP synthase near His245 and implications on gating of the proton channel. *Journal of Biological Chemistry* **273**(26): 16229-16234.

Vollmar M, Schlieper D, Winn M et al. (2009) Structure of the c(14) Rotor Ring of the Proton Translocating Chloroplast ATP Synthase. *Journal of Biological Chemistry* **284**(27): 18228-18235.

von Ballmoos C, Cook GM and Dimroth P (2008) Unique rotary ATP synthase and its biological diversity. . *Annu Rev Biophys* **37**(43-64.

von Ballmoos C and Dimroth P (2007) Two distinct proton binding sites in the ATP synthase family. *Biochemistry* **46**(42): 11800-11809.

von Ballmoos C, Wiedenmann A and Dimroth P (2009) Essentials for ATP Synthesis by F1F0 ATP Synthases. *Annual Review of Biochemistry* **78**(649-672.

Vonck J, Pisa KY, Morgner N et al. (2009) Three-dimensional structure of A1A0 ATP synthase from the hyperthermophilic archaeon Pyrococcus furiosus by electron microscopy. *Journal of Biological Chemistry* **284**(15): 10110-10119.

Vorburger T, Ebneter JZ, Wiedenmann A et al. (2008) Arginine-induced conformational change in the c-ring/a-subunit interface of ATP synthase. *Febs Journal* **275**(9): 2137-2150.

Wada W, Long JC, Zhang D et al. (1999) A novel labeling approach supports the five-transmembrane model of subunit a of the Escherichia coli ATP synthase. *J. Biol. Chemical Biology & Drug Design* **274**(17353–17357.

Walker JE (2013) The ATP synthase: the understood, the uncertain and the unknown. *Biochem Soc Trans* **41**(1): 1-16.

Walker JE and Dickson VK (2006) The peripheral stalk of the mitochondrial ATP synthase. *Biochim Biophys Acta* **1757**(5-6): 286-296.

Warshel A and Aqvist J (1991) Electrostatic energy and macromolecular function. *Annu Rev Biophys Biophys Chem* **20**(267-298.

Watanabe R, Iino R and Noji H (2010) Phosphate release in F-1-ATPase catalytic cycle follows ADP release. *Nat Chem Biol* **6**(11): 814-820.

Watanabe R, Iino R, Shimabukuro K et al. (2008) Temperature-sensitive reaction intermediate of F-1-ATPase. *EMBO Rep* **9**(1): 84-90.

Watt IN, Montgomery MG, Runswick MJ et al. (2010) Bioenergetic cost of making an adenosine triphosphate molecule in animal mitochondria. *Proceedings of the National Academy of Sciences of the United States of America* **107**(39): 16823-16827.

Weber J and Senior AE (2000) ATP synthase: what we know about ATP hydrolysis and what we do not know about ATP synthesis. *Biochimica Et Biophysica Acta-Bioenergetics* **1458**(2-3): 300-309.

Weber J, Wilkemounts S, Lee RSF et al. (1993) Specific Placement of Tryptophan in the Catalytic Sites of Escherichia-Coli F(1)-Atpase Provides a Direct Probe of Nucleotide-Binding - Maximal Atp Hydrolysis Occurs with 3 Sites Occupied. *Journal of Biological Chemistry* **268**(27): 20126-20133.

Welte C and Deppenmeier U (2014) Bioenergetics and anaerobic respiratory chains of aceticlastic methanogens. *Biochimica Et Biophysica Acta-Bioenergetics* **1837**(7): 1130-1147.

Wilkens S and Capaldi RA (1998) ATP synthase's second stalk comes into focus. *Nature* **393**(6680): 29-29.

Wiseman T, Williston S, Brandts JF et al. (1989) Rapid Measurement of Binding Constants and Heats of Binding Using a New Titration Calorimeter. *Anal Biochem* **179**(1): 131-137.

Wittig I and Schagger H (2008) Structural organization of mitochondrial ATP synthase. *Biochimica Et Biophysica Acta-Bioenergetics* **1777**(S10-S10.

Wohlert D, Kuhlbrandt W and Yildiz O (2014) Structure and substrate ion binding in the sodium/proton antiporter PaNhaP. *Elife* **3**(e03579.

Yamashita A, Singh SK, Kawate T et al. (2005) Crystal structure of a bacterial homologue of Na+/Cl--dependent neurotransmitter transporters. *Nature* **437**(7056): 215-223.

Yang J, Ellinor PT, Sather WA et al. (1993) Molecular determinants of Ca2+ selectivity and ion permeation in L-type Ca2+ channels. *Nature* **366**(6451): 158-161.

Yasuda R, Noji H, Kinosita K et al. (1998) F-1-ATPase is a highly efficient molecular motor that rotates with discrete 120 degrees steps. *Cell* **93**(7): 1117-1124.

Yasuda R, Noji H, Yoshida M et al. (2001) Resolution of distinct rotational substeps by submillisecond kinetic

analysis of F1-ATPase. *Nature* **410**(6831): 898-904.

Yerushalmi H and Schuldiner S (2000) An essential glutamyl residue in EmrE, a multidrug antiporter from Escherichia coli. *Journal of Biological Chemistry* **275**(8): 5264-5269.

Yoshida M and Allison WS (1983) Modulation by ADP and Mg2+ of the inactivation of the F1-ATPase from the thermophilic bacterium, PS3, with dicyclohexylcarbodiimide. *Journal of Biological Chemistry* **258**(23): 14407-14412.

Yoshida M, Muneyuki E and Hisabori T (2001) ATP synthase--a marvellous rotary engine of the cell. *Nat Rev Mol Cell Biol* **2**(9): 669-677.

Yoshizawa S, Kumagai Y, Kim H et al. (2014) Functional characterization of flavobacteria rhodopsins reveals a unique class of light-driven chloride pump in bacteria. *Proceedings of the National Academy of Sciences of the United States of America* **111**(18): 6732-6737.

Yu HB, Noskov SY and Roux B (2010) Two mechanisms of ion selectivity in protein binding sites. *Proceedings of the National Academy of Sciences of the United States of America* **107**(47): 20329-20334.

Zani ML, Pourcher T and Leblanc G (1993) Mutagenesis of Acidic Residues in Putative Membrane-Spanning Segments of the Melibiose Permease of Escherichia-Coli .2. Effect on Cationic Selectivity and Coupling Properties. *Journal of Biological Chemistry* **268**(5): 3216-3221.

Zhang LY, Zheng YC, Xi ZY et al. (2009) Metal ions binding to recA inteins from Mycobacterium tuberculosis. *Molecular Biosystems* **5**(6): 644-650.

Zhao JH, Benlekbir S and Rubinstein JL (2015) Electron cryomicroscopy observation of rotational states in a eukaryotic V-ATPase. *Nature* **521**(7551): 241-+.

Zscherp C, Schlesinger R, Tittor J et al. (1999) In situ determination of transient pKa changes of internal amino acids of bacteriorhodopsin by using time-resolved attenuated total reflection Fourier-transform infrared spectroscopy. *Proc Natl Acad Sci U S A* **96**(10): 5498-5503.

Duncan TM, Bulygin VV, Zhou Y et al. (1995) Rotation of Subunits during Catalysis by Escherichia-Coli F1-Atpase. *Proceedings of the National Academy of Sciences of the United States of America* **92**(24): 10964-10968.

Kinosita K, Yasuda R, Noji H et al. (1998) F-1-ATPase: A rotary motor made of a single molecule. *Cell* **93**(1): 21-24.

Mitchell P (1961) Coupling of phosphorylation to electron and hydrogen transfer by a chemi-osmotic type of mechanism. *Nature* **191**(144-148.

Noji H, Yasuda R, Yoshida M et al. (1997) Direct observation of the rotation of F1-ATPase. *Nature* **386**(6622): 299-302.